

NEAR-HORIZON BLACK HOLE PHYSICS

Thesis by
Baoyi Chen

In Partial Fulfillment of the Requirements for the
Degree of
Doctor of Philosophy in Physics

The logo for the California Institute of Technology (Caltech), featuring the word "Caltech" in a bold, orange, sans-serif font.

CALIFORNIA INSTITUTE OF TECHNOLOGY
Pasadena, California

2022
Defended Aug 9 2021

© 2022

Baoyi Chen

ORCID: 0000-0002-3927-6843

All rights reserved except where otherwise noted

ACKNOWLEDGEMENTS

I would like to express my deepest gratitude to my advisor, Yanbei Chen. He led me into the field of black hole physics, supervised me throughout my research, enlightened me with his extremely solid mathematical and physical knowledge, and constantly supported me in every way. During my time working with him, I was deeply impressed by his smart explanations of complicated physics problems. Through learning from him, I gradually built up a true physicist's way of solving all kinds of problems. Choosing Prof. Chen as my advisor is of no doubt the best decision that I have made during all these years at Caltech.

I am indebted to Leo Stein. He offered me an interesting problem to explore as my first project on black holes. Without his help, I would not have been able to switch my research directions to general relativity so quickly. I have benefited a lot from his enormous physics knowledge and smart "tricks". I really enjoyed the time we spent together discussing projects, debugging codes, writing papers, and even taking bets on the results of our work.

I am grateful to Yiqiu Ma. In addition to the countless number of valuable life and career suggestions that he offered, he also taught me the spirit to question every seemingly widely-accepted physical principles, and the ability to approach problems using physical intuitions. I really enjoyed our talks together, and I am grateful for his companion, as an excellent collaborator, a kind teacher, a good friend, and a considerate big brother.

I thank my collaborators Feng-Li Lin, Bo Ning, Qingwen Wang, and Ling Sun for all the insightful discussions. It is my honor to have worked with them on the interesting projects from weak cosmic censorship to gravitational-wave echoes. In particular, I am indebted to Feng-Li Lin. Being a very smart and senior researcher, Prof. Lin's modesty and diligence never failed to make him a role model to me. His expertise in high-energy physics also infused many interesting new ideas into our work together.

I acknowledge my other committee members, Saul Teukolsky, Mark Scheel, and Clifford Cheung, and thank them for their interest in my work, their valuable suggestions, and their investment of time.

I must also thank Fiona Harrison and Mislav Baloković for their support and help during my first year at Caltech. Many thanks to Rana Adhikari and Curt Cutler for

their patient guidance through my second year of graduate study while working on the future gravitational-wave detector project.

I thank my fellow graduate students, Zachary Mark, Songming Du, Xiang Li, Ka-Lok Lo, and Sizheng Ma, for all the insightful discussions we had together. I thank Huan Yang for kindly inviting me to visit PI, and constantly supporting me when I was applying for postdoc positions. I thank JoAnn Boyd, for her assistance on administrative matters, which helped me better focused on my research.

I thank my good friends, Jing Cai, Yunxuan Li, Hao Xie, Boqiang Shen, and Yu-An Chen during this journey, who have made my Ph.D. life not just bearable but in fact enjoyable.

I am extremely grateful to my family, especially my wife, Yingying Wu, for all the support and love. Final thanks to my daughter Claire Zimo Chen for all the joys and tears, and for making me a stronger and better person.

ABSTRACT

This thesis studies the near-horizon black hole physics in depth from three perspectives.

An important tool for studying perturbations of black hole spacetime is the linearized Einstein equations (LEE). In the Kerr spacetime, the variables in LEE do not separate, which poses a lot of difficulties to obtaining analytical solutions. By taking the near-horizon limit of extremal Kerr black holes, additional symmetries emerge to make the LEE separable. This is achieved by decomposing the metric perturbations using some basis functions adapted to the symmetry. I further show that in two string-inspired low-energy effective theories of gravity, LEE can be directly solved and analytical black hole solutions can be found.

Naively, the near-horizon perturbations of an extremal black hole may destroy the horizon and make the singularity expose itself. This is a direct challenge of the weak cosmic censorship conjecture (WCCC). Based on Wald's gendanken experiments to destroy black holes, I examine the WCCC for the extremal charged black hole in possible generalizations of Einstein-Maxwell theory due to the higher-order corrections, up to fourth-derivative terms. It turns out that, provided the null energy condition for the falling matter, the WCCC is preserved for all possible generalizations. I further find that for BTZ black holes, i.e. solutions to (2+1)-Einstein gravity with asymptotically AdS_3 boundary, WCCC is always preserved. Through the AdS/CFT correspondence, this establishes the connections between black hole thermodynamics and WCCC.

From considerations of quantum gravity and quantum information, it has been conjectured that space-time geometry near the horizon can be modified, even at scales larger than the Planck scale. The resulting spacetime is commonly referred to as the exotic compact object (ECO). A viable method to look for the near-horizon quantum structures is searching for gravitational wave echoes in the GW signals. After discussing the stability issues associated with the ECOs, I build up the phenomenology for gravitational echoes. I also introduce a new framework to deal with the near-horizon boundaries by considering the tidal response of the ECO as experienced by zero-angular-momentum fiducial observers. It is then straightforward to apply the boundary condition to computing gravitational-wave echoes from exotic compact objects.

PUBLISHED CONTENT AND CONTRIBUTIONS

- [1] Baoyi Chen and Leo C. Stein. Separating metric perturbations in near-horizon extremal Kerr. *Phys. Rev. D*, 96(6):064017, 2017. <https://journals.aps.org/prd/abstract/10.1103/PhysRevD.96.064017>. B.C was involved in developing the idea, did all the calculations, and wrote the manuscript.
- [2] Baoyi Chen and Leo C. Stein. Deformation of extremal black holes from stringy interactions. *Phys. Rev. D*, 97(8):084012, 2018. <https://journals.aps.org/prd/abstract/10.1103/PhysRevD.97.084012>. B.C was involved in developing the idea, did all the calculations, and wrote the manuscript.
- [3] Bo Ning, Baoyi Chen, and Feng-Li Lin. Gedanken Experiments to Destroy a BTZ Black Hole. *Phys. Rev. D*, 100(4):044043, 2019. <https://journals.aps.org/prd/abstract/10.1103/PhysRevD.100.044043>. B.C was involved in developing the idea, did the second-order variation calculations, and wrote half of the manuscript.
- [4] Baoyi Chen, Yanbei Chen, Yiqiu Ma, Ka-Lok R. Lo, and Ling Sun. Instability of Exotic Compact Objects and Its Implications for Gravitational-Wave Echoes. 2 2019. <https://arxiv.org/abs/1902.08180>. B.C was involved in developing the idea, did all the calculations, and wrote the manuscript.
- [5] Baoyi Chen, Feng-Li Lin, Bo Ning, and Yanbei Chen. Constraints on Low-Energy Effective Theories from Weak Cosmic Censorship. *Phys. Rev. Lett.*, 126(3):031102, 2021. [Erratum: *Phys.Rev.Lett.* 126, 119903 (2021)]. <https://journals.aps.org/prl/abstract/10.1103/PhysRevLett.126.031102>. B.C developed the idea, did all the calculations, and wrote the manuscript.
- [6] Baoyi Chen, Qingwen Wang, and Yanbei Chen. Tidal response and near-horizon boundary conditions for spinning exotic compact objects. *Phys. Rev. D*, 103(10):104054, 2021. <https://journals.aps.org/prd/abstract/10.1103/PhysRevD.103.104054>. B.C was involved in developing the idea, did all the calculations, and wrote the manuscript.

TABLE OF CONTENTS

Acknowledgements	iii
Abstract	v
Published Content and Contributions	vi
Bibliography	vi
Table of Contents	vii
List of Illustrations	x
List of Tables	xiv
Chapter I: Introduction	1
 PART I NEAR-HORIZON SYMMETRIES AND BLACK HOLE PERTURBATIONS	 9
Chapter II: Separating metric perturbations in near-horizon extremal Kerr . . .	10
2.1 Introduction	10
2.2 Kerr and the NHEK limit	12
2.3 The highest- (lowest-) weight method	15
2.4 Orthogonality in global coordinates	19
2.5 Separation of variables	21
2.6 Conclusions and future work	26
2.7 Appendix	27
Chapter III: Metric deformations from extremal Kerr black holes	38
3.1 Introduction	38
3.2 Einstein-dilaton-Gauss-Bonnet and dynamical Chern-Simons gravity	40
3.3 NHEK and separable metric perturbations	43
3.4 Solving for the metric deformations	45

3.5 Properties of solutions	49
3.6 Discussion and future work	54

PART II GEDANKEN EXPERIMENTS TO DESTROY THE EVENT HORIZON 57

Chapter IV: Gedanken experiments to destroy an extremal black hole: first-order study	58
4.1 Introduction	58
4.2 EFTs, black-hole solutions, and extremality condition	59
4.3 Gedanken experiment to destroy the horizon	61
4.4 Test particle	62
4.5 Sorce-Wald method for generic matter	63
4.6 Parameter bounds from WCCC	66
4.7 Extension to more general theories	67
4.8 Appendix	68
Chapter V: Gedanken experiments to destroy a BTZ black hole: second-order study	79
5.1 Introduction	79
5.2 BTZ black hole and variational identities	82
5.3 Gedanken experiment to destroy an extremal BTZ	91
5.4 Gedanken experiment to destroy a near-extremal BTZ	93
5.5 Conclusions and discussions	100

PART III SEARCHING FOR NEAR-HORIZON QUANTUM STRUCTURES VIA GRAVITATIONAL-WAVE ECHOES 102

Chapter VI: Instability of exotic compact objects and implications for echoes .	103
6.1 Introduction	103
6.2 Set up of the problem	104
6.3 Estimates based on the hoop conjecture	105
6.4 In-going Vaidya spacetime	107
6.5 Back reaction: static ECO with future incoming pulse	108
6.6 Back reaction: expanding ECO	109
6.7 Implications for GW-echo phenomenology	109
6.8 Discussions	111

6.9 Appendix	111
Chapter VII: Tidal response and near-horizon boundary conditions for spinning ECOs	113
7.1 Introduction	113
7.2 The reflection boundary condition from tidal response	117
7.3 Wave propagation in the vicinity of the horizon	126
7.4 Boundary condition in terms of various functions	137
7.5 Waveforms and quasi-normal modes of the ECO	141
7.6 Conclusions	146
7.7 Appendix	146
Bibliography	153

LIST OF ILLUSTRATIONS

<i>Number</i>	<i>Page</i>
3.1 The metric deformation functions δv_1 (solid) and δv_2 (dashed) as functions of u , for both dCS-deformed (red) and EdGB-deformed (blue) NHEK. Note that in D ² GB, δv_1 blows up at the two poles $u = \pm 1$	47
4.1 The gedanken experiment to destroy an extremal black hole. Charged matter, occupying the shaded region, crosses the \mathcal{H} portion of the extremal horizon.	64
4.2 Extremality contour and constant area contours. Extremal black holes live on the red solid line which divides the whole parameter space into the naked singularity region and the non-extremal black hole region. The constant area contours are always tangent to the extremal line. A small perturbation around an extremal point then shifts the spacetime to one of the following: (i) a naked singularity when the horizon area is decreased; (ii) another extremal solution when the area is unchanged; and (iii) a nonextremal black hole when the area is increased.	77
5.1 Carter-Penrose diagram of an extremal BTZ black hole. The shaded region consists of the falling matter which all goes into the black hole. The perturbation $\delta\phi$ vanishes in a neighborhood of $\Sigma_0 \cap \mathcal{H}$. . .	92
5.2 Carter-Penrose diagram of a near-extremal BTZ black hole. The shaded region consists of the falling matter which all goes into the black hole. The perturbation $\delta\phi$ and $\delta^2\phi$ vanishes in a neighborhood of B	95

- 5.3 The parameter space of BTZ black holes in chiral gravity. The black solid line corresponds to extremal BTZ black holes. Any point above this line corresponds to a non-extremal BTZ black hole, while any point below the line is a naked conical singularity. The orange dashed line is one of the lines of constant entropy, which is parallel to the line for extremal BTZ black holes. Starting with some point on the constant entropy line, any tangent vector will always be parallel to the extremal BTZ line. That is, there is no Hubeny-type violation that can overspin a near-extremal BTZ black hole in chiral gravity. 96
- 5.4 The parameter space of BTZ solutions in the three-dimensional Einstein gravity. The black solid line corresponds to extremal BTZ black holes. Any point above this line corresponds to a non-extremal BTZ black hole, while any point below the line is a naked conical singularity. The orange dashed curve is one of the curves of constant entropy, which meets the extremal BTZ line tangentially. The tangent vector at the point of an extremal BTZ black hole will always bring it to another extremal BTZ black hole. However, starting from a slightly non-extremal BTZ black hole, to linear order, the tangent vector can perturb the spacetime to become a naked conical singularity. 97
- 6.1 A pulse of GW with energy E incident on a static ECO with mass M . A hoop is placed at the Schwarzschild radius $2(M + E)$. When the spatial extent of the GWs becomes compacted within the hoop in every direction, the event horizon forms. 105
- 6.2 A Vaidya spacetime with an incoming null packet spatially bounded by the black dashed line. The trapped surface evolves along the blue solid line. The event horizon evolves along the red dashed line, and coincides with the trapped surface after all energy goes into the horizon. Any ECO with its surface crossing the pink line will promptly collapse, while those cross the green line does not. Static ECOs can then be divided into three different types (a), (b), and (c), separated by the gray dashed lines (not world lines), and are discussed in detail in the main text. 106

- 6.3 (a) A static ECO scenario where the ECO surface is outside the event horizon and, which can give rise to GW echoes. The spatially nearest incoming ray, denoted by the green dashed line, reflects at the potential barrier and the ECO surface, leading to a time delay Δt_{echo} between the main wave and the echo as observed at spatial infinity.
- (b) A static ECO scenario where part of the incoming GW energy gets reflected at the ECO surface and gives rise to echoes until “the-last-ray-to-escape”. The subsequent echoes are highly redshifted due to the formation of event horizon, leading to a weak echo signal.
- (c) Spherically symmetric ECO absorbing GWs and expanding in radius. The event horizon grows along the red dashed line. If the ECO surface always remains outside the event horizon, incoming rays can lead to GW echoes, as shown by the green dashed lines. 108
- 6.4 Contour plot for R as function of $r_{\text{ECO}}/M - 2$ and $\alpha_{\text{H}}(4\eta)^2$. Regions in red, white, and yellow indicate types (a), (b), and (c), respectively. Along the vertical axis, the ranges indicate comparable, intermediate, and extreme mass ratio inspirals. 110
- 7.1 Trajectory of the FIDO in a constant θ slice of the Kerr spacetime in the $(t, r \cos \phi, r \sin \phi)$ coordinate system. Here the green surface indicates the ECO surface with $r = b$, while the black surface indicates the Kerr horizon. Each FIDO has $r = b$, but has $(t, \phi) = (t, \phi_0 + \Omega_{\text{H}}t)$. 118
- 7.2 Waves that propagate toward the ECO surface can be approximated as propagating toward the future horizon, while those originate from the ECO surface can be approximated as originating from the past horizon. 119
- 7.3 Illustration of the constant- x contours in the $(r_*, \cos \theta)$ plane. Reflections from the same x for different θ will appear as being reflected at different r_* for different θ 128
- 7.4 The absolute values of the factor $\hat{\mathcal{M}}_{\ell\ell'm\omega}$ for various spin a and ℓ' . This factor shows the mixing between different ℓ -modes after an incoming single mode gets reflected on the surface of an exotic compact object. Here we have chosen $\ell = 2, m = 2$ as an example. In general for spacetimes with higher spins, the reflected waves gain more contributions from higher ℓ' -modes, thus the effect of mode mixing is not negligible for rapidly spinning ECOs. 131

- 7.5 Absolute values of ζ_D and ζ_M as functions of the frequency k . We have set $g_H = 1$. As indicated by Eq. (7.70), ζ and the Teukolsky reflectivity \mathcal{R} only differ by a phase, $|\zeta|$ is the same as $|\mathcal{R}|$. The blue solid line represents $|\zeta_D|$. The yellow dotted line, the green dashed line, the red dot-dashed line, and the purple long dashed line give $|\zeta_M|$ for $\mu = 0.1, 0.2, 0.5, \infty$ respectively. The Boltzman reflectivity, i.e. ξ_D , exponentially decays for higher frequencies. For our model of homogeneous stars, we have total reflection of waves on the ECO surface below a certain threshold frequency. Beyond the threshold frequency, the reflectivity gets decreased and converges to a constant. When $\mu \rightarrow \infty$, we have total reflection of waves for all the frequency range, which is equivalent to the case of inhomogeneous stars we have introduced. 136
- 7.6 Conversion factor $\mathcal{K}_{\ell m \omega}^{\text{T} \rightarrow \text{SN}}$ from the Teukolsky \mathcal{R} to the Sasaki-Nakamura \mathcal{R}_{SN} . Here we have ignored the ℓ - ℓ' mode mixing. We plot real and imaginary parts, as well as the modulus, of $\mathcal{K}_{\ell m \omega}^{\text{T} \rightarrow \text{SN}}$ for the (2, 2)-mode with $a = 0, 0.3, 0.7, 1$ respectively. The gray dot-dashed line marks the horizon frequency $m\Omega_H$. In the Schwarzschild case, the two reflection coefficients only differ by a phase. For Kerr spacetimes we have $|\mathcal{K}_{\ell m \omega}^{\text{T} \rightarrow \text{SN}}| > 1$ for both low and high frequencies, but $|\mathcal{K}_{\ell m \omega}^{\text{T} \rightarrow \text{SN}}|$ dips below 1 for some frequencies. Also note that $|\mathcal{K}_{\ell m \omega}^{\text{T} \rightarrow \text{SN}}| = 1$ when ω equals to the horizon frequency. 140

LIST OF TABLES

<i>Number</i>	<i>Page</i>
2.1 The coefficient table that gives the expressions of $\mathcal{D}_A^{(m,h)}[\mathbf{C}(u)]$, $A \in \{T, \Phi, R, u\}$ in Maxwell systems.	33
2.2 \mathcal{A} matrix.	33
2.3 \mathcal{B} matrix.	34
2.4 Part I of \mathcal{C} matrix.	35
2.5 Part II of \mathcal{C} matrix.	36
2.6 Part III of \mathcal{C} matrix.	37

Chapter 1

INTRODUCTION

A classical *black hole* is, by definition, a spacetime region where gravity is so strong that nothing can escape from it. Thus the black hole has two defining features. One is the *singularity* which is a spacetime point with infinitely large curvatures. The other is the *event horizon* which is a spacetime boundary precluding even light from escaping to infinity.

The research on black holes began after the birth of Einstein's theory of gravitation, i.e. *general relativity*, although the idea of the "surface of no escape" can be dated back to the 18th century [1]. In 1916, Schwarzschild obtained the first exact vacuum solution of Einstein's equations with spherical symmetry. About half-century after Schwarzschild's discovery, Kerr discovered the exact solution for rotating black holes. Hawking's discovery of black hole evaporation stimulated a lot of debates of quantum unitarity against semiclassical gravity. In superstring theory, those black holes with quantum hairs are actively studied as the simplest solutions to the unified theory of all interactions. The X-rays produced by accretion of gas onto central objects has also given black holes lots of attention in the astrophysical community.

More recently, a significant breakthrough in the development of black holes physics is the unprecedented discovery of gravitational waves from the binary BH merger event GW150914 [2], and follow-up observations of an order of ~ 100 binary black hole merger events [3, 4]. We now know that these dark compact objects do exist in our universe, and that their space-time geometry and dynamics are consistent with those of black holes in general relativity. The event horizon telescope has produced images from the center of the M87 galaxy that are consistent with the shadow of a black hole in general relativity [5–12]. We are now well prepared for further understanding of near-horizon black hole physics. Due to the teleological nature of the event horizon, no experiments can directly confirm the existence of this spacetime boundary. But now with the gravitational-wave detectors, we are able to *quantify* the darkness of these objects, and even search for new physics near the horizon.

This thesis can be regarded as an introduction to *near-horizon black hole physics*. Three main topics are discussed in depth.

I. Near-horizon symmetries and black hole perturbations

By focusing on the near-horizon region, the black hole spacetime may attain additional symmetries. Symmetries have been widely used in solving perturbation problems in the black hole spacetime. The equations that govern the gravitational perturbation are the *Einstein's equations*, which are coupled partial differential equations. In the Schwarzschild spacetime, by taking advantage of the spherical symmetry, one can decompose the perturbations into standard spherical harmonic bases, which makes the Einstein equations decouple. This process, however, cannot be done for spinning black holes due to lack of symmetries. Fortunately, by taking the near-horizon extremal limit, new symmetries emerge.

Extremal black holes correspond to a family of black hole solutions whose inner and outer horizons coincide. Equivalently, they are defined by their vanishing Hawking temperature,

$$T_{\text{H}} = 0. \quad (1.1)$$

Extremal black holes have gained a lot of importance in superstring theories because any supersymmetric black hole is necessarily extremal. The extremal limits of four-dimensional black holes have recently been extensively studied due to the *Kerr/CFT correspondence*, which conjectures that a Kerr black hole also has a dual three-dimensional conform field theory description.

A feature of extremal black holes is that they have a well-defined *near-horizon geometry*. By zooming onto the near-horizon region, new symmetries occur, which leads to further simplifications of solving physical problems. The method to decouple the whole black hole spacetime into a near-horizon region and an asymptotically-flat exterior region is known by taking the near-horizon scaling limit of the extremal black hole solutions. The resulting spacetime, which was first discovered by Bardeen and Horowitz [13], has an enhanced symmetry group $SL(2, \mathbb{R}) \times U(1)$, and is known as the *NHEK* spacetime. The NHEK metric is given by

$$ds^2 = \Gamma(\theta) \left[-r^2 dt^2 + \frac{dr^2}{r^2} + d\theta^2 + \Lambda(\theta)^2 (d\phi + r dt)^2 \right], \quad (1.2)$$

with

$$\Gamma(\theta) = 1 + \cos^2 \theta, \quad \Lambda(\theta) = \frac{2 \sin \theta}{1 + \cos^2 \theta}. \quad (1.3)$$

At fixed polar angle θ , this geometry is a $3d$ warped anti-de Sitter spacetime, which is a deformation of AdS_3 .

As it will turn out, the symmetry structure of NHEK spacetime finally decouples the Einstein equation for spinning black holes. There are many potential applications of the near-horizon symmetry. For instance, extreme mass-ratio inspiral (EMRI) is the main target of Laser Interferometer Space Antenna (LISA). An important part of obtaining the waveform produced by EMRI is the calculation of the gravitational self-force. However, a full analytical computation of self force is notoriously difficult. By isolating the near-horizon region, and making use of the additional symmetries in the near-horizon limit, it is possible to separate the variables in the linearized Einstein equation, and obtain the second-order metric perturbations, which are the building blocks for self-force calculation.

II. Gedanken experiments to destroy the event horizon

The singularity is always safely hidden inside the horizon. If the event horizon is somehow destroyed by external perturbations, we will then be able to directly “see” the singularity. It seems Nature itself forbids this, as have been pointed out by the weak cosmic censorship conjecture (WCCC) [14]. The WCCC asserts that all singularities, except for the big-bang singularity, must be hidden by the event horizon—no naked singularity can exist in our universe. A gravitational singularity has infinitely large curvature and is mathematically ill-defined. Philosophically, the weak cosmic censorship seems to be a smart design by the universe to avoid the awkwardness of dealing with infinity.

It might still be possible to throw charged or spinning matter into a black hole in particular ways that can destroy the horizon, revealing the singularity. For example let us consider a Kerr-Newman black hole with mass M , charge Q , and angular momentum $J = Ma$. The black hole must satisfy

$$M^2 \geq (J/M)^2 + Q^2, \quad (1.4)$$

with the equal sign corresponding to the extremal case. If we instead has a Kerr-Newman metric with the \geq -sign in Eq. (1.4) flipped to \leq , then it is a naked singularity. By throwing matters with properly tuned mass, charge, and angular momentum, it may be possible to flip the sign in the above inequality and successfully “destroy” the event horizon.

This kind of gedanken experiments was first proposed by Wald in [15]. In this paper, he proved that an extremal black holes cannot be overspun or overcharged in this

way, thus WCCC is preserved. Later, Hubeny pointed out that if one instead starts with a near-extremal black hole and then properly throws particles in, WCCC can be violated [16]. A full understanding of this problem then seems to require the full calculation of gravitational perturbations to the second order, i.e. the self-force as well as the finite size effect. Recently, significant progress has been made by Sorce and Wald [17] who derived a second order variational identity relating variations of total mass, charge, and angular momentum, and can work for general forms of falling matter obeying the Null Energy Condition (NEC). In this way, they were able to avoid solving the complicated dynamical problems of the in-falling matter involving the self-force effect, and succeeded to show that the WCCC holds for the black holes in Einstein-Maxwell theory, up to second-order variation of the black hole's mass, charge, and angular momentum. They also pointed out that Hubeny's result of WCCC violation no longer exists after taking care of the second-order variations.

Sorce and Wald's method of examining the WCCC provides a systematic framework for general theories other than Einstein-Maxwell. Following their line of thoughts, it is then particularly interesting to examine the WCCC in the low-energy effective theories of gravity, and see how the additional terms in the action alters the proof of WCCC. If WCCC turns out to be invalid for some theories, then by demanding that WCCC must hold for black hole solutions in the classical limit, we may be able to derive a bound for the coupling coefficients in the low-energy theory of quantum gravity. Due to the AdS/CFT correspondence, it would also be interesting to check the conjecture for asymptotically AdS black holes and give a holographic description of the gendanken experiments in terms of thermodynamics of the dual conformal field theory.

III. Searching for near-horizon quantum structures via gravitational-wave echoes

The event horizon cannot be directly detected due to its teleological nature. Although LIGO has made successful detections of gravitational waves from binary merger events, we do not yet have a quantitative way of saying, in which sense, and to what extent had we confirmed that these dark compact objects are black holes.

Because of the Black-Hole Information Paradox, and the singularity, many believed that GR must be modified to incorporate quantum effects, and that such modifications may affect black hole spacetimes. Many horizonless black hole mimickers have

been proposed, including gravastars, 2-2 holes, boson stars, and so on. They are commonly referred to as Exotic Compact Objects (ECOs). The idea of ECOs, although speculative, have attracted a lot of recent interest.

If ECOs, instead of black holes, are the final products of compact binary mergers, they will not completely absorb the gravitational waves that were propagating toward the black hole’s horizon, but will instead lead to gravitational-wave *echoes* [18–29]. That is, GWs that propagate toward the ECO can be reflected by the ECO surface, and bounce back and forth between the ECO’s gravitational potential barrier (at the location of the light sphere) and the ECO surface. These echoes will then become the smoking gun of modifications to relativity. Most notably, Abedi et al. claimed to have found evidence of echoes in Advanced LIGO data after the first few observed compact binary coalescence events [22, 30, 31]. Though the statistical significance of their results was questioned [32–35]. Regardless of how much one believes in ECOs, parametrizing gravitational echoes and searching for them will be an important way to quantify how “black” the dark compact objects really are. As we are approaching the stage of precision measurements with future GW detectors, the echo program is promising in helping us understand the near-horizon quantum structure of black holes.

In order to search for the near-horizon spacetime modifications, one needs to establish a template bank for gravitational-wave echoes. The numerical solution of echo waveform can be obtained by solving the Teukolsky equation with a modified near-horizon boundary. This boundary condition, is usually deemed less physical due to the unknown physical meaning of “reflecting” the curvature perturbations on the star surface. It will then be extremely helpful to have a true physical and systematic framework to deal with the near-horizon boundary conditions, and solve for the waves observed at infinity. This is the main goal of the third part of this thesis.

Organization of the thesis

The thesis is divided into three parts, which approach the near-horizon physics from three perspectives. Part I focuses on the enhanced symmetry group in the near-horizon region of the near-extremal or extremal Kerr black holes. The rich symmetry structure of the so-called NHEK or near-NHEK spacetime directly admits the separation of variables in the linearized metric perturbation equations. Part II

is about destroying the event horizon by throwing normal matter with mass, spin, and charge into the black hole. If the overspinning or overcharging occurs, this immediately means a violation of the weak cosmic censorship conjecture. Part III goes about the instability issues with ECO models, and the method to search for near-horizon modifications of spacetime by looking for the gravitational wave echoes in the late-time part of the GW signals.

A more detailed overview of the thesis is as follows.

Chapter 2, separating metric perturbations in near-horizon extremal Kerr, establishes the framework for calculating metric perturbations in the near-horizon extremal Kerr spacetime. In the general Kerr spacetime, the metric equations of motion are not separable. After taking the near-horizon extremal limit in Kerr, the new spacetime has two additional Killing vectors, and the isometry becomes $SL(2, \mathbb{R}) \times U(1)$. By choosing the scalar, vector, and tensor bases adapted to the isometry group, it is then not difficult to show that separation of variables can be achieved in NHEK spacetime for the scalar, Maxwell, and metric perturbation equations. This work was the result of a collaboration with Leo Stein and was published as Chen, B., Stein, L. (2017) *Separating metric perturbations in near-horizon extremal Kerr*, Phys. Rev. D, **96** 064017 [36].

Chapter 3, metric deformations from extremal Kerr black holes, is a direct application of the method developed in Chapter 2, which gives two analytical perturbed solutions deformed from NHEK in two string-inspired theories: Einstein-dilaton-Gauss-Bonnet, and dynamical Chern-Simons theory. We find that the EdGB metric deformation has a curvature singularity, while the dCS metric is regular. With the analytical metric forms, properties of black holes like the orbital frequencies, horizon areas, and entropies can be readily obtained. This demonstrates the power of the framework developed in Chapter 2. This work was the result of a collaboration with Leo Stein and was published as Chen, B., Stein, L. (2018) *Deformation of extremal black holes from stringy interactions*, Phys. Rev. D, **97** 084012 [37].

Chapter 4, gedanken experiments to destroy an extremal black hole: the first order study, examines the weak cosmic censorship conjecture for the extremal charged black hole in all possible generalizations of Einstein-Maxwell theory due to the higher-order corrections, up to fourth-derivative terms. Provided the null energy condition for the falling matter, the WCCC is preserved for all possible generalizations. Moreover, up to first-order variations of black hole mass and charge, WCCC is preserved for non-rotating extremal black holes in all n -dimensional

diffeomorphism-covariant theories of gravity with one $U(1)$ gauge field. This work was the result of a collaboration with Bo Ning, Feng-Li Lin, and Yanbei Chen, and was published as Chen, B., Lin, F., Ning, B. and Chen, Y. (2021) *Constraints on Low-Energy Effective Theories from Weak Cosmic Censorship*, Phys. Rev. Lett. **126** 031102 [5].

Chapter 5, gedanken experiments to destroy a BTZ black hole: the second order study, examines the weak cosmic censorship conjecture for the BTZ black holes up to second-order variations of black hole mass. Unlike in Chapter 4, the discussions only work in first order and only consider the asymptotically flat black hole solutions, this chapter focuses on BTZ black holes, which are vacuum solutions to (2+1)-dimensional gravity theories, and are asymptotically AdS_3 . The BTZ solution is interesting in its own right due to the AdS/CFT correspondence. By showing that BTZ black holes cannot be overspun or overcharged by throwing normal matter into the event horizon, one also confirms that a third law of thermodynamics holds for the holographic conformal field theories dual to three-dimensional Einstein gravity and chiral gravity. This work was the result of a collaboration with Bo Ning and Feng-Li Lin, and was published as Ning, B., Chen, B., and Lin, F. (2019) *Gedanken Experiments to Destroy a BTZ Black Hole*, Phys. Rev. D, **100** 044043 [3].

Chapter 6, instability of exotic compact objects and implications for echoes, goes about exploring the phenomenology related to the gravitational-wave echoes. By assuming the exterior spacetime of an exotic compact object is spherically-symmetric, the hoop conjecture implies that the energy carried by gravitational waves may cause the event horizon to form out of a static ECO—leaving no echo signals towards spatial infinity. Demanding that an ECO does not collapse into a black hole then puts an upper bound on the compactness of the ECO. This work was the result of a collaboration with Chen, Y., Ma, Y., Lo, K. and Sun, L [4].

Chapter 7, tidal response and near-horizon boundary conditions for spinning ECOs, approaches the problem of how to set up the physical boundary conditions near the “would-be” horizon for incoming gravitational waves towards exotic compact objects. In Kerr spacetime, imposing regularity conditions on the curvature perturbations on the future (past) horizon corresponds to imposing an in-going (out-going) wave boundary condition. These correspondences, however, do not exist for ECOs. By considering a family of zero-angular-momentum fiducial observers (FIDOs) that float right above the horizon of a linearly perturbed Kerr black hole, one can set up a physical boundary condition near horizon using the ECO’s tidal response in

the FIDO frame. This then provides a new framework for calculating the waveform of the gravitational-wave echoes. This work was the result of a collaboration with Chen, Y., and Wang, Q. and was published as Chen, B., Wang, Q. and Chen, Y. (2021) *Tidal response and near-horizon boundary conditions for spinning exotic compact objects*, Phys. Rev. D, **103** 104054 [6].

PART I

NEAR-HORIZON SYMMETRIES AND BLACK HOLE PERTURBATIONS

Chapter 2

SEPARATING METRIC PERTURBATIONS IN NEAR-HORIZON EXTREMAL KERR

Linear perturbation theory is a powerful toolkit for studying black hole spacetimes. However, the perturbation equations are hard to solve unless we can use separation of variables. In the Kerr spacetime, metric perturbations do not separate, but curvature perturbations do. The cost of curvature perturbations is a very complicated metric-reconstruction procedure. This procedure can be avoided using a symmetry-adapted choice of basis functions in highly symmetric spacetimes, such as near-horizon extremal Kerr. In this chapter, we focus on this spacetime, and (i) construct the symmetry-adapted basis functions; (ii) show their orthogonality; and (iii) show that they lead to separation of variables of the scalar, Maxwell, and metric perturbation equations. This separation turns the system of partial differential equations into one of ordinary differential equations over a compact domain, the polar angle.

2.1 Introduction

Linear metric perturbation theory is widely used in studying weakly-coupled gravity [38]. For example, it can be applied to investigating the stability of black holes, gravitational radiation produced by material sources moving in a curved background, and so on. In the context of linearized gravity, the equations that describe gravitational perturbations are the linearized Einstein equations (LEE). Although they are linear, the LEE are still difficult to solve unless we can separate variables. In the Kerr spacetime, while in Boyer-Lindquist (BL) coordinates t and ϕ can be separated, r and θ remain coupled due to lack of symmetry [39].

A successful approach towards separating wave equations for perturbations of the Kerr black hole was first developed by Teukolsky [40, 41]. Instead of looking at metric perturbations, Teukolsky adopted the Newman-Penrose (NP) formalism [42] and obtained a separable wave equation for Weyl curvature tensor components Ψ_0 and Ψ_4 . The spin-weighted version of this equation, known as the Teukolsky equation, not only works for gravitational perturbations, i.e. tensor fields, but can also be applied to scalar, vector, and spinor fields. To obtain the other Weyl scalars and recover the perturbed metric, one has to go through a complicated metric reconstruction procedure. The methods were independently developed by

Chrzanowski [43] and by Cohen and Kegeles [44], in which they obtain the perturbed metric via an analogue of Hertz potentials. However, these methods only apply to certain gauge choices and vacuum or highly-restricted source terms [45].

The desire for separable equations, the complication of metric reconstruction along with gauge- and source-restrictions, motivate us to try to develop a new formalism for studying metric perturbations in the Kerr spacetime, in a covariant, gauge-invariant way.

The metric perturbation equation may not be separable in Kerr, but Schwarzschild perturbations have long been known as separable due to the time translation invariance and spherical symmetry [46–49]. The gauge-independent language of Schwarzschild perturbations was started by Sarbach and Tiglio [50], and was brought to fruition by Martel and Poisson [51]. In the Schwarzschild background, metric perturbations are expanded in scalar, vector, and symmetric tensor spherical harmonics. These basis functions naturally lead to separation of variables in the LEE.

Schematically, the separation of variables in some differential equations of motion, such as the scalar wave equation, Maxwell’s equations, and the linearized Einstein equations, can all be understood via

$$\mathcal{D}_x \left[\left(\begin{array}{c} \text{symmetry} \\ \text{adapted} \\ \text{basis} \end{array} \right) \times \left(\begin{array}{c} \text{dependence} \\ \text{on rest of} \\ \text{coordinates} \end{array} \right) \right] = \left(\begin{array}{c} \text{symmetry} \\ \text{adapted} \\ \text{basis} \end{array} \right) \times \mathcal{D}_{x'} \left[\begin{array}{c} \text{dependence} \\ \text{on rest of} \\ \text{coordinates} \end{array} \right].$$

Here $\mathcal{D}_x[\cdot]$ is some isometry-equivariant differential operator. If the argument is decomposed in a natural isometry-adapted basis, then these basis functions pull straight through the differential operator, leaving new operators $\mathcal{D}_{x'}[\cdot]$ which only act on the remaining non-symmetry coordinates.

We show that this type of reduction is true for a special limit of Kerr spacetime: the near-horizon extremal Kerr (NHEK). This spacetime was introduced in [13] as an analogue of $AdS_2 \times S^2$. The NHEK limit exhibits a symmetry group that is “enhanced” relative to Kerr: the spacetime has four Killing vector fields that generate the isometry group $SL(2, \mathbb{R}) \times U(1)$. The three-dimensional orbit space of the isometry reduces the system of partial differential equations (PDEs) to one of ordinary differential equations (ODEs), leading to separable equations of motion. This is achieved by expanding unknown tensors into some basis functions adapted to the isometry. In this paper, we (i) construct these basis functions, (ii) prove orthogonality in geodesically-complete coordinates, and (iii) show separation of variables in the differential equations for some physical systems. With these accomplishments,

we arrive at a new formalism to deal with (extremal) Kerr perturbation that differs from using metric reconstruction on solutions to the Teukolsky equation. In this formalism there will be no gauge preference, no complications of solving PDEs, but rather only ODEs. This greatly reduces the amount of work while studying perturbations of extremal Kerr black holes, whether in GR or beyond-GR theories.

We organize the chapter as follows. In Sec. 3.3 we review the NHEK limit of the Kerr black hole, and elaborate on the structure of NHEK's isometry Lie group $SL(2, \mathbb{R}) \times U(1)$. In Sec. 2.3, we construct the highest-weight module for NHEK's isometry group, and obtain the scalar/vector/symmetric tensor basis functions. In Sec. 2.4 we present a proof of orthogonality for the basis functions in global coordinates. In Sec. 2.5 we show that with these bases, we can separate variables in the scalar Laplacian, Maxwell system, and linearized Einstein equation. Finally we conclude and discuss future work in Sec. 3.6.

2.2 Kerr and the NHEK limit

In this paper we choose geometric units ($G = c = 1$) and signature $(-+++)$ for our metric g on the spacetime manifold \mathcal{M} . A rotating, asymptotically-flat black hole in vacuum general relativity is described by the Kerr metric [52]. For simplicity we will set the mass to $M = 1$. In BL coordinates (t, r, θ, ϕ) the line element of the Kerr black hole is given by [53]

$$ds^2 = -\frac{\Delta}{\Sigma}(dt - a \sin^2 \theta d\phi)^2 + \frac{\Sigma}{\Delta} dr^2 + \Sigma d\theta^2 + \frac{\sin^2 \theta}{\Sigma} [(r^2 + a^2) d\phi - a dt]^2, \quad (2.1)$$

where $\Delta = r^2 - 2r + a^2$ and $\Sigma = r^2 + a^2 \cos^2 \theta$. The ranges of the BL coordinates are given by $t \in (-\infty, +\infty)$, $r \in (0, +\infty)$, $\theta \in [0, \pi]$, $\phi \in [0, 2\pi)$. In this paper we focus on a particular scaling limit of Kerr. This limit is usually described by the scaling coordinates (T, Φ, R) introduced in [13], which are related to the BL coordinates via

$$t = \frac{2T}{\lambda}, \quad \phi = \Phi + \frac{T}{\lambda}, \quad r = 1 + \lambda R. \quad (2.2)$$

We also introduce a new coordinate u for the polar angle via $u = \cos \theta$. The NHEK limit is then obtained by taking the $(a \rightarrow M, \lambda \rightarrow 0)$ limit of the Kerr metric in these coordinates, which yields the line element

$$ds^2 = 2\Gamma(u) \left[-R^2 dT^2 + \frac{dR^2}{R^2} + \frac{du^2}{1-u^2} + \Lambda(u)^2 (d\Phi + R dT)^2 \right], \quad (2.3)$$

where $\Gamma(u) = (1 + u^2)/2$ and $\Lambda(u) = 2\sqrt{1 - u^2}/(1 + u^2)$. This metric is interpreted on the region $T \in (-\infty, +\infty)$, $\Phi \in [0, 2\pi)$, $R \in (0, +\infty)$, $u \in [-1, 1]$.

From now on we will refer to (T, Φ, R, u) as *Poincaré coordinates*. The T, R -coordinates of NHEK are similar to the Poincaré coordinates on the two-dimensional anti-de Sitter space AdS_2 , which only cover a subspace of the global spacetime called the *Poincaré patch*. In particular, the $u = \pm 1$ submanifolds are both precisely AdS_2 . We can make this metric geodesically complete by defining the *global coordinates* (τ, φ, ψ, u) according to [13]

$$\begin{aligned} T &= \frac{\sin \tau}{\cos \tau - \cos \psi}, & R &= \frac{\cos \tau - \cos \psi}{\sin \psi}, \\ \Phi &= \varphi + \ln \left| \frac{\cos \tau - \sin \tau \cot \psi}{1 + \sin \tau \csc \psi} \right|, \end{aligned} \quad (2.4)$$

where $\tau \in (-\infty, +\infty)$, $\psi \in [0, \pi]$, $\varphi \sim \varphi + 2\pi$. The NHEK metric in global coordinates is

$$ds^2 = 2\Gamma(u) \left[(-d\tau^2 + d\psi^2) \csc^2 \psi + \frac{du^2}{1-u^2} + \Lambda(u)^2 (d\varphi - \cot \psi d\tau)^2 \right]. \quad (2.5)$$

The NHEK spacetime has four Killing vector fields (KVF), which generate the isometry group $G \equiv SL(2, \mathbb{R}) \times U(1)$. The four generators in Poincaré coordinates are given by

$$\begin{aligned} H_0 &= T \partial_T - R \partial_R, \\ H_+ &= \partial_T, \\ H_- &= \left(T^2 + \frac{1}{R^2} \right) \partial_T - 2TR \partial_R - \frac{2}{R} \partial_\Phi, \\ Q_0 &= \partial_\Phi. \end{aligned} \quad (2.6)$$

H_0 is the infinitesimal generator of *dilation*, which leaves the metric invariant under $R \rightarrow cR$ and $T \rightarrow T/c$ for some constant $c \in (0, +\infty)$. Q_0 is the generator of the rotation along Φ which generates the $U(1)$ group. H_+ is the time translation generator inherited from Kerr. The four generators form a *representation* ρ_P of the Lie algebra $\mathfrak{g} \equiv \mathfrak{sl}(2, \mathbb{R}) \times \mathfrak{u}(1)$,

$$\begin{aligned} [H_0, H_\pm] &= \mp H_\pm, \\ [H_+, H_-] &= 2H_0, \\ [H_s, Q_0] &= 0. \quad (s = 0, \pm) \end{aligned} \quad (2.7)$$

In global coordinates, we can similarly obtain four (different) generators that are KVs of the NHEK spacetime,

$$\begin{aligned} L_{\pm} &= ie^{\pm i\tau} \sin \psi (-\cot \psi \partial_{\tau} \mp i\partial_{\psi} + \partial_{\varphi}), \\ L_0 &= i\partial_{\tau}, \\ W_0 &= -i\partial_{\varphi}. \end{aligned} \tag{2.8}$$

This is a different representation, ρ_g . But since it is still a Lie algebra representation, they satisfy the same commutation relations as in Eq. (3.18) with all H 's replaced by L 's, and Q_0 replaced W_0 .

We say that the group G acts on the manifold \mathcal{M} by translation, $G \curvearrowright \mathcal{M}$. That is, every element $g \in G$ determines an isomorphism $\phi_g : \mathcal{M} \rightarrow \mathcal{M}$, and these isomorphisms, under composition, form a representation of the group G . There is an induced action on the space of functions/vector fields/forms/tensors/etc. living on \mathcal{M} by pullback under the map ϕ_g [54]. We call the pullback ϕ_g^* , overloading this symbol to mean the pullback from sections of any tensor bundle to itself. In this way, the group also acts on all spaces of (p, q) -tensors.

Studying the neighborhood of the identity $e \in G$, we get the induced action of the Lie algebra \mathfrak{g} on these same tensor bundles. The infinitesimal version of a pullback of a tensor field is the Lie derivative of that field [54]. Thus the induced action of \mathfrak{g} on tensors is Lie derivation along the representation of the Lie algebra element. That is, given a representation as tangent vector fields $\rho : \mathfrak{g} \rightarrow \mathfrak{X}(\mathcal{M})$, for some algebra element $\alpha \in \mathfrak{g}$, the induced action of α on a tensor \mathbf{t} is via the Lie derivative,

$$\alpha \cdot \mathbf{t} = \mathcal{L}_{\rho(\alpha)} \mathbf{t}. \tag{2.9}$$

One of the crucial algebra elements we will need is the Casimir element of the $\mathfrak{sl}(2, \mathbb{R})$ factor. Let $h_0, h_{\pm} \in \mathfrak{g}$ be the algebra elements whose representations are $\rho_P(h_s) = H_s$ for $s = 0, \pm$. Then the Casimir element of the $\mathfrak{sl}(2, \mathbb{R})$ factor, in this basis, is proportional to

$$\Omega \equiv h_0(h_0 - 1) - h_- h_+, \tag{2.10}$$

which commutes with every element of \mathfrak{g} . Under the Poincaré-coordinates representation ρ_P , the Casimir acts on tensors via

$$\Omega \cdot \mathbf{t} = (\mathcal{L}_{H_0}(\mathcal{L}_{H_0} - \text{id}) - \mathcal{L}_{H_-} \mathcal{L}_{H_+}) \mathbf{t}. \tag{2.11}$$

By construction, the differential operator on the right-hand side of Eq. (2.11) commutes with \mathcal{L}_X , where X is one of $\{H_0, H_\pm, Q_0\}$. Similarly, under the global-coordinates representation ρ_g , the Casimir acts as in Eq. (2.11), but with H 's replaced with L 's; and this operator will similarly commute with \mathcal{L}_X where X is one of $\{L_0, L_\pm, W_0\}$.

2.3 The highest- (lowest-) weight method

In this section we construct the scalar, vector, and symmetric tensor bases for NHEK's isometry group $SL(2, \mathbb{R}) \times U(1)$. First we briefly review the formalism of finding basis functions adapted to the isometry group in Schwarzschild spacetime. By drawing analogy to the Schwarzschild case and further utilizing the *highest-(lowest-)weight method* for non-compact groups, we will be able to construct unitary representations of NHEK's isometry group.

Review: Unitary representations of $SO(3)$ in Schwarzschild

The full spacetime manifold of Schwarzschild spacetime is $\mathcal{M}_{\text{Sch}} = M^2 \times S^2$. The two-dimensional submanifold M^2 is the (\bar{t}, \bar{r}) -plane, and S^2 is the unit two-sphere coordinated by $(\bar{\theta}, \bar{\phi})$. Here $(\bar{t}, \bar{r}, \bar{\theta}, \bar{\phi})$ are the usual Schwarzschild coordinates. Part of the isometry group of Schwarzschild is $SO(3)$, which acts on the S^2 factors. The three generators of the group are simply the rotations along each Cartesian axis, i.e. $J_x, J_y, J_z \in \mathfrak{so}(3)$. The Casimir operator of $\mathfrak{so}(3)$ is given by $J^2 = J_x^2 + J_y^2 + J_z^2$.

In any space that $SO(3)$ acts upon, we can look for bases of functions which simultaneously diagonalize J^2 and J_z —that is, they are eigenfunctions of both operators. In the space of complex functions on the unit sphere, these eigenfunctions turn out to be the spherical harmonic functions $Y^{\mu,\nu}$, where μ, ν label the functions (they are not tensor indices). The even/odd parity vector harmonics, $Y_A^{\mu,\nu}, X_A^{\mu,\nu}$, and tensor harmonics, $Y_{AB}^{\mu,\nu}, X_{AB}^{\mu,\nu}$, are also simultaneous eigenfunctions of J^2 and J_z (where now A, B are (co-)tangent indices on S^2). All of the scalars, vectors, and tensors here have eigenvalue $-\mu(\mu + 1)$ for the operator J^2 , and eigenvalue $i\nu$ for J_z .

Under any rotation, scalar spherical harmonics with different values of μ may not rotate into each other. In this sense, the function space has been split up into diagonal blocks labeled by μ . We say that each μ block “lives in” or “transforms under” a representation of $SO(3)$.

We have not yet imposed regularity or tried to make these representations unitary. Let

us define the raising and lowering operators $J_{\pm} = J_x \pm iJ_y$, which increase/decrease the ν index (eigenvalue of $-iJ_z$) by one. A *highest-weight* state is one which is annihilated by the raising operator, $J_+ f = 0$, and similarly a lowest-weight state is annihilated by the lowering operator. For spherical harmonics, we find that the highest-weight condition imposes that $\nu = \mu$, and $Y^{\mu,\mu}$ is annihilated by J_+ . Similarly, the lowest-weight condition imposes that $\nu = -\mu$.

From the representation theory of compact simple Lie groups, irreducible unitary representations must be finite-dimensional [55]. Therefore, if we start with a highest-weight state $Y^{\mu,\mu}$, after a finite number of applications of the lowering operator, we must end on a lowest-weight state $Y^{\mu,-\mu}$. This gives us the condition that $2\mu + 1$ is a positive integer, or $\mu = 0, \frac{1}{2}, 1, \dots$. Periodicity in the azimuthal angle $\bar{\phi}$ gives the condition that ν must be an integer m . This gives the ordinary spherical harmonics $Y^{l,m}$. The same arguments apply to the vector and tensor representations.

Since these bases are adapted to the isometry group of Schwarzschild, they readily lead to a separation of variables in the linearized Einstein equations [51].

Unitary representations of $SL(2, \mathbb{R}) \times U(1)$ in NHEK

We now apply the highest-/lowest-weight formalism to NHEK. In the Schwarzschild spacetime, the orbit space of the isometry $SO(3)$ is S^2 , therefore we expect a $2 + 2$ decomposition of the whole manifold. Similarly, in the NHEK spacetime, the isometry group $SL(2, \mathbb{R}) \times U(1)$ acts on the three-dimensional hypersurfaces Σ_u of constant polar angle θ (or u). This enables us to perform a $3 + 1$ decomposition of the spacetime. In both cases, we can simultaneously diagonalize some algebra elements, including the Casimir, in various tensor spaces.

However there is an important difference between the two spacetimes. In the NHEK case, we encounter the non-compact group $SL(2, \mathbb{R})$. It is known that for non-compact simple Lie groups like $SL(2, \mathbb{R})$, the only irreducible unitary finite-dimensional representation is the trivial representation [55]. As a result, one can find two distinct unitary representations of $SL(2, \mathbb{R}) \times U(1)$: the *highest-weight module* or the *lowest-weight module*. Both of them are infinite-dimensional representations in the NHEK case. For compact groups like $SO(3)$, these two modules coincide.

Our method to find the general (scalar, vector, and symmetric tensor) basis functions ξ associated with the highest-weight module of NHEK's isometry can be summarized into four steps. Notice that the method presented here is not restricted to NHEK spacetime. For instance it can also be applied to finding the basis func-

tions in near-horizon near-extremal Kerr (near-NHEK) which has the same isometry group as NHEK's [56]. This will be left for future work. For readers who are more interested in what the bases of NHEK's isometry look like either in Poincaré or global coordinates, the explicit expressions are given in App. 2.7.

Orbit space. For each point $p \in \mathcal{M}$, there is the orbit $Gp = \{\phi_g(p) | g \in G\}$, all points which are related to p by an $SL(2, \mathbb{R}) \times U(1)$ transformation. Gp is a three-dimensional submanifold of \mathcal{M} , and the collection of all the orbit spaces forms a foliation. In this case, each leaf Σ_u is a surface of constant θ (or u). Thus we can perform a $3 + 1$ decomposition of the spacetime, and look for basis functions of $SL(2, \mathbb{R}) \times U(1)$ acting on a hypersurface Σ_u .

Highest-weight states. Second, we simultaneously diagonalize $\{\mathcal{L}_{Q_0}, \mathcal{L}_{H_0}, \Omega\}$ in the space of scalar, vector, and symmetric tensor functions. We label the eigenstates by m, h, k respectively,

$$\begin{aligned}\mathcal{L}_{Q_0} \xi^{(m h k)} &= i m \xi^{(m h k)}, \\ \Omega \xi^{(m h k)} &= h(h+1) \xi^{(m h k)}, \\ \mathcal{L}_{H_0} \xi^{(m h k)} &= (-h+k) \xi^{(m h k)}.\end{aligned}\tag{2.12}$$

Then using the raising operator \mathcal{L}_{H_+} , we also impose the highest-weight condition, $k = 0$,

$$\mathcal{L}_{H_+} \xi^{(m h 0)} = 0.\tag{2.13}$$

The solutions $\xi^{(m h 0)}$ that satisfy both Eq. (2.12) and (2.13) are the highest-weight basis functions. At each point on Σ_u , the spaces of scalars, vectors, and symmetric tensors have dimensions 1, 3, and 6. Thus the space of solutions of this system of equations is a linear vector space of dimension 1, 3, and 6 for scalars, vectors, and symmetric tensors, for each choice of (m, h) . Correspondingly, for each (m, h) , there will be 1, 3, and 6 free coefficients c_β for the solution, with β ranging over the appropriate dimensionality.

Descendants. Next, we obtain basis functions with arbitrary weight by applying the lowering operator \mathcal{L}_{H_-} to the highest-weight states k times, i.e.

$$\xi^{(m h k)} = (\mathcal{L}_{H_-})^k \xi^{(m h 0)}.\tag{2.14}$$

Lifting to the whole manifold. Finally, we promote the basis functions living on Σ_u to functions living on the whole manifold \mathcal{M} by sending all unknown constant coefficients c_β (from the end of step b) to be unknown smooth functions $c_\beta(u)$. While lifting the vector and tensor bases from Σ_u to \mathcal{M} , i.e. $V_i \rightarrow V_a$ and $W_{ij} \rightarrow W_{ab}$, we also set all their projections on the u direction to be zero, i.e. $V_u = 0$, $W_{iu} = W_{ui} = W_{uu} = 0$.

To obtain the basis functions in global coordinates, one just replaces H_s by L_s , where $s = 0, \pm$, and Q_0 by iW_0 in steps b and c. To construct the lowest-weight modules of NHEK's isometry group, one should instead impose the lowest-weight condition $\mathcal{L}_{H_-} \xi^{(m h 0)} = 0$, and the condition $\Omega \xi^{(m h k)} = h(h-1) \xi^{(m h k)}$, in step b. All descendant states will then be obtained by applying the raising operator \mathcal{L}_{H_+} on the lowest-weight states. In Poincaré coordinates, we focus on the basis functions that form the highest-weight module because their expressions are simpler. In global coordinates, we show both representations explicitly in App. 2.7 and 2.7. Unless otherwise specified, our basis functions will refer to those obtained using the highest-weight method.

Let us remark on the allowed values of m, h, k . It is straightforward to see $k \in \mathbb{Z}^+$ by construction, and $m \in \mathbb{Z}$ due to the periodic boundary conditions for the azimuthal angle. In order to have a unitary representation of the isometry group, there are conditions on h as well. For the scalar case, for instance, if we apply the raising operator on a scalar in the highest-weight module, we get

$$\mathcal{L}_{H_+} F^{(m h k)} = k(k-1-2h) F^{(m h k-1)}. \quad (2.15)$$

A nontrivial unitary representation of NHEK's isometry group then requires $k-1-2h \neq 0$, otherwise there would be a lowest-weight state that would lead to a finite-dimensional (and hence non-unitary) representation. The same conclusion holds for either the vector or the tensor bases. The values of h also depend on the regularity conditions we impose. For instance, in global coordinates, the highest-weight scalar basis is proportional to

$$F^{(m h 0)} \propto (\sin \psi)^{-h} \exp[i(h\tau + m\varphi) + m\psi]. \quad (2.16)$$

Regularity at the boundaries $\psi = 0$ and $\psi = \pi$ requires $h \leq 0$. Another example is given in Sec. 2.5 when we solve for the free massless scalar wave equation in the NHEK spacetime, where h must take on some fixed values due to the regularity conditions for spheroidal harmonics.

2.4 Orthogonality in global coordinates

In this section we present a proof that all the scalar, vector, and symmetric tensor basis functions of NHEK's isometry group, when given in global coordinates, form orthogonal basis sets. In this proof we will use the vector basis functions defined on Σ_u as an example. That is, they are functions of τ, φ, ψ . As we shall see, lifting to the whole manifold \mathcal{M} and extending the proof to the scalar and symmetric tensor cases will be straightforward.

Let us introduce the metric induced on the hypersurface Σ_u as γ_{ij} , and D is the unique torsion-free Levi-Civita connection that is compatible with γ . Here Latin letters in the middle of the alphabet (i, j, k) denote three-dimensional tangent indices on Σ_u . Consider the vector basis function $\mathbf{u}^{(m h k)}(\tau, \varphi, \psi)$ and $\mathbf{v}^{(m' h' k')}(\tau, \varphi, \psi)$. We would like to show bases with different m, h, k are orthogonal,

$$\langle \mathbf{u}, \mathbf{v} \rangle \equiv \int_{\Sigma_u} d\text{Vol} \overline{u_i^{(m h k)}} v_{(m' h' k')}^i \propto \delta_{m,m'} \delta_{h,h'} \delta_{k,k'}. \quad (2.17)$$

Here the overbar denotes complex conjugation, and the volume element is given by

$$\int_{\Sigma_u} d\text{Vol} = \lim_{T \rightarrow \infty} \int_{-T}^T d\tau \int_0^{2\pi} d\varphi \int_0^\pi d\psi \sqrt{-\gamma}, \quad (2.18)$$

where γ is the determinant of the three-dimensional metric, and in these coordinates $\sqrt{-\gamma} = 2 \csc^2 \psi \sqrt{1 - u^4}$. To prove Eq. (2.17) we first note the basis components $v_j^{(m h k)}$ in global coordinates have the τ and φ dependence,

$$v_j^{(m h k)} \sim \exp(im\varphi) \exp[i(h - k)\tau]. \quad (2.19)$$

This dependence on τ and φ is the same for the scalar and tensor basis components. Once we integrate over φ and τ in Eq. (2.17), the integral will be proportional to $\delta_{m,m'} \delta_{h-k, h'-k'}$. Notice that the boundaries $\tau \rightarrow \pm\infty$ are oscillatory, so the τ integral needs to be regulated in the same way as Fourier integrals.

Now we only need to show bases with different weight k are orthogonal. Once this is done we will recover Eq. (2.17). For simplicity, from now on we only track the k -index in the vector bases. Recall that we obtain the lower weight bases by applying the lowering operator order by order,

$$\langle \mathbf{u}^{(k)}, \mathbf{v}^{(k')} \rangle = \langle \mathbf{u}^{(k)}, \mathcal{L}_{L_-} \mathbf{v}^{(k'-1)} \rangle. \quad (2.20)$$

Now we try to “integrate by parts” with the Lie derivative,

$$\langle \mathbf{u}^{(k)}, \mathcal{L}_{L_-} \mathbf{v}^{(k'-1)} \rangle = \int_{\Sigma_u} \mathcal{L}_{L_-} \left(\overline{u_i^{(k)}} v_{(k')}^i \right) d\text{Vol} - \langle \overline{\mathcal{L}_{L_-} \mathbf{u}^{(k)}}, \mathbf{v}^{(k'-1)} \rangle, \quad (2.21)$$

$$= \int_{\Sigma_u} \mathcal{L}_{L_-} \left(\overline{u_i^{(k)}} v_{(k')}^i \right) d\text{Vol} + \langle \mathcal{L}_{L_+} \mathbf{u}^{(k)}, \mathbf{v}^{(k'-1)} \rangle, \quad (2.22)$$

where in the last line we used the fact that $\overline{L_+} = -L_-$. Note that this relationship does not hold between H_{\pm} , so this type of proof will not work in Poincaré coordinates.

We would like to discard the first term on the RHS of Eq. (2.21), which would show that \mathcal{L}_{L_+} and \mathcal{L}_{L_-} are adjoints of each other. We can do this by converting the Lie derivative into a covariant derivative and then a total divergence. Since L_{\pm} are KVF's, they are automatically divergence-free, so we can pull them inside the covariant derivative:

$$\int_{\Sigma_u} d\text{Vol} \mathcal{L}_{L_-} \left(\overline{u_i^{(k)}} v_{(k')}^i \right) = \int_{\Sigma_u} d\text{Vol} L_-^j D_j \left(\overline{u_i^{(k)}} v_{(k')}^i \right) = \int_{\Sigma_u} d\text{Vol} D_j \left(L_-^j \overline{u_i^{(k)}} v_{(k')}^i \right). \quad (2.23)$$

This step is identical if we are considering scalars/vectors/tensors, since the argument of the Lie derivative has all indices contracted. Using Stokes' theorem, the integral of the total derivative becomes a boundary integral, evaluated at $\psi = 0, \pi$. This boundary contribution vanishes for $h < -1$ in the highest-weight module. To see this, one must count the powers of $\sin \psi$ which depends on h (see App. 2.7), and take into account the volume element's contribution, $\sqrt{-\gamma} \propto (\sin \psi)^{-2}$.

We repeat the procedure of extracting lowering operators from the ket as in Eq. (2.21), and arrive at

$$\langle \mathbf{u}^{(k)}, \mathbf{v}^{(k')} \rangle = \langle (\mathcal{L}_{L_+})^{k'} \mathbf{u}^{(k)}, \mathbf{v}^{(0)} \rangle. \quad (2.24)$$

Recall that the vector basis terminates at the highest weight. Therefore when $k' > k$, $(\mathcal{L}_{L_+})^{k'} \mathbf{u}^{(k)}$ will vanish. Similarly when $k' < k$, we can extract all lowering operators from the bra and raise the weight of the states in the ket, which will terminate upon raising the highest-weight state. Therefore the vector bases with different weights k, k' are orthogonal.

Since we have also proved that vector bases with different m and $h-k$ are orthogonal, the proof of orthogonality for vector bases is done. It may not be obvious that the proof holds unaltered for scalars/vectors/tensors. In all the relevant steps above, we have noted where each argument works for each of the three types of fields.

Therefore we arrive at the conclusion that the scalar, vector, and symmetric tensor bases in global coordinates form orthogonal basis sets. \square

2.5 Separation of variables

In this section we show that with the scalar, vector, and tensor bases we have obtained, it is possible to separate variables for many physical systems in NHEK spacetime. One can show that all conclusions in this section hold for both Poincaré coordinates and global coordinates. In global coordinates the results are in general more complicated. Therefore for concreteness all results in this section are given in Poincaré coordinates.

The main result of this section can be summarized with the schematic equation:

$$\mathcal{D}_x \left[\begin{array}{c} (SL(2, \mathbb{R}) \times U(1))^{(m,h,k)} \\ \text{structure} \\ (T, \Phi, R) \end{array} \right] \times \begin{array}{c} u \text{ (or } \cos \theta) \\ \text{dependence} \end{array} \Big] = \\ \begin{array}{c} (SL(2, \mathbb{R}) \times U(1))^{(m,h,k)} \\ \text{structure} \\ (T, \Phi, R) \end{array} \times \mathcal{D}_u^{(m,h)} \left[\begin{array}{c} u \text{ (or } \cos \theta) \\ \text{dependence} \end{array} \right].$$

Here, \mathcal{D}_x is an $SL(2, \mathbb{R}) \times U(1)$ -equivariant differential operator, which takes derivatives in the T, Φ, R, u directions. We completely specify the T, Φ, R dependence by being in a certain irreducible representation (irrep) of $SL(2, \mathbb{R}) \times U(1)$ labeled by (m, h, k) . Then the $SL(2, \mathbb{R}) \times U(1)$ structure factors straight through the differential operator \mathcal{D}_x , leaving a new differential operator $\mathcal{D}_u^{(m,h)}$ which only takes u derivatives. This greatly simplifies computations, since the partial differential equations have been converted into ordinary differential equations (ODEs). Because of the $SL(2, \mathbb{R}) \times U(1)$ -invariance, notice that $\mathcal{D}_u^{(m,h)}$ only depends on m and h , which label the irrep, and not on k , which labels the descendant number within the irrep.

Covariant differentiation preserves isometry group irrep labels

Let us first make a general statement about how the presence of a group of isometries acting on the manifold can be useful in separation of variables. The conclusions obtained in this subsection will also justify our motivations of finding group representations for NHEK's isometry. Consider a manifold \mathcal{M} with metric g_{ab} , metric-compatible connection ∇ , and an isometry Lie group G acting on the manifold. Let $\alpha_{(i)} \in \mathfrak{g}$ be a basis for the Lie algebra, with representation $\{X_{(i)}\}$ on the manifold. Further, let $c^{(i)(j)}$ be the inverse of the Killing form of the Lie algebra in this basis [55]. Then we also have a quadratic Casimir element, which acts on any tensor \mathbf{t} as

$$\Omega \cdot \mathbf{t} \equiv \sum_{i,j} c^{(i)(j)} \mathcal{L}_{X_{(i)}} \mathcal{L}_{X_{(j)}} \mathbf{t}. \quad (2.25)$$

Irreps of G will be labeled by eigenvalues λ_i of *some* of the KVFs, and the eigenvalue ω of the Casimir Ω .

First, we need a lemma on the commutation relation of manifold isometries and covariant derivatives,

$$[\mathcal{L}_{X_{(i)}}, \nabla_a] \mathbf{t} = 0, \quad (2.26)$$

where \mathbf{t} can be a scalar, vector, or tensor. To prove Eq. (2.26), one can start by showing the commutation relations for \mathbf{t} being a 0-form (which follows immediately from Cartan's magic formula for a 0-form) and a one-form, then use the Leibniz rule to generalize the relations to the vector and tensor cases. Eq. (2.26) says that the operator ∇_a is $SL(2, \mathbb{R}) \times U(1)$ *equivariant*: that is, its action commutes with left-translation by the group [54].

An important consequence of the commutation relation Eq. (2.26) is that the Casimir element Ω of the algebra \mathfrak{g} also commutes with the covariant derivative. Simply commute each Lie derivative one at a time, and the coefficients $c^{(i)(j)}$ are constants. As a result,

$$[\Omega, \nabla_a] \mathbf{t} = 0. \quad (2.27)$$

Now consider a tensor \mathbf{t} living in an irrep with labels λ_i and ω , meaning

$$\mathcal{L}_{X_{(i)}} \mathbf{t} = \lambda_i \mathbf{t}, \quad (2.28)$$

$$\Omega \cdot \mathbf{t} = \omega \mathbf{t}. \quad (2.29)$$

As an immediate consequence of Eq. (2.26) and Eq. (2.27) is that $\nabla \mathbf{t}$ has the same labels λ_i and ω ,

$$\mathcal{L}_{X_{(i)}} \nabla \mathbf{t} = \lambda_i \nabla \mathbf{t}, \quad (2.30)$$

$$\Omega \cdot \nabla \mathbf{t} = \omega \nabla \mathbf{t}. \quad (2.31)$$

Thus any linear differential operator which is built just from ∇_a and the metric g_{ab} can not mix tensors with different irrep labels (λ_i, ω). This even extends to differential operators which include the Levi-Civita tensor ϵ and the Riemann tensor R_{abcd} , because these two objects are also annihilated by all of the $\mathcal{L}_{X_{(i)}}$. As a result, when tensors are decomposed into a sum over irreps with different labels, they will remain separated in the same ways under this type of differential operator. This is the underlying reason why the method of finding the unitary irreps of NHEK's isometry introduced in Sec. 2.3 will lead to separation of variables in many physical systems.

Scalar Laplacian

As the first example, we look at the massless scalar wave equation $\square\psi = S$ in NHEK space time, where S is a source term (including a mass term also works). Since the scalar d'Alembert operator $\square \equiv \nabla^a \nabla_a$ is built only from g_{ab} and ∇_a , it should commute with Ω and \mathcal{L}_X where X is any KVF. To show this explicitly, note that in Poincaré coordinates, $\square\psi$ can be written as

$$\square\psi = \frac{1}{2\Gamma(u)} \left\{ (\Omega + \Xi(u)\mathcal{L}_{Q_0}^2)\psi + \mathcal{L}_{\partial_u} \left[(1-u^2)\mathcal{L}_{\partial_u}\psi \right] \right\}, \quad (2.32)$$

where $\Xi(u) \equiv \Lambda(u)^{-2} - 1$.

Assume we can decompose an arbitrary scalar field $\psi(T, \Phi, R, u)$ according to

$$\begin{aligned} \psi &= \sum_{m h k} C_{m h k}(u) F^{(m h k)}(T, \Phi, R) \\ &= \sum_{m h k} \psi_{m h k}(T, \Phi, R, u), \end{aligned} \quad (2.33)$$

where F is the scalar basis on Σ_u and $C_{m h k}$ are some unknown functions of u . We also decompose the source term using the scalar basis functions via $S = \sum_{m h k} S_{m h k} F^{(m h k)}$. The basis functions $F^{(m h k)}$ are eigenfunctions of Ω and \mathcal{L}_{Q_0} , and so $\psi_{m h k}$ are also eigenfunctions. Therefore it is straightforward to see that the (T, Φ, R) -dependence in $\psi_{m h k}$ is invariant after applying the scalar box operator. The equation for a specific mode labeled by (m, h, k) becomes

$$\begin{aligned} S_{m h k} F^{(m h k)} = \square^{(m, h)} \psi_{m h k} &= \frac{1}{2\Gamma(u)} \times \\ &\times \left\{ [h(h+1) - m^2 \Xi(u)] \psi_{m h k} + \mathcal{L}_{\partial_u} \left[(1-u^2) \mathcal{L}_{\partial_u} \psi_{m h k} \right] \right\}. \end{aligned} \quad (2.34)$$

This entire equation is proportional to the basis function $F^{(m h k)}$, which can thus be divided out, leaving an ODE for one function, $C_{m h k}(u)$.

Specializing to the homogeneous (source-free) case, we find the ODE

$$\frac{d}{du} \left[(1-u^2) \frac{d}{du} C_{m h k} \right] + [h(h+1) - \Xi(u)m^2] C_{m h k} = 0. \quad (2.35)$$

This equation has two regular singularities $u = \pm 1$ and an irregular singularity of rank 1 at $u = \infty$, which falls into the class of confluent forms of Heun's equation [57]. Explicitly, it is a spheroidal differential equation, whose standard form is

$$\frac{d}{du} \left((1-u^2) \frac{d\varphi}{du} \right) + \left(\lambda + \gamma^2(1-u^2) - \frac{\mu^2}{1-u^2} \right) \varphi = 0, \quad (2.36)$$

where we have made the substitution $\lambda = h(h+1) + 2m^2$, $\gamma^2 = -m^2/4$ and $\mu^2 = m^2$. When $\gamma = 0$, Eq. (2.36) reduces to the Legendre differential equation and the solutions are Legendre polynomials. Being second order, the space of solutions is two dimensional,

$$\varphi(u) = a_1 S_{n\mu}^{(1)}(\gamma, u) + b_1 S_{n\mu}^{(2)}(\gamma, u). \quad (2.37)$$

A solution that is regular at $u = \pm 1$ only exists for eigenvalues $\lambda = \lambda_n^m(\gamma^2)$, where $\mu = m = 0, 1, 2, \dots$, and $n = m, m+1, m+2, \dots$. Thus, there are only discrete values of the irrep label h which satisfy regularity at the poles $u = \pm 1$.

Maxwell system

Let's look at another system of physical importance, the Maxwell system, and verify that we can separate variables in Maxwell's equations (the Proca equation—i.e. adding a mass term—works as well). The inhomogeneous Maxwell equations in the presence of a source vector field \mathcal{J} are

$$\nabla^a \mathcal{F}_{ab} = \mathcal{J}_b, \quad (2.38)$$

where the electromagnetic tensor \mathcal{F} is built from the vector potential A according to

$$\mathcal{F}_{ab} = \nabla_a A_b - \nabla_b A_a. \quad (2.39)$$

We again assume that we can expand the vector potential in the scalar and vector bases. Define a one-form $n_a = du$, this expansion is given by

$$A_a = \sum_{mhk} \left(C_u(u) n_a F^{(mhk)} + \sum_B C_B(u) V_a^{B(mhk)} \right), \quad (2.40)$$

where $B \in \{T, \Phi, R\}$, $C_B(u)$ and $C_u(u)$ are unknown functions of u . Notice that B is *not* a tensor index. It is the label of a specific choice of vector bases and their corresponding unknown C -functions. The expression of $F^{(mhk)}$ and the projection of $V_a^{B(mhk)}$ onto Σ_u , i.e. $V_i^{B(mhk)}$ are both given in App. 2.7. Then at the highest weight $k = 0$, the left-hand side of Maxwell's equation can be rewritten as

$$\begin{aligned} \nabla^a \mathcal{F}_{ab}|_{k=0} &= \mathcal{D}_u^{(m,h)}[\mathbf{C}(u)] n_b F^{(mh0)} \\ &+ \sum_B \mathcal{D}_B^{(m,h)}[\mathbf{C}(u)] V_b^{B(mh0)}, \end{aligned} \quad (2.41)$$

where we have collected the four C -functions into the vector $\mathbf{C}(u)$, and defined the general differentiation as $\mathcal{D}^{(m,h)}[\mathbf{C}(u)]$, whose expressions are given in App. 2.7. As long as the source field can also be decomposed using the scalar and vector

bases, the inhomogeneous Maxwell equations in NHEK will reduce to four ordinary differential equations with four unknown C -functions. Although we only show this is true for the highest-weight case, this conclusion holds for any k . This is due to the commutation of the lowering operator and the covariant differentiation. For explicit calculations of Maxwell's system using the highest-weight vector basis we refer our readers to [58, 59].

Linearized Einstein system

In this subsection we show that we can separate variables on the left hand side of linearized Einstein equation, using our scalar, vector, and tensor bases for NHEK. Consider the metric perturbation $g'_{ab} = g_{ab} + \epsilon h_{ab} + \mathcal{O}(\epsilon^2)$, where g_{ab} is the NHEK metric and h_{ab} is a perturbation. The linearized Einstein equations (i.e. at order ϵ^1) are

$$G_{ab}^{(1)}[h] = 8\pi T_{ab}, \quad (2.42)$$

where T_{ab} is the stress-energy tensor of a source term. The linearized Einstein operator $G^{(1)}[h]$ can be written in terms of the background covariant derivative ∇ as

$$\begin{aligned} -2G_{ab}^{(1)}[h] &= \square \bar{h}_{ab} + g_{ab} \nabla^c \nabla^d \bar{h}_{cd} - 2\nabla^c \nabla_{(a} \bar{h}_{b)c} \\ &\quad - g_{ab} R^{cd} \bar{h}_{cd} + R \bar{h}_{ab}, \end{aligned} \quad (2.43)$$

where $\bar{h}_{ab} = h_{ab} - \frac{1}{2}g_{ab}g^{cd}h_{cd}$ is the trace-reverse of h_{ab} , R_{ab} is the background Ricci curvature, R is the background Ricci scalar, and parentheses around n indices means symmetrizing with a factor of $1/n!$. This operator, again, is $SL(2, \mathbb{R}) \times U(1)$ equivariant.

We assume that we can expand the metric perturbation in our scalar, vector, and tensor bases, according to

$$\begin{aligned} h_{ab} &= \sum_{mhk} h_{ab}^{(mhk)} = \sum_{mhk} \left(n_a n_b F^{(mhk)} C_{uu}(u) \right. \\ &\quad \left. + \sum_B 2n_{(a} V_{b)}^{B(mhk)} C_{uB}(u) + \sum_{A,B} W_{ab}^{AB(mhk)} C_{AB}(u) \right), \end{aligned} \quad (2.44)$$

where $A, B \in \{T, \Phi, R\}$, C_{uu}, C_{uB}, C_{AB} are unknown functions of u . Notice that A and B are *not* tensor indices but only labels of a specific choice of the vector and tensor bases (introduced in App. 2.7 and 2.7) and their corresponding unknown C -functions. Thus there are no differences between a subscript and a superscript

A or B. We choose the three highest-weight vector bases $V_b^{B(mh0)}$ and the six highest-weight tensor bases $W_{ab}^{AB(mh0)}$ such that the metric perturbation with $k = 0$ can be written as Eq. (2.45). We substitute the highest-weight metric perturbation into the left-hand side of the linearized Einstein equation and the result is given by Eq. (2.47).

$$h_{ab}^{(mh0)} = R^h e^{im\Phi} \begin{bmatrix} R^{+2}C_{TT}(u) & R^{+1}C_{T\Phi}(u) & R^{+0}C_{TR}(u) & R^{+1}C_{uT}(u) \\ * & R^{+0}C_{\Phi\Phi}(u) & R^{-1}C_{R\Phi}(u) & R^{+0}C_{u\Phi}(u) \\ * & * & R^{-2}C_{RR}(u) & R^{-1}C_{uR}(u) \\ * & * & * & R^{+0}C_{uu}(u) \end{bmatrix} \quad (2.45)$$

$$G_{ab}^{(1)}[h^{(mh0)}] = R^h e^{im\Phi} \times \begin{bmatrix} R^{+2}\mathcal{D}_{TT}^{(m,h)}[\mathbf{C}(u)] & R^{+1}\mathcal{D}_{T\Phi}^{(m,h)}[\mathbf{C}(u)] & R^{+0}\mathcal{D}_{TR}^{(m,h)}[\mathbf{C}(u)] & R^{+1}\mathcal{D}_{uT}^{(m,h)}[\mathbf{C}(u)] \\ * & R^{+0}\mathcal{D}_{\Phi\Phi}^{(m,h)}[\mathbf{C}(u)] & R^{-1}\mathcal{D}_{R\Phi}^{(m,h)}[\mathbf{C}(u)] & R^{+0}\mathcal{D}_{u\Phi}^{(m,h)}[\mathbf{C}(u)] \\ * & * & R^{-2}\mathcal{D}_{RR}^{(m,h)}[\mathbf{C}(u)] & R^{-1}\mathcal{D}_{uR}^{(m,h)}[\mathbf{C}(u)] \\ * & * & * & R^{+0}\mathcal{D}_{uu}^{(m,h)}[\mathbf{C}(u)] \end{bmatrix} \quad (2.47)$$

Again notice that the (T, Φ, R) dependence has factored straight through the differential operator, resulting in ten coupled ODEs for the ten C -functions, which we have collected together as $\mathbf{C}(u)$. The expressions for all these differential operators are given in App. 2.7.

We can easily verify that $G^{(1)}$ commutes with \mathcal{L}_{H_-} , therefore the linearized Einstein operator acting on a basis function with arbitrary weight can be obtained easily by repeatedly applying the lowering operator \mathcal{L}_{H_-} , k times, on Eq. (2.47). While applying the lowering operator, in general different components of $G_{ab}^{(1)}[h^{(mhk)}]$ will get mixed up, but the separation of variables still holds. Therefore we conclude that with these scalar, vector, and tensor bases, we can separate variables in the linearized Einstein system in NHEK.

Given some source terms, these bases can be directly applied to solving for the corresponding metric perturbations. For instance, we have obtained the highest-weight metric deformations in NHEK sourced by the decoupling limits of dynamical Chern-Simons and Einstein-dilaton-Gauss-Bonnet gravity [37].

2.6 Conclusions and future work

In this chapter, we proposed an isometry-inspired method to study metric perturbations in the near-horizon extremal Kerr spacetime. That is, we separated variables

in the metric perturbation equations in the NHEK spacetime, by expanding the perturbation in terms of basis functions adapted to the isometry group. With the separable linearized Einstein equation, one obtains the perturbed metric directly, without the complication of metric reconstruction. Further, our formalism does not depend on gauge choice. Within our formalism, partial differential equations built from $SL(2, \mathbb{R}) \times U(1)$ -equivariant operators can be converted into ordinary differential equations in the polar angle, which are simpler to solve. The price is that one must solve coupled, rather than decoupled, equations in our metric formalism.

We accomplished three things: (i) we used the highest-weight method to obtain the scalar, vector, and symmetric tensor bases for the isometry group of NHEK; (ii) in global coordinates, we showed that these bases form orthogonal basis sets when the labels of irreps satisfy $h < -1$; and (iii) with these basis functions, we separated variables in many physical equations like the scalar wave equation, Maxwell's equations, and the linearized Einstein equations.

Future work. Although we have shown that bases in global coordinates are orthogonal, we did not mention completeness. There are clues that, in global coordinates, combining the highest- and lowest-weight modules will give a complete set of states. We leave a rigorous treatment of completeness to future work. However, many problems can already be attacked without worrying about completeness—for example, if the source term lives in exactly one irrep.

Since the near-horizon near-extremal geometry exhibits the same isometry as NHEK, we expect all discussions in this paper can be applied to understanding metric perturbations in near-NHEK, which is more astrophysically relevant. With the knowledge of isometry-adapted bases in NHEK, we hope to enhance our understanding of the Kerr/CFT conjecture [60] from the gravity side.

2.7 Appendix

Scalar, vector, and symmetric tensor bases

In this subsection we present the expressions of scalar, vector, and symmetric tensor bases both in Poincaré coordinates and global coordinates, up to constant factors. All the basis functions are defined on the three-dimensional hypersurface Σ_u . To promote these basis functions to the full four-dimensional manifold \mathcal{M} , one promotes all constant coefficients c_β to become unknown functions of the (cosine) polar angle, $c_\beta(u)$. The basis functions given here are (mostly) obtained using the highest-weight method introduced in Sec. 2.3, i.e. they form the highest-weight

modules for $SL(2, \mathbb{R}) \times U(1) \cup \mathcal{M}$. Such a highest-weight module is infinite dimensional, the length of this paper, however, is supposed to be finite. Therefore, we give the highest three weights for scalar bases, the highest two weights for vector bases, and only the highest weight for tensor bases. Note all other basis functions can be generated by applying the lowering operator on the highest-weight basis order by order. In order to compare the basis functions in different modules, in global coordinates, we also give the expressions of the scalar bases obtained using the lowest-weight method.

All expressions in these appendices are also available in the companion MATHEMATICA notebooks: `Sep-met-pert-in-NHEK-Poinc.nb`, `Sep-met-pert-in-NHEK-global.nb`, and precomputed quantities in `NHEK-precomputed.mx` [61].

Basis functions in Poincaré coordinates

Scalar bases The scalar bases in Poincaré coordinates are given by

$$F^{(m h k)} \propto R^{h-k} e^{im\Phi} \times f^{(m h k)}, \quad (2.48)$$

where

$$\begin{aligned} f^{(m h 0)} &= 1, \\ f^{(m h 1)} &= -2(hRT + im), \\ f^{(m h 2)} &= -2[-2i(2h - 1)mRT + \\ &\quad + h(1 - 2h)R^2T^2 + h + 2m^2]. \end{aligned} \quad (2.49)$$

Vector bases The covector bases in Poincaré coordinates can be decomposed using the dual basis one-forms $\{dT, d\Phi, dR\}$ via

$$\mathbf{V}^{(m h k)} = V_i^{(m h k)} dx^i, \quad x \in \{T, \Phi, R\}. \quad (2.50)$$

The covector components are given by

$$V_i^{(m h k)} \propto \begin{bmatrix} v_T^{(m h k)} R^{+1} \\ v_\Phi^{(m h k)} R^{+0} \\ v_R^{(m h k)} R^{-1} \end{bmatrix} R^{h-k} e^{im\Phi}, \quad (2.51)$$

where

$$v_T^{(m h 0)} = c_1, \quad v_\Phi^{(m h 0)} = c_2, \quad v_R^{(m h 0)} = c_3, \quad (2.52)$$

and

$$\begin{aligned}
v_T^{(mh1)} &= -2[c_3 + c_1(hRT + im)], \\
v_\Phi^{(mh1)} &= -2c_2(hRT + im), \\
v_R^{(mh1)} &= -2[c_3(hRT + im) + c_1 - c_2].
\end{aligned} \tag{2.53}$$

Notice that there are three unknown coefficients, c_1 , c_2 , and c_3 . They endow us the freedom of choosing a three-dimensional basis for covectors. In particular, we introduce a specific set of covector bases labeled by B where $B \in \{T, \Phi, R\}$. They are defined by

$$\begin{aligned}
\mathbf{V}_T^{(mhk)} &= \mathbf{V}^{(mhk)}|_{c_2=c_3=0}, \\
\mathbf{V}_\Phi^{(mhk)} &= \mathbf{V}^{(mhk)}|_{c_1=c_3=0}, \\
\mathbf{V}_R^{(mhk)} &= \mathbf{V}^{(mhk)}|_{c_1=c_2=0}.
\end{aligned} \tag{2.54}$$

Symmetric tensor bases The symmetric tensor bases in Poincaré coordinates can be decomposed using the dual basis one-forms $\{dT, d\Phi, dR\}$ via

$$\mathbf{W}^{(mhk)} = W_{ij}^{(mhk)} dx^i \otimes dx^j, \quad x \in \{T, \Phi, R\}. \tag{2.55}$$

The tensor components are given by

$$W_{ij}^{(mhk)} \propto \begin{bmatrix} R^{+2} w_{TT}^{(mhk)} & R^{+1} w_{T\Phi}^{(mhk)} & R^{+0} w_{TR}^{(mhk)} \\ * & R^{+0} w_{\Phi\Phi}^{(mhk)} & R^{-1} w_{R\Phi}^{(mhk)} \\ * & * & R^{-2} w_{RR}^{(mhk)} \end{bmatrix} \times \times R^{h-k} e^{im\Phi}, \tag{2.56}$$

where

$$\begin{aligned}
w_{TT}^{(mh0)} &= c_1, & w_{\Phi\Phi}^{(mh0)} &= c_2, & w_{RR}^{(mh0)} &= c_3, \\
w_{T\Phi}^{(mh0)} &= c_4, & w_{\Phi R}^{(mh0)} &= c_5, & w_{RT}^{(mh0)} &= c_6.
\end{aligned} \tag{2.57}$$

Notice that there are six unknown c -coefficients. They endow us the freedom of choosing the six tensor bases. In particular, we introduce a specific set of highest-weight tensor bases labeled by A, B where $A, B \in \{T, \Phi, R\}$. They are defined

by

$$\begin{aligned}
\mathbf{W}_{TT}^{(m h k)} &= \mathbf{W}^{(m h k)} \Big|_{c_{\beta \neq 1}=0}, \\
\mathbf{W}_{\Phi\Phi}^{(m h k)} &= \mathbf{W}^{(m h k)} \Big|_{c_{\beta \neq 2}=0}, \\
\mathbf{W}_{RR}^{(m h k)} &= \mathbf{W}^{(m h k)} \Big|_{c_{\beta \neq 3}=0}, \\
\mathbf{W}_{T\Phi}^{(m h k)} &= \mathbf{W}^{(m h k)} \Big|_{c_{\beta \neq 4}=0}, \\
\mathbf{W}_{\Phi R}^{(m h k)} &= \mathbf{W}^{(m h k)} \Big|_{c_{\beta \neq 5}=0}, \\
\mathbf{W}_{RT}^{(m h k)} &= \mathbf{W}^{(m h k)} \Big|_{c_{\beta \neq 6}=0}.
\end{aligned} \tag{2.58}$$

This specific choice of tensor bases will be utilized to write the metric perturbation as in Eq. (2.45).

Basis functions in global coordinates

Scalar bases (highest-weight module) The scalar bases from the highest-weight module in global coordinates are given by

$$F^{(m h k)} \propto (\sin \psi)^{-h} e^{i[(h-k)\tau + m\varphi] + m\psi} \times f^{(m h k)}, \tag{2.59}$$

where

$$\begin{aligned}
f^{(m h 0)} &= 1, \\
f^{(m h 1)} &= -2(m \sin \psi - h \cos \psi), \\
f^{(m h 2)} &= 2 \left[h^2 + m^2 + (h^2 - h - m^2) \cos 2\psi + (m - 2hm) \sin 2\psi \right].
\end{aligned} \tag{2.60}$$

Scalar bases (lowest-weight module)

The scalar bases from the lowest-weight module in global coordinates are given by

$$F_L^{(m h k)} \propto (\sin \psi)^{+h} e^{i[(h+k)\tau + m\varphi] - m\psi} \times f_L^{(m h k)}, \tag{2.61}$$

where

$$\begin{aligned}
f_L^{(m h 0)} &= 1, \\
f_L^{(m h 1)} &= -2(m \sin \psi - h \cos \psi), \\
f_L^{(m h 2)} &= 2 \left[h^2 + m^2 + (h^2 + h - m^2) \cos 2\psi - (m + 2hm) \sin 2\psi \right].
\end{aligned} \tag{2.62}$$

Vector bases The covector bases in global coordinates can be decomposed using the dual basis one-forms $\{d\tau, d\varphi, d\psi\}$ via

$$\mathbf{V}^{(m h k)} = V_i^{(m h k)} dx^i, \quad x \in \{\tau, \varphi, \psi\}. \quad (2.63)$$

The covector components are given by

$$V_j^{(m h k)} \propto \begin{bmatrix} v_\tau^{(m h k)} (\sin \psi)^{-1} \\ v_\varphi^{(m h k)} (\sin \psi)^{+0} \\ v_\psi^{(m h k)} (\sin \psi)^{-1} \end{bmatrix} (\sin \psi)^{-h} e^{i[(h-k)\tau+m\varphi]+m\psi}, \quad (2.64)$$

where

$$\begin{aligned} v_\tau^{(m h 0)} &= -\frac{1}{4} (c_1 e^{-i\psi} + 2c_1 e^{i\psi} - 2c_2 e^{-i\psi} + 4c_3 e^{i\psi}), \\ v_\varphi^{(m h 0)} &= c_1, \\ v_\psi^{(m h 0)} &= +\frac{1}{4} (c_1 e^{-i\psi} + 2c_2 e^{-i\psi} + 4c_3 e^{i\psi}), \end{aligned} \quad (2.65)$$

and

$$\begin{aligned} v_\tau^{(m h 1)} &= -\frac{1}{4} \left\{ c_1 [2(h+im)e^{2i\psi} + (3h-im-1) + (h-im+1)e^{-2i\psi}] - \right. \\ &\quad \left. - 2c_2 [(h+im+1) + (h-im-1)e^{-2i\psi}] + 4c_3 [(h+im-1)e^{2i\psi} + (h-im+1)] \right\}, \\ v_\varphi^{(m h 1)} &= -2c_1 (m \sin \psi - h \cos \psi), \\ v_\psi^{(m h 1)} &= +\frac{1}{4} \left\{ c_1 [(h+im+1) + (h-im-1)e^{-2i\psi}] + 2c_2 [(h+im+1) + (h-im-1)e^{-2i\psi}] \right. \\ &\quad \left. + 4c_3 [(h+im-1)e^{2i\psi} + (h-im+1)] \right\}. \end{aligned} \quad (2.66)$$

Symmetric tensor bases The symmetric tensor bases in global coordinates can be decomposed using the dual basis one-forms $\{d\tau, d\varphi, d\psi\}$ via

$$\mathbf{W}^{(m h k)} = W_{ij}^{(m h k)} dx^i \otimes dx^j, \quad x \in \{\tau, \varphi, \psi\}. \quad (2.67)$$

The tensor components are given by

$$W_{ij}^{(m h k)} \propto \begin{bmatrix} w_{\tau\tau}^{(m h k)} (\sin \psi)^{-2} & w_{\tau\varphi}^{(m h k)} (\sin \psi)^{-1} & w_{\tau\psi}^{(m h k)} (\sin \psi)^{-2} \\ * & w_{\varphi\varphi}^{(m h k)} (\sin \psi)^{+0} & w_{\varphi\psi}^{(m h k)} (\sin \psi)^{-1} \\ * & * & w_{\psi\psi}^{(m h k)} (\sin \psi)^{-2} \end{bmatrix} (\sin \psi)^{-h} e^{i[(h-k)\tau+m\varphi]+m\psi}, \quad (2.68)$$

where

$$\begin{aligned}
w_{\tau\tau}^{(m\ h0)} &= +\frac{1}{16}(c_1e^{-2i\psi} + 4c_1e^{2i\psi} - 6c_2e^{-2i\psi} \\
&\quad + 16c_3e^{2i\psi} + 8c_5e^{-2i\psi} + 16c_6e^{2i\psi} + 4c_1 - 8c_2 + 16c_3 + 8c_4), \\
w_{\varphi\varphi}^{(m\ h0)} &= c_1, \\
w_{\psi\psi}^{(m\ h0)} &= +\frac{1}{16}(-8c_4 + 16c_6e^{2i\psi} + c_1e^{-2i\psi} + 2c_2e^{-2i\psi} + 8c_5e^{-2i\psi}), \\
w_{\tau\varphi}^{(m\ h0)} &= -\frac{1}{4}(2c_1e^{i\psi} + 4c_3e^{i\psi} + c_1e^{-i\psi} - 2c_2e^{-i\psi}), \\
w_{\varphi\psi}^{(m\ h0)} &= +\frac{1}{4}(4c_3e^{i\psi} + c_1e^{-i\psi} + 2c_2e^{-i\psi}), \\
w_{\psi\tau}^{(m\ h0)} &= -\frac{1}{16}(2c_1 + 4c_2 + 8c_3 + 8c_3e^{2i\psi} + 16c_6e^{2i\psi} + c_1e^{-2i\psi} + 2c_2e^{-2i\psi} - 8c_5e^{-2i\psi}).
\end{aligned} \tag{2.69}$$

Expressions of $\mathcal{D}_A^{(m,h)}[\mathbf{C}(u)]$ in Maxwell systems

We have decomposed the differential operators $\mathcal{D}_A^{(m,h)}[\mathbf{C}(u)]$, $A \in \{T, \Phi, R, u\}$, introduced in Sec. 2.5, by the coefficients multiplying the second, first, and zeroth derivatives of the C -functions. These coefficients are tabulated here in Table 2.1. In this table, each row is labeled by $\mathcal{D}_A^{(m,h)}$, while each column is labeled by a C -function or its derivative. Each table component is the coefficient in front of the (derivative of) corresponding C -function in $\mathcal{D}_A^{(m,h)}[\mathbf{C}(u)]$. To recover $\mathcal{D}_A^{(m,h)}[\mathbf{C}(u)]$, one just multiplies each table component with its column label and then add up all those with the same row label \mathcal{D}_A . Expressions in this appendix can be computed using the companion MATHEMATICA notebook `Sep-met-pert-in-NHEK-Poinc.nb` [61].

Expressions of $\mathcal{D}_{AB}^{(m,h)}[\mathbf{C}(u)]$ in linearized Einstein equations

The general second-order differentiation $\mathcal{D}^{(m,h)}$ on the ten unknown C -functions, denoted as $\mathcal{D}_{AB}^{(m,h)}[\mathbf{C}(u)]$, can be written compactly by putting all C -functions together to form a vector $\mathbf{C}(u)$,

$$\mathcal{D}_{AB}^{(m,h)}[\mathbf{C}(u)] = (\mathcal{A}_{AB}\partial_u^2 + \mathcal{B}_{AB}\partial_u + C_{AB}) \cdot \left(C_{TT}(u), \dots, C_{\Phi u}(u) \right)^T. \tag{2.70}$$

Here \mathcal{A}_{AB} , \mathcal{B}_{AB} , and C_{AB} are covectors whose components are obtained by collecting coefficients in front of C -functions. We further stack all the covectors \mathcal{A}_{AB} to form a matrix, and similarly do for \mathcal{B}_{AB} and C_{AB} . We label the resulting coefficient matrices as \mathcal{A} , \mathcal{B} , and C respectively. They are given in Tables 2.2, 2.7, 2.4, 2.5, and 2.6. They can also be computed using the companion MATHEMATICA notebook

\mathcal{D}_A	$C_T''(u)$	$C_\Phi''(u)$	$C_R''(u)$	$C_u''(u)$
\mathcal{D}_T	$\frac{1-u^2}{u^2+1}$	0	0	0
\mathcal{D}_Φ	0	$\frac{1-u^2}{u^2+1}$	0	0
\mathcal{D}_R	0	0	$\frac{1-u^2}{u^2+1}$	0
\mathcal{D}_u	0	0	0	0
	$C_T'(u)$	$C_\Phi'(u)$	$C_R'(u)$	$C_u'(u)$
\mathcal{D}_T	$-\frac{4u}{(u^2+1)^2}$	$-\frac{2u(u^2-3)}{(u^2+1)^2}$	0	0
\mathcal{D}_Φ	0	$-\frac{2u(u^2-1)}{(u^2+1)^2}$	0	$\frac{im(u^2-1)}{u^2+1}$
\mathcal{D}_R	0	0	$-\frac{4u}{(u^2+1)^2}$	$\frac{h(u^2-1)}{u^2+1}$
\mathcal{D}_u	$-\frac{im}{u^2+1}$	$\frac{im(u^4+6u^2-3)}{4(u^4-1)}$	$-\frac{h+1}{u^2+1}$	0
	$C_T(u)$	$C_\Phi(u)$	$C_R(u)$	$C_u(u)$
\mathcal{D}_T	$\frac{(u^4+6u^2-3)m^2}{4(u^4-1)} + \frac{(h+1)(-4u^2+h(u^2+1)^2+4)}{(u^2+1)^3}$	$\frac{h(u^4+6u^2-3)}{(u^2+1)^3}$	$-\frac{im(u^4+6u^2-3)}{(u^2+1)^3}$	$\frac{2imu(u^2-3)}{(u^2+1)^2}$
\mathcal{D}_Φ	$\frac{m^2(u^2+1)^2-4(h+1)(u^2-1)}{(u^2+1)^3}$	$\frac{h((h+1)u^4+2(h+3)u^2+h-3)}{(u^2+1)^3}$	$-\frac{im((h+1)u^4+2(h+3)u^2+h-3)}{(u^2+1)^3}$	$\frac{2imu(u^2-1)}{(u^2+1)^2}$
\mathcal{D}_R	$-\frac{i(h+1)m}{u^2+1}$	$\frac{ihm(u^4+6u^2-3)}{4(u^4-1)}$	$\frac{m^2(u^4+6u^2-3)}{4(u^4-1)}$	$\frac{4hu}{(u^2+1)^2}$
\mathcal{D}_u	0	0	0	$\frac{4(u^2-1)h^2+4(u^2-1)h+m^2(u^4+6u^2-3)}{4(u^4-1)}$

Table 2.1: The coefficient table that gives the expressions of $\mathcal{D}_A^{(m,h)}[\mathbf{C}(u)]$, $A \in \{T, \Phi, R, u\}$ in Maxwell systems.

Sep-met-pert-in-NHEK-Poinc.nb, or read from the precomputed expressions in NHEK-precomputed.mx [61].

\mathcal{D}_{AB}	$C_{TT}''(u)$	$C_{T\Phi}''(u)$	$C_{\Phi\Phi}''(u)$	$C_{RR}''(u)$	$C_{Ru}''(u)$	$C_{uu}''(u)$	$C_{TR}''(u)$	$C_{Tu}''(u)$	$C_{\Phi R}''(u)$	$C_{\Phi u}''(u)$
\mathcal{D}_{TT}	$-\frac{2(u^2-1)^2}{(u^2+1)^3}$	$\frac{u^6+5u^4-9u^2+3}{(u^2+1)^3}$	$-\frac{(u^4+6u^2-3)^2}{8(u^2+1)^3}$	$\frac{u^6+5u^4-9u^2+3}{2(u^2+1)^3}$	0	0	0	0	0	0
$\mathcal{D}_{T\Phi}$	$-\frac{2(u^2-1)^2}{(u^2+1)^3}$	$\frac{u^6+9u^4-17u^2+7}{2(u^2+1)^3}$	$-\frac{u^6+5u^4-9u^2+3}{2(u^2+1)^3}$	$\frac{2(u^2-1)^2}{(u^2+1)^3}$	0	0	0	0	0	0
$\mathcal{D}_{\Phi\Phi}$	$-\frac{2(u^2-1)^2}{(u^2+1)^3}$	$\frac{4(u^2-1)^2}{(u^2+1)^3}$	$-\frac{2(u^2-1)^2}{(u^2+1)^3}$	$\frac{2(u^2-1)^2}{(u^2+1)^3}$	0	0	0	0	0	0
\mathcal{D}_{RR}	$\frac{u^2-1}{2(u^2+1)}$	$\frac{1-u^2}{u^2+1}$	$\frac{u^4+6u^2-3}{8(u^2+1)}$	0	0	0	0	0	0	0
\mathcal{D}_{Ru}	0	0	0	0	0	0	0	0	0	0
\mathcal{D}_{uu}	0	0	0	0	0	0	0	0	0	0
\mathcal{D}_{TR}	0	0	0	0	0	0	$\frac{u^2-1}{2(u^2+1)}$	0	0	0
\mathcal{D}_{Tu}	0	0	0	0	0	0	0	0	0	0
$\mathcal{D}_{\Phi R}$	0	0	0	0	0	0	0	0	$\frac{u^2-1}{2(u^2+1)}$	0
$\mathcal{D}_{\Phi u}$	0	0	0	0	0	0	0	0	0	0

Table 2.2: \mathcal{A} matrix.

\mathcal{D}_{AB}	$C'_{TT}(u)$	$C'_{T\Phi}(u)$	$C'_{\Phi\Phi}(u)$	$C'_{RR}(u)$	$C'_{Ru}(u)$
\mathcal{D}_{TT}	$\frac{2u(u^4-4u^2+3)}{(u^2+1)^4}$	$-\frac{4u(u^2-3)(u^2-1)}{(u^2+1)^4}$	$-\frac{u(u^{10}+u^8-22u^6+66u^4-123u^2+45)}{8(u^2-1)(u^2+1)^4}$	$-\frac{u(u^6+u^4-13u^2+3)}{(u^2+1)^4}$	$-\frac{h(u^2-1)(u^4+6u^2-3)}{(u^2+1)^3}$
$\mathcal{D}_{T\Phi}$	$\frac{2u(u^4-4u^2+3)}{(u^2+1)^4}$	$-\frac{4u(u^4-4u^2+3)}{(u^2+1)^4}$	$\frac{2u(u^4-4u^2+3)}{(u^2+1)^4}$	$-\frac{2u(u^4-4u^2+3)}{(u^2+1)^4}$	$-\frac{2(2h+1)(u^2-1)^2}{(u^2+1)^3}$
$\mathcal{D}_{\Phi\Phi}$	$\frac{2u(u^4-4u^2+3)}{(u^2+1)^4}$	$-\frac{4u(u^2-3)(u^2-1)}{(u^2+1)^4}$	$\frac{2u(u^4-4u^2+3)}{(u^2+1)^4}$	$-\frac{2u(u^4-4u^2+3)}{(u^2+1)^4}$	$-\frac{4(h+1)(u^2-1)^2}{(u^2+1)^3}$
\mathcal{D}_{RR}	$-\frac{u(u^2-3)}{(u^2+1)^2}$	$\frac{2u(u^2-3)}{(u^2+1)^2}$	$\frac{u(u^2-3)^3}{8(u^2-1)(u^2+1)^2}$	0	$\frac{u^2-1}{u^2+1}$
\mathcal{D}_{Ru}	$\frac{h+1}{2(u^2+1)}$	$-\frac{2h+1}{2(u^2+1)}$	$\frac{h(u^4+6u^2-3)}{8(u^2-1)}$	$\frac{1}{2(u^2+1)}$	0
\mathcal{D}_{uu}	$-\frac{u}{2(u^4-1)}$	$\frac{u}{u^4-1}$	$-\frac{u(u^2+3)}{4(u^4-1)}$	$\frac{u}{2(u^4-1)}$	0
\mathcal{D}_{TR}	0	0	0	0	0
\mathcal{D}_{Tu}	$\frac{im}{2(u^2+1)}$	$-\frac{im(u^4+6u^2-3)}{8(u^4-1)}$	0	0	0
$\mathcal{D}_{\Phi R}$	0	0	0	0	$-\frac{im(u^2-1)}{2(u^2+1)}$
$\mathcal{D}_{\Phi u}$	$\frac{im}{2(u^2+1)}$	$-\frac{im}{2(u^2+1)}$	0	$-\frac{im}{2(u^2+1)}$	0
	$C'_{uu}(u)$	$C'_{TR}(u)$	$C'_{Tu}(u)$	$C'_{\Phi R}(u)$	$C'_{\Phi u}(u)$
\mathcal{D}_{TT}	$\frac{u(u^2-1)(u^6+11u^4-13u^2+9)}{2(u^2+1)^4}$	0	$-\frac{im(u^2-1)(u^4+6u^2-3)}{(u^2+1)^3}$	0	$\frac{im(u^4+6u^2-3)^2}{4(u^2+1)^3}$
$\mathcal{D}_{T\Phi}$	$\frac{4u(u^2-1)^3}{(u^2+1)^4}$	0	$-\frac{im(u^6+9u^4-17u^2+7)}{2(u^2+1)^3}$	0	$\frac{im(u^6+5u^4-9u^2+3)}{(u^2+1)^3}$
$\mathcal{D}_{\Phi\Phi}$	$\frac{4u(u^2-1)^3}{(u^2+1)^4}$	0	$-\frac{4im(u^2-1)^2}{(u^2+1)^3}$	0	$\frac{4im(u^2-1)^2}{(u^2+1)^3}$
\mathcal{D}_{RR}	$-\frac{u(u^2-1)}{2(u^2+1)}$	0	$\frac{im(u^2-1)}{u^2+1}$	0	$-\frac{im(u^4+6u^2-3)}{4(u^2+1)}$
\mathcal{D}_{Ru}	0	$\frac{im}{2(u^2+1)}$	0	$-\frac{im(u^4+6u^2-3)}{8(u^4-1)}$	0
\mathcal{D}_{uu}	0	0	0	0	0
\mathcal{D}_{TR}	0	$-\frac{u(u^2-3)}{(u^2+1)^2}$	$-\frac{(u^2-1)(-u^4-6u^2+h(u^2+1)^2+3)}{2(u^2+1)^3}$	$\frac{u(u^2-3)}{(u^2+1)^2}$	$-\frac{(u^2-1)(u^4+6u^2-3)}{2(u^2+1)^3}$
\mathcal{D}_{Tu}	0	$\frac{h+2}{2(u^2+1)}$	0	0	0
$\mathcal{D}_{\Phi R}$	0	0	$\frac{2(u^2-1)^2}{(u^2+1)^3}$	0	$-\frac{(u^2-1)(h(u^2+1)^2+4(u^2-1))}{2(u^2+1)^3}$
$\mathcal{D}_{\Phi u}$	0	0	0	$\frac{h+1}{2(u^2+1)}$	0

Table 2.3: \mathcal{B} matrix.

\mathcal{D}_{AB}	$C_{TT}(u)$	$C_{T\Phi}(u)$
\mathcal{D}_{TT}	$\frac{(u^2-1)(u^4+2u^2+2h^2(u^2+1)^2+6h(u^2+1)^2+9)}{(u^2+1)^5}$	$\frac{u^8-28u^6-42u^4+36u^2+2h^2(u^8+8u^6+10u^4-3)+3h(u^8+8u^6+10u^4-3)-15}{2(u^2+1)^5}$
$\mathcal{D}_{T\Phi}$	$\frac{(u^2-1)(2h^2(u^2+1)^2+5h(u^2+1)^2+8)}{(u^2+1)^5}$	$\frac{h^2(u^4+10u^2-7)(u^2+1)^2+h(u^4+10u^2-7)(u^2+1)^2-8(3u^6+4u^4-5u^2+2)}{2(u^2+1)^5}$
$\mathcal{D}_{\Phi\Phi}$	$\frac{2(u^2-1)(h^2(u^2+1)^2+2h(u^2+1)^2+4)}{(u^2+1)^5}$	$\frac{2(u^2-1)(-3u^4-6u^2+2h^2(u^2+1)^2+h(u^2+1)^2+5)}{(u^2+1)^5}$
\mathcal{D}_{RR}	$\frac{8(u^6-8u^4+9u^2-2)-m^2(u^2+1)^4}{8(u^2-1)(u^2+1)^3}$	$\frac{-3u^4+30u^2+h(u^2+1)^2-7}{2(u^2+1)^3}$
\mathcal{D}_{Ru}	$-\frac{(h+1)u}{(u^2+1)^2}$	$\frac{2u(u^2+h(u^2-1)-2)}{(u^2-1)(u^2+1)^2}$
\mathcal{D}_{uu}	$\frac{m^2(u^2+1)^4+4h^2(u^2-1)(u^2+1)^2+8h(u^2-1)(u^2+1)^2+8(u^6-u^4+u^2-1)}{8(u^2-1)^2(u^2+1)^3+5}$	$\frac{3u^4-2u^2+2h^2(u^2+1)^2+3h(u^2+1)^2+3}{2(u^2-1)(u^2+1)^3}$
\mathcal{D}_{TR}	$\frac{im(u^4-2u^2+2h(u^2+1)^2+5)}{4(u^2+1)^3}$	$\frac{im(u^4+6u^2-3)(-u^4-6u^2+h(u^2+1)^2+3)}{8(u^2-1)(u^2+1)^3}$
\mathcal{D}_{Tu}	$\frac{imu}{2-2u^4}$	$\frac{imu(u^4+6u^2-3)}{4(u^2-1)(u^2+1)^2}$
$\mathcal{D}_{\Phi R}$	$\frac{im(u^4+h(u^2+1)^2+3)}{2(u^2+1)^3}$	$\frac{im(-u^4-6u^2+h(u^2+1)^2+3)}{2(u^2+1)^3}$
$\mathcal{D}_{\Phi u}$	$\frac{imu}{2-2u^4}$	$\frac{imu}{(u^2+1)^2}$
	$C_{\Phi R}(u)$	$C_{\Phi u}(u)$
\mathcal{D}_{TT}	$\frac{ihm(u^4+6u^2-3)^2}{4(u^2-1)(u^2+1)^3}$	$\frac{imu(u^4+6u^2-3)^2}{4(u^2-1)(u^2+1)^3}$
$\mathcal{D}_{T\Phi}$	$\frac{ihm(u^4+6u^2-3)}{(u^2+1)^3}$	$\frac{imu(u^4+6u^2-3)}{(u^2+1)^3}$
$\mathcal{D}_{\Phi\Phi}$	$\frac{4ihm(u^2-1)}{(u^2+1)^3}$	$\frac{4imu(u^2-1)}{(u^2+1)^3}$
\mathcal{D}_{RR}	$\frac{im(u^4+6u^2-3)}{4(u^4-1)}$	$\frac{imu(u^6+3u^4+19u^2-15)}{4(u^2-1)(u^2+1)^2}$
\mathcal{D}_{Ru}	$\frac{imu(u^4+6u^2-3)}{4(u^2-1)(u^2+1)^2}$	$\frac{ihm(u^4+6u^2-3)}{8(u^4-1)}$
\mathcal{D}_{uu}	$\frac{i(h+1)m(u^4+6u^2-3)}{4(u^2-1)^2(u^2+1)}$	$\frac{imu(u^2+3)}{2(u^4-1)}$
\mathcal{D}_{TR}	$\frac{-u^4-12u^2+3}{(u^2+1)^3}$	$\frac{2u(u^4-14u^2+9)}{(u^2+1)^4}$
\mathcal{D}_{Tu}	$\frac{(h+2)u(u^2-3)}{(u^2-1)(u^2+1)^2}$	$\frac{(h+2)(u^4+6u^2-3)}{2(u^2+1)^3}$
$\mathcal{D}_{\Phi R}$	$\frac{6u^2-2}{(u^2+1)^3}$	$\frac{2u(h(u^2+1)^2-2(u^4-6u^2+5))}{(u^2+1)^4}$
$\mathcal{D}_{\Phi u}$	$-\frac{2(h+1)u}{(u^2-1)(u^2+1)^2}$	$\frac{(h+1)(h(u^2+1)^2+4(u^2-1))}{2(u^2+1)^3}$

Table 2.4: Part I of C matrix.

\mathcal{D}_{AB}	$C_{RR}(u)$	$C_{Ru}(u)$
\mathcal{D}_{TT}	$\frac{8(u^{10}-2u^8-6u^6-8u^4+21u^2-6)-m^2(u^6+7u^4+3u^2-3)^2}{8(u^2-1)(u^2+1)^5}$	$\frac{4u((2h+3)u^4+2(h-6)u^2+9)}{(u^2+1)^4}$
$\mathcal{D}_{T\Phi}$	$-\frac{(u^8+8u^6+10u^4-3)m^2+2h(u^2-1)(u^2+1)^2+8(u^6+u^4-3u^2+1)}{2(u^2+1)^5}$	$-\frac{4u(u^2-1)(hu^2+2u^2+h-4)}{(u^2+1)^4}$
$\mathcal{D}_{\Phi\Phi}$	$\frac{2(u^2-1)(-m^2(u^2+1)^2+h(u^2+1)^2+2(u^4+2u^2-1))}{(u^2+1)^5}$	$-\frac{4(h+1)u(u^2-1)}{(u^2+1)^3}$
\mathcal{D}_{RR}	$\frac{u^2-1}{(u^2+1)^3}$	$\frac{4u}{(u^2+1)^2}$
\mathcal{D}_{Ru}	$-\frac{u}{(u^2+1)^2}$	$\frac{8(u^6+3u^4-5u^2+1)-m^2(u^8+8u^6+10u^4-3)}{8(u^2-1)(u^2+1)^3}$
\mathcal{D}_{uu}	$-\frac{(u^8+8u^6+10u^4-3)m^2+4h(u^2-1)(u^2+1)^2+16u^2(u^2-1)}{8(u^2-1)^2(u^2+1)^3}$	$-\frac{(h+1)u}{u^4-1}$
\mathcal{D}_{TR}	$\frac{im(u^4+6u^2-3)}{4(u^2+1)^3}$	$-\frac{imu(u^2-3)}{(u^2+1)^2}$
\mathcal{D}_{Tu}	$-\frac{2(u^2-1)(u^2+1)^2}{im(u^4+4u^2-1)}$	$\frac{im(u^4+6u^2-3)}{2(u^2+1)^3}$
$\mathcal{D}_{\Phi R}$	$\frac{im(u^4+4u^2-1)}{2(u^2+1)^3}$	$-\frac{imu(u^2-1)}{(u^2+1)^2}$
$\mathcal{D}_{\Phi u}$	$\frac{imu}{2(u^4-1)}$	$\frac{im(u^4+6u^2+h(u^2+1)^2-3)}{2(u^2+1)^3}$
	$C_{uu}(u)$	$C_{Tu}(u)$
\mathcal{D}_{TT}	$\frac{4h^2(u^6+5u^4-9u^2+3)(u^2+1)^2+m^2(u^6+7u^4+3u^2-3)^2+8(5u^8+34u^6-68u^4+54u^2-9)}{8(u^2+1)^5}$	$\frac{i(2h+3)m(u^4+6u^2-3)}{2(u^2+1)^3}$
$\mathcal{D}_{T\Phi}$	$\frac{(u^2-1)((u^8+8u^6+10u^4-3)m^2+4h^2(u^2-1)(u^2+1)^2+2h(u^2-1)(u^2+1)^2+8(u^6+8u^4-11u^2+2))}{2(u^2+1)^5}$	$\frac{im(2(u^4+8u^2-5)+h(u^4+10u^2-7))}{2(u^2+1)^3}$
$\mathcal{D}_{\Phi\Phi}$	$\frac{2(u^2-1)^2(h^2(u^2+1)^2+m^2(u^2+1)^2+h(u^2+1)^2+2(u^4+9u^2-2))}{(u^2+1)^5}$	$\frac{2i(2h+3)m(u^2-1)}{(u^2+1)^3}$
\mathcal{D}_{RR}	$-\frac{(u^8+8u^6+10u^4-3)m^2+4h(u^2-1)(u^2+1)^2+8(u^4+4u^2-1)}{8(u^2+1)^3}$	$-\frac{im}{2(u^2+1)}$
\mathcal{D}_{Ru}	$-\frac{hu}{2(u^2+1)}$	$-\frac{imu}{(u^2+1)^2}$
\mathcal{D}_{uu}	$\frac{u^2(u^2+3)}{(u^2+1)^3}$	$\frac{i(2h+3)m}{2(u^4-1)}$
\mathcal{D}_{TR}	$\frac{im(u^2-1)(u^4+6u^2-3)}{4(u^2+1)^3}$	$\frac{8(u^6-7u^4+7u^2-1)-m^2(u^8+8u^6+10u^4-3)}{8(u^2-1)(u^2+1)^3}$
\mathcal{D}_{Tu}	$-\frac{imu(u^2-3)}{2(u^2+1)^2}$	$-\frac{(h+2)u}{(u^2+1)^2}$
$\mathcal{D}_{\Phi R}$	$\frac{im(u^2-1)(h(u^2+1)^2+2(u^2-1))}{2(u^2+1)^3}$	$-\frac{m^2}{2(u^2+1)}$
$\mathcal{D}_{\Phi u}$	$-\frac{imu(u^2-1)}{(u^2+1)^2}$	0

Table 2.5: Part II of C matrix.

\mathcal{D}_{AB}	$C_{\Phi\Phi}(u)$
\mathcal{D}_{TT}	$\frac{h^2(u^2-1)(u^6+7u^4+3u^2-3)^2-2(3u^{12}+68u^{10}-5u^8-128u^6+153u^4-36u^2+9)}{8(u^2-1)^2(u^2+1)^5}$
$\mathcal{D}_{T\Phi}$	$-\frac{-2(u^8+8u^6+10u^4-3)h^2+(u^8+8u^6+10u^4-3)h+4(9u^6+13u^4-9u^2+3)}{4(u^2+1)^5}$
$\mathcal{D}_{\Phi\Phi}$	$\frac{(u^2-1)(-3u^4-6u^2+2h(u^2+1)^2-2h(u^2+1)^2+5)}{(u^2+1)^5}$
\mathcal{D}_{RR}	$\frac{2(7u^8-30u^6+72u^4-42u^2+9)-h(u^2+1)^2(u^6+5u^4-9u^2+3)}{8(u^2-1)^2(u^2+1)^3}$
\mathcal{D}_{Ru}	$-\frac{u(8(u^4-4u^2+3)+h(u^6+11u^4-13u^2+9))}{8(u^4-1)^2}$
\mathcal{D}_{uu}	$\frac{(u^8+8u^6+10u^4-3)h^2+(u^8+8u^6+10u^4-3)h+2(7u^6+3u^4+9u^2-3)}{8(u^2-1)^2(u^2+1)^3}$
\mathcal{D}_{TR}	$-\frac{im(u^4+6u^2-3)^2}{16(u^2-1)(u^2+1)^3}$
\mathcal{D}_{Tu}	$-\frac{imu(u^6+3u^4-21u^2+9)}{8(u^4-1)^2}$
$\mathcal{D}_{\Phi R}$	$-\frac{im(u^4+6u^2-3)}{4(u^2+1)^3}$
$\mathcal{D}_{\Phi u}$	$-\frac{imu(u^2-3)}{2(u^2-1)(u^2+1)^2}$
	$C_{Tu}(u)$
\mathcal{D}_{TT}	$-\frac{2imu(u^2-1)(u^2+3)}{(u^2+1)^3}$
$\mathcal{D}_{T\Phi}$	$-\frac{imu(u^4+4u^2-5)}{(u^2+1)^3}$
$\mathcal{D}_{\Phi\Phi}$	$-\frac{4imu(u^2-1)}{(u^2+1)^3}$
\mathcal{D}_{RR}	$\frac{4imu}{(u^2+1)^2}$
\mathcal{D}_{Ru}	$\frac{i(h+1)m}{2(u^2+1)}$
\mathcal{D}_{uu}	$-\frac{imu}{u^4-1}$
\mathcal{D}_{TR}	$-\frac{2u(u^4-14u^2+h(u^2+1)^2+9)}{(u^2+1)^4}$
\mathcal{D}_{Tu}	$-\frac{4h^2(u^2-1)(u^2+1)^2+4h(u^6-3u^4+7u^2-5)+(u^4+6u^2-3)(-8u^2+m^2(u^2+1)^2+8)}{8(u^2-1)(u^2+1)^3}$
$\mathcal{D}_{\Phi R}$	$-\frac{4u(u^4-6u^2+5)}{(u^2+1)^4}$
$\mathcal{D}_{\Phi u}$	$-\frac{-m^2(u^2+1)^2+4h(u^2-1)+4(u^2-1)}{2(u^2+1)^3}$

Table 2.6: Part III of C matrix.

Chapter 3

METRIC DEFORMATIONS FROM EXTREMAL KERR BLACK HOLES

In Chapter II, we introduced a set of symmetry-adapted bases, which makes the metric equations separable for near-horizon extremal Kerr spacetimes. In this chapter, we apply our methods to solve for the deformations to the near-horizon extremal Kerr metric due to two example string-inspired beyond-GR theories: Einstein-dilaton-Gauss-Bonnet, and dynamical Chern-Simons theory. We accomplish this by making use of the enhanced symmetry group of NHEK and the weak-coupling limit of EdGB and dCS. We find that the EdGB metric deformation has a curvature singularity, while the dCS metric is regular. From these solutions we compute orbital frequencies, horizon areas, and entropies. This sets the stage for analytically understanding the microscopic origin of black hole entropy in beyond-GR theories.

3.1 Introduction

General relativity (GR), despite its huge success in describing gravity on large scales [62], must be corrected at high energies to reconcile with quantum mechanics. Black holes (BHs) may hold a key to developing a quantum theory of gravity: quantum effects can become important when gravity is strong, such as close to singularities. Quantum effects can also become important at the horizon over sufficiently long times, e.g. as Hawking radiation [63] shrinks a BH, generating arbitrarily large curvatures at the horizon, close to evaporation.

In order to go beyond GR, a huge class of alternative theories of gravity has been proposed and studied. Analytical black hole solutions can be sensitive to corrections to GR, but they are rare in beyond-GR theories. In the slow-rotation limit, BH solutions [64, 65] have been found for dynamical Chern-Simons theory [66]. But for many other theories or when it comes to generic spin, it is difficult to find analytic rotating solutions. In this chapter we find BH solutions in the near-horizon extremal limit for beyond-GR theories. In particular, we make use of two theories of gravity as examples, taking the weak-coupling limit, and find the corresponding deformations to near-horizon extremal Kerr (NHEK). The two theories, both inspired by string theory, are Einstein-dilaton-Gauss-Bonnet (EdGB) [67, 68] and dynamical Chern-Simons theory (dCS) [66] respectively. They both contain a dynamical scalar field

that couples to curvature, correcting GR with a (different) quadratic curvature term. After taking the weak coupling limit of a beyond-GR theory, finding the vacuum rotating solutions can be naturally formulated as finding the metric deformations to solutions in Einstein gravity, i.e. deformations to Kerr black holes (alternatively, one may expand Kerr around the $a = 0$ Schwarzschild limit, and solve for deformations around the expanded spacetime, as in [69–71]). Therefore linear metric perturbation theory is a natural tool to address the problem. However, the perturbation equations are hard to solve unless we can use separation of variables. In the Kerr spacetime, metric perturbations do not separate, but curvature perturbations do. The most common approach is to use the Newman-Penrose formalism [42] and solve the wave equations for Weyl scalars Ψ_4 or Ψ_0 . This method was developed by Teukolsky [40, 41], and the partial differential equation to solve is known as the Teukolsky equation. The cost of curvature perturbations, however, is a very complicated metric-reconstruction procedure (see e.g. discussion in [39]), which only works for certain source terms, in certain gauges, and does not recover all pieces of the metric. The main difficulty in the separation of the metric perturbation equations is insufficient symmetry in the Kerr spacetime. In the near-horizon extremal scaling limit of Kerr, additional symmetries arise, and we can separate variables, as the authors showed in [36]. Therefore in NHEK, analytical deformed solutions can be found by using linear metric perturbation theory.

The NHEK spacetime is interesting to study for several other reasons. For instance, it has been shown that the horizon instability of extremal black holes [72] can be viewed as a critical phenomenon [73]. Moreover, it was shown that near-horizon quantum states can be identified with a two-dimensional conformal field theory (CFT), via the proposed Kerr/CFT correspondence [60].

In this chapter, we focus on finding metric deformations of NHEK due to dCS and EdGB interactions in the decoupling limit. Let us emphasize, though, that this formalism is not limited to these two theories, but can be applied to finding deformed NHEK solutions in many beyond-GR theories in the decoupling limit. With the metric solutions, we compute physical properties including geodesic motion of particles and their orbital frequencies, horizon areas, and entropies. We also prove that the EdGB extremal BH is indeed singular in the decoupling limit, confirming the conjecture of [74]. One of the most important results is the calculation of the macroscopic extremal black hole entropies in beyond-GR theories. Although we only consider the near-horizon limit, the entropy results agree with extremal

BH solutions (i.e. without zooming into the near-horizon region). In the NHEK spacetime, the entropy can be computed by counting the microscopic states of a two-dimensional chiral CFT [60] via the Cardy formula, which leads to the Kerr/CFT conjecture. We also expect a dual CFT description of the extremal black hole entropy for beyond-GR theories in the decoupling limit. We will not address this issue here, but our work lays the ground for studying the microscopic states of deformed extremal black holes. This may provide insight into quantum theories beyond Einstein gravity.

We organize the chapter as follows. In Sec. 3.2 we review EdGB and dCS gravity, and introduce the decoupling limit to the two theories. In Sec. 3.3, we review the near-horizon extremal geometry, the symmetry-adapted bases, and set up the metric perturbations in near-horizon extremal Kerr spacetime as induced by the two stringy interactions. In Sec. 3.4 we solve for the dynamical scalar fields, construct the source term to the linearized Einstein field equation, and finally solve the metric perturbations in the “attractor” gauge. In Sec. 3.5 we derive the timelike geodesic equations for the deformed spacetimes, and calculate the corrections to horizon areas and black hole entropies due to the two stringy interactions. We conclude and discuss future work in Sec. 3.6.

3.2 Einstein-dilaton-Gauss-Bonnet and dynamical Chern-Simons gravity

Action

We work in units where $c = 1 = \hbar$, and choose the metric signature $(-, +, +, +)$. The theories which we are considering, namely dynamical Chern-Simons gravity and Einstein-dilaton-Gauss-Bonnet, can be motivated from both low-energy effective field theory (EFT) and high-energy fundamental theory. DCS can arise from gravitational anomaly cancellation in chiral theories [75–77], including Green-Schwarz cancellation in string theory [78]. The low-energy compactified theory was explicitly presented in [79] (and see references therein). EdGB, meanwhile, can be derived by expanding the low energy string action to two loops to find the dilaton-curvature interaction [67, 68].

The actions of dCS and EdGB both include the Einstein-Hilbert term and a scalar field that non-minimally couples to curvature. The Einstein-Hilbert action leads to standard GR. In dCS the scalar field is an axion, while in EdGB it is a dilaton. In our discussions, there is no need to distinguish between the two scalar fields. We

treat them equally as the scalar field ϑ . For both theories, we then take as our action

$$I = \int d^4x \sqrt{-g} [\mathcal{L}_{\text{EH}} + \mathcal{L}_\vartheta + \mathcal{L}_{\text{int}}], \quad (3.1)$$

with

$$\mathcal{L}_{\text{EH}} = \frac{1}{2} m_{\text{pl}}^2 R, \quad \mathcal{L}_\vartheta = -\frac{1}{2} (\partial^a \vartheta) (\partial_a \vartheta), \quad (3.2)$$

and non-minimal scalar-curvature interaction terms for dCS and EdGB respectively [66–68]

$$\mathcal{L}_{\text{int}}^{\text{CS}} = -\frac{m_{\text{pl}}}{8} \ell_{\text{CS}}^2 \vartheta {}^*RR, \quad \mathcal{L}_{\text{int}}^{\text{GB}} = -\frac{m_{\text{pl}}}{8} \ell_{\text{GB}}^2 \vartheta {}^*R^*R. \quad (3.3)$$

Here R is the Ricci scalar of the metric g_{ab} , and g is the metric determinant. The reduced Planck mass is defined through $m_{\text{pl}} \equiv (8\pi G)^{-1/2}$. The scalar field ϑ has been canonically normalized such that $[\vartheta] = [M]$. In the interaction terms, we define two coupling constant ℓ_{CS} and ℓ_{GB} for dCS and EdGB respectively. The two variables are dimensionful, specifically $[\ell_{\text{CS}}] = [\ell_{\text{GB}}] = [M]^{-1}$. That is, each of them gives the length scale of the corresponding theory, which in principle can be constrained observationally. In dCS, we encounter the Pontryagin-Chern density

$${}^*RR = {}^*R^{abcd} R_{abcd}, \quad (3.4)$$

while in EdGB we see minus the Euler (or Gauss-Bonnet) density

$${}^*R^*R = {}^*R_{abcd}^* R^{abcd} = -R^2 + 4R_{ab}R^{ab} - R_{abcd}R^{abcd}. \quad (3.5)$$

Here we have used the single- and double-dualized Riemann tensors,

$${}^*R_{abcd} \equiv \frac{1}{2} \epsilon_{ab}{}^{ef} R_{efcd}, \quad {}^*R_{abcd}^* \equiv \frac{1}{2} {}^*R_{abef} \epsilon^{ef}{}_{cd}, \quad (3.6)$$

where we dualize with the completely antisymmetric Levi-Civita tensor ϵ^{abcd} .

Equation of motion

Variation of the action in Eq. (3.1) with respect to the scalar field ϑ leads to the scalar equation of motion for dCS and EdGB respectively,

$$\square \vartheta = \frac{m_{\text{pl}}}{8} \begin{cases} \ell_{\text{CS}}^2 {}^*RR, & \text{dCS} \\ \ell_{\text{GB}}^2 {}^*R^*R, & \text{EdGB} \end{cases} \quad (3.7)$$

where $\square = \nabla^a \nabla_a$ and ∇_a is the covariant derivative compatible with the metric. Variation of the action in Eq. (3.1) with respect to g^{ab} leads to the metric equation of motion,

$$m_{\text{pl}}^2 G_{ab} = T_{ab}[\vartheta, \vartheta] - m_{\text{pl}} \begin{cases} \ell_{\text{CS}}^2 C_{ab}[\vartheta], & \text{dCS} \\ \ell_{\text{GB}}^2 H_{ab}[\vartheta]. & \text{EdGB} \end{cases} \quad (3.8)$$

Here $T_{ab}[\vartheta, \vartheta]$ is the canonical stress-energy tensor for the scalar field ϑ ,

$$T_{ab}[\vartheta, \vartheta] = \nabla_a \vartheta \nabla_b \vartheta - \frac{1}{2} g_{ab} \nabla^c \vartheta \nabla_c \vartheta. \quad (3.9)$$

We also define the C -tensor for dCS,

$$C_{ab}[\vartheta] = \nabla^c \nabla^d [{}^*R_{d(ab)c} \vartheta], \quad (3.10)$$

and introduce the H -tensor for EdGB via

$$H_{ab}[\vartheta] = \nabla^c \nabla^d [{}^*R_{dabc}^* \vartheta], \quad (3.11)$$

where parentheses around n indices means symmetrizing with a factor of $1/n!$.

Decoupling limit

We now introduce two distinct theories as the decoupling limit of dCS and EdGB respectively, namely *Decoupled dynamical Chern-Simons* ($D^2\text{CS}$) and *Decoupled dynamical Gauss-Bonnet* ($D^2\text{GB}$) [80]. We will briefly review the formalism of taking the decoupling limit in dCS (see [81] for detailed discussions). The extension of this formalism to EdGB is straightforward.

We assume the corrections to GR due to the interaction terms are small, so that in the limit $\ell \rightarrow 0$, we recover standard GR. This allows us to perform a perturbative expansion of all the fields in terms of powers of ℓ_{CS} . To make the perturbation theory simpler, we introduce a formal dimensionless order-counting parameter ε . We then consider a one-parameter family of theories defined by the action I_ε , where in I_ε , we have multiplied \mathcal{L}_{int} by ε . This parameter can be set to 1 later.

Now we expand all fields and equations of motion in a series expansion in powers of ε . Specifically, we take $\vartheta = \vartheta^{(0)} + \varepsilon \vartheta^{(1)} + \mathcal{O}(\varepsilon^2)$, and similarly $g_{ab} = g_{ab}^{(0)} + \varepsilon h_{ab}^{(1)} + \varepsilon^2 h_{ab}^{(2)} + \mathcal{O}(\varepsilon^3)$.

In order to recover GR in the limit $\varepsilon \rightarrow 0$, at order ε^0 , we have $\vartheta^{(0)} = 0$. At order ε^1 , $h_{ab}^{(1)}$ has vanishing source term and thus can be set to zero as well. It is then easy to show that the EOM for the leading order scalar field $\vartheta^{(1)}$ is at ε^1 , given by

$$\square^{(0)} \vartheta^{(1)} = \frac{m_{\text{pl}}}{8} \ell_{\text{CS}}^2 [{}^*RR]^{(0)}, \quad (3.12)$$

and the leading order metric deformation enters at ε^2 , which satisfies

$$m_{\text{pl}}^2 G_{ab}^{(1)}[h^{(2)}] + m_{\text{pl}} \ell_{\text{CS}}^2 C_{ab}[\vartheta^{(1)}] = T_{ab}[\vartheta^{(1)}, \vartheta^{(1)}]. \quad (3.13)$$

Here $G_{ab}^{(1)}[h^{(2)}]$ is the linearized Einstein operator acting on the metric deformation $h_{cd}^{(2)}$.

We now redefine our field variables in powers of ℓ_{CS} , but to do so we need another length scale against which to compare. This additional length scale is given by the typical curvature radius of the background solution, e.g. $L \sim |R_{abcd}|^{-1/2}$. For a black hole solution, this length scale will be $L \equiv GM$. We can then also pull out the scaling with powers of L from spatial derivatives and curvature tensors, by defining $\hat{\nabla} = L\nabla$ and $\hat{R}_{abcd} = L^2 R_{abcd}$. We define \hat{h}_{ab} and $\hat{\vartheta}$ via

$$\vartheta^{(1)} = m_{\text{pl}} \left(\frac{\ell_{\text{CS}}}{GM} \right)^2 \hat{\vartheta}, \quad h_{ab}^{(2)} = \left(\frac{\ell_{\text{CS}}}{GM} \right)^4 \hat{h}_{ab}. \quad (3.14)$$

Now our hatted variables satisfy the dimensionless field equations

$$\hat{\square}^{(0)} \hat{\vartheta} = \frac{1}{8} [{}^* \hat{R} \hat{R}]^{(0)}, \quad G_{ab}^{(1)}[\hat{h}] = S_{ab}, \quad (3.15)$$

with the source term $S_{ab} = T_{ab}[\hat{\vartheta}, \hat{\vartheta}] - C_{ab}[\hat{\vartheta}]$.

The equations of motion in the decoupling limit of EdGB, i.e. D²GB, are almost the same as Eq. (3.15). The only difference is that, for EdGB, we substitute ${}^* \hat{R} \hat{R}$ for ${}^* \hat{R} \hat{R}$, and the C -tensor in the source term should be replaced by the H -tensor.

3.3 NHEK and separable metric perturbations

The metric of a generic near-horizon extremal geometry (NHEG) that makes $SL(2, \mathbb{R}) \times U(1)$ symmetry manifest takes the form [82]

$$ds^2 = (GM)^2 \left[v_1(\theta) \left(-r^2 dt^2 + \frac{dr^2}{r^2} + \beta^2 d\theta^2 \right) + \beta^2 v_2(\theta) (d\phi - \alpha r dt)^2 \right], \quad (3.16)$$

where v_1 and v_2 are positive functions of the polar angle θ , and α and β are constants. The spacetime has four Killing vector fields. In these Poincaré coordinates, they are given by

$$\begin{aligned} H_0 &= t\partial_t - r\partial_r, \\ H_+ &= \partial_t, \\ H_- &= \left(t^2 + \frac{1}{r^2} \right) \partial_t - 2tr\partial_r + \frac{2\alpha}{r} \partial_\phi, \\ Q_0 &= \partial_\phi. \end{aligned} \quad (3.17)$$

The four generators form a representation of the Lie algebra $\mathfrak{g} \equiv \mathfrak{sl}(2, \mathbb{R}) \times \mathfrak{u}(1)$,

$$\begin{aligned} [H_0, H_\pm] &= \mp H_\pm, \\ [H_+, H_-] &= 2H_0, \\ [H_s, Q_0] &= 0. \quad (s = 0, \pm) \end{aligned} \tag{3.18}$$

A crucial algebra element we will need is the Casimir element of $\mathfrak{sl}(2, \mathbb{R})$. The Casimir Ω acts on a tensor \mathbf{t} via

$$\Omega \cdot \mathbf{t} = [\mathcal{L}_{H_0}(\mathcal{L}_{H_0} - \text{id}) - \mathcal{L}_{H_-} \mathcal{L}_{H_+}] \mathbf{t}, \tag{3.19}$$

where \mathcal{L}_X is the Lie derivative along the vector field X .

The generic metric in Eq. (3.16) has an Einstein gravity solution, which is found with

$$\begin{aligned} v_1(u) &= 1 + u^2, & \alpha &= -1, \\ v_2(u) &= \frac{4(1 - u^2)}{1 + u^2}, & \beta &= +1, \end{aligned} \tag{3.20}$$

where we have defined a new coordinate $u = \cos \theta$. This spacetime is called near-horizon extremal Kerr, which was first obtained by taking the near-horizon limit of extremal Kerr black holes [13].

The enhanced symmetry due to the near-horizon extremal limit enables us to separate variables in the linearized Einstein equation (LEE) in NHEK spacetime [36]. This is achieved by expanding the metric perturbations in terms of some basis functions adapted to that symmetry. For the non-compact group $SL(2, \mathbb{R})$, one can construct a *highest-weight module*, which is a unitary irreducible representation of the group. In NHEK, that is, we simultaneously diagonalize $\{\mathcal{L}_{Q_0}, \Omega, \mathcal{L}_{H_0}\}$ and label the eigenfunctions ξ by m, h, k respectively. Here m labels the azimuthal direction, h labels the representation (“weight”), and k labels “descendants” within the same representation. We impose the highest-weight condition $\mathcal{L}_{H_+} \xi = 0$, and solve for the basis functions. Expanding the metric perturbations in terms of these bases leads to separation of variables for the LEE in NHEK spacetime. As a result, the system of partial differential equations in the LEE automatically turns into one of ordinary differential equations.

If the LEE system has a source term, and that source term is a linear combination of a finite number of representations, then the metric perturbations can also be expanded as a sum of those same representations. As we will see, for both EdGB and dCS

gravity in the decoupling limit, the source term on the RHS of Eq. (3.15) will have the same $SL(2, \mathbb{R}) \times U(1)$ symmetry as the background spacetime. This enables us to solve for the linear metric deformations analytically.

3.4 Solving for the metric deformations

In this section we find solutions of the leading order scalar fields, construct the source terms on the RHS of Eq. (3.15) for D²CS and D²GB respectively, and finally solve for the metric deformations.

Solutions for scalars and construction of source

In a Ricci-flat spacetime (like Kerr), the I curvature invariant [83] agrees with $I = \frac{1}{16}(-{}^*R{}^*R + i{}^*RR)$. In NHEK, this takes the value $\hat{I} = 3/(1 - iu)^6$. The imaginary and (minus) real parts of \hat{I} thus give compact ways of expressing the source terms for the scalar equations of motion of respectively D²CS and D²GB.

In D²CS, the leading order scalar equation of motion admits an axion solution which is regular everywhere. This scalar field is given by

$$\hat{\vartheta}^{(1)} = \frac{1}{4} \left[\frac{u(u^4 + 2u^2 - 7)}{(u^2 + 1)^3} + 2 \arctan u \right] + \text{const.} \quad (3.21)$$

This also agrees with the solution presented in [84]. Because the theory is shift-symmetric, we are free to set the constant term to zero. We then construct the source $S_{ab}[\hat{\vartheta}^{(1)}, \hat{\vartheta}^{(1)}]$ in Eq. (3.15) for D²CS.

In D²GB, we find the leading order scalar solution is

$$\begin{aligned} \hat{\vartheta}^{(1)} = d_2 + \frac{\log(u^2 + 1)}{4} - \frac{u^4 + 4u^2 - 1}{2(u^2 + 1)^3} + \left(-\frac{d_1}{2} - \frac{1}{4}\right) \log(1 - u) + \\ + \left(\frac{d_1}{2} - \frac{1}{4}\right) \log(1 + u), \end{aligned} \quad (3.22)$$

where d_1 and d_2 are constants. Unlike the D²CS case, it is not possible to remove both logarithmic divergences at $u = \pm 1$ by choosing specific values of d_1 and d_2 . It is possible to cancel the divergence at one pole or the other, but not both. We set $d_1 = 0$ so that the scalar field retains the reflection symmetry, $u \rightarrow -u$, of the background spacetime. Again by shift symmetry, we are free to set the additive constant $d_2 = 0$, and then construct the source term S_{ab} accordingly. The source S_{ab} remains irregular at the two poles $u = \pm 1$.

Let us remark on an important common feature of the two source terms. For either theory,

$$\mathcal{L}_X S_{ab} = 0, \quad (3.23)$$

where $X \in \{H_0, H_{\pm}, Q_0\}$. That is, if we decompose the source term using the symmetry-adapted scalar, vector and tensor bases, the source term only contains the $m = h = k = 0$ component. Therefore on the LHS of the LEE, the metric perturbations only have stationary axisymmetric basis components, either for D²CS or D²GB. These components live in both the highest-weight and lowest-weight representations of NHEK's isometry group.

dCS-deformed NHEK

We now seek the solutions to the linearized metric perturbation equations of NHEK sourced by the two stringy interactions. Expansions of the metric perturbations into the basis functions turn the systems of partial differential equations in LEE into ten coupled ordinary differential equations (ODEs) in u , which we solve in this subsection.

So far we haven't chosen any gauge condition. Since the linear metric perturbations have the same $SL(2, \mathbb{R}) \times U(1)$ symmetry as the background NHEK spacetime, we can fix the gauge by requiring an ‘‘attractor form’’ [82] of the deformed solutions as in Eq. (3.16). That is, we only consider the following shifts in the metric parameters. Recalling that the metric is corrected at order ε^2 , we have

$$\begin{aligned} v_1(u) &\rightarrow v_1(u) + \varepsilon^2 \delta v_1(u), & \alpha &\rightarrow \alpha + \varepsilon^2 \delta \alpha, \\ v_2(u) &\rightarrow v_2(u) + \varepsilon^2 \delta v_2(u), & \beta &\rightarrow \beta + \varepsilon^2 \delta \beta. \end{aligned} \quad (3.24)$$

We call this gauge choice the *attractor gauge*. This ansatz is, by construction, in the $m = h = k = 0$ representation of NHEK's isometry group. Therefore it always makes the $SL(2, \mathbb{R}) \times U(1)$ symmetry manifest.

For D²CS, the linear metric deformations are found to be the following complicated expressions, which we also plot in Fig. 3.1:

$$\delta v_1(u) = f_1(u) + \frac{1}{53760 (u^2 + 1)^5} \mathcal{P}_1^{\text{D}^2\text{CS}}[u], \quad (3.25)$$

$$\delta v_2(u) = f_2(u) - \frac{(u^2 - 1)}{6720 (u^2 + 1)^7} \mathcal{P}_2^{\text{D}^2\text{CS}}[u], \quad (3.26)$$

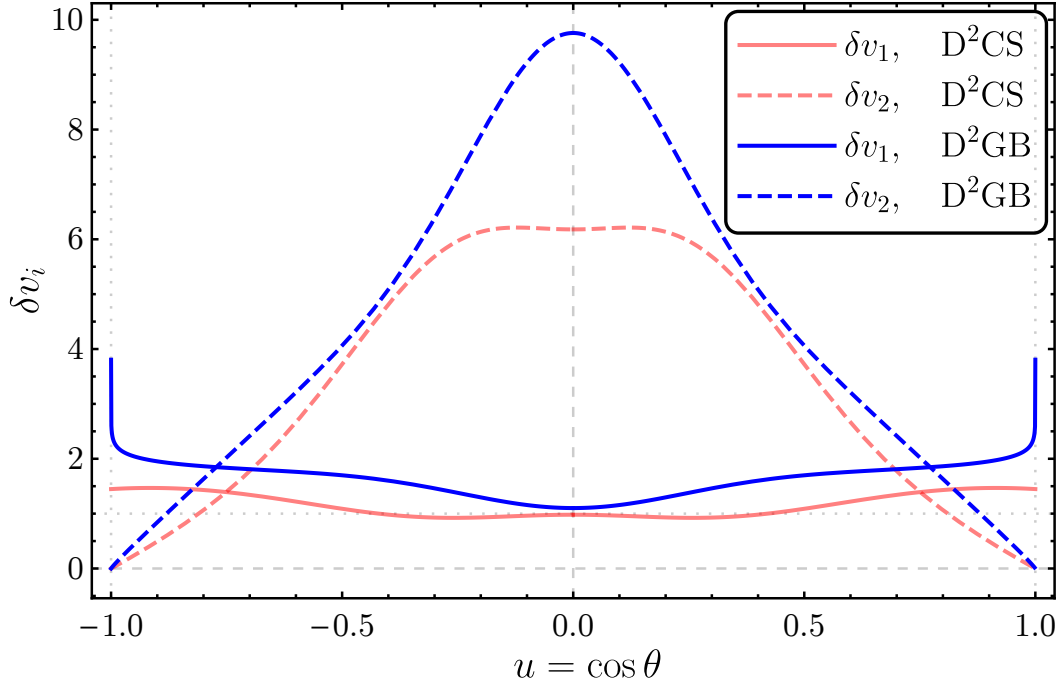


Figure 3.1: The metric deformation functions δv_1 (solid) and δv_2 (dashed) as functions of u , for both dCS-deformed (red) and EdGB-deformed (blue) NHEK. Note that in D^2GB , δv_1 blows up at the two poles $u = \pm 1$.

where

$$\begin{aligned}
 f_1(u) &= \frac{1}{3}c_1(-u^2 + 4u - 1) + \frac{1}{3}c_2(2u^2 - 5u + 2) \\
 &\quad - \frac{1}{3}c_3u\sqrt{1-u^2} - \frac{4}{3}\delta\beta(u^2 + 1) + 2\delta\beta u\sqrt{1-u^2}\sin^{-1}u \\
 &\quad + \frac{975u\sqrt{1-u^2}\tan^{-1}\left(\frac{\sqrt{2}u}{\sqrt{1-u^2}}\right)}{512\sqrt{2}} - \frac{3}{16}u\tan^{-1}u,
 \end{aligned} \tag{3.27}$$

$$\begin{aligned}
 f_2(u) &= \frac{8c_3u\sqrt{1-u^2}}{3(u^2+1)^2} + \frac{4c_1(u^4 + 4u^3 - 4u - 1)}{3(u^2+1)^2} \\
 &\quad - \frac{4c_2(2u^4 + 5u^3 - 5u - 2)}{3(u^2+1)^2} + \frac{40\delta\beta(u^2-1)}{3(u^2+1)} \\
 &\quad - \frac{16\delta\beta u\sqrt{1-u^2}\sin^{-1}u}{(u^2+1)^2} + \frac{\delta\alpha(8-8u^2)}{u^2+1} \\
 &\quad - \frac{975u\sqrt{1-u^2}\tan^{-1}\left(\frac{\sqrt{2}u}{\sqrt{1-u^2}}\right)}{64\sqrt{2}(u^2+1)^2} - \frac{3u(u^2-1)\tan^{-1}u}{4(u^2+1)^2},
 \end{aligned} \tag{3.28}$$

and the polynomials $\mathcal{P}_1^{\text{D}^2\text{CS}}[u]$ and $\mathcal{P}_2^{\text{D}^2\text{CS}}[u]$ are given by

$$\begin{aligned} \mathcal{P}_1^{\text{D}^2\text{CS}}[u] = & -58501u^{12} - 222147u^{10} - 255058u^8 \\ & + 11754u^6 + 323735u^4 - 149799u^2 + 4416, \end{aligned} \quad (3.29)$$

$$\begin{aligned} \mathcal{P}_2^{\text{D}^2\text{CS}}[u] = & 280u^{12} - 52341u^{10} - 252928u^8 \\ & - 472090u^6 - 536680u^4 + 26583u^2 - 18792. \end{aligned} \quad (3.30)$$

Here c_1 , c_2 , and c_3 are integration constants. It is straightforward to see these three constants, together with $\delta\alpha$ and $\delta\beta$, correspond to different homogeneous solutions to the LEE. These solutions are finite on the domain $u \in [-1, +1]$, but would have infinite derivative at the poles $u = \pm 1$ without an appropriate choice of $\delta\beta$. By demanding regularity at the two poles and reflection symmetry of the deformed metric, we set

$$\delta\beta = -\frac{975}{1024\sqrt{2}}, \quad c_3 = 0, \quad c_2 = \frac{4c_1}{5}. \quad (3.31)$$

Note that $\delta\alpha$ will shift the Killing vector H_- . By demanding that the perturbed spacetime has the same Killing vectors as NHEK, we also set $\delta\alpha = 0$. After inserting the solutions from (3.31) back into the metric, we only need to fix c_1 . Collecting the terms proportional to c_1 , one immediately finds that

$$\left(\text{coefficient of } c_1\right) \propto \frac{\partial g_{ab}^{(0)}}{\partial M}. \quad (3.32)$$

This means the homogeneous solution associated with c_1 shifts the mass of the black hole. Since we don't want the mass shift, we fix $c_1 = 0$. With these parameter choices, we obtain the regular solution to the LEE sourced by the dCS interaction in the decoupling limit. We call the newly-found spacetime *dCS-deformed NHEK*.

EdGB-deformed NHEK

For D²GB, in the attractor gauge, the linear metric deformations are found to be

$$\begin{aligned} \delta v_1(u) = & f_1(u) + \frac{1}{8}(-u^2 + u - 1) \log(1 - u) \\ & + \frac{1}{8}(-u^2 - u - 1) \log(1 + u) \\ & + \frac{1}{8}(u^2 + 1) \log(u^2 + 1) - \frac{3u\sqrt{1-u^2} \tan^{-1}\left(\frac{\sqrt{2}u}{\sqrt{1-u^2}}\right)}{256\sqrt{2}} \\ & + \frac{1}{53760(u^2 + 1)^5} \mathcal{P}_1^{\text{D}^2\text{GB}}[u], \end{aligned} \quad (3.33)$$

$$\begin{aligned}
\delta v_2 = f_2(u) &+ \frac{(u^4 - u^3 + u - 1) \log(1 + u)}{2(u^2 + 1)^2} \\
&+ \frac{(u^4 + u^3 - u - 1) \log(1 - u)}{2(u^2 + 1)^2} + \frac{(1 - u^2) \log(u^2 + 1)}{2u^2 + 2} \\
&+ \frac{3u\sqrt{1 - u^2} \tan^{-1}\left(\frac{\sqrt{2}u}{\sqrt{1 - u^2}}\right)}{32\sqrt{2}(u^2 + 1)^2} + \frac{(u^2 - 1)}{6720(u^2 + 1)^7} \mathcal{P}_2^{\text{D}^2\text{GB}}[u],
\end{aligned} \tag{3.34}$$

where the functions $f_1(u), f_2(u)$ are identical to the D^2CS case and given in Eqs. (3.27) and (3.28); and where the polynomials $\mathcal{P}_1^{\text{D}^2\text{GB}}[u]$ and $\mathcal{P}_2^{\text{D}^2\text{GB}}[u]$ are given by

$$\begin{aligned}
\mathcal{P}_1^{\text{D}^2\text{GB}}[u] = &-27459u^{12} - 82773u^{10} - 42302u^8 \\
&+ 81766u^6 - 18815u^4 + 298479u^2 + 11264,
\end{aligned} \tag{3.35}$$

$$\begin{aligned}
\mathcal{P}_2^{\text{D}^2\text{GB}}[u] = &35859u^{10} + 152792u^8 + 226230u^6 \\
&+ 10160u^4 + 205503u^2 - 5632.
\end{aligned} \tag{3.36}$$

As in the D^2CS case, the constant $\delta\beta$ can be chosen so as to cancel a square-root behavior at the poles which would have infinite derivative. However, the important difference from D^2CS is the appearance of log terms in Eqs. (3.33) and (3.34). There are no integration constants which can cancel these logarithmic divergences.

Still, canceling the square-root behavior and assuming reflection symmetry in u , we find

$$\delta\beta = -\frac{969}{1024\sqrt{2}}, \quad c_3 = 0, \quad c_2 = \frac{4c_1}{5}. \tag{3.37}$$

We also fix $\delta\alpha = 0$ to preserve the Killing vector fields of NHEK, and set $c_1 = 0$ to avoid a mass shift. After fixing all constants, these functions are plotted in Fig. 3.1. We call the corresponding spacetime *EdGB-deformed NHEK*. This metric deformation has a true curvature singularity at the poles, $u = \pm 1$, which we discuss further in Sec. 3.6.

3.5 Properties of solutions

Orbits

In this subsection we derive the geodesic equations for a particle in the deformed NHEK spacetime. Since the NHEK background and the deformed solutions have the same isometry group, we consider the spacetime with the general metric in

Eq. (3.16). The relativistic Hamiltonian for geodesic motion of a particle can be defined as

$$H(x^a, p_b) = \frac{1}{2} g^{ab} p_a p_b, \quad (3.38)$$

where p_a are the conjugate momenta of the particle. By drawing analogy to geodesic motion in Kerr spacetime, we can similarly find three constants of motion: energy $E \equiv -p_t$, z angular momentum $L_z \equiv p_\phi$, and Carter's constant C . The Carter constant comes from separating the radial and polar motions. Note, however, that because our Killing vector field ∂_t is different from the asymptotically timelike KVF (with norm -1 at infinity), our energy is different from the usual Kerr orbital energy [85]. Following the Hamilton-Jacobi approach [86], we define the characteristic function W via

$$W = -\frac{1}{2} \kappa \lambda - Et + \int \frac{\sqrt{R(r)}}{\beta^2 r^2} dr + \int \sqrt{\Theta(\theta)} d\theta + L_z \phi, \quad (3.39)$$

where λ is the affine parameter and $\frac{1}{2} \kappa$ is the value of the Hamiltonian evaluated along the world-line of the particle. $R(r)$ and $\Theta(\theta)$ are given by

$$\begin{aligned} R(r) &= \beta^4 (E - \alpha L_z r)^2 - \beta^2 C r^2, \\ \Theta(\theta) &= C - \frac{v_1(\theta)}{v_2(\theta)} L_z^2 + M^2 \beta^2 v_1(\theta) \kappa. \end{aligned} \quad (3.40)$$

Since $p_a = \frac{\partial W}{\partial x^a}$, we obtain the following geodesic equations of motion,

$$\begin{aligned} \Sigma \frac{dt}{d\lambda} &= \frac{\beta^2}{r^2} (E - \alpha L_z r), \\ \Sigma \frac{dr}{d\lambda} &= \pm \sqrt{R(r)}, \\ \Sigma \frac{d\theta}{d\lambda} &= \pm \sqrt{\Theta(\theta)}, \\ \Sigma \frac{d\phi}{d\lambda} &= \frac{\alpha \beta^2}{r} (E - \alpha L_z r) + \frac{v_1(\theta)}{v_2(\theta)} L_z, \end{aligned} \quad (3.41)$$

where $\Sigma = M^2 \beta^2 v_1(\theta)$. These integrals can be directly performed after defining the ‘‘Mino time’’ τ , where $d\tau = d\lambda/\Sigma$ (this again differs from the usual Mino time in the asymptotic region of Kerr, because our time coordinate differs).

In particular, let us consider circular equatorial motion, i.e. $\theta = \pi/2 = \theta_0$. For such motion we only need E and L_z to determine the orbit. For a time-like orbit with four-velocity u^a , $g_{ab} u^a u^b = -1$, we have that

$$\left(\frac{dr}{d\lambda} \right)^2 = V(r), \quad (3.42)$$

where the effective potential $V(r)$ is given by

$$V(r) = \frac{(E - \alpha L_z r)^2}{M^4 v_1^2(\theta_0)} - \frac{r^2}{M^2 v_1(\theta_0)} - \frac{L_z^2 r^2}{M^4 \beta^2 v_1(\theta_0) v_2(\theta_0)}. \quad (3.43)$$

Solving for the conditions of circular motion, we obtain

$$E = 0, \quad L_z = \pm \frac{M \beta \sqrt{v_1(\theta_0) v_2(\theta_0)}}{\sqrt{-v_1(\theta_0) + \alpha^2 \beta^2 v_2(\theta_0)}}. \quad (3.44)$$

The corresponding circular orbits $r = r_0$ are all marginally stable, i.e. $V''(r)|_{r=r_0} = 0$. After integrating out the azimuthal motion we also obtain that $\phi = \phi_0 + \omega_\phi t$, where the angular frequency ω_ϕ is given by

$$\omega_\phi = \left(\alpha - \frac{v_1(\theta_0)}{\alpha \beta^2 v_2(\theta_0)} \right) r_0. \quad (3.45)$$

The fact that all circular equatorial orbits are essentially the same, with a different angular frequency, is due to the dilation symmetry of the spacetime. That is, the metric is invariant under $r \rightarrow cr$ and $t \rightarrow t/c$ for any constant $c \in (0, +\infty)$. As a result, in Eq. (3.45), the radius-frequency relationship has to be compatible with the dilation symmetry.

Plugging in the D²CS solutions, we find the angular frequency of the equatorial circular orbits to be

$$\omega_\phi^{\text{D}^2\text{CS}} = \left[-\frac{3}{4} + \frac{25}{128} \left(\frac{\ell_{\text{CS}}}{GM} \right)^4 + \mathcal{O}(\varepsilon^3) \right] r_0. \quad (3.46)$$

Similarly for the D²GB solutions, the angular frequency is found to be

$$\omega_\phi^{\text{D}^2\text{GB}} = \left(-\frac{3}{4} + \mathcal{O}(\varepsilon^3) \right) r_0. \quad (3.47)$$

Therefore at the leading order in the metric perturbations, EdGB-type interactions do not lead to corrections to the angular frequency of circular equatorial orbits in an extremal black hole, in the near-horizon limit.

Again, because our time differs from the time coordinate in the asymptotic region, these frequencies are not the asymptotically observable orbital frequencies. Such observable quantities were computed for slowly-rotating BHs in D²CS in [65] and in D²GB in [70, 71, 87–89].

Location and area of deformed horizons

Since NHEK is not asymptotically flat, it does not have an event horizon. However, because of what the near-horizon limit is designed to do—to zoom in on the horizon region—the scaling limit of the Kerr event horizon gives rise to the horizon of the Poincaré patch. This Poincaré horizon has the same geometric properties as in Kerr, and thus it has the same area and entropy.

We can identify the location of this Killing horizon by considering observers whose world lines are along real linear combinations $c_t \partial_t + c_\phi \partial_\phi$, with c_t, c_ϕ real constants, such that their world lines are timelike. At the horizon, these world lines are forced to be null. For any metric of the NHEG form (3.16), the horizon is at $r = 0$. Therefore in attractor gauge, the coordinate location of the horizon is not deformed after including the scalar-gravity coupling in the action.

A cross section of the deformed-NHEK horizon is still homeomorphic to a two-sphere S^2 , but the total area has changed. Because the horizon is Killing, we can compute the area along any spatial cross section \mathcal{H} carrying coordinates x . The horizon areas of the two deformed solutions are both given by

$$\begin{aligned} A_{\text{deformed}} &= \oint_{\mathcal{H}} \sqrt{\gamma} d^2x \\ &= A_{\text{NHEK}} \times \left[1 + \eta \left(\frac{\ell}{GM} \right)^4 + \mathcal{O}(\varepsilon^3) \right], \end{aligned} \quad (3.48)$$

where ℓ is ℓ_{CS} or ℓ_{GB} when appropriate. Here γ is the determinant of the induced metric on \mathcal{H} . A_{NHEK} is the horizon area of an extremal Kerr black hole, which is given by $A_{\text{NHEK}} = 8\pi(GM)^2$. The constant η varies for the two deformed solutions. For D²CS and D²GB respectively we find

$$\begin{aligned} \eta_{\text{D}^2\text{CS}} &= (4875\sqrt{2} - 1380\pi - 3928) / 7680 \\ &\approx -0.18, \end{aligned} \quad (3.49)$$

$$\begin{aligned} \eta_{\text{D}^2\text{GB}} &= (1615\sqrt{2} - 300\pi - 464 - 320 \log 2) / 2560 \\ &\approx +0.26. \end{aligned} \quad (3.50)$$

Despite the fact that EdGB-deformed NHEK has a true curvature singularity, this singularity is integrable, leading to a finite correction to the horizon area.

Note that while considering deformed NHEK, the entropy no longer equals the horizon area, since the stringy interactions also contribute microscopic degrees of freedom. The horizon areas computed here will be used in the following subsection to calculate the entropy of the two deformed solutions.

Thermodynamics of horizons

The macroscopic entropy of a Killing horizon is interpreted as the Noether charge associated with the Killing vector field which generates the horizon [90, 91]. In any diffeomorphism invariant theory with a Lagrangian $\mathcal{L} = \mathcal{L}(\phi, \nabla_a \phi, g_{ab}, R_{abcd}, \nabla_e R_{abcd}, \dots)$, where ϕ is a matter field, the black hole entropy can be written as an integral over a horizon cross section \mathcal{H} [92]. Again, since the horizon is Killing, any spacelike cross section will do. This entropy integral is

$$S = -2\pi \oint_{\mathcal{H}} \frac{\delta \mathcal{L}}{\delta R_{abcd}} \hat{\epsilon}_{ab} \hat{\epsilon}_{cd} \bar{\epsilon}. \quad (3.51)$$

Here $\bar{\epsilon}$ is the induced volume form on the $D - 2$ dimensional cross section, and $\hat{\epsilon}_{ab}$ is the binormal. The binormal has been normalized such that $\hat{\epsilon}_{ab} \hat{\epsilon}^{ab} = -2$.

The NHEK solution does not have an event horizon; however, we can still get the correct entropy of the extremal black hole by performing the integral over the cross section of the Poincaré horizon. The entropy of the NHEK solution can then be obtained by evaluating Eq. (3.51) in Einstein-Hilbert theory $\mathcal{L} = \mathcal{L}_{\text{EH}}$. It is not surprising that we arrive at the Bekenstein-Hawking entropy for the extremal Kerr black hole [63, 93],

$$S_{\text{NHEK}} = 2\pi m_{\text{pl}}^2 A_{\text{NHEK}} = \frac{A_{\text{NHEK}}}{4G}. \quad (3.52)$$

Similarly in $D^2\text{CS}$ and $D^2\text{GB}$, by computing the entropy corrections due to stringy degrees of freedom, we will be able to obtain the entropies of the deformed-NHEK solutions in the two theories. Note, however, that the entropy results agree with the extremal BH solutions, since the Poincaré horizon is the scaling limit of the extremal BH event horizon. The corrections to the entropy are due to high-energy stringy degrees of freedom becoming activated.

In either $d\text{CS}$ or EdGB gravity, the scalar field Lagrangian \mathcal{L}_θ does not contribute to the entropy while the interaction term \mathcal{L}_{int} does. Therefore in a full theory with action given by Eq. (3.1), the entropy of a stationary black hole solution with horizon cross-section \mathcal{H} is

$$S = 2\pi m_{\text{pl}}^2 \oint_{\mathcal{H}} \bar{\epsilon} + S_{\text{int}}, \quad (3.53)$$

where we have defined S_{int} via

$$S_{\text{int}} = -2\pi \oint_{\mathcal{H}} \frac{\delta \mathcal{L}_{\text{int}}}{\delta R_{abcd}} \hat{\epsilon}_{ab} \hat{\epsilon}_{cd} \bar{\epsilon}. \quad (3.54)$$

Compared to Einstein gravity, $d\text{CS}$ - and EdGB -deformed NHEK receive entropy corrections from two sources: the deformation of the horizon area, and the string

interaction term S_{int} . In dCS theory, the correction to the entropy due to the scalar-gravity interaction term is given by

$$S_{\text{int}}^{\text{CS}} = \frac{\pi}{2} m_{\text{pl}} \ell_{\text{CS}}^2 \oint_{\mathcal{H}} \vartheta {}^*R^{abcd} \hat{\epsilon}_{ab} \hat{\epsilon}_{cd} \bar{\epsilon}. \quad (3.55)$$

Similarly, we find the correction to entropy via the EdGB interaction is

$$S_{\text{int}}^{\text{GB}} = \frac{\pi}{2} m_{\text{pl}} \ell_{\text{GB}}^2 \oint_{\mathcal{H}} \vartheta {}^*R^{*abcd} \hat{\epsilon}_{ab} \hat{\epsilon}_{cd} \bar{\epsilon}. \quad (3.56)$$

Now let us explore the effect of taking the decoupling limit and compute the leading order corrections to the entropy of extremal Kerr in D²CS and D²GB theories. The leading order scalar field is already at ε^1 while the metric perturbations correct at order ε^2 , thus we can evaluate Eqs. (3.55) and (3.56) using the original NHEK metric. Combining the horizon area calculations given by Eq. (3.48), the entropies of the two deformed NHEK solutions can both be written as

$$S_{\text{deformed}} = S_{\text{NHEK}} \left[1 + \xi \left(\frac{\ell}{GM} \right)^4 + \mathcal{O}(\varepsilon^3) \right], \quad (3.57)$$

where the constant ξ for D²CS and D²GB are given by

$$\begin{aligned} \xi_{\text{D}^2\text{CS}} &= (4875\sqrt{2} + 360\pi^2 - 868\pi - 3928) / 7680 \\ &\approx +0.49, \end{aligned} \quad (3.58)$$

$$\begin{aligned} \xi_{\text{D}^2\text{GB}} &= (360\pi^2 + 4845\sqrt{2} - 1392 - 960 \log 2 \\ &\quad - 4\pi(480 \log 2 - 607)) / 7680 \\ &\approx +1.54. \end{aligned} \quad (3.59)$$

Here as well, despite the EdGB scalar solution having a singularity at the poles, the singularity is integrable, leading to a finite correction to the entropy. Note that both entropy corrections are positive, as should be the case when adding new degrees of freedom to the underlying microscopic theory.

3.6 Discussion and future work

We have obtained analytic solutions for the linearized metric deformations to near-horizon extremal Kerr spacetimes as induced by dCS and EdGB interactions in the decoupling limit. In this limit, the metric deformations solve linearized Einstein equations with a source term arising from the dilaton or axion field and the background metric. We decomposed the metric perturbations using basis functions

adapted to the $SL(2, \mathbb{R}) \times U(1)$ isometry, and turn the systems of field equations into solvable ODEs. The resulting solution in D^2CS , *dCS-deformed NHEK*, is regular everywhere, while in D^2GB , *EdGB-deformed NHEK* has a true curvature singularity at the poles, discussed further below. We studied time-like orbits in these two newly found spacetimes. In particular, for circular equatorial orbits, we computed the leading order corrections to the angular frequencies, which are observables for sub-extremal black holes by gravitational wave experiments. Finally, we computed the corrections to the horizon areas and the macroscopic entropies of the extremal black hole solutions in D^2CS and D^2GB . The positive entropy corrections are related to the inclusion of new degrees of freedom in the theory.

EdGB-deformed NHEK is irregular at the poles $u = \pm 1$, no matter how we choose the constants of integration. This irregular behavior originates from the source term built from the dilaton field, since the dilaton has an unavoidable logarithmic singularity at the poles, as discussed in Sec. 3.4. This leads to a true curvature singularity, which can be seen as follows. We can find the singularity without solving for $\hat{h}^{(2)}$ by simply tracing the equation of motion Eq. (3.15). Since the background Ricci scalar and the first-order metric deformation both vanish ($\hat{R}^{(0)} = 0 = \hat{h}^{(1)}$), the deformation $\delta\hat{R}^{(2)}$ is a gauge-invariant quantity. Now, the uu component of the source tensor, $S_{ab}^{D^2GB}$, contains $(\partial_u \hat{\vartheta})^2$ and $\partial_u^2 \hat{\vartheta}$, which give a pole of order two at $u = \pm 1$. The inverse metric component g^{uu} only contributes a single zero at the poles. Thus the trace of the source term $g^{ab} S_{ab}^{D^2GB}$ blows up with a pole of order 1 at $u = \pm 1$, and we have an unavoidable curvature singularity.

This problem with extremal EdGB solutions was previously mentioned in [94] and discussed further in Appendix B of [74]. They presented numerical evidence and an analytic argument that the extremal limit does not admit regular solutions, for any values of the GB coupling parameter. Here, we have proven that there are no regular solutions, in the decoupling limit. While our analysis is restricted to the decoupling limit, based on the gauge-invariant argument above, we have proven that the extremal limit is indeed singular for EdGB.

We still lack a clear physical understanding of this curvature singularity. The simplest interpretation is that this is a sign of a breakdown of EdGB when treated as an EFT, and that this singularity is cured by the inclusion of operators at the same or higher order (such as those which were discarded in the truncation of [68]). This situation would be a counterexample to Hadar and Reall's recent claim that EFT does not break down at an extremal horizon [95].

Future work. The near-horizon near-extremal Kerr (near-NHEK) spacetime has the same $SL(2, \mathbb{R}) \times U(1)$ isometry as the NHEK spacetime. Therefore we expect all this work can be extended to near-NHEK directly. The techniques we used here can also be used for any other beyond-GR theory which has a continuous limit to GR. Therefore, we can also solve for deformed NHEK solutions in a broad class of theories. It may be possible to use matched asymptotic expansions to combine perturbation theory about (near-)NHEK and Schwarzschild, in order to build beyond-GR metric solutions valid for all values of spin, $0 \leq a \leq M$.

On the observational side, the angular frequencies of the near-extremal Kerr ISCO may be determined accurately in future gravitational wave experiments, providing a useful way to test general relativity.

Finally, this work may be helpful in understanding quantum theories beyond Einstein gravity. We have computed the macroscopic entropies of extremal black holes, which must be associated with corresponding microscopic entropies. This may be possible with an analog of the Kerr/CFT correspondence.

PART II

GEDANKEN EXPERIMENTS TO DESTROY THE EVENT HORIZON

Chapter 4

GEDANKEN EXPERIMENTS TO DESTROY AN EXTREMAL BLACK HOLE: FIRST-ORDER STUDY

We examine the weak cosmic censorship conjecture (WCCC) for the extremal charged black hole in possible generalizations of Einstein-Maxwell theory due to the higher-order corrections, up to fourth-derivative terms. Our derivation is based on Wald's gedanken experiment to destroy an extremal black hole. We find that, provided the null energy condition for the falling matter, the WCCC is preserved for all possible generalizations. Thus, the WCCC cannot serve as a constraint to the higher-order effective theories. We also show that up to first-order variations of black hole mass and charge, WCCC is preserved for nonrotating extremal black holes in all n -dimensional diffeomorphism-covariant theories of gravity and $U(1)$ gauge field.

4.1 Introduction

Even though the curvature singularity of a black hole is hidden behind the horizon, it might still be possible to throw charged or spinning matter into a black hole in particular ways that can destroy the horizon, revealing the singularity previously hidden inside. This kind of gedanken experiments was first proposed long ago by Wald [15] to test the so-called Weak Cosmic Censorship Conjecture (WCCC) [14], which asserts that the above gedanken experiments cannot succeed in order to prevent the singularity from being visible. Although the WCCC can be checked easily for extremal black holes, it is nontrivial to prove for near-extremal black holes [15, 16] and for general forms of matter. Recently, significant progress for the general proof of the WCCC has been made by Sorce and Wald [17] who adopted a general relativistic formulation of the energy conservation which can work for general forms of matter obeying the Null Energy Condition (NEC). In this way, they were able to avoid solving the complicated dynamical problems of the in-falling matter involving the self-force effect, and succeeded to show that the WCCC holds for the black holes in Einstein-Maxwell theory, up to second-order variation of the black hole's mass, charge, and angular momentum. Moreover, their method of examining the WCCC also provides a systematic framework for general theories other than Einstein-Maxwell.

One compelling reason to examine the WCCC for more general theories of gravity and electromagnetism is that the standard Einstein-Maxwell theory, which can be a good approximation at low energies, may need to be corrected at higher energies. In the low-energy Effective Field Theory (EFT), these quantum corrections can leave low-energy relics in the form of higher-order derivative terms beyond Einstein-Maxwell terms, modifying the black hole solutions, as well as the relativistic laws of the energy-momentum conservation. These terms may also make the WCCC fail. If we take the WCCC as a universal physical principle, then only those higher order EFTs that admit the WCCC should be accepted. This is in a similar spirit of using the weak gravity conjecture [96–98] which takes “gravity force is the weakest in nature” as a new physical principle to constrain the higher-order EFTs [97]. In this chapter, we would like to check to see if weak cosmic censorship can serve as a constraint on the EFTs with higher-derivative terms. By the end we will show that there is no constraint WCCC can put on the coupling coefficients of such EFTs. This calls for the further examination of preserving WCCC at the second-order variation for the EFTs considered ¹.

4.2 EFTs, black-hole solutions, and extremality condition

To demonstrate the power of the WCCC as a constraint to the EFTs, in this work we consider the most general quartic order corrections to Einstein-Maxwell theory, which is given by the following EFT action:

$$I = \int d^4x \sqrt{-g} \left(\frac{1}{2\kappa} R - \frac{1}{4} F_{\mu\nu} F^{\mu\nu} + \Delta L \right), \quad (4.1)$$

where ²

$$\begin{aligned} \Delta L = & c_1 R^2 + c_2 R_{\mu\nu} R^{\mu\nu} + c_3 R_{\mu\nu\rho\sigma} R^{\mu\nu\rho\sigma} \\ & + c_4 R F_{\mu\nu} F^{\mu\nu} + c_5 R_{\mu\nu} F^{\mu\rho} F^\nu{}_\rho + c_6 R_{\mu\nu\rho\sigma} F^{\mu\nu} F^{\rho\sigma} \\ & + c_7 F_{\mu\nu} F^{\mu\nu} F_{\rho\sigma} F^{\rho\sigma} + c_8 F_{\mu\nu} F^{\nu\rho} F_{\rho\sigma} F^{\sigma\mu}. \end{aligned} \quad (4.2)$$

We will assume c_i 's are small and restrict our consideration to $\mathcal{O}(c_i)$. The aforementioned self-interactions of four photons are the terms with coupling coefficient c_7 and c_8 respectively.

¹A technical error regarding (4.3) in the previous version of this work is pointed out by [99]. In this version we fix the error and reach the same results as in [99].

²We have neglected terms proportional to $\nabla^\mu F_{\mu\rho} \nabla_\nu F^{\nu\rho}$, as it does not affect the black hole metric or our parameter bound. Further note that terms like $(\nabla_\mu F_{\nu\rho})(\nabla^\mu F^{\nu\rho})$ and $(\nabla_\mu F_{\nu\rho})(\nabla^\nu F^{\mu\rho})$ can be recasted (up to some constant factor) into $\nabla^\mu F_{\mu\rho} \nabla_\nu F^{\nu\rho}$ plus existing terms in ΔL and an additional boundary term, upon using Bianchi identities, Ricci identities, and integrating by parts [100].

For simplicity, we will consider only the charged non-spinning black holes. The perturbative procedure of solving such black hole solutions has been outlined in [101], leading to a *family* of solutions parametrized by the mass and the charge (M, Q). Here we list some partial results relevant for our considerations³, namely the Maxwell gauge field

$$A_t = -\frac{q}{r} - \frac{q^3}{5r^5} \times \left[c_2 \kappa^2 + 4c_3 \kappa^2 + 10c_4 \kappa + c_5 \kappa - c_6 \kappa \left(9 - \frac{10mr}{q^2} \right) - 16c_7 - 8c_8 \right], \quad (4.3)$$

and the tt -component of the metric ⁴

$$\begin{aligned} -g_{tt} = & 1 - \frac{\kappa m}{r} + \frac{\kappa q^2}{2r^2} + c_2 \left(\frac{\kappa^3 m q^2}{r^5} - \frac{\kappa^3 q^4}{5r^6} - \frac{2\kappa^2 q^2}{r^4} \right) \\ & + c_3 \left(\frac{4\kappa^3 m q^2}{r^5} - \frac{4\kappa^3 q^4}{5r^6} - \frac{8\kappa^2 q^2}{r^4} \right) \\ & + c_4 \left(-\frac{6\kappa^2 m q^2}{r^5} + \frac{4\kappa^2 q^4}{r^6} + \frac{4\kappa q^2}{r^4} \right) \\ & + c_5 \left(\frac{4\kappa^2 q^4}{5r^6} - \frac{\kappa^2 m q^2}{r^5} \right) \\ & + c_6 \left(\frac{\kappa^2 m q^2}{r^5} - \frac{\kappa^2 q^4}{5r^6} - \frac{2\kappa q^2}{r^4} \right) \\ & + c_7 \left(-\frac{4\kappa q^4}{5r^6} \right) + c_8 \left(-\frac{2\kappa q^4}{5r^6} \right) + \mathcal{O}(c_i^2). \end{aligned} \quad (4.4)$$

Here we define the reduced mass $m \equiv M/4\pi$, the reduced charge $q \equiv Q/4\pi$ and $\kappa = 8\pi G_N$, where G_N is the gravitational constant. Note that in (4.4) there is no $\mathcal{O}(c_1)$ correction.

As shown by Ref. [101], as long as

$$m \geq \sqrt{\frac{2}{\kappa}} |q| \left(1 - \frac{4}{5q^2} c_0 \right), \quad (4.5)$$

the singularity of the space-time will be hidden by a horizon; more precisely, the *outer horizon* located at the outer-most solution of $g_{tt}(r_H) = 0$. Here

$$c_0 \equiv c_2 + 4c_3 + \frac{c_5}{\kappa} + \frac{c_6}{\kappa} + \frac{4c_7}{\kappa^2} + \frac{2c_8}{\kappa^2}, \quad (4.6)$$

and $c_0 \rightarrow 0$ recovers the Reissner-Nordstrom solution of Einstein-Maxwell. For a fixed m , as q increases to, and then exceeds, the critical value at which equality

³See Sec. I of the supplemental materials for the full explicit expressions.

⁴See Sec. II of the supplemental materials for the full expressions.

holds in (4.5), two horizons will merge and subsequently disappear, revealing the singularity. In this way, the *extremal solution* is defined by imposing equality in (4.5). This implicitly defines a function $q_{ext}(m)$ for the extremal solution. For each m , the horizon radius of the extremal solution is given by

$$r_H^{ext} = \frac{m\kappa}{2} + \frac{4}{5m} \left(c_2 + 4c_3 + \frac{10c_4 + c_5 + c_6}{\kappa} - \frac{16c_7 + 8c_8}{\kappa^2} \right). \quad (4.7)$$

On this extremal horizon, the electrostatic potential is

$$\Phi_H^{ext} = -(\xi^a A_a)|_{\mathcal{H}} = \sqrt{\frac{2}{\kappa}} \left(1 + \frac{4c'_0}{5q^2} \right), \quad (4.8)$$

where $\vec{\xi} = \vec{\partial}_t$ is the time-like Killing vector of the space-time, and

$$c'_0 = c_2 + 4c_3 + \frac{c_5}{\kappa} + \frac{c_6}{\kappa} + \frac{4c_7}{\kappa^2} + \frac{2c_8}{\kappa^2}. \quad (4.9)$$

One immediately notes that $c'_0 = c_0$, but we shall discuss the consequence later. We refer to (m, q) solutions that strictly satisfy the inequality (4.5) as *regular solutions*, those that take equality as *extremal solutions*, and those that violate the inequality as *singular solutions*. We may still refer to them as “black holes”—even though the horizon may or may not be destroyed.

4.3 Gedanken experiment to destroy the horizon

In gedanken experiments that attempt to destroy the horizon, e.g., as set up by Wald [15, 17], we shall always (if tacitly) assume stability of our family of solutions. That is, starting off with a regular solution (m, q) , as we “throw matter into” it, the final space-time geometry and field configuration will settle down to another solution *in our family*.

If our “way-of-throwing-matter”, for example described by the on-shell metric perturbations, field perturbations, and matter stress-energy tensor in the initial slice, is parameterized by w , then the final solution should be given by $(m(w), q(w))$.

In this language, the WCCC dictates that a starting regular solution (m, q) long before “throwing matter” will only lead to $(m(w), q(w))$ that are still regular. As a special case, let us now consider a starting extremal solution $(m, q_{ext}(m))$, and a particular approach of throwing matter, we can write

$$m(w) = m + w\delta m + O(w^2), \quad q(w) = q_{ext}(m) + w\delta q + O(w^2). \quad (4.10)$$

The condition for the starting extremal solution to not become singular, at first order in w , is given by

$$\delta m - \sqrt{\frac{2}{\kappa}} \left(1 + \frac{4c_0}{5q^2} \right) \delta q \geq 0. \quad (4.11)$$

We therefore need to find out whether physical laws in our modified theory imposes that (4.11) must hold for all infalling matter — or to find a particular way of throwing matter that violates (4.11). The advantage of starting off at the extremal solution is: once Eq. (4.11) is violated, then any infinitesimal w will lead to destruction of the horizon, and we can restrict ourselves to linear perturbation.

By contrast, starting from a non-extremal black hole with $(m, q_{ext}(m) - \epsilon)$, a *finite step size* for w must be made to surpass the extremality contour, and in this case the higher derivatives of $m(w)$ and $q(w)$ may become important, requiring the computation of higher-order variations. This was indeed the situation encountered by Hubeny [16], which was latter addressed by Sorce and Wald [17] by considering the second-order variations. Intuitively, one would expect the sub-extremal black holes will obey the WCCC if the extremal ones do, but the second-order variations are needed for a rigorous examination on the sub-extremal case. In this paper we shall restrict ourselves to the extremal black holes.

As it turns out, condition (4.11) coincides with the requirement that the horizon area must increase as matter fall into extremal black holes ⁵. More specifically, if we denote by $\mathcal{A}(m, q)$ the area of the horizon, then one can show that

$$\partial_m \mathcal{A}(m, q) / \partial_q \mathcal{A}(m, q) |_{q=q_{ext}(m)} = dq_{ext}(m) / dm, \quad (4.12)$$

and that $d\mathcal{A}(m + wdm, q_{ext}(m) + wdq) / dw = 0$ is equivalent to the equality in Eq. (4.11). In this way, the violation of condition (4.11), or the *destruction of the extremal horizon*, relies on the possibility of *area decrease* at linear order. This can be possible for the theories we consider even when the NEC is satisfied, because Raychaudhuri equation is now modified, and the NEC does not always lead to attractive gravity.

4.4 Test particle

For a regular solution (m, q) , consider a test particle with reduced mass δm_0 and reduced charge δq_0 , falling in from infinity. Using the *minimally coupled* action of

$$S_p = 4\pi \int d\tau (\delta m_0 - \delta q_0 \vec{u} \cdot \vec{A}), \quad (4.13)$$

⁵See Sec. IV of the supplemental materials for details

the reduced canonical momentum of the particle, $\vec{p} = \delta m_0 \vec{u} - \delta q_0 \vec{A}$, satisfies $\vec{\xi} \cdot \vec{p} = \text{const}$ along the particle's trajectory; at linear order in δm_0 and δq_0 , we do not have to consider the radiation reaction. Applying this to the particle at infinity and on the horizon, we obtain

$$\delta m_0(\vec{u}^H \cdot \vec{\xi}) - \Phi_H^c \delta q_0 = \delta m_0(\vec{u}^\infty \cdot \vec{\xi}) = -\delta E_\infty, \quad (4.14)$$

where \vec{u}^∞ and \vec{u}^H are the four-velocities of the particle at infinity and on the horizon, and we have used the fact that A_t does not depend on t , hence $\vec{\xi} \cdot \vec{A}$ vanishes at infinity.

For the final space-time, we assume that it still belongs to the same family, with $(m + \delta m, q + \delta q)$. We can argue from the charge conservation that $\delta q = \delta q_0$, and, from the conservation of ADM mass, as well as the fact that the energy of gravitational radiation emitted by the in-fall process is $\mathcal{O}(\delta m^2)$, that $\delta m = \delta E_\infty$: basically, *the charge and the energy of the particle are added to those of the black hole*. We will soon give a more rigorous justification, but with this in hand we can write

$$\delta m - \Phi_H^c \delta q = -\delta m_0(\vec{u}^H \cdot \vec{\xi}) \geq 0. \quad (4.15)$$

The latter inequality is because $\vec{u}^H \cdot \vec{\xi} \leq 0$: the 4-velocity of the particle must be pointed toward the future as the particle crosses the horizon. This can be saturated if the particle is able to rest right on top of the horizon. Inserting Eq. (4.8) into Eq. (4.15), we obtain the relation between δq and δm in this in-falling test particle situation:

$$\delta m \geq \sqrt{\frac{2}{\kappa}} \left(1 + \frac{4c'_0}{5q^2} \right) \delta q. \quad (4.16)$$

This is clearly the same as Eq. (4.11) since $c'_0 = c_0$. However, before discussing its consequences, we shall introduce the framework by Sorce and Wald, which provides more rigorous treatment of the energy conservation, and is able to treat more general infalling matter.

4.5 Sorce-Wald method for generic matter

We now sketch the method of Sorce and Wald developed in [17, 102]. We follow the notation of Wald, and denote by $\phi = (g_{ab}, A_a)$ the metric and field degrees of freedom. We start off with an extremal black hole, with $(m, q_{ext}(m))$, and define a Cauchy surface Σ_0 at early time, and a hypersurface Σ_1 which starts at sufficiently late time when the matter all fall in, and terminates at null infinity. We denote by \mathcal{H} the portion of the extremal horizon between Σ_0 and Σ_1 (see Fig. 4.1). We then apply perturbation $\delta\phi$, as well as matter, with stress-energy tensor δT_{ab} and electric

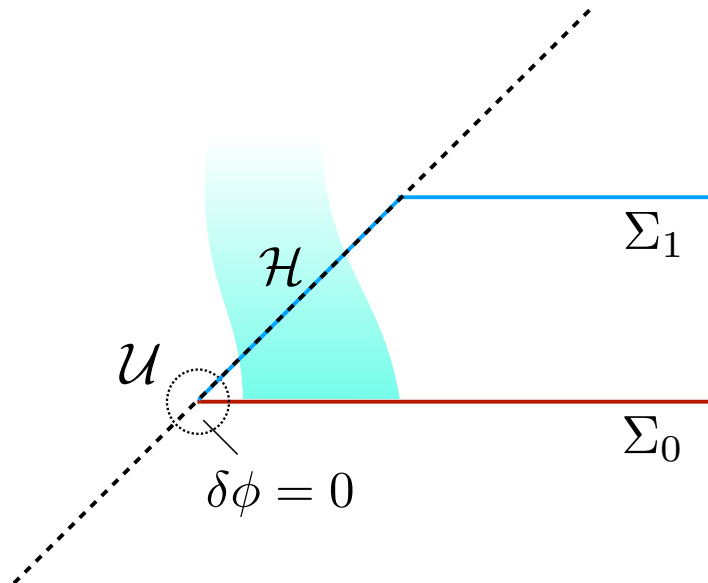


Figure 4.1: The gedanken experiment to destroy an extremal black hole. Charged matter, occupying the shaded region, crosses the \mathcal{H} portion of the extremal horizon.

current δj_a , also a form of perturbation, in an open neighborhood of Σ_0 . We will set up our initial value problem in such a way that $\delta\phi$, δT_{ab} and δj_a all vanish in an open neighborhood \mathcal{U} surrounding the intersection of \mathcal{H} and Σ_0 . In principle, $\delta\phi$ and δT_{ab} , δj_a should be evolved jointly into the future, but here we assume stability of our family of solutions, and therefore can impose that space-time geometry in an open neighborhood of Σ_1 is that of $(m + \delta m, q + \delta q)$ ⁶.

A general Noether method to derive the law of energy conservation for such an in-falling process is developed by Iyer and Wald [91], which we will briefly sketch as follows. Given a theory Lagrangian $L(\phi)$ of gravity and matter, we can introduce the Lagrangian 4-form $\mathbf{L} = L\epsilon$, where ϵ is the volume form associated with the metric. Then, variation of \mathbf{L} yields

$$\delta\mathbf{L} = \mathbf{E}(\phi)\delta\phi + d\mathbf{\Theta}(\phi, \delta\phi), \quad (4.17)$$

where $\mathbf{E}(\phi) = 0$ is Euler-Lagrangian equation, and $\mathbf{\Theta}(\phi, \delta\phi)$ is the symplectic

⁶We note that in general Σ_1 is only a portion of a ‘‘Cauchy surface’’ — with the remaining portion completed by a portion of the future null infinity. A Cauchy surface that ends at spatial infinity does not approach $(m + \delta m, q + \delta q)$, fast enough; its ADM mass is not equal to $m + \delta m$ either, because it contains the energy-momentum content of gravitational waves emitted during the in-fall process, see e.g. [102]. Sorce and Wald simply assumed that the late time solution is stable and non-radioactive to bypass the above concern [17]. On the other hand, in this paper we consider only the infall of matter into an extremal black hole for which the dynamics is non-radioactive, thus the above issue does not exist in our consideration.

potential three-form. For an arbitrary vector ξ^a , one can construct the associated Noether current $\mathbf{J}_\xi = \Theta(\phi, \mathcal{L}_\xi \phi) - i_\xi L$, which, because \mathbf{J}_ξ is conserved, i.e., $d\mathbf{J}_\xi = 0$, can be rewritten as $\mathbf{J}_\xi = d\mathbf{Q}_\xi + \xi^a \mathbf{C}_a$ with the 3-form constraint $\mathbf{C}_a = 0$ when equations of motion are satisfied. For instance, in Einstein-Maxwell theory, the 3-form constraint is given by

$$(\mathbf{C}_a)_{bcd} = \epsilon_{abcd}(T^e{}_a + j^e A_a), \quad (4.18)$$

with $T_{ab} = \frac{1}{\kappa}(G_{ab} - \kappa T_{ab}^{\text{EM}})$ the non-electromagnetic stress energy tensor, and $j^a = \nabla_b F^{ab}$ the charge current of the Maxwell source. Thus the on-shell condition $\mathbf{C}_a = 0$ gives the equations of motion $G_{ab} = \kappa T_{ab}^{\text{EM}}$ and $\nabla_b F^{ab} = 0$. The form (4.18) also holds when the higher-order derivative corrections ΔL are present. Assuming $\mathbf{E}(\phi) = 0$ and ξ^a is a Killing vector, i.e., $\mathcal{L}_\xi \phi = 0$, it is easy to show that $\delta\mathbf{J}_\xi = di_\xi \Theta(\phi, \delta\phi)$ which is then combined with $\delta\mathbf{J}_\xi = d\delta\mathbf{Q}_\xi + \xi^a \delta\mathbf{C}_a$, and is integrated over the hypersurface $\mathcal{H} \cup \Sigma_1$ to yield

$$\int_\infty [\delta\mathbf{Q}_\xi - i_\xi \Theta(\phi, \delta\phi)] = - \int_{\mathcal{H} \cup \Sigma_1} \xi^a \delta\mathbf{C}_a, \quad (4.19)$$

where we have used the Stoke's theorem to turn the 3-surface integral into the boundary integrals at the spatial infinity ∞ and at the intersection $\mathcal{H} \cap \Sigma_0$, by also imposing $\delta\phi = 0$ at $\mathcal{H} \cap \Sigma_0$.

If we assume ξ^a is the time-like Killing vector $t^a = (\partial_t)^a$ for non-spinning black holes, then we denote the change of the ADM mass as

$$\delta\mathcal{M} = \int_\infty [\delta\mathbf{Q}_\xi - i_\xi \Theta(\phi, \delta\phi)], \quad (4.20)$$

and the charge crossing the horizon as,

$$\delta Q \equiv \int_{\mathcal{H}} \epsilon_{abcd} \delta j^a, \quad (4.21)$$

where the electric current δj^a and the stress tensor $\delta T^a{}_b$ can be read off from the following on-shell relation ⁷

$$(\delta\mathbf{C}_a)_{bcd} = \epsilon_{abcd} (\delta T^e{}_a + A_a \delta j^e). \quad (4.22)$$

After combining all above and requiring vanishing of δj^e and $\delta T^e{}_a$ on Σ_1 as depicted in Fig. 4.1, we can turn (4.19) into the the following law of energy conservation for

⁷To arrive (4.22) we have imposed the on-shell conditions for the theory (4.29) along with the additional minimally coupled matter of stress tensor δT^{ab} and charge current δj^a .

the in-falling process of Wald's gedanken experiment,

$$\delta\mathcal{M} - \Phi_H^c \delta\mathcal{Q} = - \int_{\mathcal{H}} \epsilon_{abcd} \xi^a \delta T^e{}_a. \quad (4.23)$$

On horizon \mathcal{H} we can relate the 4-volume form ϵ to the 3-volume form $\tilde{\epsilon}$ by the relation $\epsilon_{abcd} = -4n_{[e}\tilde{\epsilon}_{bcd]}$ where n^e is the null vector normal to \mathcal{H} . Using this relation and the fact $\xi^a \propto n^a$ on \mathcal{H} , the R.H.S. of (4.23) turns into $4 \int_{\mathcal{H}} \tilde{\epsilon} \delta T_{ab} n^a n^b$, which is non-negative if matter's stress tensor obeys the NEC. Thus, the variational identity (4.23) becomes an inequality for matter obeying the NEC,

$$\delta\mathcal{M} - \Phi_H^c \delta\mathcal{Q} \geq 0. \quad (4.24)$$

This inequality serves as a constraint on the changes of the black hole's mass and charge for the in-falling process, and will be used to check the WCCC by comparing with the condition (4.11).

4.6 Parameter bounds from WCCC

The Noether method by Iyer and Wald provides a systematic way to calculate $\delta\mathcal{M}$ of (4.20) and $\delta\mathcal{Q}$ of (4.21) for general theory by evaluating Θ , \mathbf{Q} , and \mathbf{C}_a . For example, these quantities for Einstein-Maxwell theory have been derived in [91], and the results $\delta\mathcal{M} = 4\pi\delta m$ and $\delta\mathcal{Q} = 4\pi\delta q$ are then used to show that the WCCC holds for Einstein-Maxwell theory.

Here we apply the same method for our higher-order theory (4.29). The derivation is tedious but straightforward, and the result is given in the supplemental materials ⁸, based on which we can evaluate the corresponding $\delta\mathcal{M}$ and $\delta\mathcal{Q}$. As a result, we find that $\delta\mathcal{M} = 4\pi\delta m$ because the corrections due to higher-order Lagrangian ΔL fall off too quickly to contribute asymptotically to $\delta\mathcal{M}$. Similarly, we arrive $\delta\mathcal{Q} = 4\pi\delta q + O(c_i^2)$ after tedious calculations⁹. The results are consistent with the test particle case. Therefore, we conclude that (4.24), which holds for general forms of matter obeying the NEC, gives the same condition Eq. (4.16) as for the test particle.

⁸See Sec. III of the supplemental materials for the explicit expressions.

⁹This can also be seen as follows. By the construction of source theory, $j_a = \nabla^b(F_{ab} - S_{ab})$ in which S_{ab} is given in (5) of supplemental materials and is of $O(c_i)$, and using (3) of supplemental materials, $F_{ab} = F_{ab}^{(0,j)} + S_{ab} + O(c_i^2)$ where the superscript $(0, j)$ means to evaluate by plugging the background Reissner-Nordström configurations and keeping up to $O(c_i)$ terms. We then arrive $j_a = \nabla^b F_{ab}^{(0,j)} + O(c_i^2)$, and use the Gauss's law the integral $\mathcal{Q} = \int_{\mathcal{H}} \epsilon_{abcd} j^a = \int_B *F^{(0,j)} + O(c_i^2)$. Then, $\delta\mathcal{Q} = \int_B (*F^{(0,j)} - *F^{(0)}) + O(c_i^2) = \delta\mathcal{Q} + O(c_i^2)$, where $\delta\mathcal{Q} = 4\pi\delta q$ is the charge carried by the in-falling matter. Thus, $\delta\mathcal{Q} = 4\pi\delta q + O(c_i^2)$ is obtained.

Compare the energy condition (4.16) and the WCCC condition (4.11), it is not hard to see that we must have $c'_0 \geq c_0$ for the WCCC to hold for theory (4.29).

In our case, we simply have $c'_0 = c_0$, thus the WCCC is preserved no matter how we choose the coupling coefficients c_i . Thus there is no bound that one can put on these coefficients using the WCCC.

4.7 Extension to more general theories

We have shown that for the effective field theory with higher derivative terms, the WCCC is always preserved and it yields no bound on the coupling coefficients of the theory. This conclusion is still interesting in the following two aspects: (i) for near-extremal black holes, our result calls for check of WCCC at the quartic order for low-energy effective theories (EFTs) considered in this chapter; (ii) for extremal black holes, one might wonder whether WCCC holds for all other EFTs in general, i.e., whether c'_0 coincides with c_0 for a reason.

While more technical work is needed to clarify (i), definite conclusions can be drawn for (ii). More specifically, one can prove that WCCC is preserved for nonrotating extremal black holes in all n -dimensional diffeomorphism-covariant theories of gravity and $U(1)$ gauge field; this has also been done by Ref. [99].

As has been correctly argued in the paper, in order for matter to fall into the black hole we must have

$$\delta M - \Phi_H \delta Q \geq 0, \quad (4.25)$$

assuming that the infalling matter obeys the null energy condition. On the other hand, the condition for the extremal solution to not become singular, i.e, to preserve the WCCC, is given by

$$\delta M - \left(\frac{dM}{dQ} \right)_{\text{ext}} \delta Q \geq 0, \quad (4.26)$$

where $(dM/dQ)_{\text{ext}}$ is derivative taken along the extremal trajectory in the (M, Q) space. Here we have also assumed that $(dM/dQ)_{\text{ext}} > 0$ and that non-extremal black holes have $M > M_{\text{ext}}(Q)$. Some example violating these assumptions is discussed in [103], however, the associated physical implication is obscure.

We then write the first law of black hole thermodynamics for non-extremal black holes,

$$\delta M = T \delta S + \Phi_H \delta Q, \quad (4.27)$$

where S is the entropy of the black hole. As we approach the extremal solution, we have $T \rightarrow 0$, and

$$\left(\frac{dM}{dQ}\right)_{\text{ext}} = \Phi_H. \quad (4.28)$$

This relation can be verified explicitly for the quartic EFTs studied in this paper. Because of (4.25) and (4.28), (4.26) always holds and concludes our proof. Obviously, the above proof will not work for near-extremal cases because (4.28) does not hold.

In conclusion, no matter how we change the action of the EFTs, the condition for the matter falling into the extremal black hole always coincides with the condition for WCCC. Thus, WCCC for extremal black holes will not constrain the form of low energy EFTs. For near-extremal black holes, however, one needs to consider second-order variations of black hole mass and charge. It is still possible that after the second-order results are taken into consideration, the WCCC only permits a certain region of the parameter space. We shall leave the second-order calculations for the future work.

4.8 Appendix

Corrections to the Maxwell source and stress tensor

We consider the most general fourth-derivative higher-order corrections to Einstein-Maxwell theory, namely,

$$I = \int d^4x \sqrt{-g} \left(\frac{1}{2\kappa} R - \frac{1}{4} F_{\mu\nu} F^{\mu\nu} + \Delta L \right) \quad (4.29)$$

where

$$\begin{aligned} \Delta L = & c_1 R^2 + c_2 R_{\mu\nu} R^{\mu\nu} + c_3 R_{\mu\nu\rho\sigma} R^{\mu\nu\rho\sigma} \\ & + c_4 R F_{\mu\nu} F^{\mu\nu} + c_5 R_{\mu\nu} F^{\mu\rho} F^\nu{}_\rho + c_6 R_{\mu\nu\rho\sigma} F^{\mu\nu} F^{\rho\sigma} \\ & + c_7 F_{\mu\nu} F^{\mu\nu} F_{\rho\sigma} F^{\rho\sigma} + c_8 F_{\mu\nu} F^{\nu\rho} F_{\rho\sigma} F^{\sigma\mu}. \end{aligned} \quad (4.30)$$

The field equations obtained by the variation of the action (4.29) with respect to A_μ and $g^{\mu\nu}$ are given respectively by

$$\nabla_\nu (F^{\mu\nu} - S^{\mu\nu}) = 0, \quad (4.31)$$

and

$$R_{\mu\nu} - \frac{1}{2} g_{\mu\nu} R = \kappa T_{\mu\nu} = \kappa (\tilde{T}_{\mu\nu} + \Delta T_{\mu\nu}), \quad (4.32)$$

where $\tilde{T}_{\mu\nu} = F_{\mu}{}^\rho F_{\nu\rho} - \frac{1}{4} g_{\mu\nu} F_{\rho\sigma} F^{\rho\sigma}$ is the stress tensor of the Maxwell theory, and $\Delta T_{\mu\nu}$ and $S^{\mu\nu}$ are the corrections respectively to the stress tensor and Maxwell source field from the higher-dimension operators.

Here we list the details of the corrections to the Maxwell source field and stress tensor, i.e., $S^{\mu\nu}$ in Eq. (9) and $\Delta T_{\mu\nu}$ in Eq. (10) of the main text:

$$S^{\mu\nu} = 4c_4 R F^{\mu\nu} + 2c_5 (R^{\mu\rho} F_{\rho}{}^{\nu} - R^{\nu\rho} F_{\rho}{}^{\mu}) + 4c_6 R^{\mu\nu\rho\sigma} F_{\rho\sigma} + 8c_7 F_{\rho\sigma} F^{\rho\sigma} F^{\mu\nu} + 8c_8 F_{\rho\sigma} F^{\rho\nu} F^{\mu\sigma}, \quad (4.33)$$

and

$$\begin{aligned} \Delta T_{\mu\nu} = & c_1 (g_{\mu\nu} R^2 - 4R R_{\mu\nu} + 4\nabla_\nu \nabla_\mu R - 4g_{\mu\nu} \square R) + \\ & + c_2 (g_{\mu\nu} R_{\rho\sigma} R^{\rho\sigma} + 4\nabla_\alpha \nabla_\nu R_\mu^\alpha - 2\square R_{\mu\nu} - g_{\mu\nu} \square R - 4R_\mu^\alpha R_{\alpha\nu}) + \\ & + c_3 (g_{\mu\nu} R_{\alpha\beta\gamma\delta} R^{\alpha\beta\gamma\delta} - 4R_{\mu\alpha\beta\gamma} R_\nu{}^{\alpha\beta\gamma} - 8\square R_{\mu\nu} \\ & \quad + 4\nabla_\nu \nabla_\mu R + 8R_\mu^\alpha R_{\alpha\nu} - 8R^{\alpha\beta} R_{\mu\alpha\nu\beta}) + \\ & + c_4 (g_{\mu\nu} R F^2 - 4R F_\mu{}^\sigma F_{\nu\sigma} - 2F^2 R_{\mu\nu} + 2\nabla_\mu \nabla_\nu F^2 - 2g_{\mu\nu} \square F^2) + \\ & + c_5 (g_{\mu\nu} R^{\kappa\lambda} F_{\kappa\rho} F_{\lambda}{}^\rho - 4R_{\nu\sigma} F_{\mu\rho} F^{\sigma\rho} - 2R^{\alpha\beta} F_{\alpha\mu} F_{\beta\nu}) \\ & \quad - g_{\mu\nu} \nabla_\alpha \nabla_\beta (F^\alpha{}_\rho F^{\beta\rho} + 2\nabla_\alpha \nabla_\nu (F_{\mu\beta} F^{\alpha\beta}) - \square (F_{\mu\rho} F_\nu{}^\rho)) + \\ & + c_6 (g_{\mu\nu} R^{\kappa\lambda\rho\sigma} F_{\kappa\lambda} F_{\rho\sigma} - 6F_{\alpha\nu} F^{\beta\gamma} R^\alpha{}_{\mu\beta\gamma} - 4\nabla_\beta \nabla_\alpha (F^\alpha{}_\mu F^\beta{}_\nu)) + \\ & + c_7 (g_{\mu\nu} (F^2)^2 - 8F^2 F_\mu{}^\sigma F_{\nu\sigma}) + \\ & + c_8 (g_{\mu\nu} F^{\rho\kappa} F_{\rho\sigma} F^{\sigma\lambda} F_{\kappa\lambda} - 8F_\mu{}^\rho F_\nu{}^\sigma F_\rho{}^\kappa F_{\sigma\kappa}). \end{aligned} \quad (4.34)$$

Note that $F^2 = F_{\rho\sigma} F^{\rho\sigma}$ and $\square = \nabla_a \nabla^a$.

Corrections to the Reissner-Nordström black hole

The functions $\lambda(r)$ and $\nu(r)$ are related to the components of Ricci curvature tensor $R_{\mu\nu}$ via

$$\begin{aligned} \frac{1}{2} (R_t^t - R_r^r) - R_\theta^\theta &= \frac{1}{r^2} \frac{d}{dr} [r(e^{-\lambda(r)} - 1)], \\ R_t^t - R_r^r &= -\frac{e^{-\lambda(r)}}{r} [\nu'(r) + \lambda'(r)]. \end{aligned} \quad (4.35)$$

To solve for λ and ν explicitly, we need an additional boundary condition. Assuming that at $r \rightarrow \infty$ the metric approaches the Schwarzschild solution, the results are then given by

$$\begin{aligned} e^{-\lambda(r)} &= 1 - \frac{\kappa M}{4\pi r} - \frac{1}{r} \int_r^\infty dr r^2 \left[\frac{1}{2} (R_t^t - R_r^r) - R_\theta^\theta \right], \\ \nu(r) &= -\lambda(r) + \int_r^\infty dr r (R_t^t - R_r^r) e^{\lambda(r)}. \end{aligned} \quad (4.36)$$

We further take the trace-reverse of Eq. (10) from the main text and obtain that

$$R_{\mu\nu} = \kappa \left(T_{\mu\nu} - \frac{1}{2} T g_{\mu\nu} \right), \quad (4.37)$$

where T is the trace of the total energy-momentum tensor $T_{\mu\nu}$, and is given by $T = T_t^t + T_r^r + 2T_\theta^\theta$. Plugging the trace-reversed Einstein field equation into the integral expression (4.36), we get

$$\begin{aligned} e^{-\lambda(r)} &= 1 - \frac{\kappa M}{4\pi r} - \frac{\kappa}{r} \int_r^\infty dr r^2 T_t^t, \\ \nu(r) &= -\lambda(r) + \kappa \int_r^\infty dr r (T_t^t - T_r^r) e^{\lambda(r)}. \end{aligned} \quad (4.38)$$

Once we know the diagonal components of the energy-momentum tensor, it will be straightforward to compute the corrections to the spherically symmetric static spacetime as induced by $T_{\mu\nu}$.

We now take our background spacetime to be Reissner-Nordström black hole in four-dimension. That is,

$$\begin{aligned} e^{\nu^{(0)}} = e^{-\lambda^{(0)}} &= 1 - \frac{\kappa M}{4\pi r} + \frac{\kappa Q^2}{32\pi^2 r^2}, \\ F_{\mu\nu}^{(0)} dx^\mu \wedge dx^\nu &= \frac{Q}{4\pi r^2} dt \wedge dr. \end{aligned} \quad (4.39)$$

Here $\nu^{(0)}(r)$ and $\lambda^{(0)}(r)$ refer to the metric components in the unperturbed black hole spacetime, and $F_{\mu\nu}^{(0)}$ is the background electromagnetic energy-momentum tensor. Considering the action in Eq. (2) of the main text, we treat the corrections from higher-dimension operators as perturbations. For convenience, we also introduce a power counting parameter ε , and consider a one-parameter family of actions I_ε , which is given by

$$I_\varepsilon = \int d^4x \sqrt{-g} (L_0 + \varepsilon \Delta L). \quad (4.40)$$

The original action will be recovered after setting $\varepsilon = 1$. We then expand everything into powers series in ε . For instance,

$$g_{\mu\nu} = g_{\mu\nu}^{(0)} + \varepsilon h_{\mu\nu}^{(1)} + \mathcal{O}(\varepsilon^2), \quad F_{\mu\nu} = F_{\mu\nu}^{(0)} + \varepsilon f_{\mu\nu}^{(1)} + \mathcal{O}(\varepsilon^2). \quad (4.41)$$

At order ε^1 , the stress energy tensor is given by

$$T_{\mu\nu}^{(1)} = \tilde{T}_{\mu\nu}[g^{(0)}, f^{(1)}, F^{(0)}] + \tilde{T}_{\mu\nu}[h^{(1)}, F^{(0)}, F^{(0)}] + \Delta T_{\mu\nu}[g^{(0)}, F^{(0)}]. \quad (4.42)$$

Noting that in order to compute the corrections to the metric, we need to calculate $T_\mu{}^\nu$ instead of $T_{\mu\nu}$. At order ε^1 , $T_\mu{}^\nu{}^{(1)}$ is given by

$$T_\mu{}^\nu{}^{(1)} = \tilde{T}_\mu{}^\nu[g^{(0)}, F^{(1)}] + \Delta T_\mu{}^\nu[g^{(0)}, F^{(0)}]. \quad (4.43)$$

We solve for the corrections to Maxwell equations, and obtain that the gauge field A_a is given by

$$A_t = -\frac{q}{r} - \frac{q^3}{5r^5} \times \left[c_2 \kappa^2 + 4c_3 \kappa^2 + 10c_4 \kappa + c_5 \kappa - c_6 \kappa \left(9 - \frac{10mr}{q^2} \right) - 16c_7 - 8c_8 \right], \quad (4.44)$$

$$A_r = A_\theta = A_\phi = 0 \quad (4.45)$$

With the new A_μ , we can solve for the corrected energy-momentum tensor $T_\mu{}^{\nu(1)}$.

We then find the corrected metric tensor component to be

$$\begin{aligned} e^{-\lambda} = & 1 - \frac{\kappa m}{r} + \frac{\kappa q^2}{2r^2} + c_2 \left(\frac{3\kappa^3 m q^2}{r^5} - \frac{6\kappa^3 q^4}{5r^6} - \frac{4\kappa^2 q^2}{r^4} \right) \\ & + c_3 \left(\frac{12\kappa^3 m q^2}{r^5} - \frac{24\kappa^3 q^4}{5r^6} - \frac{16\kappa^2 q^2}{r^4} \right) + c_4 \left(\frac{14\kappa^2 m q^2}{r^5} - \frac{6\kappa^2 q^4}{r^6} - \frac{16\kappa q^2}{r^4} \right) \\ & + c_5 \left(\frac{5\kappa^2 m q^2}{r^5} - \frac{11\kappa^2 q^4}{5r^6} - \frac{6\kappa q^2}{r^4} \right) + c_6 \left(\frac{7\kappa^2 m q^2}{r^5} - \frac{16\kappa^2 q^4}{5r^6} - \frac{8\kappa q^2}{r^4} \right) \\ & + c_7 \left(-\frac{4\kappa q^4}{5r^6} \right) + c_8 \left(-\frac{2\kappa q^4}{5r^6} \right), \end{aligned}$$

$$\begin{aligned} e^{+\nu} = & 1 - \frac{\kappa m}{r} + \frac{\kappa q^2}{2r^2} + c_2 \left(\frac{\kappa^3 m q^2}{r^5} - \frac{\kappa^3 q^4}{5r^6} - \frac{2\kappa^2 q^2}{r^4} \right) \quad (4.46) \\ & + c_3 \left(\frac{4\kappa^3 m q^2}{r^5} - \frac{4\kappa^3 q^4}{5r^6} - \frac{8\kappa^2 q^2}{r^4} \right) + c_4 \left(-\frac{6\kappa^2 m q^2}{r^5} + \frac{4\kappa^2 q^4}{r^6} + \frac{4\kappa q^2}{r^4} \right) \\ & + c_5 \left(\frac{4\kappa^2 q^4}{5r^6} - \frac{\kappa^2 m q^2}{r^5} \right) + c_6 \left(\frac{\kappa^2 m q^2}{r^5} - \frac{\kappa^2 q^4}{5r^6} - \frac{2\kappa q^2}{r^4} \right) \\ & + c_7 \left(-\frac{4\kappa q^4}{5r^6} \right) + c_8 \left(-\frac{2\kappa q^4}{5r^6} \right). \quad (4.47) \end{aligned}$$

We have defined the reduced quantities $m = M/4\pi$ and $q = Q/4\pi$. Note that the R^2 -term in the action has no contributions to the equation of motion at leading order in ε . The contributions from $R_{\mu\nu}R^{\mu\nu}$ and $R_{\mu\nu\rho\theta}R^{\mu\nu\rho\theta}$ can be canceled out by choosing $c_2 = -4c_3$. This directly confirms that the Gauss-Bonnet term is a topological invariant and does not influence the equation of motion. Due to the fact that only the tr - and rt -component of $F_{\mu\nu}$ are nonzero, the term $F_{\mu\nu}F^{\mu\nu}F_{\rho\sigma}F^{\rho\sigma}$ always has twice the contributions from $F_{\mu\nu}F^{\nu\rho}F_{\rho\sigma}F^{\sigma\mu}$ towards the equation of motion.

Explicit forms of Q_ξ and C_a for the higher theory

The Lagrangian four-form L for the higher theory can be written as $L = L_0 + \sum_i c_i L_i$. In this appendix, by following the canonical method developed by Iyer and Wald,

we derive and present the Noether charge and constraint associated with each term in L .

Variation of the Lagrangian 4-form L_0 yields

$$\delta L_0 = \delta g_{ab} \left(-\frac{1}{2\kappa} G_{ab} + \frac{1}{2} T_{ab}^{\text{EM}} \right) \epsilon + \delta A_a \left(\nabla_b F^{ba} \right) \epsilon + \mathbf{d}\Theta_0, \quad (4.48)$$

where $G_{ab} = R_{ab} - \frac{1}{2}g_{ab}R$ is the Einstein tensor, and T_{ab}^{EM} is the electro-magnetic stress-energy tensor, which is defined by

$$T_{ab}^{\text{EM}} = F_{ac}F_b{}^c - \frac{1}{4}g_{ab}F_{de}F^{de}. \quad (4.49)$$

The symplectic potential can be written as

$$\Theta_0 = \Theta^{\text{GR}} + \Theta^{\text{EM}}, \quad (4.50)$$

where

$$\Theta_{abc}^{\text{GR}}(\phi, \delta\phi) = \frac{1}{2\kappa} \epsilon_{dabc} g^{de} g^{fg} \left(\nabla_g \delta g_{ef} - \nabla_e \delta g_{fg} \right), \quad (4.51)$$

$$\Theta_{abc}^{\text{EM}}(\phi, \delta\phi) = -\epsilon_{dabc} F^{de} \delta A_e. \quad (4.52)$$

Let ξ^a be any smooth vector field on the spacetime. We find that the Noether charges associated with the vector field are respectively,

$$\left(Q_{\xi}^{\text{GR}} \right)_{ab} = -\frac{1}{2\kappa} \epsilon_{abcd} \nabla^c \xi^d, \quad (4.53)$$

$$\left(Q_{\xi}^{\text{EM}} \right)_{ab} = -\frac{1}{2} \epsilon_{abcd} F^{cd} A_e \xi^e. \quad (4.54)$$

The equations of motion and constraints are given by

$$E_0 \delta\phi = -\epsilon \left(\frac{1}{2} T^{ab} \delta g_{ab} + j^a \delta A_a \right), \quad (4.55)$$

$$C_{bcda} = \epsilon_{ebcd} \left(T^e{}_a + j^e A_a \right), \quad (4.56)$$

where we have defined $T_{ab} = \frac{1}{\kappa} \left(G_{ab} - \kappa T_{ab}^{\text{EM}} \right)$ as the non-electromagnetic stress energy tensor, and $j^a = \nabla_b F^{ab}$ is the charge-current of the Maxwell sources.

We similarly obtain the Noether charges and constraints for all higher-derivative terms. The results are presented below.

L_1 Variation of L_1 yields

$$\delta L_1 = \delta g_{ab}(E_1)^{ab} \epsilon + \mathbf{d}\Theta_1, \quad (4.57)$$

where we have defined

$$(E_1)^{ab} = \frac{1}{2}g^{ab}R^2 - 2RR^{ab} + 2\nabla^b\nabla^a R - 2g^{ab}\nabla_c\nabla^c R. \quad (4.58)$$

The Noether charge associated with the vector field ξ^a is

$$(Q_\xi^1)_{ab} = \epsilon_{abcd} \left(-4\xi^c \nabla^d R + 2R \nabla^d \xi^c \right). \quad (4.59)$$

The constraints are given by

$$C_{bcda} = -2\epsilon_{ebcd} (E_1)^e{}_a. \quad (4.60)$$

L_2 Variation of L_2 yields

$$\delta L_2 = \delta g_{ab}(E_2)^{ab} \epsilon + \mathbf{d}\Theta_2, \quad (4.61)$$

where we have defined

$$(E_2)^{ab} = \frac{1}{2}g^{ab}R_{cd}R^{cd} + \nabla_c\nabla^b R^{ac} + \nabla_c\nabla^a R^{bc} - g^{ab}\nabla_d\nabla_c R^{cd} - \nabla^c\nabla_c R^{ab} - 2R^{ac}R^b{}_c. \quad (4.62)$$

The Noether charge associated with the vector field ξ^a is

$$(Q_\xi^2)_{ab} = \epsilon_{abcd} \left(4\xi^{[f} \nabla^{c]} R_f{}^d + R_f{}^d \nabla^f \xi^c + R_f{}^c \nabla^d \xi^f \right). \quad (4.63)$$

The constraints are given by

$$C_{bcda} = -2\epsilon_{ebcd}(E_2)^e{}_a. \quad (4.64)$$

L_3 Variation of L_3 yields

$$\delta L_3 = \delta g_{abc_3}(E_3)^{ab} \epsilon + \mathbf{d}\Theta_3, \quad (4.65)$$

where we have defined

$$(E_3)^{ab} = \frac{1}{2}g^{ab}R^2 + 2g^{ab}R_{cd}R^{cd} + 2R^{ab}R - 8R_{cd}R^{acbd} + 2\nabla^b\nabla^a R - 4\Box R^{ab}. \quad (4.66)$$

The Noether charge associated with the vector field ξ^a is

$$(Q_\xi^3)_{ab} = \epsilon_{abcd} \left(-4\xi^e \nabla_f R_e{}^{fcd} + 2R_{ef}{}^{cd} \nabla^f \xi^e \right). \quad (4.67)$$

The constraints are given by

$$C_{bcda} = -2\epsilon_{ebcd}(E_3)^e{}_a. \quad (4.68)$$

L_4 Variation of L_4 yields

$$\delta L_4 = \delta g_{ab}(E_4^g)^{ab} \epsilon + \delta A_a (E_4^A)^a \epsilon + \mathbf{d}\Theta_4, \quad (4.69)$$

where we have defined the equations of motion for g_{ab} and A_a respectively as

$$(E_4^g)^{ab} = \left[-R^{ab} + \frac{1}{2} g^{ab} R - g^{ab} \nabla^2 + \nabla^{(a} \nabla^{b)} \right] F^2 - 2RF^{ac} F_b{}^c, \quad (4.70)$$

$$(E_4^A)^a = 4\nabla_b (RF^{ab}). \quad (4.71)$$

The Noether charge associated with the vector field ξ^a is

$$(Q_\xi^4)_{ab} = \epsilon_{abcd} \left(F^2 \nabla^d \xi^c - 2\xi^c \nabla^d F^2 + 2RF^{cd} A_e \xi^e \right). \quad (4.72)$$

The constraints are given by

$$C_{bcda} = -2\epsilon_{ebcd} (E_4^g)^e{}_a - \epsilon_{ebcd} (E_4^A)^e A_a. \quad (4.73)$$

L_5 Variation of L_5 yields

$$\delta L_5 = \delta g_{ab}(E_5^g)^{ab} \epsilon + \delta A_a (E_5^A)^a \epsilon + \mathbf{d}\Theta_5, \quad (4.74)$$

where we have defined the equations of motion for g_{ab} and A_a respectively as

$$(E_5^g)^{ab} = 2F^{(bc} F_c{}^d R^a){}_d - F^{ac} F^{bd} R_{cd} + \frac{1}{2} F_c{}^e F^{cd} g^{ab} R_{de} \quad (4.75)$$

$$- \nabla^{(a} F^{b)c} \nabla_d F_c{}^d - F^{cd} \nabla_d \nabla^{(a} F^{b)}{}_c - F^{(bc} \nabla_d \nabla^a) F_c{}^d - F^{(bc} \square F^a){}_c$$

$$- \nabla^{(b} F_{cd} \nabla^d F^a){}_c - F^{cd} g^{ab} \nabla_{(d} \nabla_e) F_c{}^e - \nabla_d F^b{}_c \nabla^d F^{ac}$$

$$+ \frac{1}{2} g^{ab} \nabla_c F^{cd} \nabla_e F_d{}^e - \frac{1}{2} g^{ab} \nabla_d F_{ce} \nabla^e F^{cd},$$

$$(E_5^A)^a = 2\nabla_c (R^{bc} F^a{}_b + F^{bc} R^a{}_b). \quad (4.76)$$

The Noether charge associated with the vector field ξ^a is

$$(Q_\xi^5)_{ab} = \epsilon_{abcd} \left[-2\xi^e A_e F^{fc} R_f{}^d - 2\xi^c F^{f(e} \nabla_e F_f{}^d) + \xi^e \nabla^d (F^{fc} F_{ef}) + F_f{}^d F_e{}^f \nabla^{[c} \xi^{e]} \right]. \quad (4.77)$$

The constraints are given by

$$C_{bcda} = -2\epsilon_{ebcd} (E_5^g)^e{}_a - \epsilon_{ebcd} (E_5^A)^e A_a. \quad (4.78)$$

L_6 Variation of L_6 yields

$$\delta L_6 = \delta g_{ab}(E_6^g)^{ab} \epsilon + \delta A_a (E_6^A)^a \epsilon + \mathbf{d}\Theta_6, \quad (4.79)$$

where we have defined the equations of motion for g_{ab} and A_a respectively as

$$(E_6^g)^{ab} = \frac{1}{2} F^{cd} F^{ef} g^{ab} R_{cdef} - 3F^{(ac} F^{de} R^b)_{cde} \quad (4.80)$$

$$\begin{aligned} & - 2F^{(ac} \nabla_c \nabla_d F^{b)d} - 2F^{(ac} \nabla_d \nabla_c F^{b)d} - 4\nabla_c F^{(ac} \nabla_d F^{b)d}, \\ (E_6^A)^a & = 4\nabla_d (F^{bc} R^{ad}_{bc}). \end{aligned} \quad (4.81)$$

The Noether charge associated with the vector field ξ^a is

$$(Q_\xi^6)_{ab} = \epsilon_{abcd} \left[2\xi^e A_e F^{fg} R_{fg}{}^{cd} - 2\xi^e \nabla_f (F^{cd} F_e{}^f) + F^{cd} F_{ef} \nabla^f \xi^e \right]. \quad (4.82)$$

The constraints are given by

$$C_{bcda} = -2\epsilon_{ebcd} (E_6^g)^e{}_a - \epsilon_{ebcd} (E_6^A)^e A_a. \quad (4.83)$$

L_7 Variation of L_7 yields

$$\delta L_7 = \delta g_{ab}(E_7^g)^{ab} \epsilon + \delta A_a (E_7^A)^a \epsilon + \mathbf{d}\Theta_7, \quad (4.84)$$

where we have defined the equations of motion for g_{ab} and A_a respectively as

$$(E_7^g)^{ab} = \frac{1}{2} g^{ab} F^2 F^2 - 4F^{ac} F^b{}_c F^2, \quad (4.85)$$

$$(E_7^A)^a = 8\nabla_b (F^{ab} F^2). \quad (4.86)$$

The Noether charge associated with the vector field ξ^a is

$$(Q_\xi^7)_{ab} = \epsilon_{abcd} (4\xi^e A_e F^{cd} F^2). \quad (4.87)$$

The constraints are given by

$$C_{bcda} = -2\epsilon_{ebcd} (E_7^g)^e{}_a - \epsilon_{ebcd} (E_7^A)^e A_a. \quad (4.88)$$

L_8 Variation of L_8 yields

$$\delta L_8 = \delta g_{ab}(E_8^g)^{ab} \epsilon + \delta A_a (E_8^A)^a \epsilon + \mathbf{d}\Theta_8, \quad (4.89)$$

where we have defined the equations of motion for g_{ab} and A_a respectively as

$$(E_8^g)^{ab} = \frac{1}{2} g^{ab} F_c^d F_d^e F_e^f F_f^c - 4F^{ac} F^{bd} F_c^e F_{de}, \quad (4.90)$$

$$(E_8^A)^a = -8\nabla_d (F^a{}_b F^b{}_c F^{cd}). \quad (4.91)$$

The Noether charge associated with the vector field ξ^a is

$$(Q_\xi^8)_{ab} = \epsilon_{abcd} (4\xi^e A_e F_f^d F_g^c F^{gf}). \quad (4.92)$$

The constraints are given by

$$C_{bcda} = -2\epsilon_{ebcd} (E_8^g)^e{}_a - \epsilon_{ebcd} (E_8^A)^e A_a. \quad (4.93)$$

Finally, the above results can be summarized in the following compact form:

$$(\mathbf{Q}_\xi)_{c_3c_4} = \epsilon_{abc_3c_4} (M^{abc} \xi_c - E^{abcd} \nabla_{[c} \xi_{d]}), \quad (4.94)$$

where

$$M^{abc} \equiv -2\nabla_d E^{abcd} + E_F^{ab} A^c, \quad (4.95)$$

and

$$(\mathbf{C}^d)_{abc} = \epsilon_{eabc} (2E^{pqre} R_{pqr}{}^d + 4\nabla_f \nabla_h E^{efdh} + 2E_F^{eh} F^d{}_h - 2A^d \nabla_h E_F^{eh} - g^{ed} \mathbf{L}) \quad (4.96)$$

with

$$E^{abcd} \equiv \frac{\delta \mathbf{L}}{\delta R_{abcd}}, \quad E_F^{ab} \equiv \frac{\delta \mathbf{L}}{\delta F_{ab}}. \quad (4.97)$$

Proof that constant area direction is along the extremality curve

Suppose the radius, hence area A of the horizon is determined implicitly by the following equation

$$F(M, Q, A) = 0. \quad (4.98)$$

The extremality condition requires, in addition, that

$$\partial_A F(M, Q, A) = 0. \quad (4.99)$$

This is because the two roots of $1/g_{rr}$ coincide at this location.

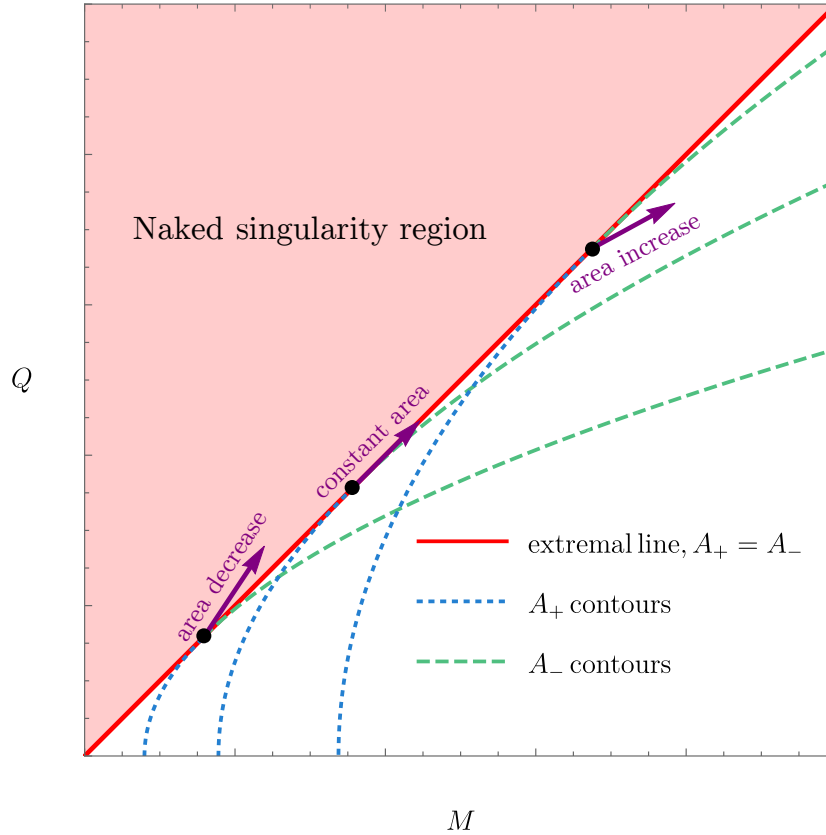


Figure 4.2: Extremality contour and constant area contours. Extremal black holes live on the red solid line which divides the whole parameter space into the naked singularity region and the non-extremal black hole region. The constant area contours are always tangent to the extremal line. A small perturbation around an extremal point then shifts the spacetime to one of the following: (i) a naked singularity when the horizon area is decreased; (ii) another extremal solution when the area is unchanged; and (iii) a nonextremal black hole when the area is increased.

Extremal black holes are of a one-parameter family, with $Q_{\text{ext}}(M)$, $A_{\text{ext}}(M)$ determined jointly by Eqs. (4.98) and (4.99). In practice, when $Q < Q_{\text{ext}}(M)$, we will have contours of constant A (as shown in Fig. 6.4), determined by

$$\partial_M F dM + \partial_Q F dQ = 0, \quad (4.100)$$

or

$$(dQ/dM)_A = -\partial_M F / \partial_Q F. \quad (4.101)$$

On the other hand, we can find out the direction of the extremality curve in the (M, Q, A) space. The tangent vector satisfies

$$\partial_M F \Delta M + \partial_Q F \Delta Q + \partial_A F \Delta A = 0. \quad (4.102)$$

However, because we have $\partial_A F$ on that curve, we have $\partial_A F = 0$ and also

$$(dQ/dM)_{ext} = -\partial_M F / \partial_Q F . \quad (4.103)$$

This means, on the extremality contour, the direction at which area remains constant is the same as the contour itself. This does not mean that the contour all has the same area — instead, constant area contours reach the extremality contour in a tangential way, as shown in the figure.

Chapter 5

GEDANKEN EXPERIMENTS TO DESTROY A BTZ BLACK HOLE: SECOND-ORDER STUDY

We consider gedanken experiments to destroy an extremal or near-extremal BTZ black hole by throwing matter into the horizon. These black holes are vacuum solutions to (2+1)-dimensional gravity theories, and are asymptotically AdS_3 . Provided the null energy condition for the falling matter, we prove the following: (i) in a Mielke-Baekler model without ghost fields, when torsion is present, an extremal BTZ black hole can be overspun and becomes a naked conical singularity; (ii) in three-dimensional Einstein gravity and chiral gravity, which both live in the torsionless limits of Mielke-Baekler model, an extremal BTZ black hole cannot be overspun; and (iii) in both Einstein gravity and chiral gravity, a near-extremal BTZ black hole cannot be overspun, leaving the weak cosmic censorship preserved. To obtain these results, we follow the analysis of Sorce and Wald on their gedanken experiments to destroy a Kerr-Newman black hole, and calculate the second-order variation of the black hole mechanics. Furthermore, Wald's type of gedanken experiments provides an operational procedure of proving the third law of black hole dynamics. Through the AdS/CFT correspondence, our results on BTZ black holes also indicate that a third law of thermodynamics holds for the holographic conformal field theories dual to three-dimensional Einstein gravity and chiral gravity.

5.1 Introduction

Weak cosmic censorship conjecture (WCCC) was formulated by Penrose [14] to postulate that a gravitational singularity should not be naked and should be hidden inside a black hole horizon. A gravitational singularity is usually mathematically ill-defined due to the divergent spacetime curvature. Thus, the WCCC helps to avoid seeing such an unphysical part of the universe and retains the predicted power of physical laws. Its philosophical incarnation was summarized by Hawking that "nature abhors a naked singularity"¹. In this sense, a special case worthy of consideration is the three-dimensional Banados-Teitelboim-Zanelli (BTZ) black hole, for which there is no curvature singularity but a conical one. The conical

¹See the story in <https://www.nytimes.com/1997/02/12/us/a-bet-on-a-cosmic-scale-and-a-concession-sort-of.html>

singularity will thus cause no physical divergence unlike the curvature one. It is then interesting to check if WCCC holds for this case or not, and partly motivates the study of this chapter.

The general proof or demonstration of WCCC is notoriously difficult. One way is to find the critical situation in which a black hole almost turns into a naked singularity due to small perturbations. This is when a Kerr-Newman black hole is in its near-extremal regime. A super-extremal solution possesses the naked singularity, thus checking WCCC is to see if a sub-extremal black hole in the near-extremal limit can turn into a super-extremal one by throwing some matter. Along this line of thought, a gedanken experiment was first proposed by Wald [15] to demonstrate the impossibility of destroying an extremal Kerr-Newman black hole by throwing the matter obeying the null energy condition. The key ingredient in [15] is the linear variation of black hole mechanics [104, 105], i.e.,

$$\delta M - \Omega_H \delta J - \Phi_H \delta Q \geq 0, \quad (5.1)$$

where M is the mass of the black hole, J the angular momentum, Q the charge, and Ω_H and Φ_H are respectively the angular velocity and chemical potential evaluated on the horizon. A similar consideration for the near-extremal Reissner-Nordstrom black hole was examined by Hubeny [16], who found that it can be overcharged to violate WCCC by throwing a charged particle. See [106–109] for follow-up works.

Recently, it was realized by Sorce and Wald [17] that the analysis in Hubeny's type of gedanken experiments is insufficient at the linear order so that the second-order variation must be taken into account to check WCCC for near-extremal black holes. Based on an earlier development of the second-order variation of black hole mechanics [102], they went beyond the first-order analysis in [16] and derived the following inequality

$$\delta^2 M - \Omega_H \delta^2 J - \Phi_H \delta^2 Q \geq -T_H \delta^2 S, \quad (5.2)$$

with T_H the Hawking temperature and S the Wald's black hole entropy [90][91], which equals to the Bekenstein-Hawking entropy of area law for the case of Einstein's theory of gravity, but receives modifications for non-Einstein theories of gravity [92] ((5.40) for the case of Mielke-Barkler gravity). Under the situation that the linear variation is optimally done, i.e., the inequality (5.1) is saturated, Sorce and Wald adopted (5.2) to show that the WCCC holds for Kerr-Newman black holes in four-dimensional Einstein-Maxwell gravity. In [17] it is assumed that the near-extremal

black hole is linearly stable, so that at very late time the linear perturbation induced by falling matter becomes the perturbation towards another Kerr-Newman black hole. Thus, the WCCC prohibits the possibility of a naked singularity, and can be formally described as the condition for a one-parameter family of black hole solutions

$$f(\lambda) > 0, \quad \text{for all } \lambda \geq 0 \quad (5.3)$$

with $f(\lambda) = 0$ being the condition for extremal black hole. For examples, $f(\lambda) = M(\lambda)^2 - \frac{J(\lambda)^2}{M(\lambda)^2} - Q(\lambda)^2$ for a Kerr-Newman black hole of mass $M(\lambda)$, angular momentum $J(\lambda)$ and charge $Q(\lambda)$, and $f(\lambda) = M(\lambda)^2 + \Lambda J(\lambda)^2$ for a BTZ black hole in three-dimensional anti-de Sitter (AdS) space of cosmological constant $\Lambda < 0$. Note that there is no need in this formulation of examining WCCC to consider the self-force effects of the in-falling matter as done in [110–114].

In this chapter, we will check WCCC for a BTZ black hole in three-dimensional torsional Mielke-Barkler gravity (MBG) [115–117] with the general falling matter². In some special limits of MBG, we have either Einstein gravity or chiral gravity [120], both of which have the known dual descriptions by a two-dimensional conformal field theory (CFT) in the context of AdS/CFT correspondence [121]. Especially, the extremal black hole has zero surface gravity, and corresponds to a dual CFT state at zero temperature. The motivation of our study is two-fold. First, we would like to see if WCCC holds even for the naked conical singularity such as the one in BTZ, and at the same time extend the formulation of [17] to more general gravity theories. Second, Wald’s type of gedanken experiments provide an operational procedure of proving the third law of black hole dynamics [107, 122]: One cannot turn the non-extremal black hole into an extremal one in the finite time-interval by throwing into the black hole the matter satisfying the null energy condition. We can turn the above third law into the one of black hole thermodynamics if we adopt Bekenstein and Hawking’s point of view. Moreover, through the AdS/CFT correspondence, this third law also corresponds to the third law of thermodynamics for the dual two-dimensional CFT³. Our results indicate that such a third law of thermodynamics holds for the holographic CFTs dual to three-dimensional Einstein gravity and chiral gravity. Intuitively, the cooling procedure can be holographically understood as throwing the coolant, i.e., matter of spin J and energy E with $J > E$, into the black hole.

²See also recent papers [118, 119] for the related discussion for special falling matter.

³See [123] for the earlier discussion on AdS₅ cases in context other than WCCC.

We organize the rest of the chapter as follows. In Sec. 5.2 we derive the linear and second-order variational identities for the MB model, with which we can proceed to the consideration of gedanken experiments for three ghost-free limits of MB model, i.e., the Einstein gravity, chiral gravity and torsional chiral gravity. In Sec. 5.3 we consider the gedanken experiments for an extremal BTZ black hole by using the linear variational identity and the null energy condition. In Sec. 5.4 we check WCCC for nonextremal BTZ black holes for the chiral gravity and Einstein gravity. Finally in Sec. 5.5 we summarize our results and conclude with some discussions on the issue of proving the third law and its implication to the holographic dual CFTs.

5.2 BTZ black hole and variational identities

BTZ black holes are topologically non-trivial solutions to the three-dimensional Einstein gravity as well as the topological massive gravity (TMG) [124–126]. In fact, they are solutions to a quite general category of gravity theories called Mielke-Baekler (MB) model [115, 116] which also incorporates torsion, with Einstein gravity and TMG arising as special limits in its parameter space. In this section, we derive the variational identities and canonical energy for this model following Wald’s formulation.

In three-dimensional spacetime, it is convenient to express the gravity theory in the first-order formalism. The Lagrangian of a general chiral gravity with torsion, namely the MB model, is as follows:

$$L = L_{\text{EC}} + L_{\Lambda} + L_{\text{CS}} + L_{\text{T}} + L_{\text{M}}, \quad (5.4)$$

where

$$L_{\text{EC}} = \frac{1}{\pi} e^a \wedge R_a, \quad (5.5)$$

$$L_{\Lambda} = -\frac{\Lambda}{6\pi} \epsilon_{abc} e^a \wedge e^b \wedge e^c, \quad (5.6)$$

$$L_{\text{CS}} = -\theta_{\text{L}} \left(\omega^a \wedge d\omega_a + \frac{1}{3} \epsilon_{abc} \omega^a \wedge \omega^b \wedge \omega^c \right), \quad (5.7)$$

$$L_{\text{T}} = \frac{\theta_{\text{T}}}{2\pi^2} e^a \wedge T_a, \quad (5.8)$$

in which $\Lambda < 0$ is the cosmological constant, θ_{L} and θ_{T} are coupling constants, L_{EC} is the Einstein-Cartan term, L_{Λ} is the cosmological constant term, L_{CS} is the Chern-Simons (CS) terms for curvature, L_{T} is a translational Chern-Simons term, and L_{M} is the Lagrangian for the matter. T_a is the torsion 2-form defined

by $T^a = de^a + \omega^a_b \wedge e^b$ with e^a the dreibeins. We have also defined the dual spin connection ω^a and the dual curvature 2-form R^a for simplicity:

$$\omega^a = \frac{1}{2} \epsilon^a_{bc} \omega^{bc}, \quad R^a = \frac{1}{2} \epsilon^a_{bc} R^{bc}, \quad (5.9)$$

Variations of the Lagrangian (5.4–5.8) with respect to the dreibeins e^a and the dual spin connections ω^a give rise to the equations of motion $E_a^{(e)} = 0$ and $E_a^{(\omega)} = 0$ with

$$E_a^{(e)} = \frac{1}{\pi} \left(R_a + \frac{\theta_T}{\pi} T_a - \frac{\Lambda}{2} \epsilon_{abc} e^b \wedge e^c \right), \quad (5.10)$$

$$E_a^{(\omega)} = \frac{1}{\pi} \left(T_a - 2\pi\theta_L R_a + \frac{\theta_T}{2\pi} \epsilon_{abc} e^b \wedge e^c \right) \quad (5.11)$$

for vanishing matter. For the case $1 + 2\theta_T\theta_L \neq 0$, the equations of motion are solved by

$$T^a = \frac{\mathcal{T}}{\pi} \epsilon^a_{bc} e^b \wedge e^c, \quad (5.12)$$

$$R^a = -\frac{\mathcal{R}}{2\pi^2} \epsilon^a_{bc} e^b \wedge e^c, \quad (5.13)$$

in which

$$\mathcal{T} \equiv \frac{-\theta_T + 2\pi^2\Lambda\theta_L}{2 + 4\theta_T\theta_L}, \quad \mathcal{R} \equiv -\frac{\theta_T^2 + \pi^2\Lambda}{1 + 2\theta_T\theta_L}. \quad (5.14)$$

The MB model was originally proposed as a torsional generalization of TMG. It has a Poincaré gauge theory description, and there are propagating massive gravitons just like in TMG. We will be especially interested in three limits:

(i) Einstein gravity (with negative cosmological constant). This could be approached by taking the limit $\theta_L \rightarrow 0$ and $\theta_T \rightarrow 0$.

(ii) Chiral gravity. The torsionless branch of the MB model, which is equivalent to TMG, could be obtained by setting $\mathcal{T} = 0$ according to (5.12). It was pointed out in [120] that TMG is only well defined at the critical point in which the dual CFT becomes chiral. In our convention, the critical point is located at $\theta_L = -1/(2\pi\sqrt{-\Lambda})$. Hence the chiral gravity is approached by setting $\mathcal{T} = 0$ first and then taking the limit $\theta_L \rightarrow -1/(2\pi\sqrt{-\Lambda})$.

(iii) Torsional chiral gravity. For the branch with non-vanishing torsion, we note from the Lagrangian (5.4-5.8) that the torsion field T_a could not be kinematic since there is no second-order derivative of ω^a . The torsion field should just contribute to the interaction term in the linearized theory, while the propagators of the gravitons should not be changed compared with TMG. We then expect that the MB model

also behaves well with no ghost at the critical point $\theta_L \rightarrow -1/(2\pi\sqrt{-\Lambda})$. Note that by taking this limit first, we obtain $\mathcal{T} \rightarrow \pi\sqrt{-\Lambda}/2$ hence the torsion field could not be vanishing. This is a different limit from the case (ii), and we refer it as the torsional chiral gravity.

An interesting class of solutions to the Eqs. (5.12)(5.13) are the BTZ-like solutions with non-vanishing torsion [127]. They are described by the following dreibeins,

$$e^0 = Ndt, \quad e^1 = \frac{dr}{N}, \quad e^2 = r(d\phi + N^\phi dt), \quad (5.15)$$

and the dual spin connections,

$$\omega^a = \tilde{\omega}^a + \frac{\mathcal{T}}{\pi} e^a, \quad (5.16)$$

with the torsion free parts

$$\tilde{\omega}^0 = Nd\phi, \quad \tilde{\omega}^1 = -\frac{N^\phi}{N}dr, \quad \tilde{\omega}^2 = -\Lambda_{\text{eff}}r dt + rN^\phi d\phi, \quad (5.17)$$

in which

$$N^2(r) = -M - \Lambda_{\text{eff}}r^2 + \frac{J^2}{4r^2}, \quad N^\phi(r) = -\frac{J}{2r^2}, \quad (5.18)$$

where M and J are constants corresponding to mass and angular momentum of BTZ black hole, respectively, for the case of Einstein's gravity, and

$$\Lambda_{\text{eff}} \equiv -\frac{\mathcal{T}^2 + \mathcal{R}}{\pi^2}. \quad (5.19)$$

Taking the torsion free limit $\mathcal{T} \rightarrow 0$, the above solutions recover the usual BTZ black holes with $\Lambda_{\text{eff}} = \Lambda$. The horizons are located at

$$r_\pm^2 = \frac{1}{2\Lambda_{\text{eff}}} \left(-M \mp \sqrt{M^2 + \Lambda_{\text{eff}}J^2} \right), \quad (5.20)$$

(note that $\Lambda_{\text{eff}} < 0$ for asymptotic AdS solutions), and the angular velocity of the outer horizon is

$$\Omega_{\text{H}} = \frac{J}{2r_+^2} = \frac{r_-}{r_+} \sqrt{-\Lambda_{\text{eff}}}. \quad (5.21)$$

The black hole temperature is fixed by the vanishing of the conical singularity of the corresponding Euclidean metric:

$$T_{\text{H}} = -\frac{\Lambda_{\text{eff}}(r_+^2 - r_-^2)}{2\pi r_+}, \quad (5.22)$$

and the surface gravity is $\kappa_{\text{H}} = 2\pi T_{\text{H}}$.

First-order variations

Wald's gedanken experiment to destroy a black hole begins with considering a general off-shell variation of the fields, which in principle incorporates all kinds of possible perturbations of a black hole, including throwing matter into it. From the variational identities one obtains general constraints obeyed by these perturbations.

The first-order variation of the Lagrangian (5.4-5.8) gives rise to the equations of motion as well as a surface term:

$$\delta L = \delta e^a \wedge E_a^{(e)} + \delta \omega^a \wedge E_a^{(\omega)} + d\Theta(\phi, \delta\phi), \quad (5.23)$$

in which $\phi = (e^a, \omega^a)$, $E_a^{(e)}$ and $E_a^{(\omega)}$ are given by (5.10) and (5.11). The surface term $\Theta(\phi, \delta\phi)$, called the symplectic potential, is evaluated to be

$$\Theta(\phi, \delta\phi) = \frac{1}{\pi} \delta \omega^a \wedge e_a + \frac{\theta_T}{2\pi^2} \delta e^a \wedge e_a - \theta_L \delta \omega^a \wedge \omega_a. \quad (5.24)$$

In Wald's approach, the space of field configurations is the phase space of the theory, and the variation $\delta\phi \equiv (d\phi/d\lambda)|_{\lambda=0}$ is the phase space flow vector associated with a one-parameter family of field configurations $\phi(\lambda)$. For a two-parameter family of field configurations $\phi(\lambda_1, \lambda_2)$, one could define the symplectic current

$$\Omega(\phi, \delta_1\phi, \delta_2\phi) = \delta_1\Theta(\phi, \delta_2\phi) - \delta_2\Theta(\phi, \delta_1\phi), \quad (5.25)$$

in which δ_1, δ_2 denote derivatives with respect to parameters λ_1, λ_2 :

$$\delta_1 = \left. \frac{\partial}{\partial \lambda_1} \right|_{\lambda=0}, \quad \delta_2 = \left. \frac{\partial}{\partial \lambda_2} \right|_{\lambda=0}. \quad (5.26)$$

One can show that the symplectic current is conserved when the linearized equations of motion are satisfied:

$$d\Omega = 0. \quad (5.27)$$

The Noether current two-form associated with a vector field ξ is defined by

$$j_\xi = \Theta(\phi, \mathcal{L}_\xi\phi) - i_\xi L, \quad (5.28)$$

in which $i_\xi L$ represents the interior derivative which contracts ξ^μ into the first index of the three-form L . Then, j_ξ could be written in the form

$$j_\xi = dQ_\xi + C_\xi, \quad (5.29)$$

in which the Noether charge Q_ξ and the constraints C_ξ are given by

$$Q_\xi = \frac{1}{\pi} (\mathbf{i}_\xi \omega^a) \wedge e_a + \frac{\theta_\Gamma}{2\pi^2} (\mathbf{i}_\xi e^a) \wedge e_a - \theta_L (\mathbf{i}_\xi \omega^a) \wedge \omega_a, \quad (5.30)$$

$$C_\xi = -(\mathbf{i}_\xi e^a) \wedge E_a^{(e)} - (\mathbf{i}_\xi \omega^a) \wedge E_a^{(\omega)}. \quad (5.31)$$

Suppose the field configuration is a family of asymptotic AdS spacetime. Variation of (5.28)(5.29) gives rise to the following linear variational identity after integrating over an achronal hypersurface Σ :

$$\int_{\partial\Sigma} \delta Q_\xi - \mathbf{i}_\xi \Theta(\phi, \delta\phi) = \int_\Sigma \Omega(\phi, \delta\phi, \mathcal{L}_\xi \phi) - \int_\Sigma \delta C_\xi - \int_\Sigma \mathbf{i}_\xi (E\delta\phi). \quad (5.32)$$

The first term on the right hand side is recognized as the variation of the Hamiltonian h_ξ associated with the diffeomorphism generated by the vector field ξ

$$\delta h_\xi = \int_\Sigma \Omega(\phi, \delta\phi, \mathcal{L}_\xi \phi). \quad (5.33)$$

Note that δh_ξ (or the first term on the R.H.S. of (5.32)) vanishes if ξ is a Killing field, i.e., $\mathcal{L}_\xi \phi = 0$. If the ϕ is on-shell so that $E_a = 0$, then the last two terms on the R.H.S. of (5.32) also vanish. This then motivates the following definition of the conserved ADM quantity H_ξ conjugate to the Killing field ξ for an on-shell ϕ [90][91]:

$$\delta H_\xi = \int_\infty \delta Q_\xi - \mathbf{i}_\xi \Theta(\phi, \delta\phi), \quad (5.34)$$

where \int_∞ is the integration over the circle at spatial infinity. For a black hole solution, the boundary of Σ contains also horizon as the ‘‘inner boundary’’ besides the ‘‘outer boundary’’ at spatial infinity, then there will be contribution to the L.H.S. of (5.32) from the ‘‘inner boundary’’ as well (i.e., the area law term for Einstein gravity). Combining all the above, (5.32) finally yields the first law of black hole mechanics/thermodynamics.

For the timelike Killing field $\partial/\partial t$ and the rotational Killing field $\partial/\partial\varphi$, the above integration gives rise to the variation of the total mass \mathcal{M} and the total angular momentum \mathcal{J} , respectively. For the BTZ-like black holes (5.15-5.17), it could be evaluated that [128]

$$\mathcal{M} = M - 2\theta_L (\mathcal{T}M + \pi\Lambda_{\text{eff}}J), \quad (5.35)$$

$$\mathcal{J} = J + 2\theta_L (\pi M - \mathcal{T}J). \quad (5.36)$$

For the case that the equations of motion are satisfied and ξ is a Killing field, the linear variational identity (5.32) yields

$$\int_{\partial\Sigma} \delta Q_\xi - i_\xi \Theta(\phi, \delta\phi) = - \int_\Sigma \delta C_\xi. \quad (5.37)$$

For nonextremal black holes, the boundaries include infinity as well as the bifurcation surface B . If ξ is the horizon Killing field $\xi^a = \partial/\partial t + \Omega_H \partial/\partial \varphi$, the boundary integral over infinity is given by

$$\int_\infty \delta Q_\xi - i_\xi \Theta(\phi, \delta\phi) = \delta M - \Omega_H \delta \mathcal{J}. \quad (5.38)$$

For Einstein's theory of gravity, the boundary contribution from the bifurcation surface B turns out to be proportional to the variation of the Bekenstein-Hawking entropy [90][91]:

$$\int_B \delta Q_\xi - i_\xi \Theta(\phi, \delta\phi) = T_H \delta S, \quad (5.39)$$

in which $S = A_B/4$ where A_B is the area of the bifurcation surface. We will take the above equation as a rightful definition of the modified black hole entropy in the MB model so that the first law of the black hole thermodynamics still holds but with Wald's generalized black hole entropy. It has been evaluated for the BTZ-like black holes that [128]

$$S = 4\pi r_+ - 8\pi\theta_L \left(\mathcal{T} r_+ - \pi \sqrt{-\Lambda_{\text{eff}}} r_- \right). \quad (5.40)$$

(5.37) then takes the form

$$\delta M - \Omega_H \delta \mathcal{J} - T_H \delta S = - \int_\Sigma \delta C_\xi. \quad (5.41)$$

We will consider the special situation the perturbation vanishes near the internal boundary of the surface Σ , (5.41) with $\delta S = 0$ would hold for both extremal and non-extremal black holes. Noting (5.35)(5.36) and $\delta S = 0$, (5.41) turns out to be

$$(1 - 2\theta_L \mathcal{T} - 2\pi\theta_L \Omega_H) (\delta M - \Omega_H \delta J) - 2\pi\theta_L \Lambda_{\text{eff}} \left(\frac{r_+^2 - r_-^2}{r_+^2} \right) \delta J = - \int_\Sigma \delta C_\xi. \quad (5.42)$$

for BTZ-like black holes in the MB model.

(5.41)(5.42) are derived from the Lagrangian without matter. It might be puzzling that the vacuum configuration could be perturbed without matter; however, this is physically possible since there are gravitational waves in the MB model with general couplings. In general, δM and δJ should be understood as variations

allowed mathematically in the parameter space, rather than consequences of certain physical evolutions. On the other hand, since we didn't enforce the linearized equations of motion to be satisfied, it should be expected that these equations could also be used for considering perturbed configurations due to matter contribution⁴. The right hand side of (5.42) would be related to the energy-momentum tensor of the matter. To see this explicitly, we first define the ‘‘energy-momentum 2-form’’ Σ_a and ‘‘spin current 2-form’’ τ_a as follows:

$$\Sigma_a \equiv \frac{\delta L_{\mathbf{M}}}{\delta e^a}, \quad \tau_a \equiv \frac{\delta L_{\mathbf{M}}}{\delta \omega^a}. \quad (5.43)$$

The equations of motion with matter would be

$$E_a^{(e)} = -\Sigma_a, \quad E_a^{(\omega)} = -\tau_a. \quad (5.44)$$

Since $\Sigma_a = \tau_a = 0$ in the background spacetime, from (5.31) we get

$$\delta C_\xi = (i_\xi e^a) \wedge \delta \Sigma_a + (i_\xi \omega^a) \wedge \delta \tau_a. \quad (5.45)$$

Σ_a should be related to the conserved canonical energy-momentum tensor Σ_a^μ defined by

$$\sqrt{-g} \Sigma_a^\mu \equiv \frac{\partial \mathcal{L}}{\partial e^a_\mu} = e_a^\mu \mathcal{L} - \frac{\partial \mathcal{L}}{\partial (\partial_\mu \psi)} D_a \psi, \quad (5.46)$$

in which ψ is the matter field, \mathcal{L} is the Lagrangian density of the matter related to $L_{\mathbf{M}}$ by $L_{\mathbf{M}} = \mathcal{L} d^3x$, and D_a is the covariant derivative defined by $D_a = e_a^\mu (\partial_\mu + \omega_\mu^{bc} f_{cb})$ where f_{ab} are the representations of the generators of the Lorentz group associated with ψ . From (5.46) we obtain

$$\Sigma_a = \frac{1}{2} \epsilon_{\mu\nu\lambda} \Sigma_a^\lambda dx^\mu \wedge dx^\nu. \quad (5.47)$$

Note that

$$\epsilon_{\mu\nu\lambda} = -3k_{[\mu} \hat{\epsilon}_{\nu\lambda]}, \quad (5.48)$$

in which k^μ is the future-directed normal vector to the horizon, and $\hat{\epsilon}$ is the volume element on the horizon. The first term on the right hand side of (5.45) then turns out to be

$$(i_\xi e^a) \wedge \delta \Sigma_a = -\xi_\mu k_\nu \delta \Sigma^{\mu\nu} \sqrt{-\gamma} d^2x, \quad (5.49)$$

⁴For the matter field, we impose Dirichlet condition on asymptotic AdS boundary, as conventionally used in AdS/CFT dictionary for black holes dual to thermal states in CFT. This choice will not affect the argument for WCCC as we only care about the matter that falls in.

as $\xi^\mu \propto k^\mu$, thus the contribution of this term to the right-hand side of equations (5.42) is non-negative if and only if the null energy condition of matter energy-momentum tensor $\delta\Sigma_{\mu\nu}$ is satisfied:

$$k^\mu k^\nu \delta\Sigma_{\mu\nu} \geq 0. \quad (5.50)$$

For the second term on the right hand side of (5.45), our ‘‘spin current two-form’’ τ_a is related to the canonical spin angular momentum tensor $\tau_{ab}{}^\mu$ defined by

$$\sqrt{-g} \tau_{ab}{}^\mu \equiv \frac{\partial \mathcal{L}}{\partial \omega_\mu{}^{ab}} = -\frac{\partial \mathcal{L}}{\partial (\partial_\mu \psi)} f_{ab} \psi, \quad (5.51)$$

Comparing (5.51) with (5.43), we obtain

$$\tau_a = -\frac{1}{2} \epsilon_a{}^{bc} \epsilon_{\mu\nu\lambda} \tau_{bc}{}^\lambda dx^\mu \wedge dx^\nu, \quad (5.52)$$

hence the second term on the right hand side of (5.45) is reduced to

$$(\mathbf{i}_\xi \omega^a) \wedge \delta\tau_a = -(\xi^\sigma \omega^{ab}{}_\sigma) k_\lambda \delta\tau_{ab}{}^\lambda \sqrt{-\gamma} d^2x. \quad (5.53)$$

For axially symmetric stationary black holes, in general we have [128]

$$\mathbf{i}_\xi \omega^a|_{\mathcal{H}} = -\frac{1}{2} \kappa_{\mathcal{H}} \epsilon^a{}_{bc} n^{bc} + \mathbf{i}_\xi K^a|_{\mathcal{H}}, \quad (5.54)$$

in which n^{ab} is the binormal to the horizon and K^a is the dual contorsion one-form defined by $T^a = \epsilon^a{}_{bc} K^b \wedge e^c$, satisfying the identity $\omega^a = \tilde{\omega}^a + K^a$. For BTZ-like black holes, (5.16) gives

$$K^a = \frac{\mathcal{T}}{\pi} e^a. \quad (5.55)$$

Using (5.54)(5.55), (5.53) turns out to be

$$(\mathbf{i}_\xi \omega^a) \wedge \delta\tau_a = \left(\kappa_{\mathcal{H}} n_{\mu\nu} + \frac{\mathcal{T}}{\pi} \epsilon_{\mu\nu}{}^\sigma \xi_\sigma \right) k_\lambda \delta\tau^{\mu\nu\lambda} \sqrt{-\gamma} d^2x. \quad (5.56)$$

The first term on the right hand side is vanishing for extremal black holes. We note that the sign of the second term could not be determined for torsional chiral gravity unless the spin angular momentum tensor satisfies $\epsilon_{\mu\nu}{}^\sigma k_\sigma k_\lambda \delta\tau^{\mu\nu\lambda} \geq 0$, of which the physical meaning is not clear yet for us.

Combining all the results above, we obtain the following linear variational identity for the BTZ-like black holes in the MB model, with the additional assumption that

the perturbation $\delta\phi$ vanishes near the internal boundary of Σ

$$\begin{aligned}
& \delta\mathcal{M} - \Omega_{\text{H}}\delta\mathcal{J} \\
&= (1 - 2\theta_{\text{L}}\mathcal{T} - 2\pi\theta_{\text{L}}\Omega_{\text{H}}) (\delta\mathcal{M} - \Omega_{\text{H}}\delta\mathcal{J}) - 2\pi\theta_{\text{L}}\Lambda_{\text{eff}} \left(\frac{r_+^2 - r_-^2}{r_+^2} \right) \delta\mathcal{J} \\
&= \int_{\Sigma} d^2x \sqrt{-\gamma} \left\{ \xi_{\mu} k_{\nu} \delta\Sigma^{\mu\nu} - \left(\kappa_{\text{H}} n_{\mu\nu} + \frac{\mathcal{T}}{\pi} \epsilon_{\mu\nu}{}^{\sigma} \xi_{\sigma} \right) k_{\lambda} \delta\tau^{\mu\nu\lambda} \right\}. \quad (5.57)
\end{aligned}$$

For extremal BTZ black holes with $\kappa_{\text{H}} = 0$ and $r_+ = r_-$, the above identity takes the following simpler form:

$$\begin{aligned}
\delta\mathcal{M} - \Omega_{\text{H}}\delta\mathcal{J} &= (1 - 2\theta_{\text{L}}\mathcal{T} - 2\pi\theta_{\text{L}}\sqrt{-\Lambda_{\text{eff}}}) (\delta\mathcal{M} - \sqrt{-\Lambda_{\text{eff}}}\delta\mathcal{J}) \\
&= \int_{\Sigma} d^2x \sqrt{-\gamma} \left\{ \xi_{\mu} k_{\nu} \delta\Sigma^{\mu\nu} - \frac{\mathcal{T}}{\pi} \epsilon_{\mu\nu}{}^{\sigma} \xi_{\sigma} k_{\lambda} \delta\tau^{\mu\nu\lambda} \right\}. \quad (5.58)
\end{aligned}$$

Second order variations

As pointed out in [17], for near-extremal black holes it is in general not sufficient to consider just the linear order variation due to Hubeny-type violations. We therefore construct further the second-order variational identity. A second variation of (5.32) gives rise to

$$\mathcal{E}_{\Sigma}(\phi; \delta\phi) = \int_{\partial\Sigma} [\delta^2\mathcal{Q}_{\xi} - i_{\xi}\delta\Theta(\phi, \delta\phi)] + \int_{\Sigma} \delta^2\mathcal{C}_{\xi} + \int_{\Sigma} i_{\xi}(\delta E \wedge \delta\phi), \quad (5.59)$$

in which

$$\mathcal{E}_{\Sigma}(\phi; \delta\phi) \equiv \int_{\Sigma} \Omega(\phi, \delta\phi, \mathcal{L}_{\xi}\delta\phi) \quad (5.60)$$

is Wald's canonical energy of the off-shell perturbation $\delta\phi$ on Σ . For the case that the background ϕ is a stationary black hole solution and ξ is the horizon Killing field, the boundary contribution from infinity is simply

$$\int_{\infty} \delta^2\mathcal{Q}_{\xi} - i_{\xi}\delta\Theta(\phi, \delta\phi) = \delta^2\mathcal{M} - \Omega_{\text{H}}\delta^2\mathcal{J} \quad (5.61)$$

according to (5.38). The contribution from interior boundary would be vanishing if there's no perturbation in its neighborhood, as supposed before. Then (5.59) turns out to be

$$\delta^2\mathcal{M} - \Omega_{\text{H}}\delta^2\mathcal{J} = \mathcal{E}_{\Sigma}(\phi; \delta\phi) - \int_{\Sigma} i_{\xi}(\delta E \wedge \delta\phi) - \int_{\Sigma} \delta^2\mathcal{C}_{\xi}. \quad (5.62)$$

Noting (5.44), (5.47), and (5.52), the integrand of the second term on the right hand side is evaluated to be

$$\begin{aligned}
i_{\xi}(\delta E \wedge \delta\phi) &\equiv i_{\xi}(\delta E_a^{(e)} \wedge \delta e^a + \delta E_a^{(\omega)} \wedge \delta\omega^a) \\
&= \xi^{\tau} \Xi_{[\mu\nu\tau]} dx^{\mu} \wedge dx^{\nu}, \quad (5.63)
\end{aligned}$$

in which

$$\Xi_{\mu\nu\tau} = -\frac{3}{2} \epsilon_{\mu\nu\lambda} \left(\delta\Sigma_a^\lambda \delta e^a_\tau + \delta\tau_{ab}^\lambda \delta\omega^{ab}_\tau \right). \quad (5.64)$$

Since ξ is tangent to the horizon, the pullback of (5.63) to the horizon vanishes, hence this term gives no contribution. From (5.31), it turns out that

$$\delta^2 C_\xi = \delta^2 \left\{ -d^2 x \sqrt{-\gamma} \left[\xi_\mu k_\nu \Sigma^{\mu\nu} - \left(\kappa_H n_{\mu\nu} + \frac{\mathcal{T}}{\pi} \epsilon_{\mu\nu}^\sigma \xi_\sigma \right) k_\lambda \tau^{\mu\nu\lambda} \right] \right\}. \quad (5.65)$$

Substituting the above expression into (5.62) leads to the following identity for the second-order variation:

$$\begin{aligned} \delta^2 \mathcal{M} - \Omega_H \delta^2 \mathcal{J} &= \mathcal{E}_\Sigma(\phi; \delta\phi) \\ &+ \delta^2 \int_\Sigma d^2 x \sqrt{-\gamma} \left\{ \xi_\mu k_\nu \Sigma^{\mu\nu} - \left(\kappa_H n_{\mu\nu} + \frac{\mathcal{T}}{\pi} \epsilon_{\mu\nu}^\sigma \xi_\sigma \right) k_\lambda \tau^{\mu\nu\lambda} \right\}. \end{aligned} \quad (5.66)$$

5.3 Gedanken experiment to destroy an extremal BTZ

We now consider our gedanken experiment to destroy a BTZ black hole along the line of Wald's proposals [15, 17]. In this section, we will deal with an extremal BTZ black hole with mass parameter M and angular momentum parameter J . We wish to see if a naked singularity can be made via throwing matter into the extremal black hole. Without losing generality, we take our gravity theory as MB model, and then discuss its three limits, torsional chiral gravity, chiral gravity, and three-dimensional Einstein gravity.

Considering a one-parameter family of solutions $\phi(\lambda)$, $\phi_0 = \phi(0)$ is an extremal BTZ black hole, which is a vacuum solution in MB model. The existence of event horizon is determined by a function,

$$f(\lambda) = M(\lambda)^2 + \Lambda_{\text{eff}} J(\lambda)^2. \quad (5.67)$$

If $f(\lambda) \geq 0$, the spacetime is a BTZ black hole. If $f(\lambda) < 0$, it is a naked conical singularity and WCCC is violated. We now consider perturbations to the extremal black hole ϕ_0 . Then, to the first order in λ , we have

$$f(\lambda) = 2\lambda \sqrt{-\Lambda_{\text{eff}}} |J| \left(\delta M - \sqrt{-\Lambda_{\text{eff}}} \delta J \right) + \mathcal{O}(\lambda^2), \quad (5.68)$$

where we have used the extremal condition $M = \sqrt{-\Lambda_{\text{eff}}} |J|$ to eliminate M . It is then evident that if $\delta M < \sqrt{-\Lambda_{\text{eff}}} \delta J$, $f(\lambda)$ can be negative.

We would like to see whether this sort of violation of WCCC is possible if we throw matter into the BTZ black hole in a certain way. Let Σ_0 be an asymptotically

AdS hypersurface which extends from the future horizon to the spatial infinity. We consider a perturbation $\delta\phi$ whose initial data for both fields δe^a and $\delta\omega^a$ on Σ_0 vanish in the neighborhood of the intersection between Σ_0 and the horizon. We assume that the initial data for the matter sources $\delta\Sigma_{\mu\nu}$ and $\delta\tau^{\mu\nu\lambda}$ also vanish in this neighborhood, and, only exist in a compact region of Σ_0 . That is, we consider perturbations whose effects at sufficiently early times are negligibly small. To simplify the discussion, we only consider the case where, as we evolve the perturbation, all of the matter will fall through the horizon. Therefore, the whole evolution of the matter source $\delta\Sigma_{\mu\nu}$ and $\delta\tau^{\mu\nu\lambda}$ stays in a shaded region as shown in Fig. 5.1. As matter falls in, we further define a hypersurface Σ in the following way—it starts on the future horizon in the region where the perturbation vanishes and extends along the future horizon till all matter falls into the horizon; then it becomes spacelike, approaches the spatial infinity and becomes asymptotically AdS. We denote the horizon portion of Σ as \mathcal{H} , and the spatial portion as Σ_1 .

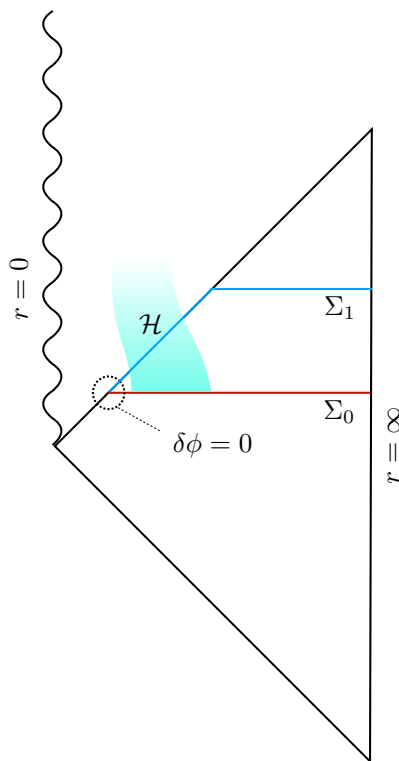


Figure 5.1: Carter-Penrose diagram of an extremal BTZ black hole. The shaded region consists of the falling matter which all goes into the black hole. The perturbation $\delta\phi$ vanishes in a neighborhood of $\Sigma_0 \cap \mathcal{H}$.

We now use the linear variational identity with vanishing inner boundary contribu-

tions (5.58) for this choice of Σ . As we will show later, this identity constrains the sign of $f(\lambda)$. We notice that in e.q. (5.58), the integral in the second line is not positive definite due to the spin angular momentum term and its coupling to torsion. That is, in torsional chiral gravity, whether WCCC can hold depends on an additional relation between the spin angular momentum and the torsion. The physical origin of this additional information needed is unclear, and is beyond our scope of this chapter. We will leave it to a future work. In the torsionless limit $\mathcal{T} \rightarrow 0$, however, this integral would be non-negative as long as the null energy condition is satisfied. From now on, we will focus on this limit, and assume the falling matter satisfies the null energy condition. Then $f(\lambda)$ is non-negative only if the constant factor on the right hand side of the first line of Eq. (5.58) is non-negative,

$$1 - 2\theta_L \mathcal{T} - 2\pi\theta_L \sqrt{-\Lambda_{\text{eff}}} \geq 0. \quad (5.69)$$

For chiral gravity, we choose $\theta_L = -1/(2\pi\sqrt{-\Lambda})$, and send $\mathcal{T} \rightarrow 0$. The inequality (5.69) is then satisfied. Therefore extremal BTZ black hole in chiral gravity cannot be destroyed in our experiment, and WCCC is preserved.

For three-dimensional Einstein gravity with a negative cosmological constant, both torsion and Chern-Simons interaction vanish, thus we set $\theta_L \rightarrow 0$ and $\theta_T \rightarrow 0$. The inequality (5.69) is then satisfied. Consequently, extremal BTZ black hole in three-dimensional Einstein gravity cannot be destroyed, leaving WCCC preserved.

5.4 Gedanken experiment to destroy a near-extremal BTZ

For extremal BTZ black holes, we have found that WCCC can be violated in the presence of torsion. With torsion being turned off, we have seen that WCCC is preserved in both chiral gravity and three-dimensional Einstein gravity, provided that the matter obeys the null energy condition. In four-dimensional Einstein gravity, Hubeny [16] proposed that violations of WCCC might be possible if one threw matter into a near-extremal black hole in an appropriate manner. In order to examine whether Hubeny-type violations can truly happen, one has to calculate the energy and momentum of the matter beyond the linear order. In this section, we will examine the Hubeny-type violations for a near-extremal BTZ black hole in chiral gravity and three-dimensional Einstein gravity respectively.

As shown in Fig. 5.2, we make similar choices of Σ_0 and Σ like those for the extremal BTZ case. The only difference is that, the two hypersurfaces now terminate at the bifurcation surface B . We further assume that the second-order perturbation $\delta^2\phi$ for

both fields δe^a and $\delta \omega^a$ also vanishes in a neighborhood of B . Again, we simplify our discussions by restricting to the case where all matter falls into the black hole. We will also make the following additional assumption:

Assumption: The non-extremal BTZ black hole is linearly stable to perturbations, i.e., any source-free linear perturbation $\delta\phi$ approaches a perturbation $\delta\phi^{\text{BTZ}}$ towards another BTZ black hole at sufficiently late times.

Although our perturbations are not source-free in general, we will only apply the above assumption on the late-time spatial surface Σ_1 long after all of the matter has fallen in the the black hole. We emphasize that this linear stability assumption does not indicate WCCC which we wish to prove. This is because a finite perturbation is needed to overspin a non-extremal black hole, while a linear perturbation can always be scaled down to a infinite small one. Hence the linear instability of a non-extremal BTZ black hole should be independent of the instability associated with overspinning, i.e., a linearly stable non-extremal BTZ black hole could possibly be overspun by a finite perturbation, just like the situation for the Kerr-Newman black hole in [17].

Chiral gravity

We now consider our thought experiment to destroy a near-extremal BTZ black hole (M, J) in chiral gravity for which $\mathcal{T} = 0$ and $\theta_L = -\frac{1}{2\pi\sqrt{-\Lambda}}$. Thus, using (5.35–5.36) it is straightforward to see

$$\delta\mathcal{M} - \Omega_H\delta\mathcal{J} = \left(1 + \frac{\Omega_H}{\sqrt{-\Lambda}}\right) (\delta M - \sqrt{-\Lambda}\delta J), \quad (5.70)$$

and the first law of black hole thermodynamics yields

$$T_H\delta S = \delta\mathcal{M} - \Omega_H\delta\mathcal{J}. \quad (5.71)$$

where the black hole entropy is given by [128]

$$S = 4\pi (r_+ - r_-). \quad (5.72)$$

Recall (5.57), the null energy condition for the falling matter yields the first-order relation that

$$\delta M \geq \sqrt{-\Lambda}\delta J. \quad (5.73)$$

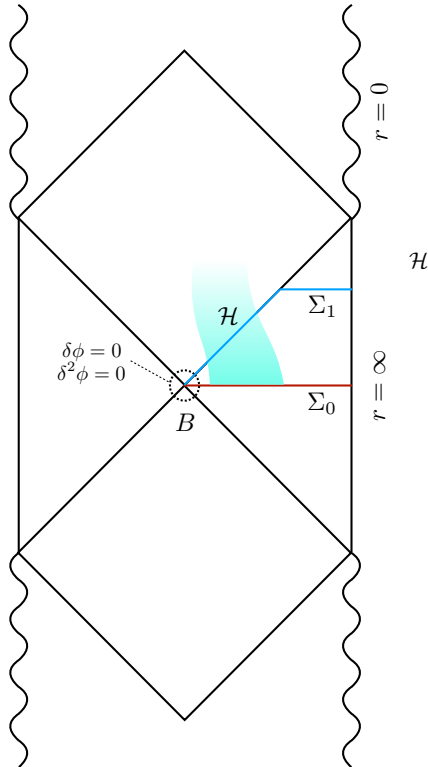


Figure 5.2: Carter-Penrose diagram of a near-extremal BTZ black hole. The shaded region consists of the falling matter which all goes into the black hole. The perturbation $\delta\phi$ and $\delta^2\phi$ vanishes in a neighborhood of B .

The first-order perturbation has been optimally done, i.e. $\delta S = 0$, such that

$$\delta M = \sqrt{-\Lambda} \delta J. \quad (5.74)$$

For some constant entropy S , we can then plot the line of constant entropy in the parameter space of BTZ black holes, which is shown in Fig. 5.3.

We are now ready to discuss our experiment to destroy the near-extremal BTZ black hole. Starting from a point (M_0, J_0) in the parameter space, after a perturbation of the spacetime as induced by falling matter, we will always arrive at another point (M_1, J_1) . At the linear order, the change from one point to another will correspond to a tangent vector in the parameter space. For any S , the line of constant entropy is given by

$$M = (\sqrt{-\Lambda}) J - \frac{\Lambda}{16\pi^2} S^2. \quad (5.75)$$

The slope of the constant entropy line is then equal to that of the line representing extremal BTZ black holes. Since the tangent to the constant entropy line is a lower

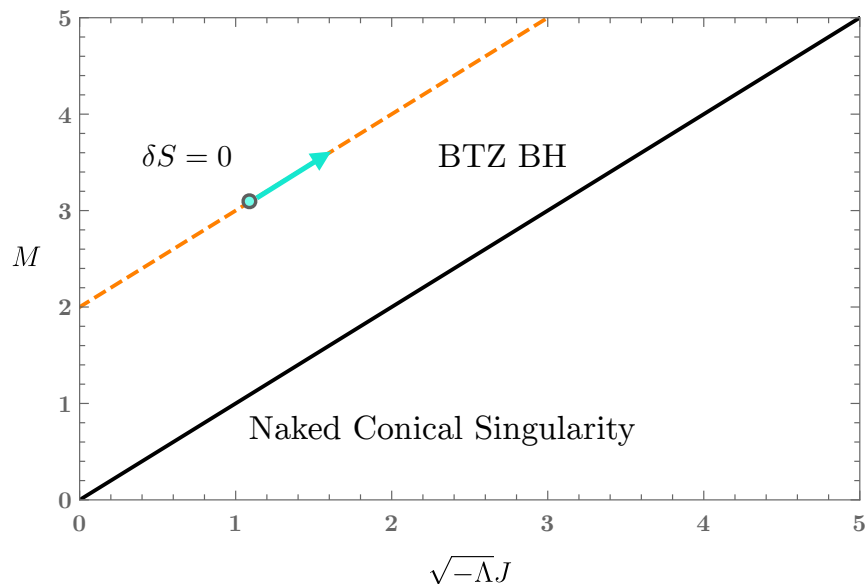


Figure 5.3: The parameter space of BTZ black holes in chiral gravity. The black solid line corresponds to extremal BTZ black holes. Any point above this line corresponds to a non-extremal BTZ black hole, while any point below the line is a naked conical singularity. The orange dashed line is one of the lines of constant entropy, which is parallel to the line for extremal BTZ black holes. Starting with some point on the constant entropy line, any tangent vector will always be parallel to the extremal BTZ line. That is, there is no Hubeny-type violation that can overspin a near-extremal BTZ black hole in chiral gravity.

bound to all physically-realizable perturbations, a non-extremal BTZ black hole will at most be perturbed to another BTZ black hole with the same entropy. There is no Hubeny-type violation of weak cosmic censorship for the BTZ black hole in three-dimensional chiral gravity, thus WCCC is preserved.

Einstein gravity

The discussions above can be applied to the BTZ black holes in three-dimensional Einstein gravity as well, for which we turn off both torsion and Chern-Simons interactions in MB model. In this theory, the linear variational identity is given by

$$\delta \mathcal{M} - \Omega_{\text{H}} \delta \mathcal{J} = \delta M - \Omega_{\text{H}} \delta J. \quad (5.76)$$

Given the material null energy condition, we similarly find that

$$\delta M - \Omega_{\text{H}} \delta J \geq 0. \quad (5.77)$$

Once a first-order perturbation is optimally done by choosing $\delta M = \Omega_H \delta J$, according to the first law of black hole thermodynamics, we will also find a lower bound for all perturbations given by $\delta S = 0$. In Einstein gravity, the entropy of the BTZ black hole is $S = 4\pi r_+$, and the curve of constant entropy is given by

$$M = \frac{4\pi^2}{S^2} J^2 - \frac{\Lambda}{16\pi^2} S^2. \quad (5.78)$$

We plot one of such curves in Fig. 5.4.

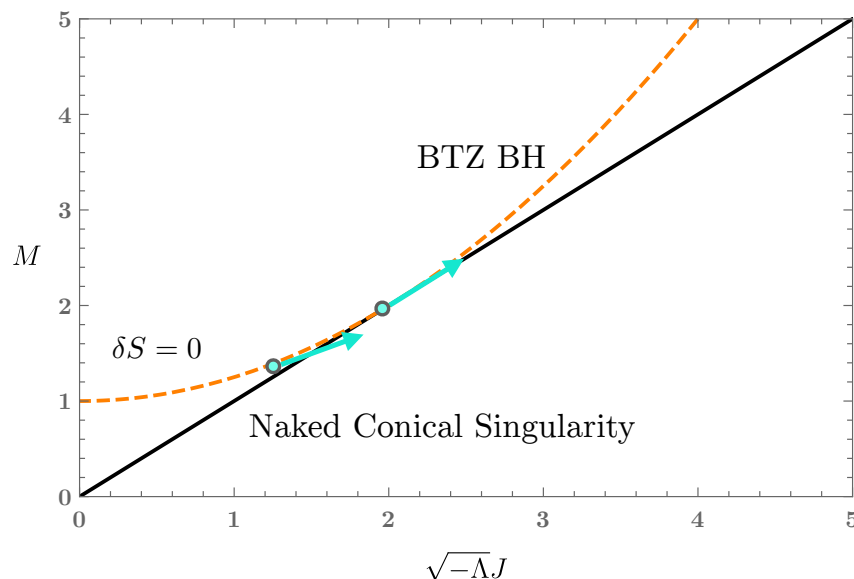


Figure 5.4: The parameter space of BTZ solutions in the three-dimensional Einstein gravity. The black solid line corresponds to extremal BTZ black holes. Any point above this line corresponds to a non-extremal BTZ black hole, while any point below the line is a naked conical singularity. The orange dashed curve is one of the curves of constant entropy, which meets the extremal BTZ line tangentially. The tangent vector at the point of an extremal BTZ black hole will always bring it to another extremal BTZ black hole. However, starting from a slightly non-extremal BTZ black hole, to linear order, the tangent vector can perturb the spacetime to become a naked conical singularity.

As shown in Fig. 5.4, if the initial spacetime is an extremal BTZ black hole, a tangent vector at this point is also tangent to the line representing extremal BTZ solutions. Therefore given extremality, the best one can do is to deform the black hole to another extremal BTZ black hole. WCCC is then preserved and no naked singularities will form. However, if one starts at a slightly non-extremal BTZ black hole, the tangent to the curve of constant entropy is possible to move the original

point to another point located in the region representing naked conical singularities. This type of violation of WCCC is exactly the Hubeny-type violation, which can be found at the linear order for near-extremal black holes. As we will see in the following discussions, a conclusive answer to whether this type of perturbations truly leads to a violation of WCCC requires calculations to the second order.

Now we consider a one-parameter family of solutions $\phi(\lambda)$, $\phi_0 = \phi(0)$ is a nearly extremal BTZ black hole in three-dimensional Einstein gravity. We then expand $f(\lambda)$ in e.q. (5.67) to second order in λ ,

$$f(\lambda) = (M^2 - \alpha^2 J^2) + 2\lambda (M\delta M - \alpha^2 J\delta J) + \lambda^2 [(\delta M)^2 - \alpha^2 (\delta J)^2 + M\delta^2 M - \alpha^2 J\delta^2 J] + O(\lambda^3), \quad (5.79)$$

where we have introduced a parameter $\alpha = \sqrt{-\Lambda}$. For convenience we also introduce a parameter ϵ according to

$$\epsilon = \frac{r_+^2 - r_{+, \text{extremal}}^2}{r_{+, \text{extremal}}^2} = \frac{\sqrt{M^2 - \alpha^2 J^2}}{M}. \quad (5.80)$$

The background spacetime corresponds to $\epsilon \ll 1$, and $\epsilon \rightarrow 0$ is the extremal limit. The null energy condition for the matter fields yields $\delta M - \Omega_H \delta J \geq 0$, which is equivalent to the statement that black hole entropy always increases. If we only consider perturbations to first order in λ , that entropy always increases will constrain $f(\lambda)$ by

$$f(\lambda) \geq M^2 \epsilon^2 - 2\lambda \epsilon (\alpha^2 J \delta J) + O(\lambda^2). \quad (5.81)$$

It is then evident from this inequality that, when $\delta J \sim \epsilon M / \alpha$, it is possible to make $f(\lambda) < 0$ by some careful choice of δJ . This is exactly the Hubeny-type violation of WCCC. The problem is that when $\delta J \sim \epsilon M / \alpha$, the violation of $f(\lambda) \geq 0$ is of order $M^2 \epsilon^2 \sim \alpha^2 (\delta J)^2$, which is not fully captured to first order in λ . Therefore to determine whether there is a true violation of WCCC, one needs to calculate all quantities in (5.81) to the appropriate order.

We now consider the second-order variations in order to give a bound for $f(\lambda)$. Given the null energy conditions for the falling matter, we can obtain the following relation from the second-order variational identity with no inner boundary contributions (5.66),

$$\delta^2 M - \Omega_H \delta^2 J \geq \mathcal{E}_\Sigma(\phi; \delta\phi), \quad (5.82)$$

where the canonical energy \mathcal{E}_Σ is given by

$$\begin{aligned}\mathcal{E}_\Sigma(\phi; \delta\phi) &= \mathcal{E}_\mathcal{H}(\phi; \delta\phi) + \mathcal{E}_{\Sigma_1}(\phi; \delta\phi) \\ &= \int_{\mathcal{H}} \Omega(\phi, \delta\phi, \mathcal{L}_\xi \delta\phi) + \int_{\Sigma_1} \Omega(\phi, \delta\phi, \mathcal{L}_\xi \delta\phi).\end{aligned}\quad (5.83)$$

In (3+1)-dimension, the term $\mathcal{E}_\mathcal{H}(\phi; \delta\phi)$ is identified as the total flux of gravitational wave energy into the black hole [102]. In (2+1)-dimensional Einstein gravity, however, there is no propagating degree of freedom in the bulk, i.e. there is no gravitational wave solution. Thus $\mathcal{E}_\mathcal{H}(\phi; \delta\phi) = 0$. A more rigorous way to see this can be done by following the calculation of the canonical energy as in [102], and we similarly find that

$$\int_{\mathcal{H}} \Omega(\phi, \delta\phi, \mathcal{L}_\xi \delta\phi) = \frac{1}{4\pi} \int_{\mathcal{H}} (\kappa u) \delta\sigma_{ab} \delta\sigma^{ab} \hat{\epsilon} + \frac{1}{16\pi} \int_{\mathcal{H} \cap \Sigma_1} (\kappa u) \delta g^{ab} \delta\sigma_{ab} \hat{\epsilon}, \quad (5.84)$$

where κ is the surface gravity, u is an affine parameter on the future horizon, $\delta\sigma_{ab}$ is the perturbed shear of the horizon generators, and $\hat{\epsilon}$ is the volume element. In three dimension, it is found that every null geodesic congruence is shear-free [129], i.e. $\sigma_{ab} = 0$, therefore $\delta\sigma_{ab} = 0$ on \mathcal{H} and the canonical energy on \mathcal{H} vanishes.

Then we only need to calculate the canonical energy on Σ_1 . According to our assumption, the perturbation $\delta\phi$, as induced by the falling matter, approaches a perturbation $\delta\phi^{\text{BTZ}}$ towards another BTZ black hole on Σ_1 . Also since $\delta\phi^{\text{BTZ}}$ has no gravitational wave energy through \mathcal{H} , we may replace Σ_1 by Σ and obtain that

$$\mathcal{E}_{\Sigma_1}(\phi; \delta\phi) = \mathcal{E}_\Sigma(\phi; \delta\phi^{\text{BTZ}}). \quad (5.85)$$

We use the general second-order variational identity (5.59) on this Σ . As before, we consider a one-parameter family of BTZ black holes, $\phi^{\text{BTZ}}(\beta)$. The black hole mass and angular momentum are given by $M(\beta) = M + \beta \delta M^{\text{BTZ}}$ and $J(\beta) = J + \beta \delta J^{\text{BTZ}}$, where δM^{BTZ} and δJ^{BTZ} are fixed by the first-order perturbation for $\phi(\lambda)$. Therefore for this family of solutions, we have $\delta^2 M = \delta^2 J = \delta E = \delta^2 C = 0$. In Eq. (5.59), the only nonvanishing contribution in the evaluation of the canonical energy $\mathcal{E}_\Sigma(\phi; \delta\phi^{\text{BTZ}})$ then comes from the integral over the bifurcation surface B , which yields

$$\mathcal{E}_{\Sigma_1}(\phi; \delta\phi) = -T_{\text{H}} \delta^2 S^{\text{BTZ}}. \quad (5.86)$$

Here, the minus sign is due to the fact that the bifurcation surface is the inner boundary of Σ .

With the canonical energy being calculated, (5.82) now reads

$$\delta^2 M - \Omega_{\text{H}} \delta^2 J \geq -T_{\text{H}} \delta^2 S^{\text{BTZ}}. \quad (5.87)$$

Here the temperature of the BTZ black hole is given by

$$T_{\text{H}} = -\frac{\Lambda(r_+^2 - r_-^2)}{2\pi r_+} = \frac{\alpha M \epsilon}{\pi \sqrt{2M(1 + \epsilon)}}. \quad (5.88)$$

The second-order variation of the black hole entropy is calculated as

$$\begin{aligned} \delta^2 S^{\text{BTZ}} = & (\delta J)^2 \left(-\frac{\pi \alpha M [\alpha^2 J^2 (3\epsilon + 2) + 2M^2 \epsilon^2 (\epsilon + 1)]}{\sqrt{2}\epsilon^3 [M^3(\epsilon + 1)]^{3/2}} \right) \\ & + (\delta J \delta M) \left(\frac{\pi \sqrt{2}\alpha J(\epsilon + 2)}{M\epsilon^3 \sqrt{M^3(\epsilon + 1)}} \right) + (\delta M)^2 \left(\frac{\pi(\epsilon - 2)(\epsilon + 1)}{\sqrt{2}\alpha\epsilon^3 \sqrt{M^3(\epsilon + 1)}} \right). \end{aligned} \quad (5.89)$$

where we have used the relation that for this family of solutions, $\delta^2 M = \delta^2 J = 0$. We assume that the first-order perturbation is optimally done, i.e. $\delta M = \Omega_{\text{H}} \delta J$, and we use the inequality (5.87) to constrain $f(\lambda)$ in (5.79). We obtain that

$$f(\lambda) \geq M^2 \epsilon^2 - 2\lambda \epsilon \left(\alpha^2 J \delta J \right) + \lambda^2 \frac{\alpha^4 J^2 (\delta J)^2}{M^2} + \mathcal{O}(\lambda^3, \epsilon \lambda^2, \epsilon^2 \lambda, \epsilon^3), \quad (5.90)$$

which can be further written as

$$f(\lambda) \geq \left(M\epsilon - \lambda \frac{\alpha^2 J \delta J}{M} \right)^2 + \mathcal{O}(\lambda^3, \epsilon \lambda^2, \epsilon^2 \lambda, \epsilon^3). \quad (5.91)$$

Consequently, $f(\lambda) \geq 0$ when second-order variations in λ are also taken into account. Our gedanken experiment cannot destroy a near-extremal BTZ black hole in three-dimensional Einstein gravity, leaving WCCC preserved.

5.5 Conclusions and discussions

Along the line of Wald's proposals [15, 17] for 4D Einstein gravity, in this chapter we have considered the gedanken experiments of destroying a BTZ black hole for three different limits of Mielke-Baekler (MB) model of 3D gravity. They are (i) Einstein gravity, (ii) chiral gravity, and (iii) torsional chiral gravity. All three limits are free of perturbative ghosts and show different behaviors in the gedanken experiments. We find that there are Hubeny-type violations for Einstein gravity but none for chiral gravity when trying to destroy a nonextremal BTZ black hole. However, in these two theories, the WCCC holds for both extremal and nonextremal BTZ black holes if the falling matter obeys the null energy condition. It is philosophically interesting

to see that WCCC prevails here even though the BTZ singularity is just a conical one.

On the other hand, for the torsional chiral gravity there is an additional contribution to the null energy condition from the spin angular momentum tensor even at the linear order of variations. Thus, that the WCCC will hold or not depends on the imposition of additional null energy-like condition for the spin angular momentum tensor. If WCCC does not hold for the first-order variations, one needs to check the second-order variation to see if there is Hubeny-type violation. However, the full formalism of deriving the second-order variational identity for MB model is out of scope of this chapter, and it deserves to be a future work.

The third law of black hole dynamics was first proposed by Israel and a sketchy proof was also given [122], which states that one cannot turn a nonextremal black hole into an extremal one by throwing the matter in a finite time interval. Later, the detailed proof was given by Sorce and Wald [17] as described and adopted in this chapter. In the context of AdS/CFT correspondence, the temperature of the boundary CFT is the same as the Hawking temperature of the black hole in the bulk. Thus, our results in this chapter can serve as an operational proof of the third law of thermodynamics by holographically mapping our gedanken experiments around a near-extremal BTZ black hole into the cooling processes of the boundary CFT toward zero temperature. Generalizations to BTZ black holes though seems straightforward, its implication to the third law of thermodynamics for holographic condensed matter systems is nontrivial and deserves further study. Especially, the generalization to the higher-dimensional AdS black holes for more general gravity theories will give holographic tests of the third law of thermodynamics for the more realistic systems. We plan to attack this problem in the near future.

Before ending the chapter, we comment on one more point about the proof of the third law by noticing that the equality of (5.91) holds for one particular choice of parameter λ . This implies that one can reach the extremal black hole at the second order for this particular case. To pin down the issue, one needs to check the third order of variation for this particular λ value. This is too involved to carry out just for a measure-zero possibility. However, it is still an interesting issue for the future work.

PART III

SEARCHING FOR NEAR-HORIZON QUANTUM STRUCTURES VIA GRAVITATIONAL-WAVE ECHOES

Chapter 6

INSTABILITY OF EXOTIC COMPACT OBJECTS AND IMPLICATIONS FOR ECHOES

Exotic compact objects (ECOs) have recently become an exciting research subject, since they are speculated to have a special response to the incident gravitational waves (GWs) that leads to GW echoes. We show that energy carried by GWs can easily cause the event horizon to form out of a static ECO — leaving no echo signals towards null infinity. To show this, we use ingoing Vaidya spacetime and take into account the back reaction due to incoming GWs. Demanding that an ECO does not collapse into a black hole puts an upper bound on the compactness of the ECO, at the cost of less distinct echo signals for smaller compactness. The trade-off between echoes' detectability and distinguishability leads to a fine tuning of ECO parameters for LIGO to find distinct echoes. We also show that an extremely compact ECO that can survive the gravitational collapse and give rise to GW echoes might have to expand its surface in a non-causal way.

6.1 Introduction

Black holes are important predictions of classical general relativity, and shown to be robust products of gravitational collapses. The *event horizon*, describing the boundary within which the future null infinity cannot be reached, is the defining feature of a black hole [130]. It is hoped that gravitational-wave (GW) observations can provide evidence for the event horizon. Absence of the event horizon, as well as deviations from the Kerr geometry near the horizon, can be motivated by quantum-gravity and quantum-information considerations. Objects whose spacetime geometries mimic that of a black hole, except in the near-horizon region, have been speculated to exist, and are referred to as exotic compact objects (ECOs) [131, 132]. The boundary between the Kerr and non-Kerr regions of the ECO are often placed at Planck scale above the horizon.

Pani *et al.* argued that GWs emitted from a gravitational collapse or a compact binary coalescence (CBC), which results in an ECO, should be followed by *echoes* [18, 19, 133, 134]. GWs that propagate toward the ECO can be reflected by the ECO surface — or penetrate through the ECO and re-merge at its surface — and bounce back and forth between the ECO's gravitational potential barrier (at the location of

the light sphere) and the ECO itself [21, 135–138]. GW echoes, as the smoking gun of ECOs [20], have generated enormous interest. Most notably, Abedi et al. claimed to have found evidence of echoes in Advanced Laser Interferometer Gravitational Wave Observatory (Advanced LIGO) data after the first few observed CBC events [22, 30, 31], and the statistical significance of these signatures was being questioned [32–35]. Alternative techniques in searching for echoes have been proposed [33–35, 139, 140].

It was realized that ECOs may suffer from nonlinear instabilities [141]. Moreover, the accreting matter can trigger the instability of ECOs, which then puts a bound on the compactness of the existing ECO models, using the Vaidya geometry [142]. We would like to consider the possible instability of ECOs induced by incoming gravitational wave radiations. As radiations propagate near the ECO surface, they get increasingly blue shifted (for observers with constant Schwarzschild/Boyer-Lindquist r , e.g., those who sit on the ECO surface); energy is also crammed into a compact region (in terms of Δr), and we need to consider its back reaction to the spacetime geometry [143]. As Eardley [144] and Redmount [145] were studying the stability of white holes and worm holes in an astrophysical environment, they concluded that the “blue sheet” made up by in-falling material and radiations can cause the formation of an event horizon. Another point of view of such instability is through Thorne’s hoop conjecture [146], as shown in Fig. 6.1, which says a certain amount of mass/energy will collapse into a black hole when it is inside the “hoop” located at its own Schwarzschild radius. Similarly, ECOs may suffer from such instability caused by GWs and collapse into black holes. In this paper, we study the condition for ECO to remain stable and the impact of back reaction on GW echoes.

6.2 Set up of the problem

We would like to consider a particle (or a star) plunging into an ECO. During the ringdown process, gravitational waves can be emitted near the light ring both towards the ECO and the infinity. For simplicity, we consider a spherically symmetric initial ECO with mass M and areal radius $r_{\text{ECO}} = 2M + \epsilon$, and an incident GW packet with energy E . Here ϵ is a small distance that quantifies the compactness of the ECO; $\Delta \equiv \sqrt{8M\epsilon}$ is also used to characterize “the spatial distance between ECO surface and the horizon”. For the ringdown phase of a CBC, cumulative energy emitted from the potential barrier towards the ECO, up to Schwarzschild time t is given by

$$E_{\text{RD}}(t) \approx \alpha_{\text{H}}(4\eta)^2 M(1 - e^{-2\gamma t}), \quad (6.1)$$

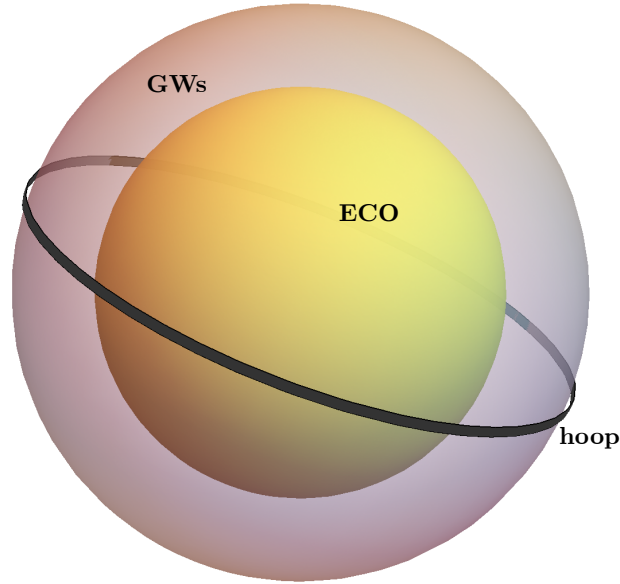


Figure 6.1: A pulse of GW with energy E incident on a static ECO with mass M . A hoop is placed at the Schwarzschild radius $2(M + E)$. When the spatial extent of the GWs becomes compacted within the hoop in every direction, the event horizon forms.

where γ is the imaginary part of the quasinormal modes (QNM) frequency, $\eta = M_1 M_2 (M_1 + M_2)^{-2}$ is the symmetric mass ratio, with M_1 and M_2 being the masses of the two objects in the binary, and the numerical factor α_H is typically estimated to be 3%-10% depending on the choice of ringdown time [147]. Here we fix this parameter to be 5%. We define the tortoise coordinate r_* from the Schwarzschild radius r as $r_* = r + 2M \log(r/2M - 1)$. The conventional estimate for the time lag between the first echo and the beginning of the ringdown signal is given by

$$\Delta t_{\text{echo}}^{\text{conv}} = 2|r_*^{\text{LR}} - r_*^{\text{ECO}}| \approx 2M + 4M \log(M/\epsilon). \quad (6.2)$$

where LR stands for the light ring at $r^{\text{LR}} = 3M$, and r_*^{ECO} is the tortoise coordinate for r_{ECO} ¹.

6.3 Estimates based on the hoop conjecture

According to the *hoop conjecture* [146], the event horizon forms when a certain amount of mass gets compacted within its own Schwarzschild radius. This corresponds to a zeroth-order estimate on the effect of the incoming energy towards an ECO, in the sense that we neglect the back reactions of the GWs to the ECO

¹In some existing literature, the time lag between the first echo and the beginning of the ringdown signal is denoted by t_{echo} , and notation Δt_{echo} is used to denote the time lag between two echoes.

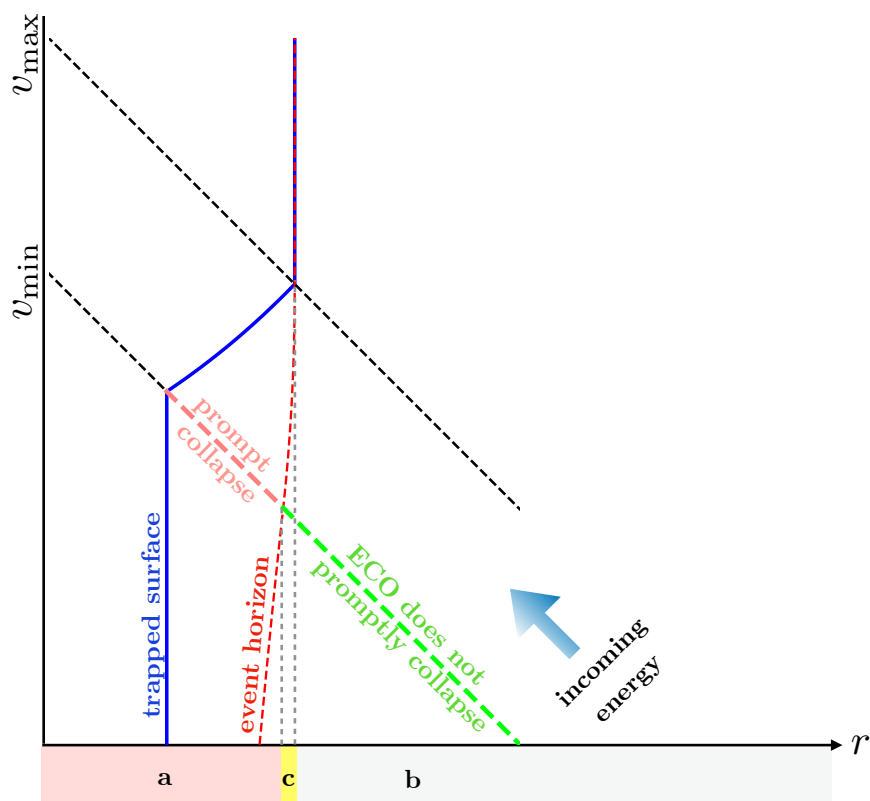


Figure 6.2: A Vaidya spacetime with an incoming null packet spatially bounded by the black dashed line. The trapped surface evolves along the blue solid line. The event horizon evolves along the red dashed line, and coincides with the trapped surface after all energy goes into the horizon. Any ECO with its surface crossing the pink line will promptly collapse, while those cross the green line does not. Static ECOs can then be divided into three different types (a), (b), and (c), separated by the gray dashed lines (not world lines), and are discussed in detail in the main text.

Schwarzschild spacetime. As shown in Fig. 6.1, at the instant when all incoming energy gets compacted within the “hoop”, the event horizon forms. If we consider the null packet carrying the ringdown energy (6.1), to prevent horizon formation, the location of the ECO surface must satisfy

$$r_{\text{ECO}} - 2M > 0.015(4\eta)^2 M (M\gamma/0.1)(\alpha_H/0.05). \quad (6.3)$$

This means, stable, static ECOs cannot be very compact— ϵ or Δ are far from Planck scale.

6.4 In-going Vaidya spacetime

To approach a more accurate study of the back reaction of the incoming GWs, we consider a Vaidya geometry,

$$ds^2 = -[1 - 2M(v)/r] dv^2 + 2drdv + r^2 d\Omega^2, \quad (6.4)$$

where v is the advanced time, and $M(v)$ is the total gravitational mass that has entered the spacetime up to v . The Vaidya geometry, as an approximation, describes a spherically symmetric spacetime with (gravitating) in-falling dust along radial null rays, but does not capture the fact that GW energy is not spherically symmetrically distributed — nor does it capture GW oscillations. For incident GWs during $v_{\min} < v < v_{\max}$, we have

$$M(v) = M_{\min} + E(v), \quad (6.5)$$

where $E(v)$ is total GW energy that has entered since v_{\min} . M grows from M_{\min} to $M_{\max} \equiv M_{\min} + E_{\text{tot}}$. During the process of incoming GWs, as shown in Fig. 6.2, the apparent horizon (AH) traces the total energy content, and is located at $r_{\text{AH}} = 2M(v)$. The event horizon (EH), on the other hand, follows out-going radial null geodesics, parameterized by $r(v)$, which satisfies

$$2dr/dv = 1 - 2M(v)/r(v). \quad (6.6)$$

We also need to impose a *final condition* of $r_{\text{EH}}(v_{\max}) = 2M_{\max}$. Assuming $\dot{M} \ll 1$, writing $r_{\text{EH}}(v) = 2M(v) + \delta(v)$ with $\delta \ll M$, we have $\dot{\delta} - \delta/(4M) = -2\dot{M}$, and the solution is given by

$$\delta(v) = 2 \int_v^{v_{\max}} dv' \dot{M}(v') \exp \left[- \int_v^{v'} dv'' \frac{1}{4M(v'')} \right]. \quad (6.7)$$

The required final condition for δ , as well as the dependency of $\delta(v)$ on $\dot{M}(v')$ at $v' > v$, embodies the *teleological nature* of the EH: the location of the EH right now is determined by what shall happen in the future.

For the ringdown of a CBC, we substitute $E(v) = E_{\text{RD}}(v - v_{\min})$ into the solution and obtain

$$\delta(v) = \frac{16(4\eta)^2 \alpha_{\text{H}} M(M\gamma)}{1 + 8M\gamma} e^{-2(v-v_{\min})} \equiv \epsilon_{\text{th}} e^{-2(v-v_{\min})}. \quad (6.8)$$

Next, we use Vaidya spacetime only as the *exterior* of the ECO, and consider two scenarios: (i) GW-induced collapse of a static ECO and (ii) an ECO with expanding surface.

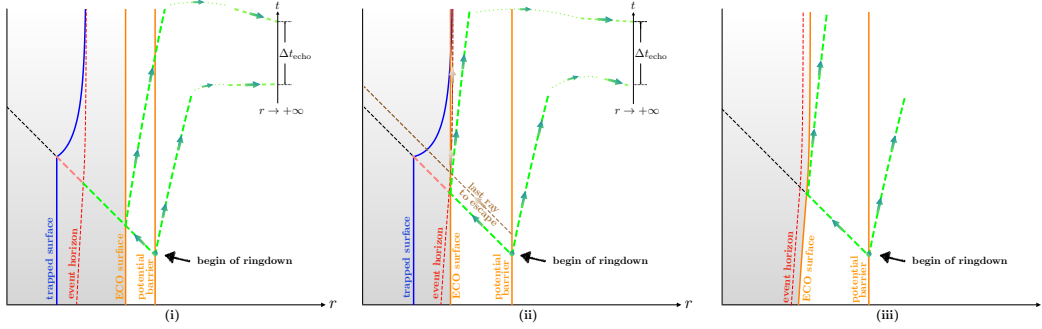


Figure 6.3: (a) A static ECO scenario where the ECO surface is outside the event horizon and, which can give rise to GW echoes. The spatially nearest incoming ray, denoted by the green dashed line, reflects at the potential barrier and the ECO surface, leading to a time delay Δt_{echo} between the main wave and the echo as observed at spatial infinity. (b) A static ECO scenario where part of the incoming GW energy gets reflected at the ECO surface and gives rise to echoes until “the-last-ray-to-escape”. The subsequent echoes are highly redshifted due to the formation of event horizon, leading to a weak echo signal. (c) Spherically symmetric ECO absorbing GWs and expanding in radius. The event horizon grows along the red dashed line. If the ECO surface always remains outside the event horizon, incoming rays can lead to GW echoes, as shown by the green dashed lines.

6.5 Back reaction: static ECO with future incoming pulse

For static ECOs with radius $r = r_{\text{ECO}}$ and initial mass M_{min} , we can divide them into three types as in Fig. 6.2:

- (a) For $r_{\text{ECO}} < 2M_{\text{min}} + \epsilon_{\text{th}}$, the ECO will promptly collapse and there will be no GW echoes, since the first incoming ray reaches the ECO inside the EH.
- (b) For $r_{\text{ECO}} > 2M_{\text{max}}$, the ECO does not collapse, and conventional echoes (generally more than one) will form, as individually shown in Fig. 6.3(i).
- (c) For $2M_{\text{min}} + \epsilon_{\text{th}} < r_{\text{ECO}} < 2M_{\text{max}}$, the ECO enters the EH (hence collapses) during the incoming GW pulse. Only one echo, with reduced magnitude, could form, as individually shown in Fig. 6.3(ii).

The magnitude of ϵ_{th} indicates that static ECOs that can produce echoes will deviate from a black hole at a distance far from Planck scale above the horizon. In terms of compactness, for $M\gamma \approx 0.1$, we have

$$\epsilon_{\text{th}}/(2M) = 0.022(\alpha_{\text{H}}/0.05)(4\eta)^2. \quad (6.9)$$

For a comparable-mass binary (e.g., $\eta = 0.25$), this corresponds to a moderate bound on the compactness; for extreme mass-ratio inspirals (EMRIs) with $\eta = 10^{-7}$,

compactness $\epsilon_{\text{th}}/(2M)$ reaches 3.5×10^{-15} for typical values of α_{H} and $M\gamma$. In terms of proper distance above the horizon, we have, $M\gamma \approx 0.1$,

$$\Delta_{\text{th}} = 8\sqrt{\frac{2\alpha_{\text{H}}(4\eta)^2 M^3 \gamma}{1 + 8M\gamma}} \approx 2.4\eta M \sqrt{\alpha_{\text{H}}/0.05}. \quad (6.10)$$

For stellar mass CBC, Δ_{th} is at least kilometer-scale, far from Planck scale.

6.6 Back reaction: expanding ECO

If the ECO has an expanding surface, as shown in Fig. 6.3c, its increasing radius could *in principle* keep up with the influx of GW energy, so that the horizon will not form. For example, *if*

$$r_{\text{ECO}}(v) = r_{\text{EH}}(v) + \epsilon = 2M(v) + \delta(v) + \epsilon, \quad (6.11)$$

with a constant positive ϵ which can be arbitrarily small, ECO surface will be time-like. We need to emphasize that the expansion trajectory (6.11), although being time-like, is *teleological* in nature, since its rate of expansion must be determined by the *future* in-going GW flux. In other words, internal physics of the ECO must know how much energy is going to come in the future, and adjust the ECO radius accordingly, before the waves arrive.

6.7 Implications for GW-echo phenomenology

The back reaction of incoming GWs substantially affects the phenomenology of GW echoes by imposing constraints on Δt_{echo} , which is the first echo's time lag behind the main wave. When Δt_{echo} is comparable to the ringdown time scale $1/\gamma$, the echoes will interfere with the main wave [21], giving rise to less distinct echo signals. To better illustrate this, we define a ratio R between these two time scales via $R \equiv \gamma \Delta t_{\text{echo}}$. Then the echo is separated from the main wave when $R \geq 1$.

For static ECOs of type (a), which promptly collapse, there are no echoes. For types (b) [Fig. 6.3a] and (c) [Fig. 6.3(ii)], the ratio R can be obtained from

$$r_{\text{ECO}}/M - 2 = \epsilon_{\text{th}}/M + \exp[-R/(4M\gamma) + 1/2]. \quad (6.12)$$

In Fig. 6.4, we plot the contour of R as function of $r_{\text{ECO}}/M - 2$ and $\alpha_{\text{H}}(4\eta)^2$. For type (b), echo arises from the entire duration of incoming GW, there will be *subsequent echoes*, when GW reflected from the ECO further travel back and forth between the potential barrier and the ECO. For type (c), echo arises only from the first part of the incoming GW, up till the “last ray to escape” shown in Fig. 6.3(ii), and *there*

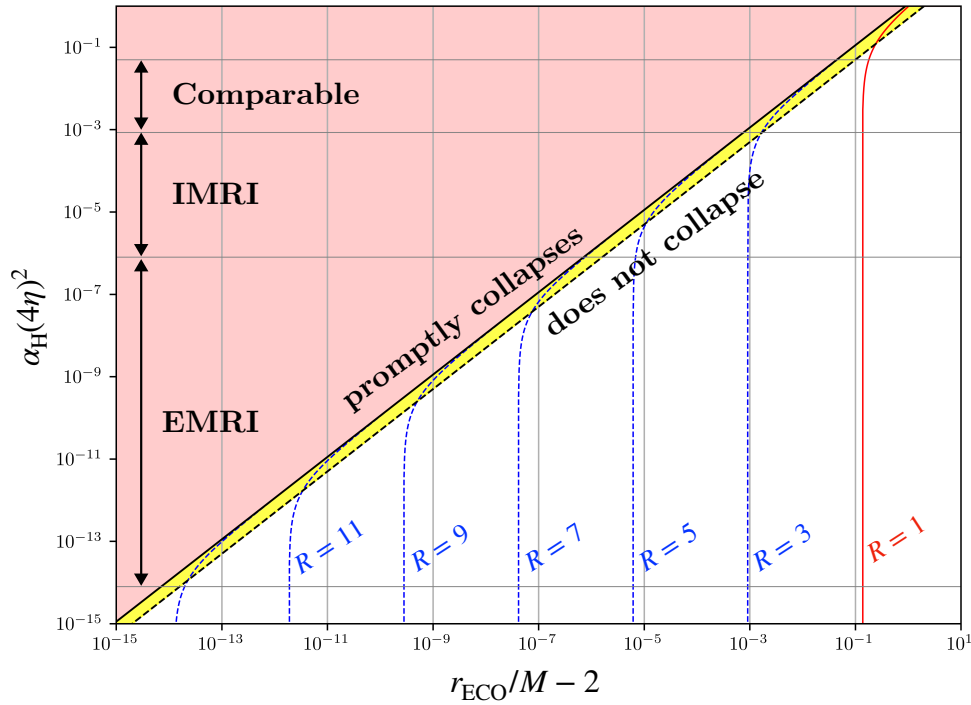


Figure 6.4: Contour plot for R as function of $r_{\text{ECO}}/M - 2$ and $\alpha_{\text{H}}(4\eta)^2$. Regions in red, white, and yellow indicate types (a), (b), and (c), respectively. Along the vertical axis, the ranges indicate comparable, intermediate, and extreme mass ratio inspirals.

can only be one echo. The reflected GW will first oscillate and then be “frozen” due to ECO gravitational collapse. Since the low-frequency component of the reflected GW can not propagate to infinity due to the filtering of the frequency-dependent potential barrier, the distant observer will just see a weakened QNM waveform.

For CBCs observable by LIGO, we choose, for instance, $\eta = 0.25$, $\alpha_{\text{H}} = 0.05$ and $M\gamma = 0.1$, which are consistent with GW150914 [148]. We then have $\epsilon_{\text{th}} = 0.044M$. Type (b) ECOs should have $r_{\text{ECO}} > 2.1M$. In particular, for $2.1M < r_{\text{ECO}} < 2.18M$, we have $1 < R < 1.4$. For type (c) ECOs, we could have much larger R , but that would correspond to a small region in parameter space.

Previously, one could have argued that exotic physics could create static ECOs that have r_{ECO}/M very close to 2. However, to have a moderately large R , Eq. (6.12) requires that r_{ECO}/M be exponentially close to $2 + \epsilon_{\text{th}}$, with ϵ_{th} depending on the incoming GW. This seems a fine tuning for static ECOs which is very unlikely to

happen.

For EMRIs targeted by Laser Interferometer Space Antenna (LISA), less incoming GWs allows more compact ECOs to be probed. Let us consider $\alpha_H = 0.05$, $\eta = 10^{-7}$ and $M\gamma = 0.1$, and use the boundary between type (b) and type (c) as the typical ECO compactness. In this case, we will have $R^{\text{typical}} \approx 13$, which corresponds to a distinct echo signal.

In the case of expanding ECOs with $r_{\text{ECO}} = 2M(v) + \epsilon$, under the approximation that $\dot{M}(v) \ll 1$, Δt_{echo} is given by $\Delta t_{\text{echo}}^{\text{expand}} = 2M + 4M \log[M/\epsilon]$, which is equal to $\Delta t_{\text{echo}}^{\text{conv}}$. Here we see that a teleologically expanding ECO has the same phenomenology proposed in existing literature.

6.8 Discussions

As an attempt to use simplified analytical solutions to capture features of a highly complex spacetime geometry, governed by yet unknown physics, our work has several limitations. (i) We have focused on the echo of *reflective type*, i.e., the echo generated by the reflection of the main wave on the ECO surface. For those echoes of *transmissive type*, i.e., the echo generated by the GW penetration into and re-emerging out of the ECO surface, the delay of echo signal depends on the specific ECO model. (ii) Our Vaidya spacetime model only captures the back reaction of the ingoing GW flux, while in reality the reflected outgoing GWs also gravitate. The back reaction of the reflected waves may have qualitatively significant effects on the echoes when the surface reflectivity is large. (iii) We have not attempted to describe what happens as the other object impacts the ECO, which takes place roughly at the same time as the ringdown wave starts to impinge on the final compact object. Finally, while the teleological response necessary for the expanding ECO sounds unnatural, it might arise due to *non-local* interactions that were speculated to exist near the event horizon [149]; we also note that the final-state projection model [150, 151] may also be regarded as teleological in nature.

6.9 Appendix

Derivation of the ECO compactness bound via the hoop conjecture

In this section, we present a derivation of Eq. (6.3), which gives the compactness bound on ECOs using the hoop conjecture. For simplicity, we assume that there is a pulse of gravitational wave carrying energy E and incidenting on a static ECO with mass M , as shown in We further assume that the spatial extents of the gravitational

wave are bounded by r_*^{\max} and r_*^{\min} . Therefore at any given moment, we have

$$r_*^{\max} - r_*^{\min} = T, \quad (6.13)$$

where T is the duration of the GW pulse measured in Schwarzschild time. According to the hoop conjecture, when the spatial extents of the gravitational wave are all within a ‘‘hoop’’ located at the Schwarzschild radius $2(M + E)$, a black hole forms. Therefore in a threshold case, when r_*^{\min} coincides with the ECO surface, r_*^{\max} happens to coincide with the location of the event horizon (or the ‘‘hoop’’). That is, to avoid the event horizon formation, it requires

$$T < 2E + 2M \log \left(\frac{2E}{r_{\text{ECO}} - 2M} \right). \quad (6.14)$$

In the threshold case, we can solve for a critical duration T_c using

$$T_c = 2E(T_c) + 2M \log \left(\frac{2E(T_c)}{r_{\text{ECO}} - 2M} \right). \quad (6.15)$$

We plug in the ringdown energy $E(T) = \alpha_{\text{H}}(4\eta)^2 M(1 - e^{-2\gamma T})$, and take T -derivative on both sides. For the threshold case, we obtain

$$4\alpha_{\text{H}}\gamma\eta M e^{-2\gamma T_c} + \frac{4\gamma M e^{-2\gamma T_c}}{1 - e^{-2\gamma T_c}} = 1. \quad (6.16)$$

The critical duration T_c is then given by

$$e^{-2\gamma T_c} = -\frac{\sqrt{(4\alpha_{\text{H}}\gamma(4\eta)^2 M + 4\gamma M + 1)^2 + 16\alpha_{\text{H}}\gamma(4\eta)^2 M}}{8\alpha_{\text{H}}\gamma(4\eta)^2 M} + \frac{1}{2} + \frac{1}{2\alpha_{\text{H}}(4\eta)^2} + \frac{1}{8\alpha_{\text{H}}\gamma(4\eta)^2 M}. \quad (6.17)$$

Thus using (6.14), one can show that, in order to avoid horizon formation, the bound on the ECO compactness is given by

$$r_{\text{ECO}} - 2M > \frac{32\alpha_{\text{H}}\eta^2(M\gamma)}{e} M + \mathcal{O}(\alpha_{\text{H}}^2, (M\gamma)^2), \quad (6.18)$$

which reduces to Eq. (6.3) when α_{H} and $M\gamma$ are both small.

TIDAL RESPONSE AND NEAR-HORIZON BOUNDARY CONDITIONS FOR SPINNING ECOS

Teukolsky equations for $|s| = 2$ provide efficient ways to solve for curvature perturbations around Kerr black holes. Imposing regularity conditions on these perturbations on the future (past) horizon corresponds to imposing an ingoing (outgoing) wave boundary condition. For exotic compact objects (ECOs) with external Kerr space time, however, it is not yet clear how to physically impose boundary conditions for curvature perturbations on their boundaries. We address this problem using the Membrane Paradigm, by considering a family of zero-angular-momentum fiducial observers (FIDOs) that float right above the horizon of a linearly perturbed Kerr black hole. From the reference frame of these observers, the ECO will experience tidal perturbations due to ingoing gravitational waves, respond to these waves, and generate outgoing waves. As it also turns out, if both ingoing and outgoing waves exist near the horizon, the Newman Penrose (NP) quantity ψ_0 will be numerically dominated by the ingoing wave, while the NP quantity ψ_4 will be dominated by the outgoing wave — even though both quantities contain full information regarding the wave field. In this way, we obtain the ECO boundary condition in the form of a relation between ψ_0 and the complex conjugate of ψ_4 , in a way that is determined by the ECO’s tidal response in the FIDO frame. We explore several ways to modify gravitational-wave dispersion in the FIDO frame, and deduce the corresponding ECO boundary condition for Teukolsky functions. Using the Starobinsky-Teukolsky identity, we subsequently obtain the boundary condition for ψ_4 alone, as well as for the Sasaki-Nakamura and Detweiler’s functions. As it also turns out, reflection of spinning ECOs will generically mix between different ℓ components of the perturbations fields, and be different for perturbations with different parities. It is straightforward to apply our boundary condition to computing gravitational-wave echoes from spinning ECOs, and to solve for the spinning ECOs’ quasi-normal modes.

7.1 Introduction

A black hole (BH) is characterized by the event horizon, a boundary of the space-time region within which the future null infinity cannot be reached. The existence

of a horizon has led to the simplicity of black-hole solutions in general relativity and modified theories of gravity, although the notion of a horizon has also led to technical and conceptual problems. First of all, at the classical level, the event horizon has a *teleological nature*: its shape at a particular time-slice of a spacetime depends on what happens to the future of that slice. Even if we are provided with a full numerical solution of the Einstein's equation (e.g., in the form of all metric components in a particular coordinate system), it is much harder to determine the location of the event horizon than *trapped surfaces*, whose definitions are more local.

In classical general relativity, it has been shown that a singularity (or singularities) should always exist inside the event horizon [14]. This requires that quantum gravity must be used to study the space-time geometry inside black holes. Naively, one expects corrections when space-time curvature is at the Planck scale. However, the unique causal structure of the horizon already leads to non-trivial quantum effects, e.g., Hawking radiation [63, 152]. From considerations of quantum gravity, it has been proposed that space-time geometry near the horizon can be modified, even at scales larger than the Planck scale [153, 153–163]. It has also been conjectured that a phase transition might occur during the formation of black holes, leading to non-singular, yet extremely compact objects [164, 165]. All these considerations (or speculations) lead to a similar class of objects: their external space-time geometries mimic those of black holes except very close to the horizon. We shall refer to these objects as *Exotic Compact Objects* (ECOs).

Followed by the unprecedented discovery of gravitational waves from the binary BH merger event GW150914 [2], and follow-up observations of an order of ~ 100 binary black-hole merger events [3, 4], we now know that dark compact objects do exist in our universe, and that their space-time geometry and dynamics are consistent with those of black holes in general relativity, better than order unity, and at scales comparable to the sizes of the black holes. Observations by the Event Horizon Telescope (EHT) provides yet another avenue toward near-horizon physics of black holes [5–12].

Since the horizon is defined as the boundary of the unreachable region, hence it “absorbs” all radiation. Instead of asking whether the horizon exists, a more testable question might be how absorptive the horizon is: any potential modifications to classical general relativity near the surface of an ECO, be it quantum or not, may impose a different physical boundary condition near the horizon. That is, for any

incoming gravitational radiations, they not only can fall into the dark object, but may also get reflected, and then propagate to the infinity. In the context of a point particle orbiting a black-hole candidate, this was studied as a modified tidal interaction [166–168]. Alternatively, a stronger probe of the reflectivity is provided by waves that propagate toward the horizon of the final (remnant) black hole after the merger of two black holes — in the form of repeated GW echoes at late times in the ringdown signal of a binary merger event [18–29]. Following this line of thought, the gravitational echoes have been extensively studied in different models of near-horizon structures [140, 169–175]. Even though the idea of ECOs might be speculative, one can always regard the search for ECOs as one to quantify the darkness of the final objects in binary merger events, and in this way its importance cannot be overstated.

The key problem for calculating the echoes from spinning ECOs is how to apply boundary conditions near the horizon for curvature perturbations obtained from the Teukolsky equation. This was discussed, by Nakano et al. [176] and Wang and Afshordi [170], but for Kerr there are still more details to fill in — even though Kerr echoes have already been studied by several authors [23–27]. This is the main problem we would like to address in this paper.

Imposing a near-horizon boundary condition is more straightforward in Schwarzschild spacetime. The Schwarzschild metric perturbations can be fully constructed from solutions of the Regge-Wheeler equation [46] and the Zerilli equation [49], both of which are wave equations that have regular asymptotic behaviors at horizon and infinity. These metric perturbations can then be used to connect to the response of the ECO to external perturbations. In the Kerr spacetime, perturbations are most efficiently described by the $s = \pm 2$ Teukolsky equations [41] for curvature components that are projected along null directions, and therefore are less directly connected to tidal perturbations and responses of an ECO. Furthermore, the Teukolsky equations for the $s = \pm 2$ cases do not have short-range potentials, and result in solutions that do not have the standard form of incoming and outgoing waves, leading to certain difficulties in finding numerical solutions.

To solve the second issue, the Teukolsky equations can be transformed into wave-like equations with short-ranged potentials, namely the Sasaki-Nakamura (SN) equations, via the Chandrasekhar-Sasaki-Nakamura (CSN) transformation [177–179]. In order to define the near-horizon reflection of waves in the Kerr spacetime, it was proposed that the reflection should be applied to the SN functions — as has

been widely used in many literatures regarding gravitational wave echoes [23–26, 26, 136, 138, 140, 167]. Despite the short-rangedness of the SN equation, the physical meaning of SN functions are less clear than the Teukolsky functions, especially in the Kerr case.

For the Kerr spacetime, Thorne, Price, and MacDonald introduced the “Membrane Paradigm” (MP) [180], by considering a family of fiducial observers (FIDOs) with zero angular momentum. World lines of the collection of these observers form a “membrane”—which can be used as a proxy to think about the interaction between the black hole and the external universe. In order to recover the pure darkness of the black hole, the membrane must have the correct complex (in fact purely resistive) impedance for each type of flux/current, so that nothing is reflected. For example, the membrane must have the correct specific viscosity in order for gravitational waves not to be reflected, and the correct (electric) resistivity in order for electromagnetic waves not to be reflected. Extensive discussions were made on the physics viewed by the FIDOs, in particular tidal tensors measured by these observers in the presence of gravitational waves. The picture was more recently used to visualize space-time geometry using Tendex and Vortex picture [181–183].

It has been proposed that reflectivity of ECOs can be modeled by altering the impedance of the ECO surface [170, 176, 184]. In this paper, we generalize this point of view to ECOs with nonzero spins. It is worth mentioning that the the membrane paradigm point of view has been taken by Datta *et al.* [168, 185] to study the tidal heating of Kerr-like ECOs, although reflection of waves by the ECO was not described. In this paper we shall continue along with the membrane paradigm, and propose a physical definition of the ECO’s reflectivity.

In order to do so, we make a careful connection between Teukolsky functions, which efficiently describe wave propagation between the near-horizon region and infinity, and ingoing and outgoing tidal waves in the FIDO frame of the Membrane Paradigm. We then obtain boundary conditions for the Teukolsky equations in terms of tidal responses of the ECO in the FIDO frame. Here the *fundamental assumption* that we rely upon — as has also been made implicitly in previous ECO reflectivity literatures — is that the ECO has a simple structure in the FIDO frame — for example as a distribution of exotic matter that modifies dispersion relation of gravitational waves in the FIDO frame.

We organize the paper as follows. In Sec. 7.2, by considering individual FIDOs, we introduce the modified boundary conditions in Teukolsky equations based on

the tidal response of the ECO, and obtain input-output relations for Teukolsky equations in terms of that tidal response. In Sec. 7.3, we more specifically consider a Rindler coordinate system near the horizon, and put our discussion into a more firm ground by relating the Teukolsky functions to Riemann tensor components in this coordinate system. We further consider modified gravitational-wave dispersion relations in the Rindler frame, and relate these relations to the ECO’s tidal response. In Sec. 7.4, we translate our reflection model into a model which fits most literatures on gravitational-wave echoes, in particular making connections to the SN formalism. In Sec. 7.5, we apply our method to obtain the echo waveform as well as the quasi-normal modes (QNMs) of the ECOs. Showing that even- and odd-parity waves will generate different echoes, and generalize the breaking of QNM *isospectrality* found by Maggio *et al.* [184] to the spinning case. In Sec. 7.6, we summarize all results and propose possible future works.

Notation. We choose the natural units $G = c = 1$, and set the black hole mass $M = 1$. The following symbols are also used throughout the paper:

$$\Delta = r^2 - 2r + a^2, \quad (7.1)$$

$$\Sigma = r^2 + a^2 \cos^2 \theta, \quad (7.2)$$

$$\rho = -(r - ia \cos \theta)^{-1}. \quad (7.3)$$

Here (t, r, θ, ϕ) are the Boyer-Lindquist coordinates for Kerr black holes and a is the black hole spin. The Kerr horizons are at the Boyer-Lindquist radius $r_H = 1 + \sqrt{1 - a^2}$, while the inner horizons are at $r_C = 1 - \sqrt{1 - a^2}$. The angular velocity of the horizon is given by $\Omega_H = a / (2r_H)$. The tortoise coordinate is defined by

$$r_* = r + \frac{2r_H}{r_H - r_C} \ln \left(\frac{r - r_H}{2} \right) - \frac{2r_C}{r_H - r_C} \ln \left(\frac{r - r_C}{2} \right). \quad (7.4)$$

7.2 The reflection boundary condition from tidal response

In a $(3 + 1)$ -splitting of the spacetime, the Weyl curvature tensor C_{abcd} naturally gets split into an “electric” part, which is responsible for the *tidal effect*, and a “magnetic” part, which is responsible for the *frame-dragging effect*. From now on, we will focus on the electric part, as it gives rise to the gravitational stretching and squeezing, i.e. the tidal force, which drives the geodesic deviations of particles that are *slowly moving with respect to that slicing*.

In MP, a relation is established between the Newman-Penrose quantity ψ_0 near the future horizon and components of the tidal tensors in the FIDO frame. In this

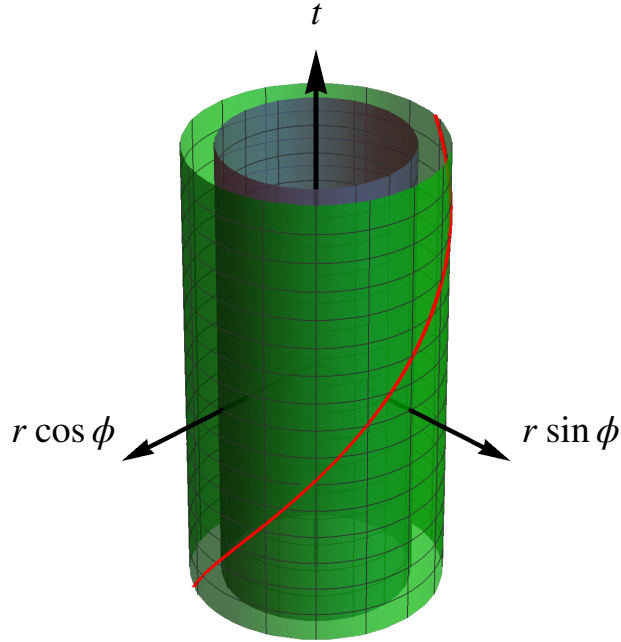


Figure 7.1: Trajectory of the FIDO in a constant θ slice of the Kerr spacetime in the $(t, r \cos \phi, r \sin \phi)$ coordinate system. Here the green surface indicates the ECO surface with $r = b$, while the black surface indicates the Kerr horizon. Each FIDO has $r = b$, but has $(t, \phi) = (t, \phi_0 + \Omega_H t)$.

section, we will extend this to include waves “originating from past horizon”, which really are waves in the vicinity of the horizon but propagate toward the positive r direction, see Fig. 7.2. More specifically, we seek to derive the relation among the tidal tensor components, the incoming waves, and the “reflected” (outgoing) waves due to the tidal response. This will establish our model of near-horizon reflection for the Teukolsky equations.

FIDOs

Starting from the Boyer-Lindquist coordinate system (t, r, θ, ϕ) , FIDOs in the MP are characterized by constant r and θ , but $\phi = \text{const} + \omega_\phi t$, with

$$\omega_\phi = \frac{2ar}{\Xi}. \quad (7.5)$$

and

$$\Xi = (r^2 + a^2)^2 - a^2 \Delta \sin^2 \theta. \quad (7.6)$$

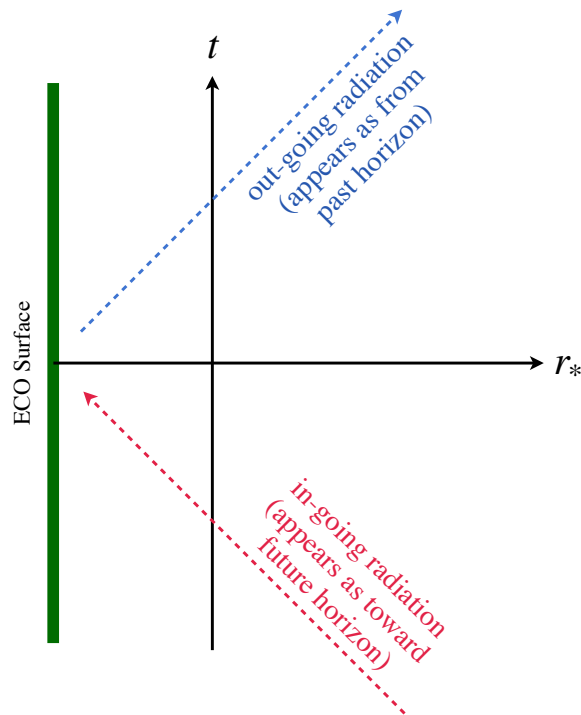


Figure 7.2: Waves that propagate toward the ECO surface can be approximated as propagating toward the future horizon, while those originate from the ECO surface can be approximated as originating from the past horizon.

Each FIDO carries an orthonormal tetrad of ¹

$$\begin{aligned} \vec{e}_{\hat{r}} &= \sqrt{\frac{\Delta}{\Sigma}} \vec{\partial}_r, & \vec{e}_{\hat{\theta}} &= \frac{\vec{\partial}_\theta}{\sqrt{\Sigma}}, \\ \vec{e}_{\hat{\phi}} &= \sqrt{\frac{\Sigma}{\Xi}} \frac{\vec{\partial}_\phi}{\sin \theta}, & \vec{e}_{\hat{0}} &= \frac{1}{\alpha} (\vec{\partial}_t + \omega_\phi \vec{\partial}_\phi), \end{aligned} \quad (7.7)$$

with

$$\alpha = \sqrt{\frac{\Sigma \Delta}{\Xi}}. \quad (7.8)$$

Here $\vec{e}_{\hat{0}}$ is the four-velocity of the FIDO. The FIDOs have zero angular momentum (hence are also known as Zero Angular-Momentum Observers, or ZAMOs), since $\vec{e}_{\hat{0}}$ has zero inner product with $\vec{\partial}_\phi$. Here α is called the redshift factor, also known as the lapse function, since it relates the proper time of the FIDOs and the coordinate time t .

Near the horizon, we have $\alpha \rightarrow 0$; FIDO's tetrads are related to the Kinnersly

¹Note that MP uses different notations for the ρ , Σ .

tetrad [186] via

$$\vec{l} \approx \sqrt{\frac{\Sigma}{\Delta}}(\vec{e}_{\hat{0}} + \vec{e}_{\hat{r}}), \vec{n} \approx \sqrt{\frac{\Delta}{\Sigma}} \frac{\vec{e}_{\hat{0}} - \vec{e}_{\hat{r}}}{2}, \vec{m} \approx \frac{e^{i\beta}(\vec{e}_{\hat{\theta}} + i\vec{e}_{\hat{\phi}})}{\sqrt{2}}, \quad (7.9)$$

where

$$\beta = -\tan^{-1}\left(\frac{a \cos \theta}{r_H}\right). \quad (7.10)$$

Tidal Tensor Components

Let us now introduce the *electric-type* tidal tensor \mathcal{E} as viewed by FIDOs, which can be formally defined as [182]

$$\mathcal{E}_{ij} = h_i^a h_j^c C_{abcd} U^b U^d. \quad (7.11)$$

Here $U = \vec{e}_{\hat{0}}$ is the four-velocity of FIDOs as in Eq. (7.7), and $h_i^a = \delta_i^a + U_i U^a$ is the projection operator onto the spatial hypersurface orthogonal to U . In particular, we look at the mm -component of the tidal tensor, as the gravitational-wave stretching and squeezing will be along these directions. Near the horizon, the tidal tensor component is then given by

$$\mathcal{E}_{mm} = C_{\hat{0}m\hat{0}m} \approx -\frac{\Delta}{4\Sigma} \psi_0 - \frac{\Sigma}{\Delta} \psi_4^*. \quad (7.12)$$

For convenience, let us define a new variable ${}_s\Upsilon$ which is the solution to the Teukolsky equation with spin weight s . For $s = \pm 2$ we have

$${}_{-2}\Upsilon \equiv \rho^{-4} \psi_4, \quad {}_{+2}\Upsilon \equiv \psi_0. \quad (7.13)$$

We briefly review the Teukolsky formalism in Appendix. 7.7. For perturbations that satisfy the linearized vacuum Einstein's equation (in this case the Teukolsky equation), at $r_* \rightarrow -\infty$, in general we can decompose ${}_s\Upsilon$ using the spin-weighted spheroidal harmonics ${}_sS_{\ell m \omega}(\theta)$, and write

$${}_{-2}\Upsilon(t, r_*, \theta, \phi) = \sum_{\ell m} \int \frac{d\omega}{2\pi} e^{-i\omega t} {}_{-2}S_{\ell m \omega}(\theta) e^{im\phi} \quad (7.14)$$

$$\times \left[Z_{\ell m \omega}^{\text{hole}} \Delta^2 e^{-ikr_*} + Z_{\ell m \omega}^{\text{refl}} e^{ikr_*} \right],$$

$${}_{+2}\Upsilon(t, r_*, \theta, \phi) = \sum_{\ell m} \int \frac{d\omega}{2\pi} e^{-i\omega t} {}_{+2}S_{\ell m \omega}(\theta) e^{im\phi} \quad (7.15)$$

$$\times \left[Y_{\ell m \omega}^{\text{hole}} \Delta^{-2} e^{-ikr_*} + Y_{\ell m \omega}^{\text{refl}} e^{ikr_*} \right],$$

where $k \equiv \omega - m \Omega_H$. We use the shorthand $\sum_{\ell m} \equiv \sum_{\ell=2}^{\infty} \sum_{m=-\ell}^{\ell}$, in which ℓ is the multipolar index, and m is the azimuthal quantum number. Note this m here should

not be confused with the label m in the Kinnersly tetrad basis. Here $Z_{\ell m \omega}$ and $Y_{\ell m \omega}$ are amplitudes for the radial modes, with “hole” labeling the left-propagation modes into the compact object (in this paper, left means toward direction with decreasing r), and “refl” labeling the right-propagation (reflected) modes (in this paper, “right” means toward direction with increasing r)².

Note that for outgoing modes of either ${}_{+2}\Upsilon$ or ${}_{-2}\Upsilon$, we have

$$e^{-i\omega t} e^{ikr_*} e^{im\phi} = e^{-i\omega(t-r_*)} e^{im(\phi-\Omega_H r_*)}, \quad (7.16)$$

therefore the outgoing modes are functions of the retarded time $u = t - r_*$, and the position-dependent angular coordinate $\phi - \Omega_H r_*$. Similarly for ingoing modes, we have

$$e^{-i\omega t} e^{-ikr_*} e^{im\phi} = e^{-i\omega(t+r_*)} e^{im(\phi+\Omega_H r_*)}, \quad (7.17)$$

indicating that the ingoing modes are functions of the advanced time $v = t + r_*$, and another position-dependent angular coordinate $\phi + \Omega_H r_*$. We can then write down one schematic expression for either ${}_{+2}\Upsilon$ or ${}_{-2}\Upsilon$, by decomposing both of them into left- and right- propagation components:

$${}_{+2}\Upsilon(t, r_*, \theta, \phi) = {}_{+2}\Upsilon^R(u, \theta, \varphi_-) + \frac{1}{\Delta^2} {}_{+2}\Upsilon^L(v, \theta, \varphi_+), \quad (7.18)$$

$${}_{-2}\Upsilon(t, r_*, \theta, \phi) = {}_{-2}\Upsilon^R(u, \theta, \varphi_-) + \Delta^2 {}_{-2}\Upsilon^L(v, \theta, \varphi_+), \quad (7.19)$$

where we have defined

$$\varphi_- = \phi - \Omega_H r_*, \quad \varphi_+ = \phi + \Omega_H r_*. \quad (7.20)$$

Here both the L and R components are finite, and the Δ represents the divergence/convergence behaviors of the components. As we can see here, once we specify these L , and R components on a constant t slice, as functions of (r_*, θ, ϕ) , we will be able to obtain their future, or past, values by inserting t .

Here we also note that, while the *vacuum/homogeneous* perturbation of space-time geometry encoded in both ψ_0 and ψ_4 — either of them suffices to describe the perturbation field [187, 188]³. Near the horizon, the numerical value of ψ_0 is

²Of course here we refer to ECOs instead of black holes, the label “hole” is for matching the notations from [187].

³One may imagine a very rough electromagnetic analogy: for a vacuum EM wave (without electro- or magneto-static fields), both E and B fields contain the full information of the wave, since one can use Maxwell equations to convert one to the other. Nevertheless, when it comes to interacting with charges and currents, E and B play very different roles, and sometimes it is important to evaluate both E and B fields.

dominated by left-propagating waves, while the numerical value of ψ_4 is dominated by right-propagating waves. According to Eq. (7.12), we then have

$$\mathcal{E}_{mm} \approx -\frac{1}{4\Sigma\Delta} {}_{+2}\Upsilon^L(v, \theta, \varphi_+) - \frac{\rho^{*4}\Sigma}{\Delta} \left[{}_{-2}\Upsilon^R(u, \theta, \varphi_-) \right]^* . \quad (7.21)$$

Note that both terms diverge toward $r_* \rightarrow -\infty$ and at the same order. This divergence correctly reveals the fact that the FIDOs will observe gravitational waves with the same fractional metric perturbation, but because the frequency of the wave gets increased, the curvature perturbation will diverge as α^{-2} .

Linear Response Theory

Now, suppose we have a surface, \mathcal{S} at a constant radius $r_* = b_*$ (or in the Boyer-Lindquist coordinates $r = b$), with $e^{\kappa b_*} \ll 1$. Here $\kappa = (r_H - r_C)/2(r_H^2 + a^2)$ is the surface gravity of the Kerr black hole. To the right of the surface, for $r_* > b_*$, we have completely vacuum, and to the left of the surface, we have matter that are relatively at rest in the FIDO frame, we shall refer to this as the ECO region. The ECO is assumed to be extremely compact and \mathcal{S} is close to the position, as viewed as part of its external Kerr spacetime.

For the moment, let us assume that linear perturbation theory holds throughout the external Kerr spacetime of the ECO. On \mathcal{S} and to its right, \mathcal{E}_{mm} will be the sum of two pieces,

$$\mathcal{E}_{mm} = \mathcal{E}_{mm}^{\text{src}} + \mathcal{E}_{mm}^{\text{resp}} , \quad (7.22)$$

with the first term

$$\mathcal{E}_{mm}^{\text{src}} = -\frac{\Delta}{4\Sigma} {}_{+2}\Upsilon^{\text{src}}(v, \theta, \varphi_+) \quad (7.23)$$

a purely left-propagating wave that is *sourced* by processes away from the surface, e.g., an orbiting or a plunging particle. The second term can be written as

$$\mathcal{E}_{mm}^{\text{resp}} = -\frac{\rho^{*4}\Sigma}{\Delta} \left[{}_{-2}\Upsilon^{\text{refl}}(u, \theta, \varphi_-) \right]^* , \quad (7.24)$$

as the ECO's *response* to the incoming gravitational wave.

Now we are prepared to discuss the reflecting boundary condition of the Teukolsky equations in terms of the tidal response of the ECO. According to the linear response theory, we can assume the linear tidal response of the ECO is proportional to the total tidal fields near the surface of the ECO. That is, we may introduce a new parameter η , and write

$$\mathcal{E}_{mm}^{\text{resp}} = \eta(b, \theta) \mathcal{E}_{mm} . \quad (7.25)$$

Here η is analogous to the *tidal love number*. This leads to the following relation at $r_* = b_*$:

$$\frac{\left[-_2\Upsilon^{\text{refl}}(t - b_*, \theta, \phi - \Omega_H b_*)\right]^*}{+_2\Upsilon^{\text{src}}(t + b_*, \theta, \phi + \Omega_H b_*)} = \frac{\eta}{1 - \eta} \frac{e^{-4i\beta}}{4} \Delta^2. \quad (7.26)$$

In particular, when $\eta \rightarrow \infty$, we will have the Dirichlet boundary condition,

$$\frac{\left[-_2\Upsilon^{\text{refl}}(t - b_*, \theta, \phi - \Omega_H b_*)\right]^*}{+_2\Upsilon^{\text{src}}(t + b_*, \theta, \phi + \Omega_H b_*)} = -\frac{e^{-4i\beta}}{4} \Delta^2. \quad (7.27)$$

This then provides us with a prescription for obtaining the boundary condition at $r_* = b_*$. Once we know the left-propagating ψ_0^{src} , the reflected waves due to the tidal response are simply given by Eq. (7.26).

Let us now define a new parameter $\mathcal{R}(b, \theta)$ as

$$\mathcal{R}(b, \theta) \equiv -\frac{\eta}{1 - \eta}. \quad (7.28)$$

This parameter has the physical meaning of being the *reflectivity* of the tidal fields on the ECO surface. This *local* response assumes that different angular elements of the ECO act independently, which is reasonable since on the ECO surface, and in the FIDO frame, the gravitational wavelength is blue shifted by α , hence, much less than the radius of the ECO.

This parameter has the physical meaning of being the *reflectivity* of the tidal fields on the ECO surface. In terms of $\mathcal{R}(b, \theta)$, we can write

$$\begin{aligned} & \left[-_2\Upsilon^{\text{refl}}(t - b_*, \theta, \phi - \Omega_H b_*)\right]^* \\ &= -\frac{e^{-4i\beta}}{4} \mathcal{R}(b, \theta) \Delta^2 + _2\Upsilon^{\text{src}}(t + b_*, \theta, \phi + \Omega_H b_*) \end{aligned} \quad (7.29)$$

This *local* response, constructed for the surface element with Boyer-Lindquist coordinates (t, b, θ, ϕ) , assumes that different angular elements of the ECO act independently, which is reasonable since on the ECO surface, and in the FIDO frame, the gravitational wavelength is blue shifted by α , hence, much less than the radius of the ECO.

Furthermore, the ECO's response may not be instantaneous, but may instead depend on the history of the exerted tidal perturbation. In order to account for this, we should construct a more general boundary condition, in which reflected field emitted at (t, b, θ, ϕ) — more specifically, emitted by a FIDO at spatial coordinates (b, θ, ϕ) at

Boyer-Lindquist time t — is the result of incoming fields at $(t', b, \theta, \phi - \Omega_H(t - t'))$, with $t' \leq t$; these are points on the past of the world line of this same FIDO [See Fig. 7.1]. To implement this, we rewrite the right-hand side of Eq. (7.29) as an integral. In this integral, we evaluate the incoming tidal field ${}_{+2}\Upsilon^{\text{src}}$ at arguments $t \rightarrow t'$, $\theta \rightarrow \theta$, and $\phi \rightarrow \phi - \Omega_H(t - t')$ ($t' \leq t$). For the response, we replace the instantaneous response $\mathcal{R}(b, \theta)$ by a Green function, which, assuming stationarity, only depends on the time difference $t - t'$: $\mathcal{R}(b, \theta; t - t')$. In this way, we can now write

$$\begin{aligned} & \left[{}_{-2}\Upsilon^{\text{refl}}(t - b_*, \theta, \phi - \Omega_H b_*) \right]^* = \\ & - \frac{e^{-4i\beta}}{4} \int_{-\infty}^t dt' \mathcal{R}(b, \theta; t - t') \Delta^2 {}_{+2}\Upsilon^{\text{src}}(t' + b_*, \theta, \phi + \Omega_H b_* - \Omega_H(t - t')). \end{aligned} \quad (7.30)$$

Here the $-\Omega_H(t - t')$ term has been inserted into the argument of ${}_{+2}\Upsilon^{\text{src}}$ because the FIDO follows $\phi = \phi_0 + \Omega_H t$ (see Fig. 7.1). This is the key equation of our reflection model.

Mode Decomposition

We now have obtained the modified boundary condition (7.30) in terms of the Newman-Penrose quantities, and are ready to apply it to the Teukolsky formalism. The solutions to the $s = -2$ Teukolsky equation, ${}_{-2}\Upsilon$, admits the near-horizon decomposition as in Eq. (7.14). In this equation, Z^{hole} is the amplitude of the ingoing wave down to the ECO, which is contributed by the source, and Z^{refl} is the amplitude of the reflected wave due to the tidal response. For $s = +2$, the corresponding amplitudes are Y^{hole} and Y^{refl} . We would like to derive a relation among the four amplitudes.

Near the ECO surface \mathcal{S} , ${}_{+2}\Upsilon^{\text{src}}$ is given by

$${}_{+2}\Upsilon^{\text{src}}(v, \theta, \varphi_+) = \sum_{\ell m} \int \frac{d\omega}{2\pi} e^{-i\omega v} Y_{\ell m \omega}^{\text{hole}} \Delta^{-2} {}_{+2}S_{\ell m \omega}(\theta, \varphi_+), \quad (7.31)$$

where we have kept only the dominant piece—the left-propagating mode, and $Y_{\ell m \omega}^{\text{hole}}$ is the amplitude of that mode. The quantity ${}_{-2}\Upsilon^{\text{refl}}$ is given by

$${}_{-2}\Upsilon^{\text{refl}}(u, \theta, \varphi_-) = \sum_{\ell m} \int \frac{d\omega}{2\pi} e^{-i\omega u} Z_{\ell m \omega}^{\text{refl}} {}_{-2}S_{\ell m \omega}(\theta, \varphi_-). \quad (7.32)$$

Inserting the above two equations into Eq. (7.30), we obtain

$$\begin{aligned} & \sum_{\ell} Z_{\ell m \omega}^{\text{refl}} {}_{-2}S_{\ell m \omega}(\theta, \phi) \\ &= \frac{1}{4} \sum_{\ell'} e^{4i\beta - 2ikb_*} (-1)^{m+1} \mathcal{R}_{-k_*}^* Y_{\ell' - m - \omega^*}^{\text{hole}^*} {}_{-2}S_{\ell' m \omega^*}(\theta, \phi), \end{aligned} \quad (7.33)$$

where $\mathcal{R}_{\omega}(b, \theta)$ is the Fourier transform of $\mathcal{R}(b, \theta; t - t')$, and $k \equiv \omega - m\Omega_H$. During the derivation, we have used the fact that the spheroidal harmonic functions satisfy the relation

$${}_{-2}S_{\ell m \omega}^*(\theta, \phi) = (-1)^m {}_{+2}S_{\ell - m - \omega^*}(\theta, \phi). \quad (7.34)$$

Assuming the normalization that

$$\int_0^{2\pi} \int_0^{\pi} {}_{-2}S_{\ell m \omega}(\theta, \phi) {}_{-2}S_{\ell' m' \omega}(\theta, \phi) \sin \theta d\theta d\phi = \delta_{\ell}^{\ell'} \delta_m^{m'}, \quad (7.35)$$

from Eq. (7.33), we can write

$$Z_{\ell m \omega}^{\text{refl}} = (-1)^{m+1} \frac{1}{4} e^{-2ikb_*} \sum_{\ell'} \mathcal{M}_{\ell \ell' m \omega} Y_{\ell' - m - \omega^*}^{\text{hole}^*}, \quad (7.36)$$

with

$$\begin{aligned} \mathcal{M}_{\ell \ell' m \omega} &= \int_0^{\pi} \mathcal{R}_{-\omega^* + m\Omega_H}^*(b, \theta) e^{4i\beta(\theta)} \times \\ &\times {}_{-2}S_{\ell' m \omega}(\theta) {}_{-2}S_{\ell m \omega}^*(\theta) \sin \theta d\theta. \end{aligned} \quad (7.37)$$

In general the reflection will mix between modes with different ℓ , but not different m . Note that the mixing not only arises from the θ dependence of $\mathcal{R}(\theta, b)$, but also from the θ dependence of β . This mixing vanishes for the Schwarzschild case. For our calculation, it will be good to discard the phase term $e^{4i\beta}$ and make the assumption that \mathcal{R} is independent of the angle θ . But we should keep in mind that these assumptions only work well in the Schwarzschild limit $a \rightarrow 0$.

In the simplified scenario where mode mixing is ignored, we can write

$$Z_{\ell m \omega}^{\text{refl}} \approx (-1)^{m+1} \frac{1}{4} e^{-2ikb_*} \mathcal{R}_{-\omega^* + m\Omega_H}^* Y_{\ell - m - \omega^*}^{\text{hole}^*}, \quad (7.38)$$

In this way, the ω frequency component of the ψ_4 amplitude of each (l, m) mode is related to the $-\omega^*$ frequency component of ψ_0 of the $(l, -m)$ mode. Here in a Fourier analysis, ω is always real, but we have kept ω^* so that our notation will directly apply to quasi-normal modes, where frequency can be complex.

7.3 Wave propagation in the vicinity of the horizon

In the previous section, we have obtained a new reflecting boundary condition (7.30) relating Newman-Penrose quantity ψ_0 and ψ_4 on a spherical surface near the Kerr horizon. This was further converted as a relation between frequency components of the in-coming ψ_0 and the outgoing ψ_4 . Before moving on to the applications of these boundary conditions, in this section, we put the discussions of the previous section onto a more solid ground. We consider a concrete coordinate system associated with the FIDOs, and relate condition (7.30) to modified refractive indices or dispersion relations of gravitational waves in this coordinate system. This way of modeling the ECO can be thought of as a generalization of Refs. [169, 170, 176] to the spinning case.

Rindler approximations

Let us now study the propagation of waves near the horizon, and explore how emergent gravity might influence the boundary condition there.

Inside the ECO boundary \mathcal{S} , we can consider propagation of metric perturbations in the near-horizon FIDO coordinate system. According to MP, the unperturbed metric takes the simple form [180]:

$$ds^2 = -\alpha^2 d\bar{t}^2 + \frac{d\alpha^2}{g_H^2} + \Sigma_H d\bar{\theta}^2 + \frac{4r_H^2}{\Sigma_H} \sin^2 \bar{\theta} d\bar{\phi}^2, \quad (7.39)$$

where

$$g_H = \frac{r_H - 1}{2r_H}, \quad \Sigma_H = r_H^2 + a^2 \cos^2 \bar{\theta}. \quad (7.40)$$

This metric, only valid for $\alpha \ll 1$, is a Rindler-like spacetime with spherical symmetry, with horizon located at $\alpha = 0$. According to the membrane paradigm [189], the new radial coordinates $(\alpha, \bar{\theta}, \bar{\phi})$ are defined as

$$\bar{t} = t, \quad (7.41)$$

$$\alpha = \left(2g_H - 2a\Omega_H g_H \sin^2 \theta \right)^{\frac{1}{2}} (r - r_H)^{\frac{1}{2}}, \quad (7.42)$$

$$\bar{\theta} = \theta - \frac{\Sigma_{H,\theta}}{4g_H^2 \Sigma_H^2} \alpha^2, \quad (7.43)$$

$$\bar{\phi} = \phi - \Omega_H t. \quad (7.44)$$

The Kinnersley tetrad, near the horizon, can then be expressed in terms of the

Rindler coordinates as

$$\vec{l} = \frac{2r_H}{\Delta} (\vec{\partial}_t + g_H \alpha \vec{\partial}_\alpha), \quad (7.45)$$

$$\vec{n} = \frac{r_H}{\Sigma} (\vec{\partial}_t - g_H \alpha \vec{\partial}_\alpha), \quad (7.46)$$

$$\begin{aligned} \vec{m} = \frac{-\rho^*}{\sqrt{2}} & \left[ia \sin \bar{\theta} \vec{\partial}_t - \frac{a\Omega_H \sin \bar{\theta} \cos \bar{\theta}}{1 - a\Omega_H \sin^2 \bar{\theta}} \alpha \vec{\partial}_\alpha \right. \\ & \left. + \vec{\partial}_{\bar{\theta}} + \left(\frac{i}{\sin \bar{\theta}} - ia\Omega_H \sin \bar{\theta} \right) \vec{\partial}_{\bar{\phi}} \right], \end{aligned} \quad (7.47)$$

where we have used the near-horizon approximations and discarded all $O(\alpha^2)$ corrections.

For convenience, we introduce a new radial coordinate x , which is related to the lapse function via

$$\alpha = e^{g_H x}. \quad (7.48)$$

The regime $x \rightarrow -\infty$ is the horizon, where $\alpha \rightarrow 0$. In fact, (t, x) is exactly the Cartesian coordinate of the Minkowski space in which this Rindler space is embedded. Now we consider metric perturbations of the trace-free form

$$h_{\bar{\theta}\bar{\theta}}(t, x, \bar{\theta}, \bar{\phi}) = \Sigma_H H_+(t, x, \bar{\theta}, \bar{\phi}), \quad (7.49)$$

$$h_{\bar{\theta}\bar{\phi}}(t, x, \bar{\theta}, \bar{\phi}) = 2r_H \sin \bar{\theta} H_\times(t, x, \bar{\theta}, \bar{\phi}), \quad (7.50)$$

$$h_{\bar{\phi}\bar{\phi}}(t, x, \bar{\theta}, \bar{\phi}) = -4r_H^2 \sin^2 \bar{\theta} H_+(t, x, \bar{\theta}, \bar{\phi}) / \Sigma_H. \quad (7.51)$$

Note that $H_{+, \times}$ are metric perturbations in the angular directions, measured in orthonormal bases. We first find that the Einstein's equations reduce to

$$(-\partial_t^2 + \partial_x^2) H_p = 0, \quad p = +, \times. \quad (7.52)$$

Again, to obtain the equations above we have only kept the leading terms in α -series. The absence of $\bar{\theta}$ and $\bar{\phi}$ derivatives in this equation supports the argument that tidal response of the ECO is *local* to each angular element on its surface, as we have made in Sec. 7.2.

We can further decompose $H_p(t, x)$ to the left- and right-propagating piece as

$$H_p(t, x, \bar{\theta}, \bar{\phi}) = H_p^L(t + x, \bar{\theta}, \bar{\phi}) + H_p^R(t - x, \bar{\theta}, \bar{\phi}), \quad (7.53)$$

Using the Rindler approximations, we then find that the Weyl quantities ψ_0 and ψ_4 near horizon can be written as

$$\psi_0(t, x, \bar{\theta}, \bar{\phi}) = \frac{8r_H^2 e^{2i\beta}}{\Delta^2} (\partial_t^2 - g_H \partial_x) \mathcal{H}^L(t, x, \bar{\theta}, \bar{\phi}), \quad (7.54)$$

$$[\rho^{-4} \psi_4(t, x, \bar{\theta}, \bar{\phi})]^* = 2r_H^2 e^{-2i\beta} (\partial_t^2 - g_H \partial_x) \mathcal{H}^R(t, x, \bar{\theta}, \bar{\phi}), \quad (7.55)$$

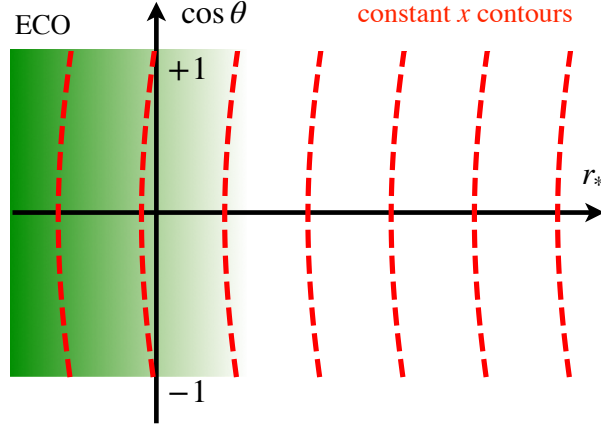


Figure 7.3: Illustration of the constant- x contours in the $(r_*, \cos \theta)$ plane. Reflections from the same x for different θ will appear as being reflected at different r_* for different θ .

where we have defined

$$\mathcal{H}^L = H_+^L + iH_\times^L, \quad \mathcal{H}^R = H_+^R + iH_\times^R. \quad (7.56)$$

Note that in this approximation, we only extract the leading behavior of ψ_0 and ψ_4 near the horizon, namely a left-going wave $\sim (r - r_H)^{-2}$ for ψ_0 , and a right-going wave $\sim (r - r_H)^0$ for ψ_4 . Here, we are considering wave propagation and reflection independently for each $(\bar{\theta}, \bar{\phi})$. Eq. (7.54) and Eq. (7.55) are consistent with our reflection model given in Eq. (7.30). For instance, in the case of total reflection, we have $\mathcal{R} = -1$, and all left-propagating modes H_p^L become right-propagating modes H_p^R .

Let us now evaluate the Riemann tensor components in an orthonormal basis whose vectors point along the $(t, x, \bar{\theta}, \bar{\phi})$ coordinate axes. The results are

$$R_{\hat{t}\hat{\theta}\hat{t}\hat{\theta}} = -R_{\hat{t}\hat{\phi}\hat{t}\hat{\phi}} = -\frac{e^{-2g_H x}}{2} \left[-\partial_t^2 + g_H \partial_x \right] H_+, \quad (7.57)$$

$$R_{\hat{t}\hat{\theta}\hat{t}\hat{\phi}} = -\frac{e^{-2g_H x}}{2} \left[-\partial_t^2 + g_H \partial_x \right] H_\times. \quad (7.58)$$

This also confirms the reflection model that we have obtained from the previous section.

We also point out that near the horizon, x and r_* differ by an additive constant for each $(\bar{\theta}, \bar{\phi})$. Let's work out the $\bar{\theta}$ dependence of the asymptotic shift between x and r_* . More specifically, near the horizon, the tortoise coordinate r_* is approximately

given by

$$r_* \approx \frac{1}{2g_H} \ln[2g_H(r - r_H)] + \mathcal{I}, \quad (7.59)$$

with a constant

$$\mathcal{I} = r_H + \ln\left(\frac{r_H}{2}\right) - \frac{1}{2r_H g_H} \ln(8r_H g_H^2). \quad (7.60)$$

Here we have neglected $O(r - r_H)$ terms. Note that r_* is independent of $\bar{\theta}$. We define the difference between the two radial coordinates as

$$x - r_* \equiv \delta(\bar{\theta}) - \mathcal{I}, \quad (7.61)$$

where

$$\delta(\bar{\theta}) = \frac{1}{2g_H} \ln(1 - a\Omega_H \sin^2 \bar{\theta}). \quad (7.62)$$

This may influence the mode mixing of reflected waves from an ECO whose surface has a constant redshift. In Fig. 7.3, we illustrate constant- x contours in the $(r_*, \cos \theta)$ plane.

Finally let us derive the Teukolsky reflectivity \mathcal{R} using the Rindler approximation. Supposing for x in certain regions we can write the wave solution as

$$\mathcal{H}(t, x, \bar{\theta}, \bar{\phi}) = \mathcal{H}^L(t, x, \bar{\theta}, \bar{\phi}) + \mathcal{H}^R(t, x, \bar{\theta}, \bar{\phi}), \quad (7.63)$$

with

$$\mathcal{H}^L(t, x, \bar{\theta}, \bar{\phi}) = \sum_m \int \frac{dk}{2\pi} \Theta_k(\bar{\theta}) e^{-ikx} e^{-ikt} e^{im\bar{\phi}}, \quad (7.64)$$

$$\mathcal{H}^R(t, x, \bar{\theta}, \bar{\phi}) = \sum_m \int \frac{dk}{2\pi} \Theta_k(\bar{\theta}) \zeta_k e^{ikx} e^{-ikt} e^{im\bar{\phi}}. \quad (7.65)$$

Here $\Theta_k(\bar{\theta})$ gives the k -dependent angular distribution. $\zeta_k \equiv \zeta(k)$ is the reflection coefficient that converts left-propagating to right-propagating gravitational waves.

Thus ψ_0 and ψ_4 are respectively given by

$$\psi_0(t, x, \bar{\theta}, \bar{\phi}) = \frac{8r_H^2 e^{2i\beta(\bar{\theta})}}{\Delta^2} \sum_m \int \frac{dk}{2\pi} \Theta_k(\bar{\theta}) (-k^2 + ig_H k) e^{-ikx} e^{-ikt} e^{im\bar{\phi}}, \quad (7.66)$$

$$(\rho^{-4}\psi_4)^*(t, x, \bar{\theta}, \bar{\phi}) = 2r_H^2 e^{-2i\beta(\bar{\theta})} \sum_m \int \frac{dk}{2\pi} \Theta_k(\bar{\theta}) (-k^2 - ig_H k) \zeta_k e^{ikx} e^{-ikt} e^{im\bar{\phi}}. \quad (7.67)$$

Now that we have obtained ψ_0 and ψ_4 using the Rindler approximations, and would like to relate ζ to the Teukolsky reflectivity \mathcal{R} . To accomplish this, recall that in

Sec. 7.2 we have obtained a reflection relation (7.30) between ψ_0 and ψ_4 on the ECO surface. Since the relation is written in the Boyer-Lindquist coordinates, we first perform the coordinate transformations on ψ_0 and ψ_4 according to $x = r_* + \delta(\theta) - \mathcal{I}$, $\bar{\theta} = \theta$, and $\bar{\phi} = \phi - \Omega_H t$. During the coordinate transformation, we have used the near-horizon approximations and discarded all $O(\alpha^2)$ terms. The results are given by

$$\psi_0(v, \theta, \varphi_+) = \frac{8r_H^2 e^{2i\beta(\theta)}}{\Delta^2} \sum_m \int \frac{dk}{2\pi} \Theta_k(\theta) (-k^2 + ig_H k) e^{-i(k+m\Omega_H)v} e^{-ik\delta(\theta)} e^{ik\mathcal{I}} e^{im\varphi_+}, \quad (7.68)$$

$$(\rho^{-4}\psi_4)^*(u, \theta, \varphi_-) = 2r_H^2 e^{-2i\beta(\theta)} \sum_m \int \frac{dk}{2\pi} \Theta_k(\theta) (-k^2 - ig_H k) \zeta_k e^{-i(k+m\Omega_H)u} e^{ik\delta(\theta)} e^{-ik\mathcal{I}} e^{im\varphi_-}. \quad (7.69)$$

Using the reflection model (7.30), we obtain that

$$\mathcal{R}_k = \zeta_k \left(\frac{-k - ig_H}{-k + ig_H} \right) \exp[2ikb_* + 2ik\delta(\theta) - 2ik\mathcal{I}]. \quad (7.70)$$

Thus once we know ζ , the Teukolsky reflectivity \mathcal{R} can be readily obtained. Here we point out that the phase factor e^{2ikb_*} here will cancel the e^{-2ikb_*} factors in Sec. 7.2. This is because in the previous section we chose b_* as the location for the ‘‘surface of the ECO’’, while in this section, the ECO is embedded into the x coordinate system, therefore we no longer need to introduce a reference location b_* as ‘‘surface of the ECO’’. The information of ECO location will now be incorporated into ζ_k .

Before the end of this subsection, let us look at the factor $\mathcal{M}_{\ell\ell'm\omega}$ in Eq. (7.37), and see how the mode mixing shows up in the reflected waves. We can pull out the angular dependence of this factor by defining

$$\mathcal{M}_{\ell\ell'm\omega} = \left(\frac{-k - ig_H}{-k + ig_H} \right) \zeta_{-\omega^* + m\Omega_H}^* e^{2ikb_* - 2ik\mathcal{I}} \hat{\mathcal{M}}_{\ell\ell'm\omega}, \quad (7.71)$$

where

$$\hat{\mathcal{M}}_{\ell\ell'm\omega} = \int_0^\pi e^{i\Phi_{m\omega}(\theta)} {}_{-2}S_{\ell'm\omega}(\theta) {}_{-2}S_{\ell m\omega}^*(\theta) \sin\theta d\theta, \quad (7.72)$$

with

$$\Phi_{m\omega}(\theta) = 2(\omega - m\Omega_H)\delta(\theta) + 4\beta(\theta). \quad (7.73)$$

This $\hat{\mathcal{M}}_{\ell\ell'm\omega}$ directly shows the mixing of modes due to the phases $\delta(\theta)$ and $\beta(\theta)$, which arises due to the non-spherical nature of the ECO surface. Since $e^{i\Phi_{m\omega}(\theta)}$ is

a unitary operator, we must have

$$\sum_{\ell} \hat{M}_{\ell\ell'm\omega} \hat{M}_{\ell\ell''m\omega}^* = \delta_{\ell\ell''}. \quad (7.74)$$

We plot the absolute value of $\hat{M}_{\ell\ell'm\omega}$ for $\ell = 2$, $m = 2$ and for various spin and ℓ' in Fig. 7.4. For $a = 0$, we have $\hat{M}_{\ell\ell'm\omega} = 1$, indicating no mode mixing. As we raise the spin, modes get more mixed and the reflected waves attain more contributions from $\ell' > 2$ modes. This quantitatively shows the mixing of different ℓ -modes is a significant feature for reflection of waves near horizon.

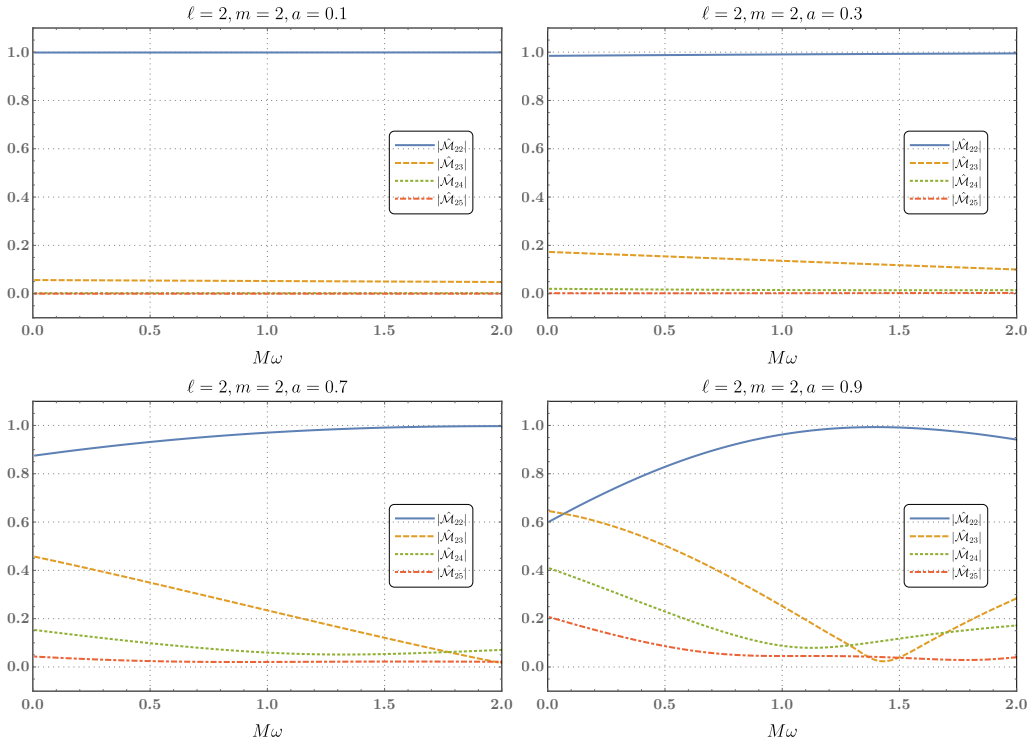


Figure 7.4: The absolute values of the factor $\hat{M}_{\ell\ell'm\omega}$ for various spin a and ℓ' . This factor shows the mixing between different ℓ -modes after an incoming single mode gets reflected on the surface of an exotic compact object. Here we have chosen $\ell = 2$, $m = 2$ as an example. In general for spacetimes with higher spins, the reflected waves gain more contributions from higher ℓ' -modes, thus the effect of mode mixing is not negligible for rapidly spinning ECOs.

Position-dependent damping of gravitational waves

We now calculate the reflectivity \mathcal{R} in a simplest setting — by adding dissipating terms in the linearized Einstein equation in the Rindler coordinate system, obtaining ζ , and then converting to \mathcal{R} . Wang et al. already introduced a model in which the

wave is damped, by introducing a complex ‘‘Young’s modulus’’ of space-time [170]. They name the reflection coefficient they found as the *Boltzman reflectivity*. As an alternative approach, let us introduce a position-dependent damping to gravitational waves, which increases as we approach the horizon. This model has the feature of being able to provide more well-posed differential equations.

To do so, we modify the linearized Einstein equation by adding an extra dissipation term, with coupling coefficient ϵ , to the equation satisfied by the perturbation \mathcal{H} defined in Eq. (7.63):

$$-\partial_t^2 \mathcal{H} - \epsilon e^{-g_H x} \partial_t \mathcal{H} + \partial_x^2 \mathcal{H} = 0. \quad (7.75)$$

Assuming harmonic time decomposition $\mathcal{H}(x, t) = \tilde{\mathcal{H}}(x) e^{-ikt}$, we have

$$\left[\frac{d^2}{dx^2} + k^2 + ik\epsilon e^{-g_H x} \right] \tilde{\mathcal{H}}(x) = 0. \quad (7.76)$$

Here k has the physical meaning of being the angular frequency of the perturbation measured by FIDOs, before blue shift. The modified Einstein equation then admits a general solution given by

$$\tilde{\mathcal{H}}(x) = C_1 \Gamma(1 - i\nu) J_{-i\nu}^{(1)}(z) + C_2 \Gamma(1 + i\nu) J_{i\nu}^{(1)}(z), \quad (7.77)$$

where

$$\nu = 2k/g_H, \quad z = 2e^{\frac{i\pi}{4} - \frac{g_H x}{2}} \sqrt{\epsilon k/g_H}, \quad (7.78)$$

and $J_\nu^{(1)}(z)$ is the Bessel function of the first kind. The appropriate solution which damps on the horizon is given by

$$\frac{C_1}{C_2} = -\frac{\Gamma(1 + i\nu)}{\Gamma(1 - i\nu)} e^{-\pi\nu}. \quad (7.79)$$

Here we shall assume $\epsilon \ll 1$. In this way, there is a region where $x \ll -1$, but still with $\epsilon e^{-g_H x} \ll 1$. In other words, this is a region very close to the Kerr horizon, but here the damping has not yet turned on. In this region, the damping solution can be written as

$$\tilde{\mathcal{H}}(x) \propto e^{-ikx} + \zeta_D e^{ikx}, \quad (7.80)$$

with

$$\zeta_D(k) = -\frac{\Gamma(1 + 2ik/g_H)}{\Gamma(1 - 2ik/g_H)} e^{-\frac{2ik}{g_H} \ln \frac{k}{g_H}} e^{-\frac{\pi k}{g_H}} e^{-\frac{2ik}{g_H} \ln \epsilon}, \quad k > 0. \quad (7.81)$$

Here we have imposed $k > 0$ because the sense of ingoing and outgoing waves changes for $k < 0$, where we need to write

$$\zeta_D(-k) = \zeta_D^*(k). \quad (7.82)$$

This is the same form of reflectivity proposed by Wang *et al.* In Eq. (7.81), the first factor involving two Γ functions is a pure phase factor that has a moderate variation at the scale $k \sim g_H$, and the phase factor $e^{-\frac{2ik}{g_H} \ln \frac{k}{g_H}}$ is similar; the amplitude factor $e^{-\frac{\pi k}{g_H}}$ provides unity reflectivity for $k \sim 0$ and this reflectivity decreases as $|k|$ increases. We plot $|\zeta_D(k)|$ for $g_H = 1$ in Fig. 7.5.

The final phase factor in ζ_D can be written in the form of

$$e^{-\frac{2ik}{g_H} \ln \epsilon} = e^{-2ikx_{\text{eff}}}, \quad x_{\text{eff}} = \frac{1}{g_H} \ln \epsilon. \quad (7.83)$$

This provides an effective x location around which most of the wave is reflected — as we can see, we no longer have a single location $r = b$ for the ECO surface at which all the waves are reflected. To obtain the reflectivity \mathcal{R} , we simply insert ζ_D into Eq. (7.70), which adds an additional θ -dependent phase factor.

GW Propagation in Matter

The damping term in the linearized Einstein equation causes reflection in the near-horizon region. In this subsection we consider another scenario where there exists some effective matter fields in the vicinity of the horizon. The effective stress-energy tensor is denoted as T_{AB}^{eff} , and its existence may be related to the emergent nature of gravity. We now modify the linearized (1 + 1)-Einstein equation (7.52) by adding the effective source, and get

$$-\partial_t^2 \mathcal{H} + \partial_x^2 \mathcal{H} = -16\pi e^{2g_H x} T_{AB}^{\text{eff}}. \quad (7.84)$$

In this equation, on the left-hand side, we have a freely propagating GW in (1 + 1)-Minkowski spacetime, while on the right-hand side, we have the effect of emergent gravity.

Tidal response of matter

We now discuss how T_{AB}^{eff} should respond to \mathcal{H} . Suppose these effective degrees of freedom act as matters that stay at rest in the FIDO frame. The AB component of the Riemann tensor is given by

$$R_{tAtB} = \frac{1}{2} \left(-\partial_t^2 + g_H \partial_x \right) \mathcal{H}. \quad (7.85)$$

We postulate that the response of the effective matter is given by

$$T_{AB}^{\text{eff}} = \frac{\mu}{8\pi} R_{\tau A \tau B}, \quad (7.86)$$

where τ is the proper time for the Rindler metric (7.39), and μ is a physical coupling constant measured in the local Lorentz frame of the FIDO, which can be dependent on the driving frequency felt by the FIDO. Physically speaking, μ is the linear response of the matter towards external perturbations, which is similar to the permeability of gravitational waves in matter. Thus we have

$$T_{AB}^{\text{eff}} = \frac{\mu}{8\pi\alpha^2} R_{tAtB} = \frac{\mu}{16\pi\alpha^2} (-\partial_t^2 + g_H \partial_x) \mathcal{H}. \quad (7.87)$$

Note that the Einstein's equation is now modified into

$$G_{AB} = \mu R_{\tau A \tau B}. \quad (7.88)$$

With the effective stress-energy tensor, the metric equation of motion can now be written as

$$\left[-(1 + \mu) \partial_t^2 + g_H \mu \partial_x + \partial_x^2 \right] \mathcal{H} = 0. \quad (7.89)$$

Here $(1 + \mu)$ acts as the permeability of gravitational waves in matter, and decreases the speed of gravitational waves. Now let us consider two kinds of matter distributions for the exotic compact object.

Homogeneous star

For simplest model, let us look at a homogeneous star with uniform μ in the interior region. For a frequency-independent μ , we can write $\mathcal{H} \propto e^{-ikt+i\tilde{k}x}$, and the modified dispersion relation is given by $\tilde{k} = \tilde{k}_+$ or \tilde{k}_- , with

$$\tilde{k}_{\pm} = \frac{ig_H\mu}{2} \pm \sqrt{(1 + \mu)k^2 - \frac{g_H^2\mu^2}{4}}. \quad (7.90)$$

We immediately note that gravitational waves become evanescent when

$$|k| \leq |k_{\text{th}}| = \frac{|g_H\mu|}{2\sqrt{1 + \mu}}. \quad (7.91)$$

That is, we have a total reflection of all waves below ω_{th} . Substantial reflection also takes place near the ω_{th} frequency. For $|k| > k_{\text{th}}$ and positive μ , waves will be amplified when propagating towards the $x \rightarrow -\infty$ direction, i.e., towards the horizon.

We may further postulate that μ is of order unity inside a surface at which the surface gravity is blue-shifted to the Planck frequency ω_P :

$$\mu = \begin{cases} \mu_0, & \alpha^{-1} g_H > \omega_P, \\ 0, & \text{otherwise.} \end{cases} \quad (7.92)$$

The surface is then located at $x = x_P$, where

$$x_P = \frac{1}{g_H} \ln \left(\frac{g_H}{\omega_P} \right). \quad (7.93)$$

As before, we write down the general solutions to Eq. (7.89) as $\mathcal{H}(x, t) = \tilde{\mathcal{H}}(x)e^{-ikt}$. Outside the surface, we can write

$$\tilde{\mathcal{H}}(x) \propto e^{-ikx} + \zeta_M e^{ikx}. \quad (7.94)$$

Inside the surface we have

$$\tilde{\mathcal{H}}(x) \propto e^{i\tilde{k}x}. \quad (7.95)$$

Matching the solutions on the surface gives

$$\zeta_M = \left(\frac{k + \frac{ig_H\mu}{2} - \sqrt{(1+\mu)k^2 - \frac{g_H^2\mu^2}{4}}}{k - \frac{ig_H\mu}{2} + \sqrt{(1+\mu)k^2 - \frac{g_H^2\mu^2}{4}}} \right) e^{-2ikx_P}, \quad k > 0. \quad (7.96)$$

Similarly to the previous section, $\zeta_M(-k) = \zeta_M^*(k)$. For $|k| \leq k_{\text{th}}$, we have $|\zeta_M| = 1$, indicating a total reflection of low frequency waves. For higher frequencies, $|\zeta_M|$ approaches a constant

$$\lim_{k \rightarrow \infty} |\zeta_M| = \frac{\sqrt{1+\mu} - 1}{1 + \sqrt{1+\mu}}. \quad (7.97)$$

We plot $|\zeta_M|$ for different μ s in Fig. 7.5. Since μ is supposed to be a small number, high-frequency waves have nearly zero reflection near the surface. This ζ_M is qualitatively similar to the Lorentzian reflectivity model adopted, e.g., by Ref. [138].

Inhomogeneous star

Let us make μ grow as a function of the location, with

$$\mu = \mu_0 e^{-\eta x}, \quad (7.98)$$

where μ_0 and η are positive constants. In this way, we successfully “revive” μ near the horizon.

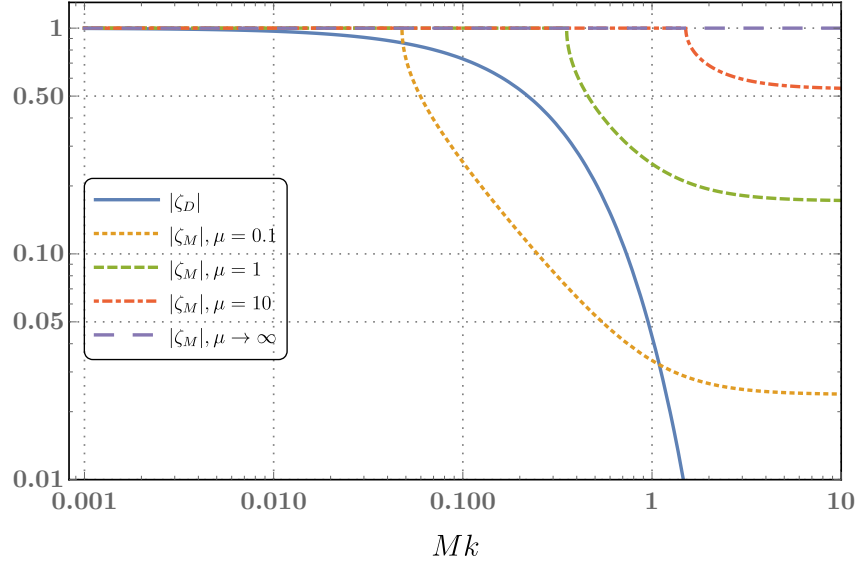


Figure 7.5: Absolute values of ζ_D and ζ_M as functions of the frequency k . We have set $g_H = 1$. As indicated by Eq. (7.70), ζ and the Teukolsky reflectivity \mathcal{R} only differ by a phase, $|\zeta|$ is the same as $|\mathcal{R}|$. The blue solid line represents $|\zeta_D|$. The yellow dotted line, the green dashed line, the red dot-dashed line, and the purple long dashed line give $|\zeta_M|$ for $\mu = 0.1, 0.2, 0.5, \infty$ respectively. The Boltzman reflectivity, i.e. ξ_D , exponentially decays for higher frequencies. For our model of homogeneous stars, we have total reflection of waves on the ECO surface below a certain threshold frequency. Beyond the threshold frequency, the reflectivity gets decreased and converges to a constant. When $\mu \rightarrow \infty$, we have total reflection of waves for all the frequency range, which is equivalent to the case of inhomogeneous stars we have introduced.

We write down the general solutions to Eq. (7.89) as $\mathcal{H}(x, t) = \tilde{\mathcal{H}}(x)e^{-ikt}$, and obtain that

$$\begin{aligned} \tilde{\mathcal{H}}(x) = & A_1 e^{-ikx} e^{\frac{ik}{\eta} \ln\left(\frac{\mu_0 g_H}{\eta}\right) - \frac{\pi k}{\eta}} M(a, b, z) + \\ & A_2 e^{ikx} e^{-\frac{ik}{\eta} \ln\left(\frac{\mu_0 g_H}{\eta}\right) + \frac{\pi k}{\eta}} M(a^*, b^*, z), \end{aligned} \quad (7.99)$$

where

$$a = \frac{ik}{\eta} - \frac{k^2}{g_H \eta}, \quad b = 1 + \frac{2ik}{\eta}, \quad z = \frac{\mu_0 g_H}{\eta} e^{-\eta x}, \quad (7.100)$$

A_1, A_2 are some constants, and $M(a, b, z)$ is the confluent hypergeometric function.

The hypergeometric function behaves asymptotically as

$$M(a, b, z) \sim e^z z^{a-b} \frac{\Gamma(b)}{\Gamma(a)}, \quad z \rightarrow \infty, \quad (7.101)$$

$$M(a, b, z) \sim 1, \quad z \rightarrow 0. \quad (7.102)$$

The solution that damps on the horizon is then given by

$$\frac{A_2}{A_1} = -e^{-\frac{2\pi\omega}{\eta}} \frac{\Gamma(b) \Gamma(a^*)}{\Gamma(b^*) \Gamma(a)}. \quad (7.103)$$

For x in the region that $\mu_0 g_H e^{-\eta x} \ll 1$ and positive k , this solution can then be written as

$$\tilde{\mathcal{H}}(x) = e^{-ikx} + \zeta_N e^{ikx}, \quad (7.104)$$

where

$$\zeta_N = -e^{\left[-\frac{2ik}{\eta} \ln\left(\frac{\mu_0 g_H}{\eta}\right)\right]} \frac{\Gamma\left(1 + \frac{2ik}{\eta}\right) \Gamma\left(-\frac{ik}{\eta} - \frac{k^2}{g_H \eta}\right)}{\Gamma\left(1 - \frac{2ik}{\eta}\right) \Gamma\left(\frac{ik}{\eta} - \frac{k^2}{g_H \eta}\right)}. \quad (7.105)$$

One immediately notes that $|\zeta_N| = 1$ for all real k , indicating a total reflection of waves. This may be due to the fact that our assumption of μ in (7.98) is equivalent to putting infinite numbers of reflecting surfaces near the horizon, i.e. the $\mu \rightarrow \infty$ case in Fig. 7.5.

7.4 Boundary condition in terms of various functions

In calculations for gravitational waveforms, one does not usually compute both ψ_0 and ψ_4 ; the Sasaki-Nakamura formalism was also used to obtain faster numerical convergence. In this section, let us convert our boundary condition (7.36), which involves both ψ_0 and ψ_4 amplitudes, into those that only involve ψ_4 amplitudes, and compare our reflectivity with the one defined using the Sasaki-Nakamura functions.

Reflectivity for ψ_4 mode amplitudes

The Newman-Penrose quantities ψ_0 and ψ_4 can be transformed into each other using the Teukolsky-Starobinsky identities. The amplitude Z^{hole} and Y^{hole} are related by [187]

$$C_{\ell m \omega} Y_{\ell m \omega}^{\text{hole}} = D_{\ell m \omega} Z_{\ell m \omega}^{\text{hole}}, \quad (7.106)$$

with

$$D_{\ell m \omega} = 64(2r_H)^4 (ik) \left(k^2 + 4\varepsilon^2\right) (-ik + 4\varepsilon), \quad (7.107)$$

and C is given by

$$\begin{aligned} |C_{\ell m \omega}|^2 &= \left((\lambda + 2)^2 + 4a\omega m - 4a^2\omega^2\right) \\ &\times \left[\lambda^2 + 36a\omega m - 36a^2\omega^2\right] \\ &+ (2\lambda + 3)(96a^2\omega^2 - 48a\omega m) + 144\omega^2(1 - a^2), \end{aligned} \quad (7.108)$$

with

$$\text{Im } C = 12\omega, \quad (7.109)$$

$$\text{Re } C = +\sqrt{|C|^2 - (\text{Im } C)^2}. \quad (7.110)$$

Here we have defined

$$\varepsilon = \frac{\sqrt{1 - a^2}}{4r_H}, \quad (7.111)$$

and $\lambda \equiv -2\lambda_{\ell m \omega}$ is the eigenvalue of the $s = -2$ spin-weighted spheroidal harmonic. See Sec. 7.7 for more discussions on the Teukolsky-Starobinsky identity.

Combining Eq. (7.36) with Eq. (7.106), we finally arrive at the relation between Z^{refl} and Z^{in} , which is given by

$$Z_{\ell m \omega}^{\text{refl}} = \sum_{\ell'} \mathcal{G}_{\ell \ell' m \omega} Z_{\ell' -m -\omega^*}^{\text{hole}^*}, \quad (7.112)$$

where

$$\mathcal{G}_{\ell \ell' m \omega} = (-1)^{m+1} \frac{1}{4} e^{-2ikb_*} \mathcal{M}_{\ell \ell' m \omega} \frac{D_{\ell' m \omega}}{C_{\ell' m \omega}}. \quad (7.113)$$

We have used the relations $D_{\ell m \omega} = D_{\ell -m -\omega^*}^*$ and $C_{\ell m \omega} = C_{\ell -m -\omega^*}^*$ in order to obtain the above equation.

If we restrict ourselves to the simple case where ℓ - and ℓ' - modes do not mix up, we may simply write Eq. (7.112) as

$$Z_{\ell m \omega}^{\text{refl}} = \hat{\mathcal{G}}_{\ell m \omega} Z_{\ell -m -\omega^*}^{\text{hole}^*}, \quad (7.114)$$

with

$$\hat{\mathcal{G}}_{\ell m \omega} \equiv \frac{D_{\ell m \omega}}{4C_{\ell m \omega}} \mathcal{R}_{-\omega+m\Omega_H}^* e^{i\varphi_{\ell m \omega}^{\text{refl}}}, \quad (7.115)$$

and

$$\varphi_{\ell m \omega}^{\text{refl}} = (m+1)\pi - 2kb_*. \quad (7.116)$$

Eq. (7.114) says that, *the (ℓ, m, ω) -mode of gravitational-wave echoes is not induced by the reflection of the incoming (ℓ, m, ω) -mode but the $(\ell, -m, -\omega^*)$ -mode instead.* The mixing of these two types of modes essentially indicates the breaking of isospectrality as pointed out by Ref. [184]. We will get back to this point later. The other new result is the extra phase term φ^{refl} for the reflected waves, which may be important for observations.

Reflectivity for Sasaki-Nakamura Mode Amplitudes

Since most previous literatures on gravitational wave echoes based their models on the reflection of Sasaki-Nakamura (SN) functions, one may ask how the tidal reflectivity can be related to the SN reflectivity. (See Appendix 7.7 for a brief review of the SN formalism.) In the vicinity of the horizon, the $s = -2$ SN function, i.e., the one associated with ψ_4 , can be written as

$$X_{\ell m \omega}^{\text{ECO}} = \xi_{\ell m \omega}^{\text{hole}} e^{-ikr_*} + \xi_{\ell m \omega}^{\text{refl}} e^{ikr_*}. \quad r_* \rightarrow b_*. \quad (7.117)$$

Under the Chandrasekhar-Sasaki-Nakamura transformation, we have

$$\xi_{\ell m \omega}^{\text{hole}} = Z_{\ell m \omega}^{\text{hole}} d_{\ell m \omega}, \quad \xi_{\ell m \omega}^{\text{refl}} = \frac{Z_{\ell m \omega}^{\text{refl}}}{f_{\ell m \omega}} \quad (7.118)$$

with

$$\begin{aligned} d_{\ell m \omega} = & \sqrt{2r_H} [(8 - 24i\omega - 16\omega^2)r_H^2 \\ & + (12iam - 16 + 16am\omega + 24i\omega)r_H \\ & - 4a^2m^2 - 12iam + 8], \end{aligned} \quad (7.119)$$

and

$$f_{\ell m \omega} = -\frac{4k\sqrt{2r_H} [2kr_H + i(r_H - 1)]}{\eta(r_H)}. \quad (7.120)$$

Inserting Eqs. (7.118) into Eq. (7.112), we obtain boundary condition for the $\ell m \omega$ components of the SN functions:

$$\xi_{\ell m \omega}^{\text{refl}} = \frac{(-1)^{m+1} e^{-2ikb_*}}{4f_{\ell m \omega}} \sum_{\ell'} \mathcal{M}_{\ell \ell' m \omega} \frac{D_{\ell' m \omega}}{C_{\ell' m \omega} d_{\ell' m \omega}} \xi_{\ell' -m -\omega^*}^{\text{hole}*}, \quad (7.121)$$

Here we have used the identity that

$$d_{\ell m \omega} = d_{\ell -m -\omega^*}^*. \quad (7.122)$$

As we will see later, the fact that reflection at the ECO surface turns the ingoing $(\ell, -m, -\omega)$ SN components into outgoing (ℓ, m, ω) SN components leads to the breaking of isospectrality, which has also been pointed out by Maggio *et al.* [184]; here we take the further step of relating these coefficients to the tidal response of the ECO.

For the most simplified scenario where $Z_{\ell -m -\omega^*}^{\text{hole}*} = Z_{\ell m \omega}^{\text{hole}}$ and different ℓ' -modes do not mix, we may simply write

$$\xi_{\ell m \omega}^{\text{refl}} = \mathcal{R}_{\ell m \omega}^{\text{SN}} \xi_{\ell m \omega}^{\text{hole}}, \quad (7.123)$$

where

$$\mathcal{R}_{\ell m \omega}^{\text{SN}} = \mathcal{K}_{\ell m \omega}^{\text{T} \rightarrow \text{SN}} \mathcal{R}_{-\omega + m \Omega_H}^*, \quad (7.124)$$

with

$$\mathcal{K}_{\ell m \omega}^{\text{T} \rightarrow \text{SN}} = \frac{(-1)^{m+1} D_{\ell m \omega}}{4 C_{\ell m \omega} f_{\ell m \omega} d_{\ell m \omega}}. \quad (7.125)$$

This is a simple linear factor that converts \mathcal{R} into the \mathcal{R}^{SN} that are used in SN calculations. In the Schwarzschild limit, we have

$$\mathcal{K}_{\ell m \omega}^{\text{T} \rightarrow \text{SN}} = \frac{(-1)^m (4\omega - i) [12\omega + i\lambda(\lambda + 2)]}{(4\omega + i) [12\omega - i\lambda(\lambda + 2)]}, \quad a = 0, \quad (7.126)$$

where $\lambda = (\ell - 1)(\ell + 2)$. One immediately notes that $|\mathcal{K}_{\ell m \omega}^{\text{T} \rightarrow \text{SN}}| = 1$ in the Schwarzschild limit. For spinning ECOs, we numerically investigate $\mathcal{K}_{\ell m \omega}^{\text{T} \rightarrow \text{SN}}$ for the (2, 2) mode for different spins in Fig. 7.6.

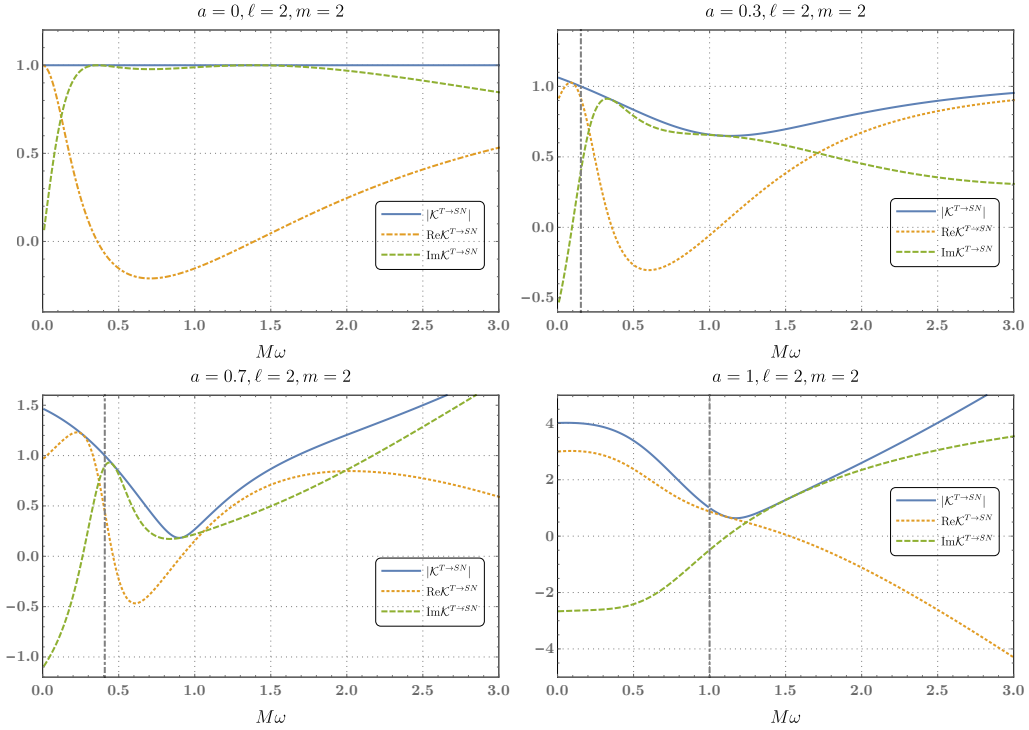


Figure 7.6: Conversion factor $\mathcal{K}_{\ell m \omega}^{\text{T} \rightarrow \text{SN}}$ from the Teukolsky \mathcal{R} to the Sasaki-Nakamura \mathcal{R}_{SN} . Here we have ignored the ℓ - ℓ' mode mixing. We plot real and imaginary parts, as well as the modulus, of $\mathcal{K}_{\ell m \omega}^{\text{T} \rightarrow \text{SN}}$ for the (2, 2)-mode with $a = 0, 0.3, 0.7, 1$ respectively. The gray dot-dashed line marks the horizon frequency $m\Omega_H$. In the Schwarzschild case, the two reflection coefficients only differ by a phase. For Kerr spacetimes we have $|\mathcal{K}_{\ell m \omega}^{\text{T} \rightarrow \text{SN}}| > 1$ for both low and high frequencies, but $|\mathcal{K}_{\ell m \omega}^{\text{T} \rightarrow \text{SN}}|$ dips below 1 for some frequencies. Also note that $|\mathcal{K}_{\ell m \omega}^{\text{T} \rightarrow \text{SN}}| = 1$ when ω equals to the horizon frequency.

Energy Contents of Incoming and Reflected Waves

The reflection coefficient we defined in last subsection is indeed the (square root of) power reflectivity of the gravitational waves on the ECO boundary. To see this, consider a solution to $s = -2$ Teukolsky equation near the ECO surface. The energy flux down to the surface is given by [187]

$$\frac{dE_{\text{hole}}}{d\omega} = \sum_{\ell m} \frac{\omega}{64\pi k(k^2 + 4\epsilon^2)(2r_H)^3} |Y_{\ell m \omega}^{\text{hole}}|^2, \quad (7.127)$$

while the energy propagating outward from the surface is given by

$$\frac{dE^{\text{refl}}}{d\omega} = \sum_{\ell m} \frac{\omega}{4\pi k(k^2 + 4\epsilon^2)(2r_H)^3} |Z_{\ell m \omega}^{\text{refl}}|^2. \quad (7.128)$$

Here ω are all taken as real numbers. See Appendix 7.7 for detailed discussions on the energy flux and the energy conservation law. In the simple case of neglecting ℓ - ℓ' mixing, incoming energy from the $(\ell - m - \omega)$ -mode will return from the $(\ell m \omega)$ -mode, with

$$\left(\frac{dE_{\text{refl}}}{d\omega} \right)_{\ell m \omega} = |\mathcal{R}_{-\omega+m\Omega_H}|^2 \left(\frac{dE_{\text{hole}}}{d\omega} \right)_{\ell - m - \omega}. \quad (7.129)$$

This means our reflectivity \mathcal{R} indeed acts as an energy reflectivity.

7.5 Waveforms and quasi-normal modes of the ECO

In this section, we show how our ECO boundary conditions can be applied to echo computations and resonant conditions for quasi-normal modes. We shall also restrict ourselves to the case of

$$\hat{\mathcal{G}}_{\ell m \omega} = \hat{\mathcal{G}}_{\ell - m - \omega}^*. \quad (7.130)$$

This is satisfied by all the reflectivity models discussed in this paper, since in these cases the tidal response in the time-domain, $\mathcal{R}(b, \theta; t)$ [Cf. (7.30)] is real-valued.

Even and Odd-Parity Echoes

In this subsection, we derive the gravitational-wave echo waveform based on our reflection model. Note that this echo can be the additional wave due to the reflection at the ECO surface during the inspiral phase — it does not necessarily has to be the echo that follows the ringdown phase of the coalescence wave.

Suppose now we have some small perturbations towards the ECO spacetime. We assume that the source in the Teukolsky equation drives a ${}_{-2}\Upsilon^{(0)}$, which has the following form at $r_* \rightarrow -\infty$:

$${}_{-2}\Upsilon^{(0)} = \sum_{\ell m} \int \frac{d\omega}{2\pi} Z_{\ell m \omega}^{\text{hole}(0)} \Delta^2 e^{-ikr_*} {}_{-2}S_{\ell m \omega}(\theta, \phi) e^{-i\omega t}. \quad (7.131)$$

This satisfies the Teukolsky equation with the appropriate source term away from the horizon, the outgoing condition at infinity, but not the ECO boundary condition near the horizon. We will need to add an additional homogeneous solution, which satisfies the outgoing boundary condition at infinity. Recall that for the radial part, we have

$$R_{\ell m \omega}^{+\infty} = \begin{cases} D_{\ell m \omega}^{\text{in}} \Delta^2 e^{-ikr_*} + D_{\ell m \omega}^{\text{out}} e^{ikr_*}, & r \rightarrow b, \\ r^3 e^{i\omega r_*}, & r \rightarrow +\infty. \end{cases}$$

Thus we add the following homogeneous solution to $\Upsilon^{(0)}$:

$${}_{-2}\Upsilon^{\text{echo}} = \sum_{\ell m} \int \frac{d\omega}{2\pi} c_{\ell m \omega} R_{\ell m \omega}^{+\infty} {}_{-2}S_{\ell m \omega}(\theta, \phi) e^{-i\omega t}, \quad (7.132)$$

so that ${}_{-2}\Upsilon^{(0)} + {}_{-2}\Upsilon^{\text{echo}}$ is of the form (7.14), also satisfying (7.114). The asymptotic behavior of ${}_{-2}\Upsilon^{\text{echo}}$ is given by

$${}_{-2}\Upsilon^{\text{echo}} = \begin{cases} \sum_{\ell m} \int \frac{d\omega}{2\pi} c_{\ell m \omega} r^3 e^{+i\omega r_*} e^{-i\omega t} {}_{-2}S_{\ell m \omega}(\theta, \phi), & r_* \rightarrow +\infty, \\ \sum_{\ell m} \int \frac{d\omega}{2\pi} c_{\ell m \omega} [D_{\ell m \omega}^{\text{in}} \Delta^2 e^{-ikr_*} + D_{\ell m \omega}^{\text{out}} e^{ikr_*}] e^{-i\omega t} {}_{-2}S_{\ell m \omega}(\theta, \phi), & r_* \rightarrow b_*. \end{cases} \quad (7.133)$$

Here we already see that the amplitudes $c_{\ell m \omega}$ directly give us the *additional* gravitational waves due to the reflecting surface. Identifying term by term between ${}_{-2}\Upsilon^{(0)} + {}_{-2}\Upsilon^{\text{echo}}$ and Eq. (7.14), we find

$$Z_{\ell m \omega}^{\text{hole}} = Z_{\ell m \omega}^{\text{hole}(0)} + c_{\ell m \omega} D_{\ell m \omega}^{\text{in}}, \quad Z_{\ell m \omega}^{\text{refl}} = c_{\ell m \omega} D_{\ell m \omega}^{\text{out}}. \quad (7.134)$$

Applying Eq. (7.112), we obtain

$$\begin{aligned} c_{\ell m \omega} D_{\ell m \omega}^{\text{out}} &= \sum_{\ell'} \mathcal{G}_{\ell \ell' m \omega} [Z_{\ell' -m -\omega}^{\text{hole}(0)*} + c_{\ell' -m -\omega}^* D_{\ell' -m -\omega}^{\text{in}*}], \\ c_{\ell -m -\omega}^* D_{\ell -m -\omega}^{\text{out}*} &= \sum_{\ell'} \mathcal{G}_{\ell \ell' -m -\omega}^* [Z_{\ell' m \omega}^{\text{hole}(0)} + c_{\ell' m \omega} D_{\ell' m \omega}^{\text{in}}]. \end{aligned} \quad (7.135)$$

Here we restrict ourselves to real-valued ω only. Using the symmetry of the Teukolsky equation, for real-valued ω , it is straightforward to show that the homogeneous solutions have the symmetry that

$$D_{\ell m \omega}^{\text{in}} = D_{\ell -m -\omega}^{\text{in}*}, \quad D_{\ell m \omega}^{\text{out}} = D_{\ell -m -\omega}^{\text{out}*}. \quad (7.136)$$

We can then write

$$\begin{pmatrix} \delta_{\ell\ell'} D_{\ell m \omega}^{\text{out}} & -\mathcal{G}_{\ell\ell'm\omega} D_{\ell m \omega}^{\text{in}} \\ -\overline{\mathcal{G}}_{\ell\ell'm\omega} D_{\ell m \omega}^{\text{in}} & \delta_{\ell\ell'} D_{\ell m \omega}^{\text{out}} \end{pmatrix} \begin{pmatrix} c_{\ell'm\omega} \\ c_{\ell'-m-\omega}^* \end{pmatrix} = \begin{pmatrix} \mathcal{G}_{\ell\ell'm\omega} & 0 \\ 0 & \overline{\mathcal{G}}_{\ell\ell'm\omega} \end{pmatrix} \begin{pmatrix} Z_{\ell'-m-\omega}^{\text{in}(0)*} \\ Z_{\ell'm\omega}^{\text{in}(0)} \end{pmatrix}, \quad (7.137)$$

$$\overline{\mathcal{G}}_{\ell\ell'm\omega} \equiv \mathcal{G}_{\ell\ell'-m-\omega}^*, \quad (7.138)$$

where the components in all matrices are also block matrices with ℓ and ℓ' representing sections of rows and columns. This will allow us to solve for $c_{\ell m \omega}$, therefore leading to the additional outgoing waves at infinity, i.e. the gravitational-wave echoes.

In the simple case where there is no ℓ - ℓ' mixing for reflected waves (so that the relation between reflected waves and incoming waves is simply given by Eq. (7.114)), and that

$$\hat{\mathcal{G}}_{\ell-m-\omega}^* \equiv \hat{\mathcal{G}}_{\ell m \omega}, \quad (7.139)$$

we can have simpler results. For each harmonic for the Z components (similar for the c components), we can define symmetric and anti-symmetric quadrature amplitudes

$$Z_{\ell m \omega}^{\text{hole}(0),S} \equiv \frac{Z_{\ell m \omega}^{\text{hole}(0)} + Z_{\ell-m-\omega}^{\text{hole}(0)*}}{\sqrt{2}}, \quad (7.140)$$

$$Z_{\ell m \omega}^{\text{hole}(0),A} \equiv \frac{Z_{\ell m \omega}^{\text{hole}(0)} - Z_{\ell-m-\omega}^{\text{hole}(0)*}}{\sqrt{2}i}. \quad (7.141)$$

We then have

$$c_{\ell m \omega}^S = \frac{\hat{\mathcal{G}}_{\ell m \omega}}{D_{\ell m \omega}^{\text{out}} - \hat{\mathcal{G}}_{\ell m \omega} D_{\ell m \omega}^{\text{in}}} Z_{\ell m \omega}^{\text{hole}(0),S}, \quad (7.142)$$

$$c_{\ell m \omega}^A = -\frac{\hat{\mathcal{G}}_{\ell m \omega}}{D_{\ell m \omega}^{\text{out}} + \hat{\mathcal{G}}_{\ell m \omega} D_{\ell m \omega}^{\text{in}}} Z_{\ell m \omega}^{\text{hole}(0),A}. \quad (7.143)$$

Here we see that the A quadrature has a reflectivity of $-\hat{\mathcal{G}}_{\ell m \omega}$, compared with $\hat{\mathcal{G}}_{\ell m \omega}$ for the S quadrature. These quadratures correspond to electric- and magnetic-type perturbations.

As it turns out, non-spinning binaries, or those with spins aligned with the orbital angular momentum, only excite the S quadrature — although generically both quadratures are excited — they will have different echoes. In the case when echoes are well-separated in the time domain, the first, third, and other odd echoes, the A

and S will have transfer functions negative to each other, while for even echoes, they will have the same transfer function.

If we further simplify the problem by demanding $c_{\ell m \omega} = c_{\ell -m -\omega}^*$, Eq. (7.137) gives that

$$c_{\ell m \omega} = \frac{\hat{\mathcal{G}}_{\ell m \omega}^{\text{hole}}}{D_{\ell m \omega}^{\text{out}} - \hat{\mathcal{G}}_{\ell m \omega}^{\text{hole}} D_{\ell m \omega}^{\text{in}}} Z_{\ell m \omega}^{\text{hole}(0)}. \quad (7.144)$$

This expression coincides, for instance, with the one obtained in [21] for the spherically-symmetric spacetime with a reflecting surface. Note that the phase factor e^{-2ikb_*} has been absorbed into our definition of $\hat{\mathcal{G}}$.

Echoes driven by symmetric source terms

In our reflection model (7.114), as discussed in Ref. [190], the coefficients $Z_{\ell -m -\omega}^{\text{hole}*}$ and $Z_{\ell m \omega}^{\text{hole}}$ are related for quasi-circular orbits. For such orbits, one can define a series of frequencies as

$$\omega_{mk} = m\Omega_\phi + k\Omega_\theta, \quad (7.145)$$

where Ω_ϕ and Ω_θ are two fundamental frequencies defined for periodic motions in ϕ and θ . Then, for real frequencies, we can decompose the amplitude $Z_{\ell m \omega}^{\text{in}}$ according to

$$Z_{\ell m \omega}^{\text{hole}} = \sum_k Z_{\ell m k}^{\text{hole}} \delta(\omega - \omega_{mk}). \quad (7.146)$$

It is easy to check that for Kerr black holes,

$$Z_{\ell -m -k}^{\text{hole}*} = (-1)^{\ell+k} Z_{\ell m k}^{\text{hole}}. \quad (7.147)$$

That is, if we consider a specific circular orbit, we have the symmetry that $Z_{\ell -m -\omega}^{\text{hole}*}$ is either equal to $Z_{\ell m \omega}^{\text{hole}}$, or they differ by a minus sign. In this simple case, our reflection model (7.114) does not involve different modes, and the model becomes similar to those reflection models based on Sasaki-Nakamura functions like in Ref. [170]. However, if we consider the full quasi-circular motions, i.e. adding up all orbits, this symmetry no longer exists, and one has to consider the mixing of modes when dealing with the reflecting boundary. For general orbits that are not quasi-circular, the symmetry between $Z_{\ell -m -\omega}^{\text{hole}*}$ and $Z_{\ell m \omega}^{\text{hole}}$ may not exist.

Now for the symmetric source, where there is no mode mixing, let us consider a solution ${}_{-2}\Upsilon^{(0)}$ to the Teukolsky equation, which has the following form at $r_* \rightarrow -\infty$:

$${}_{-2}\Upsilon^{(0)} = \sum_{\ell m} \int \frac{d\omega}{2\pi} Z_{\ell m \omega}^{\text{hole}(0)} \Delta^2 e^{-ikr_*} {}_{-2}S_{\ell m \omega}(\theta, \phi) e^{-i\omega t}. \quad (7.148)$$

Following the same steps as in the last subsection, it is straightforward to show that the echo solution to the Teukolsky equation at infinity is given by

$${}_{-2}\Upsilon^{\text{echo}} = \sum_{\ell m} \int \frac{d\omega}{2\pi} Z_{\ell m \omega}^{\text{echo}} {}_{-2}S_{\ell m \omega}(\theta, \phi) e^{-i\omega t}, \quad (7.149)$$

with

$$Z_{\ell m \omega}^{\text{echo}} = \frac{\hat{\mathcal{G}}_{\ell m \omega}}{D_{\ell m \omega}^{\text{out}} - \hat{\mathcal{G}}_{\ell m \omega} D_{\ell m \omega}^{\text{in}}} Z_{\ell m \omega}^{\text{hole}(0)}, \quad (7.150)$$

where we have chosen the normalization $D_{\ell m \omega}^{\infty} = 1$. The tidal reflectivity can also be directly related to the SN reflectivity as

$$\mathcal{R}_{\ell m \omega}^{\text{SN}} = (-1)^{m+1} \frac{D_{\ell m \omega}}{4C_{\ell m \omega} f_{\ell m \omega} d_{\ell m \omega}} \mathcal{R}_{-\omega+m\Omega_H}^*. \quad (7.151)$$

In this simple scenario, the tidal reflectivity is exactly the energy reflectivity for each mode.

Quasi-Normal Modes and Breakdown of Isospectrality

For Quasi-Normal Modes, we set Z to zero, and analytically continue Eq. (7.137) to complex ω . The QNM frequencies can be directly solved by setting the determinant of the lhs matrix of Eq. (7.137) to zero, i.e.

$$\det \begin{pmatrix} \delta_{\ell\ell'} D_{\ell m \omega}^{\text{out}} & -\mathcal{G}_{\ell\ell' m \omega} D_{\ell m \omega}^{\text{in}} \\ -\mathcal{G}_{\ell\ell' -m -\omega}^* D_{\ell m \omega}^{\text{in}} & \delta_{\ell\ell'} D_{\ell m \omega}^{\text{out}} \end{pmatrix} = 0. \quad (7.152)$$

This will in general cause a mixing between QNMs with different ℓ , and break the *isospectrality property* of the Kerr spacetime and lead to *two distinct QNMs* for each (ℓ, m) .

Neglecting the ℓ - ℓ' mixing, we can simply write

$$\left[D_{\ell m \omega}^{\text{out}} \right]^2 = \hat{\mathcal{G}}_{\ell m \omega} \bar{\hat{\mathcal{G}}}_{\ell m \omega} \left[D_{\ell m \omega}^{\text{in}} \right]^2, \quad \bar{\hat{\mathcal{G}}}_{\ell m \omega} \equiv \hat{\mathcal{G}}_{\ell -m -\omega}^*. \quad (7.153)$$

In the special case of $\hat{\mathcal{G}}_{\ell m \omega} = \bar{\hat{\mathcal{G}}}_{\ell m \omega}$ (which is satisfied by all the reflectivity models discussed in this paper), we note that the ECO's QNMs split into S and A modes, with $\omega_{\ell m}^S$ and $\omega_{\ell m}^A$ satisfying different equations:

$$D_{\ell m \omega_S}^{\text{out}} - \hat{\mathcal{G}}_{\ell m \omega_S} D_{\ell m \omega_S}^{\text{in}} = 0, \quad (7.154)$$

$$D_{\ell m \omega_A}^{\text{out}} + \hat{\mathcal{G}}_{\ell m \omega_A} D_{\ell m \omega_A}^{\text{in}} = 0. \quad (7.155)$$

This still breaks the isospectrality properties of Kerr spacetime. Note that this property has also been found and studied in Ref. [184] with their echo model which describes the ECO as a dissipative fluid. Since modes of the ECO are usually excited collectively, the main signature of the breakdown of isospectrality is still the fact that S and A echoes have alternating sign differences in even and odd echoes.

7.6 Conclusions

In this paper, we developed a more physical way to impose boundary conditions for Teukolsky functions near the surface of extremely compact objects. We adopted the Membrane Paradigm, and assumed that the ECO structure is well adapted to the coordinate system of the Fiducial Observers, which is an approximate Rindler coordinate system near the horizon. More specifically, assuming that the additional physics near an ECO can be viewed as modified propagation laws of gravitational waves in the Rindler coordinate system, we were able to obtain reflectivity models for spinning ECOs that are similar to those proposed by previous literature, when taking the Schwarzschild limit. In particular, the Boltzmann reflectivity of Oshita *et al.* was obtainable from a position-dependent damping of gravitational waves in the Rindler coordinate system, which might be thought of as due to the emergent nature of gravity.

As it has turned out, the most directly physical condition is between ingoing components of ψ_0 and outgoing components of ψ_4 , although relations between ingoing and outgoing components of ψ_4 , as well as those of the Sasaki-Nakamura functions, can be obtained by using the Starobinsky-Teukolsky transformation, as well as the Chandrasekhar-Sasaki-Nakamura relations.

The deformation of space-time geometry due to the spin of the ECO causes a mixing between different ℓ modes during reflection at the ECO surface; reflection at the ECO also takes $(m, \omega) \rightarrow (-m, -\omega^*)$. This means an incoming (ℓ, m, ω) mode is reflected into $(\ell', -m, -\omega^*)$ modes. For moderately rapidly spinning holes, such ℓ - ℓ' mixing is moderate, but non-negligible, which means accurately modeling echoes will indeed have to take such mixing into account. For incoming waves toward the ECO caused by a quasi-circular inspiral of a non-spinning particle, the waveform has a *definite parity*, and is invariant under the $(m, \omega) \rightarrow (-m, -\omega^*)$ transformation. For more general waves, the $(m, \omega) \rightarrow (-m, -\omega^*)$ map causes echoes from even- and odd-parity waves to differ from each other; it also causes the breakdown of quasi-normal mode isospectrality, as has been pointed out by Maggio *et al.* in the Schwarzschild case.

7.7 Appendix

The homogeneous Teukolsky and Sasaki-Nakamura equations

Perturbations of Kerr spacetime can be described by the Teukolsky equations [41]. In the vacuum case, one can decompose solutions to the homogeneous Teukolsky

equation as

$${}_s\Upsilon = \sum_{\ell m} \int \frac{d\omega}{2\pi} e^{-i\omega t + im\phi} {}_sR_{\ell m\omega}(r) {}_sS_{\ell m\omega}(\theta), \quad (7.156)$$

where ${}_sS_{\ell m\omega}(\theta)$ is the spin-weighted spheroidal harmonic function, and s is the spin weight. The Teukolsky equations are then separable, and the equations for R and S are respectively

$$\left[\Delta^{-s} \frac{d}{dr} \left(\Delta^{s+1} \frac{d}{dr} \right) + \frac{K^2 - 2is(r-1)K}{\Delta} + 4is\omega r - {}_s\lambda_{\ell m\omega} \right] {}_sR_{\ell m\omega} = 0, \quad (7.157)$$

$$\left[\frac{1}{\sin\theta} \frac{d}{d\theta} \left(\sin\theta \frac{d}{d\theta} \right) - a^2\omega^2 \sin^2\theta - \frac{(m + s \cos\theta)^2}{\sin^2\theta} - 2a\omega s \cos\theta + s + 2ma\omega + {}_s\lambda_{\ell m\omega} \right] {}_sS_{\ell m\omega} = 0, \quad (7.158)$$

where $K = (r^2 + a^2)\omega - ma$, and ${}_s\lambda_{\ell m\omega}$ is the eigenvalue of the spin-weighted spheroidal harmonic.

For $s = -2$, the radial equation (7.157) admits two independent solutions, ${}_{-2}R_{\ell m\omega}^H$ and ${}_{-2}R_{\ell m\omega}^\infty$, which have the following asymptotic forms:

$${}_{-2}R_{\ell m\omega}^H = \begin{cases} B_{\ell m\omega}^{\text{out}} r^3 e^{i\omega r_*} + B_{\ell m\omega}^{\text{in}} r^{-1} e^{-i\omega r_*}, & r \rightarrow \infty, \\ B_{\ell m\omega}^{\text{hole}} \Delta^2 e^{-ikr_*}, & r \rightarrow r_H; \end{cases} \quad (7.159)$$

$${}_{-2}R_{\ell m\omega}^\infty = \begin{cases} D_{\ell m\omega}^\infty r^3 e^{i\omega r_*}, & r \rightarrow \infty, \\ D_{\ell m\omega}^{\text{out}} e^{ikr_*} + D_{\ell m\omega}^{\text{in}} \Delta^2 e^{-ikr_*}, & r \rightarrow r_H. \end{cases} \quad (7.160)$$

The Sasaki-Nakamura-Chandrasekar transformation [178] takes the Teukolsky radial function ${}_{-2}R(r)$ to the Sasaki-Nakamura function $X(r)$, and the Teukolsky equation becomes the Sasaki-Nakamura equation. The homogeneous SN equation is given by

$$\frac{d^2 X_{\ell m\omega}}{dr_*^2} - F(r) \frac{dX_{\ell m\omega}}{dr_*} - U(r) X_{\ell m\omega} = 0. \quad (7.161)$$

The explicit expressions for $F(r)$ and $U(r)$ are given in Ref. [191]'s Eqs. (51-58). The SN equation also admits two independent solutions, $X_{\ell m\omega}^H$ and $X_{\ell m\omega}^\infty$, which

have the asymptotic values:

$$X_{\ell m \omega}^H = \begin{cases} A_{\ell m \omega}^{\text{out}} e^{i\omega r_*} + A_{\ell m \omega}^{\text{in}} e^{-i\omega r_*}, & r \rightarrow \infty, \\ A_{\ell m \omega}^{\text{hole}} e^{-ikr_*}, & r \rightarrow r_H; \end{cases} \quad (7.162)$$

$$X_{\ell m \omega}^\infty = \begin{cases} C_{\ell m \omega}^\infty e^{i\omega r_*}, & r \rightarrow \infty, \\ C_{\ell m \omega}^{\text{out}} e^{ikr_*} + C_{\ell m \omega}^{\text{in}} e^{-ikr_*}, & r \rightarrow r_H. \end{cases} \quad (7.163)$$

The amplitudes A and C can be related to the amplitudes B and D by matching the asymptotic solutions to the SN and the Teukolsky equation on the horizon and at infinity. The B -coefficients and A -coefficients are related by

$$B_{\ell m \omega}^{\text{in}} = -\frac{1}{4\omega^2} A_{\ell m \omega}^{\text{in}}, \quad (7.164)$$

$$B_{\ell m \omega}^{\text{out}} = -\frac{4\omega^2}{c_0} A_{\ell m \omega}^{\text{out}}, \quad (7.165)$$

$$B_{\ell m \omega}^{\text{hole}} = \frac{1}{d_{\ell m \omega}} A_{\ell m \omega}^{\text{hole}}, \quad (7.166)$$

and the D -coefficients and C -coefficients are related by

$$D_{\ell m \omega}^{\text{in}} = \frac{1}{d_{\ell m \omega}} C_{\ell m \omega}^{\text{in}}, \quad (7.167)$$

$$D_{\ell m \omega}^{\text{out}} = f_{\ell m \omega} C_{\ell m \omega}^{\text{out}}, \quad (7.168)$$

$$D_{\ell m \omega}^\infty = -\frac{4\omega^2}{c_0} C_{\ell m \omega}^\infty, \quad (7.169)$$

where

$$d_{\ell m \omega} = \sqrt{2r_H} [(8 - 24i\omega - 16\omega^2)r_H^2 \quad (7.170)$$

$$+ (12iam - 16 + 16am\omega + 24i\omega)r_H$$

$$- 4a^2m^2 - 12iam + 8],$$

$$(7.171)$$

and

$$f_{\ell m \omega} = -\frac{4k\sqrt{2r_H} [2kr_H + i(r_H - 1)]}{\eta(r_H)}. \quad (7.172)$$

Here $\eta(r)$ is defined by

$$\eta(r) = c_0 + \frac{c_1}{r} + \frac{c_2}{r^2} + \frac{c_3}{r^3} + \frac{c_4}{r^4}, \quad (7.173)$$

with

$$c_0 = -12i\omega + \lambda(\lambda + 2) - 12a\omega(a\omega - m), \quad (7.174)$$

$$c_1 = 8ia[3a\omega - \lambda(a\omega - m)],$$

$$c_2 = -24ia(a\omega - m) + 12a^2[1 - 2(a\omega - m)^2], \quad (7.175)$$

$$c_3 = 24ia^3(a\omega - m) - 24a^2,$$

$$c_4 = 12a^4,$$

where $\lambda \equiv -2\lambda_{\ell m \omega}$ is the eigenvalue of the $s = -2$ spin-weighted spheroidal harmonic.

Conservation of energy for gravitational perturbations

In this section, we derive a new conservation relation among four energies, which corresponds to waves that are outgoing at infinity, ingoing at infinity, coming down to the “horizon”, and being reflected from the “horizon”, respectively. A derivation has been done by Teukolsky and Press in [187] for the relation among the first three energies. Here we extend their results to include the reflected one.

From the Newman-Penrose equations, one can derive the Teukolsky-Starobinsky identities for $s = \pm 2$, which can be written as

$$\mathcal{L}_{-1}\mathcal{L}_0\mathcal{L}_1\mathcal{L}_2{}_2S + 12i\omega{}_2S = C{}_2S, \quad (7.176)$$

$$\mathcal{D}\mathcal{D}\mathcal{D}\mathcal{D}{}_2R = \frac{1}{4}{}_2R, \quad (7.177)$$

where we have omitted $(\ell m \omega)$ -indices in R and S for the sake of brevity. We will adopt these abbreviated notations throughout this section. The operators \mathcal{L} and \mathcal{D} are defined by

$$\mathcal{L}_n = \partial_\theta + m \csc \theta - a\omega \sin \theta + n \cot \theta, \quad (7.178)$$

$$\mathcal{D} = \partial_r - iK/\Delta, \quad (7.179)$$

and C is given by

$$\begin{aligned} |C|^2 &= ((\lambda + 2)^2 + 4a\omega m - 4a^2\omega^2) \\ &\times [\lambda^2 + 36a\omega m - 36a^2\omega^2] \\ &+ (2\lambda + 3)(96a^2\omega^2 - 48a\omega m) + 144\omega^2(1 - a^2), \end{aligned} \quad (7.180)$$

with

$$\text{Im } C = 12\omega, \quad (7.181)$$

$$\text{Re } C = +\sqrt{|C|^2 - (\text{Im } C)^2}. \quad (7.182)$$

Similarly we define

$$\mathcal{L}_n^\dagger = \mathcal{L}_n(-\omega, -m), \quad (7.183)$$

$$\mathcal{D}^\dagger = \mathcal{D}(-\omega, -m) = \partial_r + iK/\Delta. \quad (7.184)$$

A complementary set of equations to Eqs. (7.176) and (7.177) then gives

$$\mathcal{L}_{-1}^\dagger \mathcal{L}_0^\dagger \mathcal{L}_1^\dagger \mathcal{L}_2^\dagger C_{-2} S + 12i\omega C^* {}_2S = C^2 {}_2S, \quad (7.185)$$

$$\mathcal{D}^\dagger \mathcal{D}^\dagger \mathcal{D}^\dagger \mathcal{D}^\dagger \Delta^2 {}_2R = 4|C|^2 \Delta^{-2} {}_2R. \quad (7.186)$$

Now let us derive the relation between ψ_0 and ψ_4 by using the Teukolsky-Starobinsky identities. Note that at large r , the radial function ${}_sR$ has the following asymptotic behavior,

$${}_2R = Y_{\text{in}} \frac{e^{-i\omega r_*}}{r} + Y_{\text{out}} \frac{e^{i\omega r_*}}{r^5}, \quad (7.187)$$

$${}_{-2}R = Z_{\text{in}} \frac{e^{-i\omega r_*}}{r} + Z_{\text{out}} r^3 e^{i\omega r_*}. \quad (7.188)$$

Plugging these asymptotic expressions into Eq. (7.177), and keep the terms leading in $(1/r)$ -expansions, we have

$$CY_{\text{in}} = 64\omega^4 Z_{\text{in}}. \quad (7.189)$$

A set of useful identities can be used during the derivations are

$$\Delta \mathcal{D} \mathcal{D} = 2(-iK + r - 1) \mathcal{D} + 6i\omega r + \lambda, \quad (7.190)$$

$$\begin{aligned} \Delta^2 \mathcal{D} \mathcal{D} \mathcal{D} &= [4iK(iK - r + 1) + (\lambda + 2 + 2i\omega r)\Delta] \mathcal{D} \\ &\quad - 2iK(\lambda + 6i\omega r) + 6i\omega \Delta, \end{aligned} \quad (7.191)$$

$$\begin{aligned} \Delta^3 \mathcal{D} \mathcal{D} \mathcal{D} \mathcal{D} &= [\Delta(-4iK(\lambda + 2) - 8i\omega r(r - 1)) \\ &\quad + 8iK(K^2 + (r - 1)^2) + 8i\omega \Delta^2] \mathcal{D} \\ &\quad + \Delta[(\lambda + 2 - 2i\omega r)(\lambda + 6i\omega r) \\ &\quad - 12i\omega(iK + r - 1)] \\ &\quad + 4iK(iK + r - 1)(\lambda + 6i\omega r). \end{aligned} \quad (7.192)$$

Similarly, plugging the asymptotic expressions of the radial functions ${}_{\pm 2}R$ into Eq. (7.186), we obtain that

$$4\omega^4 Y_{\text{out}} = C^* Z_{\text{out}}. \quad (7.193)$$

On the horizon, the radial function ${}_sR$ is given by

$${}_2R = Y_{\text{hole}}\Delta^{-2}e^{-ikr_*} + Y_{\text{refl}}e^{ikr_*}, \quad (7.194)$$

$${}_{-2}R = Z_{\text{hole}}\Delta^{+2}e^{-ikr_*} + Z_{\text{refl}}e^{ikr_*}. \quad (7.195)$$

Plugging these expressions into Eq. (7.177) and (7.186), we obtain that

$$CY_{\text{hole}} = 64(2r_H)^4(ik)(-ik + 4\epsilon)(k^2 + 4\epsilon^2)Z_{\text{hole}}, \quad (7.196)$$

$$4(2r_H)^4(ik)(-ik - 4\epsilon)(k^2 + 4\epsilon^2)Y_{\text{refl}} = C^*Z_{\text{refl}}. \quad (7.197)$$

In the Schwarzschild case, the energy conservation relations can be most easily seen from the Wronskian of two linearly independent homogeneous solutions to the perturbation equations such as the Regge-Wheeler equation. In the Teukolsky equation, due to the existence of the dR/dr_* -term, the Wronskian is then dependent on r . To resolve this, one can rewrite the radial Teukolsky equation (7.157) in a form of

$$d^2Y/dr_*^2 + VY = 0, \quad (7.198)$$

which is possible if one defines

$$Y = \Delta^{s/2}(r^2 + a^2)^{1/2}R, \quad (7.199)$$

$$V = \frac{[K^2 - 2isK(r-1) + \Delta(4ir\omega s - \lambda - 2) - s^2(1-a^2)]}{(r^2 + a^2)^2} - \frac{\Delta(2r^3 + a^2r^2 - 4ra^2 + a^4)}{(r^2 + a^2)^4}. \quad (7.200)$$

The Wronskian of any two solutions of Eq. (7.198) is then conserved. By equating the Wronskian evaluated at infinity and that on the horizon, we have

$$\left(\frac{d_s Y}{dr_*} {}_{-s}Y^* - {}_sY \frac{d_{-s} Y^*}{dr_*}\right)_{r=r_H} = \left(\frac{d_s Y}{dr_*} {}_{-s}Y^* - {}_sY \frac{d_{-s} Y^*}{dr_*}\right)_{r=\infty}. \quad (7.201)$$

For $s = 2$, we substitute Eqs. (7.187), (7.188), (7.194), and (7.195) into the Wronskian equation, and we use Eqs. (7.189), (7.193), (7.196), and (7.197) to obtain that

$$\frac{-iC^*|Y_{\text{hole}}|^2}{32k(2r_H)^3(k^2 + 4\epsilon^2)} + \frac{256(ik)r_H^5(k^2 + 4\epsilon^2)(k^2 + 16\epsilon^2)|Y_{\text{refl}}|^2}{C} = \frac{-iC^*|Y_{\text{in}}|^2}{32\omega^3} + \frac{8i\omega^5|Y_{\text{out}}|^2}{C}, \quad (7.202)$$

where ϵ is defined in Eq. (7.111).

This is indeed the energy conservation law relating the ingoing energy at infinity E_{in} , the outgoing energy at infinity E_{out} , the energy absorbed by the ‘‘horizon’’ E_{hole} ,

and the energy reflected from the horizon E_{refl} . The conservation law can be written as

$$\frac{dE_{\text{in}}}{d\omega} - \frac{dE_{\text{out}}}{d\omega} = \frac{dE_{\text{hole}}}{d\omega} - \frac{dE_{\text{refl}}}{d\omega}, \quad (7.203)$$

in which the explicit expressions for the four energies are

$$\frac{dE_{\text{in}}}{d\omega} = \sum_{\ell m} \frac{1}{64\pi\omega^2} |Y_{\text{in}}|^2 = \sum_{\ell m} \frac{64\omega^6}{\pi|C|^2} |Z_{\text{in}}|^2, \quad (7.204)$$

$$\frac{dE_{\text{out}}}{d\omega} = \sum_{\ell m} \frac{1}{4\pi\omega^2} |Z_{\text{out}}|^2 = \sum_{\ell m} \frac{4\omega^6}{\pi|C|^2} |Y_{\text{in}}|^2, \quad (7.205)$$

$$\frac{dE_{\text{hole}}}{d\omega} = \sum_{\ell m} \frac{\omega}{64\pi k(k^2 + 4\epsilon^2)(2r_H)^3} |Y_{\text{hole}}|^2 \quad (7.206)$$

$$= \sum_{\ell m} \frac{64\omega k(k^2 + 4\epsilon^2)(k^2 + 16\epsilon^2)(2r_H)^5}{\pi|C|^2} |Z_{\text{hole}}|^2, \quad (7.207)$$

$$\frac{dE_{\text{refl}}}{d\omega} = \sum_{\ell m} \frac{\omega}{4\pi k(k^2 + 4\epsilon^2)(2r_H)^3} |Z_{\text{refl}}|^2, \quad (7.208)$$

$$= \sum_{\ell m} \frac{4\omega k(k^2 + 4\epsilon^2)(k^2 + 16\epsilon^2)(2r_H)^5}{\pi|C|^2} |Y_{\text{refl}}|^2. \quad (7.209)$$

BIBLIOGRAPHY

- [1] V. P. Frolov and I. D. Novikov, editors. *Black hole physics: Basic concepts and new developments*. 1998.
- [2] B.P. Abbott et al. Observation of Gravitational Waves from a Binary Black Hole Merger. *Phys. Rev. Lett.*, 116(6):061102, 2016.
- [3] B.P. Abbott et al. GWTC-1: A Gravitational-Wave Transient Catalog of Compact Binary Mergers Observed by LIGO and Virgo during the First and Second Observing Runs. *Phys. Rev. X*, 9(3):031040, 2019.
- [4] R. Abbott et al. GWTC-2: Compact Binary Coalescences Observed by LIGO and Virgo During the First Half of the Third Observing Run. 10 2020.
- [5] Kazunori Akiyama et al. First M87 Event Horizon Telescope Results. I. The Shadow of the Supermassive Black Hole. *Astrophys. J.*, 875(1):L1, 2019.
- [6] Kazunori Akiyama et al. First M87 Event Horizon Telescope Results. II. Array and Instrumentation. *Astrophys. J. Lett.*, 875(1):L2, 2019.
- [7] Kazunori Akiyama et al. First M87 Event Horizon Telescope Results. III. Data Processing and Calibration. *Astrophys. J. Lett.*, 875(1):L3, 2019.
- [8] Kazunori Akiyama et al. First M87 Event Horizon Telescope Results. IV. Imaging the Central Supermassive Black Hole. *Astrophys. J. Lett.*, 875(1):L4, 2019.
- [9] Kazunori Akiyama et al. First M87 Event Horizon Telescope Results. V. Physical Origin of the Asymmetric Ring. *Astrophys. J. Lett.*, 875(1):L5, 2019.
- [10] Kazunori Akiyama et al. First M87 Event Horizon Telescope Results. VI. The Shadow and Mass of the Central Black Hole. *Astrophys. J. Lett.*, 875(1):L6, 2019.
- [11] Samuel E. Gralla, Daniel E. Holz, and Robert M. Wald. Black Hole Shadows, Photon Rings, and Lensing Rings. *Phys. Rev. D*, 100(2):024018, 2019.
- [12] Steven B. Giddings. Searching for quantum black hole structure with the Event Horizon Telescope. *Universe*, 5(9):201, 2019.
- [13] James M. Bardeen and Gary T. Horowitz. The Extreme Kerr throat geometry: A Vacuum analog of $AdS(2) \times S^{*2}$. *Phys. Rev.*, D60:104030, 1999.
- [14] R. Penrose. Gravitational collapse: The role of general relativity. *Riv. Nuovo Cim.*, 1:252–276, 1969.

- [15] Robert Wald. Gedanken experiments to destroy a black hole. *Annals of Physics*, 82(2):548–556, 1974.
- [16] Veronika E. Hubeny. Overcharging a black hole and cosmic censorship. *Phys. Rev. D*, 59:064013, 1999.
- [17] Jonathan Sorce and Robert M. Wald. Gedanken experiments to destroy a black hole. II. Kerr-Newman black holes cannot be overcharged or overspun. *Phys. Rev. D*, 96(10):104014, 2017.
- [18] Vitor Cardoso, Edgardo Franzin, and Paolo Pani. Is the gravitational-wave ringdown a probe of the event horizon? *Phys. Rev. Lett.*, 116(17):171101, 2016. [Erratum: *Phys.Rev.Lett.* 117, 089902 (2016)].
- [19] Vitor Cardoso, Seth Hopper, Caio F. B. Macedo, Carlos Palenzuela, and Paolo Pani. Gravitational-wave signatures of exotic compact objects and of quantum corrections at the horizon scale. *Phys. Rev. D*, 94(8):084031, 2016.
- [20] Vitor Cardoso and Paolo Pani. Tests for the existence of black holes through gravitational wave echoes. *Nature Astron.*, 1(9):586–591, 2017.
- [21] Zachary Mark, Aaron Zimmerman, Song Ming Du, and Yanbei Chen. A recipe for echoes from exotic compact objects. *Phys. Rev. D*, 96(8):084002, 2017.
- [22] Jahed Abedi, Hannah Dykaar, and Niayesh Afshordi. Echoes from the Abyss: Tentative evidence for Planck-scale structure at black hole horizons. *Phys. Rev. D*, 96(8):082004, 2017.
- [23] Luis Felipe Longo Micchi, Niayesh Afshordi, and Cecilia Chirenti. How loud are echoes from Exotic Compact Objects? 10 2020.
- [24] Luis Felipe Longo Micchi and Cecilia Chirenti. Spicing up the recipe for echoes from exotic compact objects: orbital differences and corrections in rotating backgrounds. *Phys. Rev. D*, 101(8):084010, 2020.
- [25] Randy S. Conklin. Gravitational Wave Perturbations on a Kerr Background and Applications for Echoes. *Phys. Rev. D*, 101(4):044045, 2020.
- [26] Norichika Sago and Takahiro Tanaka. Gravitational wave echoes induced by a point mass plunging to a black hole. 9 2020.
- [27] C.P. Burgess, Ryan Plestid, and Markus Rummel. Effective Field Theory of Black Hole Echoes. *JHEP*, 09:113, 2018.
- [28] Sayak Datta and Sukanta Bose. Probing the nature of central objects in extreme-mass-ratio inspirals with gravitational waves. *Phys. Rev. D*, 99(8):084001, 2019.

- [29] Sayak Datta, Khun Sang Phukon, and Sukanta Bose. Recognizing black holes in gravitational-wave observations: Telling apart impostors in mass-gap binaries. 4 2020.
- [30] Jahed Abedi, Hannah Dykaar, and Niayesh Afshordi. Echoes from the Abyss: The Holiday Edition! 1 2017.
- [31] Jahed Abedi and Niayesh Afshordi. Echoes from the Abyss: A highly spinning black hole remnant for the binary neutron star merger GW170817. *JCAP*, 11:010, 2019.
- [32] Gregory Ashton, Ofek Birnholtz, Miriam Cabero, Collin Capano, Thomas Dent, Badri Krishnan, Grant David Meadors, Alex B. Nielsen, Alex Nitz, and Julian Westerweck. Comments on: "Echoes from the abyss: Evidence for Planck-scale structure at black hole horizons". 12 2016.
- [33] Julian Westerweck, Alex Nielsen, Ofek Fischer-Birnholtz, Miriam Cabero, Collin Capano, Thomas Dent, Badri Krishnan, Grant Meadors, and Alexander H. Nitz. Low significance of evidence for black hole echoes in gravitational wave data. *Phys. Rev. D*, 97(12):124037, 2018.
- [34] R. K. L. Lo, T. G. F. Li, and A. J. Weinstein. Template-based Gravitational-Wave Echoes Search Using Bayesian Model Selection. *Phys. Rev. D*, 99(8):084052, 2019.
- [35] Alex B. Nielsen, Collin D. Capano, Ofek Birnholtz, and Julian Westerweck. Parameter estimation and statistical significance of echoes following black hole signals in the first Advanced LIGO observing run. *Phys. Rev. D*, 99(10):104012, 2019.
- [36] Baoyi Chen and Leo C. Stein. Separating metric perturbations in near-horizon extremal Kerr. *Phys. Rev.*, D96(6):064017, 2017.
- [37] Baoyi Chen and Leo C. Stein. Deformation of extremal black holes from stringy interactions. *Phys. Rev. D*, 97(8):084012, 2018.
- [38] Robert M. Wald. *General Relativity*. University of Chicago Press, Chicago and London, 1984.
- [39] Saul A. Teukolsky. The Kerr Metric. *Class. Quant. Grav.*, 32(12):124006, 2015.
- [40] S. A. Teukolsky. Rotating black holes - separable wave equations for gravitational and electromagnetic perturbations. *Phys. Rev. Lett.*, 29:1114–1118, 1972.
- [41] Saul A. Teukolsky. Perturbations of a rotating black hole. 1. Fundamental equations for gravitational electromagnetic and neutrino field perturbations. *Astrophys. J.*, 185:635–647, 1973.

- [42] Ezra Newman and Roger Penrose. An Approach to gravitational radiation by a method of spin coefficients. *J. Math. Phys.*, 3:566–578, 1962.
- [43] P. L. Chrzanowski. Vector Potential and Metric Perturbations of a Rotating Black Hole. *Phys. Rev.*, D11:2042–2062, 1975.
- [44] L. S. Kegeles and J. M. Cohen. Constructive Procedure For Perturbations Of Space-Times. *Phys. Rev.*, D19:1641–1664, 1979.
- [45] B. F. Whiting and L. R. Price. Metric reconstruction from Weyl scalars. *Class. Quant. Grav.*, 22:S589–S604, 2005.
- [46] Tullio Regge and John A. Wheeler. Stability of a Schwarzschild singularity. *Phys. Rev.*, 108:1063–1069, 1957.
- [47] C. V. Vishveshwara. Stability of the schwarzschild metric. *Phys. Rev.*, D1:2870–2879, 1970.
- [48] Frank J. Zerilli. Effective potential for even parity Regge-Wheeler gravitational perturbation equations. *Phys. Rev. Lett.*, 24:737–738, 1970.
- [49] F. J. Zerilli. Gravitational field of a particle falling in a schwarzschild geometry analyzed in tensor harmonics. *Phys. Rev.*, D2:2141–2160, 1970.
- [50] Olivier Sarbach and Manuel Tiglio. Gauge invariant perturbations of Schwarzschild black holes in horizon penetrating coordinates. *Phys. Rev.*, D64:084016, 2001.
- [51] Karl Martel and Eric Poisson. Gravitational perturbations of the Schwarzschild spacetime: A Practical covariant and gauge-invariant formalism. *Phys. Rev.*, D71:104003, 2005.
- [52] Roy P. Kerr. Gravitational field of a spinning mass as an example of algebraically special metrics. *Phys. Rev. Lett.*, 11:237–238, 1963.
- [53] Robert H. Boyer and Richard W. Lindquist. Maximal analytic extension of the Kerr metric. *J. Math. Phys.*, 8:265, 1967.
- [54] John M. Lee. *Introduction to smooth manifolds*, volume 218 of *Graduate Texts in Mathematics*. Springer, New York, second edition, 2013.
- [55] A. O. Barut and R. Raczka. *Theory of Group Representations and Applications*. Singapore: World Scientific, 1986.
- [56] Irene Bredberg, Thomas Hartman, Wei Song, and Andrew Strominger. Black Hole Superradiance From Kerr/CFT. *JHEP*, 04:019, 2010.
- [57] NIST Digital Library of Mathematical Functions. <http://dlmf.nist.gov/>, Release 1.0.15 of 2017-06-01. F. W. J. Olver, A. B. Olde Daalhuis, D. W. Lozier, B. I. Schneider, R. F. Boisvert, C. W. Clark, B. R. Miller and B. V. Saunders, eds.

- [58] Alexandru Lupsasca, Maria J. Rodriguez, and Andrew Strominger. Force-Free Electrodynamics around Extreme Kerr Black Holes. *JHEP*, 12:185, 2014.
- [59] G. Compère and R. Oliveri. Near-horizon Extreme Kerr Magnetospheres. *Phys. Rev.*, D93(2):024035, 2016. [Erratum: *Phys. Rev.*D93,no.6,069906(2016)].
- [60] Monica Guica, Thomas Hartman, Wei Song, and Andrew Strominger. The Kerr/CFT Correspondence. *Phys. Rev.*, D80:124008, 2009.
- [61] See Supplemental Material at <http://link.aps.org/supplemental/10.1103/PhysRevD.96.064017> or <https://arxiv.org/src/1707.05319/anc> for MATHEMATICA notebooks which compute highest-weight bases and Maxwell/linearized Einstein operators.
- [62] Clifford M. Will. The Confrontation between General Relativity and Experiment. *Living Rev. Rel.*, 17:4, 2014.
- [63] S. W. Hawking. Particle Creation by Black Holes. *Commun. Math. Phys.*, 43:199–220, 1975.
- [64] Nicolas Yunes and Frans Pretorius. Dynamical Chern-Simons Modified Gravity. I. Spinning Black Holes in the Slow-Rotation Approximation. *Phys. Rev.*, D79:084043, 2009.
- [65] Kent Yagi, Nicolas Yunes, and Takahiro Tanaka. Slowly Rotating Black Holes in Dynamical Chern-Simons Gravity: Deformation Quadratic in the Spin. *Phys. Rev.*, D86:044037, 2012. [Erratum: *Phys. Rev.*D89,049902(2014)].
- [66] Stephon Alexander and Nicolas Yunes. Chern-Simons Modified General Relativity. *Phys. Rept.*, 480:1–55, 2009.
- [67] R.R. Metsaev and Arkady A. Tseytlin. Order alpha-prime (Two Loop) Equivalence of the String Equations of Motion and the Sigma Model Weyl Invariance Conditions: Dependence on the Dilaton and the Antisymmetric Tensor. *Nucl.Phys.*, B293:385–419, 1987.
- [68] Kei-ichi Maeda, Nobuyoshi Ohta, and Yukinori Sasagawa. Black Hole Solutions in String Theory with Gauss-Bonnet Curvature Correction. *Phys.Rev.*, D80:104032, 2009.
- [69] P. Kanti, N. E. Mavromatos, J. Rizos, K. Tamvakis, and E. Winstanley. Dilatonic black holes in higher curvature string gravity. *Phys. Rev.*, D54:5049–5058, 1996.
- [70] Paolo Pani and Vitor Cardoso. Are black holes in alternative theories serious astrophysical candidates? The Case for Einstein-Dilaton-Gauss-Bonnet black holes. *Phys. Rev.*, D79:084031, 2009.

- [71] Paolo Pani, Caio F. B. Macedo, Luis C. B. Crispino, and Vitor Cardoso. Slowly rotating black holes in alternative theories of gravity. *Phys. Rev.*, D84:087501, 2011.
- [72] Stefanos Aretakis. Horizon Instability of Extremal Black Holes. *Adv. Theor. Math. Phys.*, 19:507–530, 2015.
- [73] Samuel E. Gralla and Peter Zimmerman. Critical Exponents of Extremal Kerr Perturbations. *Class. Quant. Grav.*, 35(9):095002, 2018.
- [74] Burkhard Kleihaus, Jutta Kunz, Sindy Mojica, and Eugen Radu. Spinning black holes in Einstein–Gauss-Bonnet–dilaton theory: Nonperturbative solutions. *Phys. Rev.*, D93(4):044047, 2016.
- [75] Robert Delbourgo and Abdus Salam. The gravitational correction to pcc. *Phys. Lett.*, 40B:381–382, 1972.
- [76] Tohru Eguchi and Peter G. O. Freund. Quantum Gravity and World Topology. *Phys. Rev. Lett.*, 37:1251, 1976.
- [77] Luis Alvarez-Gaume and Edward Witten. Gravitational Anomalies. *Nucl. Phys.*, B234:269, 1984.
- [78] Michael B. Green and John H. Schwarz. Anomaly Cancellation in Supersymmetric D=10 Gauge Theory and Superstring Theory. *Phys. Lett.*, 149B:117–122, 1984.
- [79] Bruce A. Campbell, Malcolm J. Duncan, Nemanja Kaloper, and Keith A. Olive. Gravitational dynamics with Lorentz Chern-Simons terms. *Nucl. Phys.*, B351:778–792, 1991.
- [80] Kent Yagi, Leo C. Stein, and Nicolas Yunes. Challenging the Presence of Scalar Charge and Dipolar Radiation in Binary Pulsars. *Phys. Rev.*, D93(2):024010, 2016.
- [81] Leo C. Stein. Rapidly rotating black holes in dynamical Chern-Simons gravity: Decoupling limit solutions and breakdown. *Phys. Rev.*, D90(4):044061, 2014.
- [82] Dumitru Astefanesei, Kevin Goldstein, Rudra P. Jena, Ashoke Sen, and Sandip P. Trivedi. Rotating attractors. *JHEP*, 10:058, 2006.
- [83] Hans Stephani, Eduard Herlt, Malcolm MacCullum, Cornelius Hoenselaers, and Dietrich Kramer. *Exact Solutions of Einstein's Equations*. Cambridge Univ. Press, Cambridge, 2003.
- [84] Robert McNees, Leo C. Stein, and Nicolás Yunes. Extremal black holes in dynamical Chern–Simons gravity. *Class. Quant. Grav.*, 33(23):235013, 2016.

- [85] Geoffrey Compère, Kwinten Fransen, Thomas Hertog, and Jiang Long. Gravitational waves from plunges into Gargantua. 2017.
- [86] Wolfram Schmidt. Celestial mechanics in Kerr space-time. *Class. Quant. Grav.*, 19:2743, 2002.
- [87] Dimitry Ayzenberg and Nicolas Yunes. Slowly-Rotating Black Holes in Einstein-Dilaton-Gauss-Bonnet Gravity: Quadratic Order in Spin Solutions. *Phys. Rev.*, D90:044066, 2014. [Erratum: *Phys. Rev.* D91,no.6,069905(2015)].
- [88] Andrea Maselli, Paolo Pani, Leonardo Gualtieri, and Valeria Ferrari. Rotating black holes in Einstein-Dilaton-Gauss-Bonnet gravity with finite coupling. *Phys. Rev.*, D92(8):083014, 2015.
- [89] Pedro V. P. Cunha, Carlos A. R. Herdeiro, Burkhard Kleihaus, Jutta Kunz, and Eugen Radu. Shadows of Einstein–dilaton–Gauss–Bonnet black holes. *Phys. Lett.*, B768:373–379, 2017.
- [90] Robert M. Wald. Black hole entropy is the Noether charge. *Phys. Rev.*, D48(8):R3427–R3431, 1993.
- [91] Vivek Iyer and Robert M. Wald. Some properties of Noether charge and a proposal for dynamical black hole entropy. *Phys. Rev.*, D50:846–864, 1994.
- [92] Ted Jacobson, Gungwon Kang, and Robert C. Myers. On black hole entropy. *Phys. Rev.*, D49:6587–6598, 1994.
- [93] Jacob D. Bekenstein. Black holes and entropy. *Phys. Rev.*, D7:2333–2346, 1973.
- [94] Burkhard Kleihaus, Jutta Kunz, and Eugen Radu. Rotating Black Holes in Dilatonic Einstein-Gauss-Bonnet Theory. *Phys. Rev. Lett.*, 106:151104, 2011.
- [95] Shahar Hadar and Harvey S. Reall. Is there a breakdown of effective field theory at the horizon of an extremal black hole? *JHEP*, 12:062, 2017.
- [96] Cumrun Vafa. The String landscape and the swampland. 9 2005.
- [97] Nima Arkani-Hamed, Lubos Motl, Alberto Nicolis, and Cumrun Vafa. The String landscape, black holes and gravity as the weakest force. *JHEP*, 06:060, 2007.
- [98] Clifford Cheung, Junyu Liu, and Grant N. Remmen. Proof of the Weak Gravity Conjecture from Black Hole Entropy. 2018.
- [99] Jie Jiang, Aofei Sang, and Ming Zhang. Comment on "Constraints on Low-Energy Effective Theories from Weak Cosmic Censorship". 1 2021.

- [100] Stanley Deser and P. van Nieuwenhuizen. One Loop Divergences of Quantized Einstein-Maxwell Fields. *Phys. Rev. D*, 10:401, 1974.
- [101] Yevgeny Kats, Lubos Motl, and Megha Padi. Higher-order corrections to mass-charge relation of extremal black holes. *JHEP*, 12:068, 2007.
- [102] Stefan Hollands and Robert M. Wald. Stability of Black Holes and Black Branes. *Commun. Math. Phys.*, 321:629–680, 2013.
- [103] Jie Jiang and Ming Zhang. Testing the Weak Cosmic Censorship Conjecture in Lanczos-Lovelock gravity. *Phys. Rev. D*, 102(8):084033, 2020.
- [104] Gabor Zsolt Toth. Test of the weak cosmic censorship conjecture with a charged scalar field and dyonic Kerr-Newman black holes. *Gen. Rel. Grav.*, 44:2019–2035, 2012.
- [105] Jose Natario, Leonel Queimada, and Rodrigo Vicente. Test fields cannot destroy extremal black holes. *Class. Quant. Grav.*, 33(17):175002, 2016.
- [106] F. de Felice and Yun-Qiang Yu. Turning a black hole into a naked singularity. *Class. Quant. Grav.*, 18:1235–1244, 2001.
- [107] Goffredo Chirco, Stefano Liberati, and Thomas P. Sotiriou. Gedanken experiments on nearly extremal black holes and the Third Law. *Phys. Rev. D*, 82:104015, 2010.
- [108] Alberto Saa and Raphael Santarelli. Destroying a near-extremal Kerr-Newman black hole. *Phys. Rev. D*, 84:027501, 2011.
- [109] Sijie Gao and Yuan Zhang. Destroying extremal Kerr-Newman black holes with test particles. *Phys. Rev. D*, 87(4):044028, 2013.
- [110] Enrico Barausse, Vitor Cardoso, and Gaurav Khanna. Test bodies and naked singularities: Is the self-force the cosmic censor? *Phys. Rev. Lett.*, 105:261102, 2010.
- [111] Enrico Barausse, Vitor Cardoso, and Gaurav Khanna. Testing the Cosmic Censorship Conjecture with point particles: the effect of radiation reaction and the self-force. *Phys. Rev. D*, 84:104006, 2011.
- [112] Peter Zimmerman, Ian Vega, Eric Poisson, and Roland Haas. Self-force as a cosmic censor. *Phys. Rev. D*, 87(4):041501, 2013.
- [113] Marta Colleoni and Leor Barack. Overspinning a Kerr black hole: the effect of self-force. *Phys. Rev. D*, 91:104024, 2015.
- [114] Marta Colleoni, Leor Barack, Abhay G. Shah, and Maarten van de Meent. Self-force as a cosmic censor in the Kerr overspinning problem. *Phys. Rev. D*, 92(8):084044, 2015.

- [115] Eckehard W. Mielke and Peter Baekler. Topological gauge model of gravity with torsion. *Phys. Lett. A*, 156:399–403, 1991.
- [116] P. Baekler, E. W. Mielke, and F. W. Hehl. Dynamical symmetries in topological 3-D gravity with torsion. *Nuovo Cim. B*, 107:91–110, 1992.
- [117] F. W. Hehl, P. Von Der Heyde, G. D. Kerlick, and J. M. Nester. General Relativity with Spin and Torsion: Foundations and Prospects. *Rev. Mod. Phys.*, 48:393–416, 1976.
- [118] Koray Düztaş, Mubasher Jamil, Sanjar Shaymatov, and Bobomurat Ahmedov. Testing cosmic censorship conjecture for extremal and near-extremal (2 + 1)-dimensional MTZ black holes. *Class. Quant. Grav.*, 37(17):175005, 2020.
- [119] Deyou Chen. Weak cosmic censorship conjecture in BTZ black holes with scalar fields. *Chin. Phys. C*, 44(1):015101, 2020.
- [120] Wei Li, Wei Song, and Andrew Strominger. Chiral Gravity in Three Dimensions. *JHEP*, 04:082, 2008.
- [121] Juan Martin Maldacena. The Large N limit of superconformal field theories and supergravity. *Int. J. Theor. Phys.*, 38:1113–1133, 1999.
- [122] W. Israel. Third Law of Black-Hole Dynamics: A Formulation and Proof. *Phys. Rev. Lett.*, 57(4):397, 1986.
- [123] Eric D’Hoker and Per Kraus. Charged Magnetic Brane Solutions in AdS (5) and the fate of the third law of thermodynamics. *JHEP*, 03:095, 2010.
- [124] Stanley Deser, R. Jackiw, and S. Templeton. Topologically Massive Gauge Theories. *Annals Phys.*, 140:372–411, 1982. [Erratum: *Annals Phys.* 185, 406 (1988)].
- [125] Stanley Deser, R. Jackiw, and S. Templeton. Three-Dimensional Massive Gauge Theories. *Phys. Rev. Lett.*, 48:975–978, 1982.
- [126] Stanley Deser and Bayram Tekin. Massive, topologically massive, models. *Class. Quant. Grav.*, 19:L97–L100, 2002.
- [127] Alberto A. Garcia, Friedrich W. Hehl, Christian Heinicke, and Alfredo Macias. Exact vacuum solution of a (1+2)-dimensional Poincare gauge theory: BTZ solution with torsion. *Phys. Rev. D*, 67:124016, 2003.
- [128] Cheng-Hao Wei and Bo Ning. Quasi-local Energy in 3D Gravity with Torsion. 7 2018.
- [129] David D. K. Chow, C. N. Pope, and Ergin Sezgin. Kundt spacetimes as solutions of topologically massive gravity. *Class. Quant. Grav.*, 27:105002, 2010.

- [130] S. W. Hawking. Black holes in general relativity. *Commun. Math. Phys.*, 25:152–166, 1972.
- [131] Pawel O. Mazur and Emil Mottola. Gravitational condensate stars: An alternative to black holes. 9 2001.
- [132] Franz E. Schunck and Eckehard W. Mielke. General relativistic boson stars. *Class. Quant. Grav.*, 20:R301–R356, 2003.
- [133] Paolo Pani, Emanuele Berti, Vitor Cardoso, Yanbei Chen, and Richard Norte. Gravitational wave signatures of the absence of an event horizon. I. Nonradial oscillations of a thin-shell gravastar. *Phys. Rev. D*, 80:124047, 2009.
- [134] Paolo Pani, Emanuele Berti, Vitor Cardoso, Yanbei Chen, and Richard Norte. Gravitational-wave signatures of the absence of an event horizon. II. Extreme mass ratio inspirals in the spacetime of a thin-shell gravastar. *Phys. Rev. D*, 81:084011, 2010.
- [135] Richard H. Price and Gaurav Khanna. Gravitational wave sources: reflections and echoes. *Class. Quant. Grav.*, 34(22):225005, 2017.
- [136] Hiroyuki Nakano, Norichika Sago, Hideyuki Tagoshi, and Takahiro Tanaka. Black hole ringdown echoes and howls. *PTEP*, 2017(7):071E01, 2017.
- [137] Qingwen Wang and Niayesh Afshordi. Black hole echology: The observer’s manual. *Phys. Rev. D*, 97(12):124044, 2018.
- [138] Song Ming Du and Yanbei Chen. Searching for near-horizon quantum structures in the binary black-hole stochastic gravitational-wave background. *Phys. Rev. Lett.*, 121(5):051105, 2018.
- [139] Ka Wa Tsang, Michiel Rollier, Archisman Ghosh, Anuradha Samajdar, Michalis Agathos, Katerina Chatziioannou, Vitor Cardoso, Gaurav Khanna, and Chris Van Den Broeck. A morphology-independent data analysis method for detecting and characterizing gravitational wave echoes. *Phys. Rev. D*, 98(2):024023, 2018.
- [140] Randy S. Conklin, Bob Holdom, and Jing Ren. Gravitational wave echoes through new windows. *Phys. Rev. D*, 98(4):044021, 2018.
- [141] Pedro V. P. Cunha, Emanuele Berti, and Carlos A. R. Herdeiro. Light-Ring Stability for Ultracompact Objects. *Phys. Rev. Lett.*, 119(25):251102, 2017.
- [142] Raúl Carballo-Rubio, Pawan Kumar, and Wenbin Lu. Seeking observational evidence for the formation of trapping horizons in astrophysical black holes. *Phys. Rev. D*, 97(12):123012, 2018.
- [143] Raúl Carballo-Rubio, Francesco Di Filippo, Stefano Liberati, and Matt Visser. Phenomenological aspects of black holes beyond general relativity. *Phys. Rev. D*, 98(12):124009, 2018.

- [144] Douglas M. Eardley. Death of White Holes in the Early Universe. *Phys. Rev. Lett.*, 33:442–444, 1974.
- [145] Ian H Redmount. Blue-sheet instability of schwarzschild wormholes. *Progress of theoretical physics*, 73(6):1401–1426, 1985.
- [146] K. S. Thorne. NONSPHERICAL GRAVITATIONAL COLLAPSE: A SHORT REVIEW. 1972.
- [147] Eanna E. Flanagan and Scott A. Hughes. Measuring gravitational waves from binary black hole coalescences: 1. Signal-to-noise for inspiral, merger, and ringdown. *Phys. Rev. D*, 57:4535–4565, 1998.
- [148] B. P. Abbott et al. Tests of general relativity with GW150914. *Phys. Rev. Lett.*, 116(22):221101, 2016. [Erratum: *Phys.Rev.Lett.* 121, 129902 (2018)].
- [149] Steven B. Giddings. Gravitational wave tests of quantum modifications to black hole structure – with post-GW150914 update. *Class. Quant. Grav.*, 33(23):235010, 2016.
- [150] Rainald Flume, Francesco Fucito, Jose F. Morales, and Rubik Poghossian. Matone’s relation in the presence of gravitational couplings. *JHEP*, 04:008, 2004.
- [151] Seth Lloyd and John Preskill. Unitarity of black hole evaporation in final-state projection models. *JHEP*, 08:126, 2014.
- [152] S.W. Hawking. Breakdown of Predictability in Gravitational Collapse. *Phys. Rev. D*, 14:2460–2473, 1976.
- [153] Oleg Lunin and Samir D. Mathur. AdS / CFT duality and the black hole information paradox. *Nucl. Phys. B*, 623:342–394, 2002.
- [154] Samir D. Mathur. The Fuzzball proposal for black holes: An Elementary review. *Fortsch. Phys.*, 53:793–827, 2005.
- [155] Chanda Prescod-Weinstein, Niayesh Afshordi, Michael L. Balogh, Niayesh Afshordi, and Michael L. Balogh. Stellar Black Holes and the Origin of Cosmic Acceleration. *Phys. Rev. D*, 80:043513, 2009.
- [156] Samuel L. Braunstein, Stefano Pirandola, and Karol Życzkowski. Better Late than Never: Information Retrieval from Black Holes. *Phys. Rev. Lett.*, 110(10):101301, 2013.
- [157] Ahmed Almheiri, Donald Marolf, Joseph Polchinski, and James Sully. Black Holes: Complementarity or Firewalls? *JHEP*, 02:062, 2013.
- [158] Massimo Bianchi, Dario Consoli, Alfredo Grillo, Jose Francisco Morales, Paolo Pani, and Guilherme Raposo. The multipolar structure of fuzzballs. 8 2020.

- [159] Massimo Bianchi, Dario Consoli, Alfredo Grillo, Josè Francisco Morales, Paolo Pani, and Guilherme Raposo. Distinguishing fuzzballs from black holes through their multipolar structure. *Phys. Rev. Lett.*, 125(22):221601, 2020.
- [160] Steven B. Giddings. Astronomical tests for quantum black hole structure. *Nature Astron.*, 1:0067, 2017.
- [161] Iosif Bena and Daniel R. Mayerson. Multipole Ratios: A New Window into Black Holes. *Phys. Rev. Lett.*, 125(22):221602, 2020.
- [162] Iosif Bena and Daniel R. Mayerson. Black Holes Lessons from Multipole Ratios. 7 2020.
- [163] Daniel R. Mayerson. Fuzzballs and Observations. *Gen. Rel. Grav.*, 52(12):115, 2020.
- [164] Pawel O. Mazur and Emil Mottola. Gravitational vacuum condensate stars. *Proc. Nat. Acad. Sci.*, 101:9545–9550, 2004.
- [165] Samir D. Mathur. Fuzzballs and the information paradox: A Summary and conjectures. 10 2008.
- [166] Hua Fang and Geoffrey Lovelace. Tidal coupling of a Schwarzschild black hole and circularly orbiting moon. *Phys. Rev. D*, 72:124016, 2005.
- [167] Chao Li and Geoffrey Lovelace. A Generalization of Ryan’s theorem: Probing tidal coupling with gravitational waves from nearly circular, nearly equatorial, extreme-mass-ratio inspirals. *Phys. Rev. D*, 77:064022, 2008.
- [168] Sayak Datta, Richard Brito, Sukanta Bose, Paolo Pani, and Scott A. Hughes. Tidal heating as a discriminator for horizons in extreme mass ratio inspirals. *Phys. Rev. D*, 101(4):044004, 2020.
- [169] Naritaka Oshita and Niayesh Afshordi. Probing microstructure of black hole spacetimes with gravitational wave echoes. *Phys. Rev. D*, 99(4):044002, 2019.
- [170] Qingwen Wang, Naritaka Oshita, and Niayesh Afshordi. Echoes from Quantum Black Holes. *Phys. Rev. D*, 101(2):024031, 2020.
- [171] Vitor Cardoso, Valentino F. Foit, and Matthew Kleban. Gravitational wave echoes from black hole area quantization. *JCAP*, 08:006, 2019.
- [172] Luca Buoninfante. Echoes from corpuscular black holes. 5 2020.
- [173] Pablo Bueno, Pablo A. Cano, Frederik Goelen, Thomas Hertog, and Bert Vercknocke. Echoes of Kerr-like wormholes. *Phys. Rev. D*, 97(2):024040, 2018.

- [174] Bob Holdom. Damping of gravitational waves in 2-2-holes. *Phys. Lett. B*, 813:136023, 2021.
- [175] Randy S. Conklin and Bob Holdom. Gravitational wave echo spectra. *Phys. Rev. D*, 100(12):124030, 2019.
- [176] Naritaka Oshita, Qingwen Wang, and Niayesh Afshordi. On Reflectivity of Quantum Black Hole Horizons. *JCAP*, 04:016, 2020.
- [177] Misao Sasaki and Takashi Nakamura. A Class of New Perturbation Equations for the Kerr Geometry. *Phys. Lett. A*, 89:68–70, 1982.
- [178] Misao Sasaki and Takashi Nakamura. Gravitational Radiation From a Kerr Black Hole. 1. Formulation and a Method for Numerical Analysis. *Prog. Theor. Phys.*, 67:1788, 1982.
- [179] Scott A. Hughes. Computing radiation from Kerr black holes: Generalization of the Sasaki-Nakamura equation. *Phys. Rev. D*, 62:044029, 2000. [Erratum: *Phys.Rev.D* 67, 089902 (2003)].
- [180] Kip S. Thorne, R.H. Price, and D.A. Macdonald, editors. *BLACK HOLES: THE MEMBRANE PARADIGM*. 1986.
- [181] David A. Nichols et al. Visualizing Spacetime Curvature via Frame-Drag Vortexes and Tidal Tendexes I. General Theory and Weak-Gravity Applications. *Phys. Rev. D*, 84:124014, 2011.
- [182] Fan Zhang, Aaron Zimmerman, David A. Nichols, Yanbei Chen, Geoffrey Lovelace, Keith D. Matthews, Robert Owen, and Kip S. Thorne. Visualizing Spacetime Curvature via Frame-Drag Vortexes and Tidal Tendexes II. Stationary Black Holes. *Phys. Rev. D*, 86:084049, 2012.
- [183] David A. Nichols, Aaron Zimmerman, Yanbei Chen, Geoffrey Lovelace, Keith D. Matthews, Robert Owen, Fan Zhang, and Kip S. Thorne. Visualizing Spacetime Curvature via Frame-Drag Vortexes and Tidal Tendexes III. Quasinormal Pulsations of Schwarzschild and Kerr Black Holes. *Phys. Rev. D*, 86:104028, 2012.
- [184] Elisa Maggio, Luca Buoninfante, Anupam Mazumdar, and Paolo Pani. How does a dark compact object ringdown? *Phys. Rev. D*, 102(6):064053, 2020.
- [185] Sayak Datta. Tidal heating of Quantum Black Holes and their imprints on gravitational waves. *Phys. Rev. D*, 102(6):064040, 2020.
- [186] William Kinnersley. Type D Vacuum Metrics. *J. Math. Phys.*, 10:1195–1203, 1969.
- [187] S.A. Teukolsky and W.H. Press. Perturbations of a rotating black hole. III - Interaction of the hole with gravitational and electromagnetic radiation. *Astrophys. J.*, 193:443–461, 1974.

- [188] Alexei A. Starobinskii and S.M. Churilov. Amplification of electromagnetic and gravitational waves scattered by a rotating "black hole". *Sov. Phys. JETP*, 65(1):1–5, 1974.
- [189] W.M. Suen, R.H. Price, and I.H. Redmount. Membrane Viewpoint on Black Holes: Gravitational Perturbations of the Horizon. *Phys. Rev. D*, 37:2761–2789, 1988.
- [190] Scott A. Hughes. The Evolution of circular, nonequatorial orbits of Kerr black holes due to gravitational wave emission. *Phys. Rev. D*, 61(8):084004, 2000. [Erratum: *Phys.Rev.D* 63, 049902 (2001), Erratum: *Phys.Rev.D* 65, 069902 (2002), Erratum: *Phys.Rev.D* 67, 089901 (2003), Erratum: *Phys.Rev.D* 78, 109902 (2008), Erratum: *Phys.Rev.D* 90, 109904 (2014)].
- [191] Misao Sasaki and Hideyuki Tagoshi. Analytic black hole perturbation approach to gravitational radiation. *Living Rev. Rel.*, 6:6, 2003.